Understanding the interconnection between carbon metabolism, electron transport chain and envelope redox homeostasis in *Escherichia coli*

KANCHAN JASWAL

A thesis submitted for the partial fulfillment of

the degree of the Doctor of Philosophy

Department of Biological Sciences

Indian Institute of Science Education and Research Mohali

Knowledge city, Sector 81, SAS Nagar, Manauli PO, Mohali 140306, Punjab, India.

September 2020

Dedicated to my family

Declaration

The work presented in this thesis has been carried out by me under the guidance of Dr. Rachna Chaba at the Indian Institute of Science Education and Research Mohali. This work has not been submitted in part or in full for a degree, a diploma, or a fellowship to any other university or institute. Whenever contributions of others are involved, every effort is made to indicate this clearly, with due acknowledgement of collaborative research and discussions. This thesis is a bona fide record of original work done by me and all sources listed within have been detailed in the bibliography.

Kanchan Jaswal

In my capacity as the supervisor of the candidate's thesis work, I certify that the above statements by the candidate are true to the best of my knowledge.

Dr. Rachna Chaba

Acknowledgments

The successful completion of my Ph.D. thesis is an outcome of the efforts put in by many people, and I am indebted to them for helping me on this adventurous journey. First, I express my heartfelt gratitude to my Ph.D. supervisor and coach, Dr. Rachna Chaba, who not only provided the support, guidance, and encouragement for my research work but has developed scientific aptitude in me. She is my guide, friend, and confidant. She instilled the values of hard work, dedication, punctuality, and consistency in me. She has always been encouraging and motivational, and I will miss our long-lasting discussions on the project. I owe a great deal to her. Many thanks!

I am sincerely thankful to my doctoral committee members, Dr. Shravan Kumar Mishra and Dr. Sudip Mandal, for their critical suggestions and motivation that has greatly influenced the quality of my research work and presentation. The discussions with them have always given a new perspective to my ideas and reasoning, which will be indispensable in my future endeavors. I would also like to thank Prof. Anand K. Bachhawat for his suggestions and encouragement throughout my research. I would especially like to mention the course BIO610 taught by Prof. Anand K. Bachhawat, which has improved my ability to grasp research papers. I am also grateful to Dr. Mahak Sharma and Dr. Vishal Agrawal (PU, Chandigarh, IN) for their critical suggestions while troubleshooting some crucial experiments.

I express my sincere gratitude to IISER Mohali directors, Prof. N. Sathyamurthy, Prof. Debi P. Sarkar, and Dr. J. Gowrishankar, for providing with an excellent academic environment, a cooperative IISER community, and the exceptional lab facilities throughout these years.

I thank my collaborator, Dr. Anthony L. Shiver (Stanford University, CA, USA), for the comparative analysis performed on the datasets obtained from the genetic screens. I

would also like to thank Dr. Frédéric Barras (CNRS, Marseille, France), Dr. Gisela Storz (NIH, Maryland, USA), Dr. Abhijit A Sardesai (CDFD, Hyderabad, IN), Dr. Carol Gross (UC, San Francisco, USA), Dr. Sarah Ades (Penn State University, USA), and Dr. Manjula Reddy (CSIR-CCMB, Hyderabad, IN) for providing different strains and reporter constructs used for the study.

Getting through my Ph.D. was fun and adventurous, and I owe this to the members of the Chaba lab. My seniors, Shashank and Bhupinder, not only taught me the experiments but also provided me with useful scientific insights. I was fortunate to have such generous and kind seniors. A very special gratitude goes out to all the members of Chaba lab, with whom I share an exceptional bond. Garima's great attitude towards life, Megha's happy-go-lucky attitude, Swati's kindness, Neeladrita's fun attitude, and Deeptodeep's persistency, has made my day-to-day work so easy and pleasurable. My special thanks to the 'project mates', Shashank, Megha, and Deeptodeep, for sharing the highs and lows during this period. A heartfelt thanks to the previous BS-MS students, Himanshi, Akshay, Shachikanta, Yatendera, and Bhargesh, and post-docs, Tapas, Prakram, and Mohinder. I also thank Liz and Aadra for their cheerful presence. A special mention to Apurtha for his insights and encouragement. It was great sharing lab space with you all throughout these years.

During these six and a half years, I have many people to thank for providing me with more than academic support. Special thanks to Muskan, Manpreet, Gayathri, and Anuj for listening to and, at times, having to tolerate me. I cherish our beautiful memories and friendship. I thank Deepinder, Twinkle, and Nitin for many memorable evenings. I will always be thankful to Bhisem, Richa, Kiran, Shalini, Nisha, Sonal, Prince, Krishna, and Devashish for their precious time during my journey at IISER Mohali.

Most importantly, none of this could have happened without the incomparable love and care of my family, who are always there unconditionally. My Parents are my pillar of strength. I am fortunate to have such an understanding and amazing parents. I would also like to express my appreciation for my loving brother, Sahil, and my dearest sister, Himani. I thank my eternal cheerleader-cum-husband, Neeraj, for his enduring support and patience. I thank my forever encouraging brother-in-law, Ankush. And, lastly, my sweet niece, Inaya, whose smile and charm make you forget all the hardships.

Kanchan Jaswal

Publications

A part of the work embodied in this thesis has been published in:

Agrawal S*, **Jaswal K***, Shiver A. L, Balecha H, Patra T, Chaba R. A genome-wide screen in *Escherichia coli* reveals that ubiquinone is a key antioxidant for metabolism of long-chain fatty acids. **J Biol Chem** 2017; 292: 20086-20099, PMID: 15161972; http://www.jbc.org/content/early/2017/10/17/jbc.M117.806240

Jaswal K*, Shrivastava M*, Roy D, Agrawal S, Chaba R. Metabolism of long-chain fatty acids affects disulfide bond formation in *Escherichia coli* and activates envelope stress response pathways as a combat strategy. **PloS Genetics** 2020; 16(10): e1009081, PMID: 33079953; https://doi.org/10.1371/journal.pgen.1009081

*co-first author

Abstract

Escherichia coli, a common gut microbe, can utilize a wide variety of fermentable and non-fermentable carbon sources (NFCs) for heterotrophic growth. In contrast to fermentable carbon sources, growth on NFCs requires the optimal functioning of electron transport chain (ETC) for energy production. Because different NFCs enter central metabolism at different steps and theoretically generate varied amounts of reduced cofactors, even amongst NFCs, there could be a difference in the requirement of ETC components. Besides a fundamental understanding, the information on the requirement of ETC components for growth on different NFCs can be exploited to manipulate commensal/ pathogenic *E. coli* strains. Here, we performed a comparative analysis of the existing high-throughput datasets of genetic screens of the single-gene deletion library of *E. coli* K-12 on multiple carbon sources. Our results showed that the requirement of ETC components for growth is inversely correlated with the energy yield of NFCs; however, the requirement of ubiquinone, a lipid-soluble electron carrier in the ETC, is highest for growth on long-chain fatty acids (LCFAs), an energy-rich NFCs. Our detailed analysis revealed that besides its electron carrier function in the ETC, ubiquinone functions as a key antioxidant during LCFA metabolism.

Besides transferring electrons generated by carbon metabolism, ubiquinone plays a pivotal role in taking up electrons from the disulfide bond-forming machinery, which catalyzes disulfide bond formation in the oxidizing environment of the envelope compartment. Because metabolism and disulfide bond formation converge at ubiquinone in the ETC, it is plausible that metabolic conditions that generate a large number of reduced cofactors render ubiquinone unavailable for disulfide bond formation. Disulfide bonds are required for the activity of several proteins including virulence factors, therefore, understanding the interconnection between carbon metabolism and disulfide bond

formation is of tremendous importance to envision how carbon metabolism impacts bacterial survival and pathogenesis. In this direction, we investigated the influence of metabolism of LCFA on the redox state of the envelope. We found that LCFA-utilizing cells exhibit characteristics of insufficient disulfide bond formation; these hallmarks are averted in cells exogenously provided with ubiquinone. Importantly, the envelope stress response (ESR) pathways, Cpx and σ^E, are activated by envelope signals generated by LCFA metabolism with Cpx being the primary ESR that monitors problems in disulfide bond formation. Taken together, our results demonstrate an intricate relationship between carbon metabolism and disulfide bond formation dictated by ETC and ESR, and provide the basis for examining whether similar mechanisms control envelope redox status in other gram-negative bacteria.

Thesis Synopsis

Title – Understanding the interconnection between carbon metabolism, electron transport chain and envelope redox homeostasis in *Escherichia coli*

Supervisor – Dr. Rachna Chaba

Department – Department of Biological Sciences

Institute – Indian Institute of Science Education and Research (IISER)-Mohali

Escherichia coli, a gram-negative facultative anaerobe, exhibits tremendous metabolic flexibility. *E. coli* can utilize a broad range of organic carbon sources for heterotrophic growth, which includes both fermentable (e.g., glucose, glucosamine, and maltose) and non-fermentable (e.g., acetate, fatty acids, and succinate) carbon sources. Depending on the availability and nature of electron acceptors, *E. coli* is able to operate three modes of metabolism: aerobic respiration, anaerobic respiration, and fermentation. During aerobic (in the presence of oxygen as a terminal electron acceptor) and anaerobic (in the presence of alternative electron acceptors such as nitrate) respiration, oxidation of reduced cofactors in the electron transport chain (ETC) generates proton motive force (PMF), which enables the production of ATP via oxidative phosphorylation. On the other hand, during fermentation, ATP can be produced through substrate-level phosphorylation. Thus, compared to fermentable carbon sources, the optimal functioning of ETC is critical for energy production during growth on non-fermentable carbon sources. Different non-fermentable carbon sources enter into the tricarboxylic acid cycle at varied steps and are theoretically expected to produce different amount of reduced cofactors. This raises the possibility that even amongst non-fermentable carbon sources, there could be a differential requirement of ETC components. However, this aspect has not been studied so far. Besides a fundamental understanding, the ETC components identified to be critical for growth on

non-fermentable carbon sources can be targeted to influence the growth of commensal/ pathogenic *E. coli* strains.

In the present study, by comparing the existing high-throughput datasets of genetic screens of the single-gene deletion library of *E. coli* on multiple carbon sources, we investigated whether there is a differential requirement of ETC components amongst non-fermentable carbon sources. Our results showed that the requirement of ETC components for growth is inversely correlated with the energy yield of non-fermentable carbon sources; however, the requirement of ubiquinone, a lipid-soluble electron carrier in the ETC, is highest for growth on long-chain fatty acids (LCFAs). Our follow-up study on the increased requirement of ubiquinone for growth on LCFAs revealed that ubiquinone is the cell's first line of defense against LCFA-induced oxidative stress, which likely limits the formation of reactive oxygen species by enabling rapid transfer of electrons from a large number of reduced cofactors produced by LCFA degradation.

In the presence of oxygen as the terminal electron acceptor, besides transferring electrons generated by the metabolism of carbon sources from respiratory dehydrogenases to the terminal oxidases, ubiquinone transfers electrons from the disulfide oxidoreductases, which catalyze disulfide bond formation in a large number of secreted proteins. The convergence of aerobic metabolism and disulfide bond formation at the level of ubiquinone in the ETC makes it tempting to speculate that metabolic conditions that increase electron flow in the ETC might limit ubiquinone from taking up electrons from the disulfide bond-forming machinery, thereby compromising envelope redox homeostasis. Because disulfide bonds are required for the activity of several proteins, including virulence factors, these studies are of tremendous importance to envision how carbon metabolism impacts bacterial survival and pathogenesis. The LCFA degradation pathway suggests the generation of a large number of reduced cofactors during its metabolism, which might increase electron

flow in the ETC, therefore, we chose LCFAs as a carbon source to investigate the interconnection between carbon metabolism and the redox status of the envelope. Our results showed that LCFA metabolism indeed increases electron flow in the ETC. Further, we found that during LCFA metabolism, ubiquinone is limiting for disulfide bond formation leading to redox imbalance in the envelope. Finally, our results showed that of the five major envelope stress response (ESR) pathways in *E. coli*, Cpx and σ^E are activated during LCFA metabolism, with Cpx playing a primary role in sensing envelope redox imbalance. Collectively, our results demonstrate an intricate relationship between carbon metabolism and disulfide bond formation dictated by ETC and ESR, and provide the basis for examining whether similar mechanisms control envelope redox status in other gram-negative bacteria.

This thesis is divided into six chapters organized as below:

Chapter I includes an extensive review of literature on topics relevant to this study. The first part of the present work deals with investigating the differential requirement of ETC components on non-fermentable carbon sources, and the second part examines the impact of carbon metabolism on envelope redox homeostasis. To encompass all topics included in the study, this chapter is divided into two sections. *Section I* of Chapter I describes the metabolism of fermentable and non-fermentable carbon sources with a particular focus on the LCFA metabolic pathway. This is followed by a thorough description of the ETC components with special emphasis on aerobic respiratory chain and PMF generation. Finally, this section provides information on metabolism induced oxidative stress and enzymatic and non-enzymatic antioxidants in *E. coli*. *Section II* of Chapter I describes the architecture of *E. coli* cell envelope, the role of envelope stress response pathways in maintaining envelope homeostasis and the process of disulfide bond formation in *E. coli*.

Chapter II describes the materials and methods that have been used in this study.

Chapters III, IV and V cover the results obtained in this study.

Chapter III: Systems-level analysis reveals a differential requirement of electron transport chain for the metabolism of non-fermentable carbon sources

In this section, we investigated the requirement of ETC components amongst non-fermentable carbon sources. For this, we re-analyzed data from previous high-throughput genetic screens of the single-gene deletion library of *E. coli* on various fermentable (glucose, glucosamine, N-acetyl glucosamine and maltose) and non-fermentable (acetate, glycerol, and succinate) carbon sources. In addition, the data from the genetic screens performed by Dr. Rachna Chaba on fermentable (glucose) and non-fermentable (oleate, a C18 LCFA) carbon sources were also included in the comparative analysis. As expected, this large scale analysis showed that ETC is critical for the growth of *E. coli* on non-fermentable carbon sources. Importantly, this analysis revealed that even amongst non-fermentable carbon sources, there is a difference in the requirement of various ETC components. We verified the growth phenotype of ETC components at a candidate level in liquid media. Importantly, we found that the requirement of ETC components is inversely correlated with the energy yield of non-fermentable carbon sources; however, the requirement of ubiquinone is maximal in oleate. Previous work from our lab showed that LCFA transport and degradation results in oxidative stress in *E. coli*. Following up on these observations that ubiquinone is maximally required for growth on LCFAs amongst all tested non-fermentable carbon sources and LCFA degradation generates oxidative stress, we showed that the increased requirement of ubiquinone on LCFAs is to mitigate oxidative stress. Further, our results suggest that a mechanism in addition to the known electron carrier function of ubiquinone is required to explain its antioxidant role in LCFA metabolism.

Chapter IV: Long-chain fatty acid metabolism compromises envelope redox homeostasis

Disulfide bonds contribute to the folding and stability of many extracytoplasmic proteins in all domains of life. In gram-negative bacteria, disulfide bond formation occurs in the oxidizing environment of the periplasmic space enclosed within the outer and inner membrane layers of the envelope. In *E. coli*, the periplasmic oxidoreductase, DsbA catalyzes the formation of disulfide bonds in substrate proteins. DsbB, an inner membrane disulfide oxidoreductase, performs the re-oxidation of DsbA. The reduced form of DsbB is re-oxidized by transferring electrons to ubiquinone. The terminal oxidases finally shuttle electrons from reduced ubiquinone (ubiquinol) to the terminal electron acceptors. Because electrons from aerobic metabolism of carbon sources and disulfide bond-forming machinery converge at the level of ubiquinone in the ETC, it is an intriguing possibility that envelope redox homeostasis is influenced by electron flow from the degradation of carbon sources. In this section, we investigated the influence of the metabolism of LCFA, an energy-rich carbon source, on the redox state of the envelope. By measuring $NADH/NAD^+$ ratio and the activity of respiratory dehydrogenases, we showed that LCFA degradation increases electron flow in the ETC. Further, we showed that cells metabolizing LCFAs exhibit several characteristics of insufficient disulfide bond formation, and these are prevented in cells exogenously provided with ubiquinone. Collectively, these data establish that during LCFA metabolism, ubiquinone is limiting for disulfide bond formation.

Chapter V: Envelope stress response pathways monitor redox imbalance during long-chain fatty acid metabolism

In *E. coli*, the integrity of the multilayered envelope is continuously monitored by at least five dedicated ESR systems (Bae, Cpx, Psp, Rcs, and σ^E), which sense problems in the

envelope and change the transcriptional program to combat stress. In this chapter, we investigated the activation of the ESR pathways during LCFA metabolism. Our results showed that envelope signals generated during LCFA metabolism induce Cpx and σ^E pathways. Further, several observations suggest that Cpx is the primary ESR that monitors envelope redox status during LCFA metabolism. Future investigations are required to understand the mechanism of activation of the Cpx pathway by LCFAs and the nature of feedback exerted by this ESR system to maintain envelope redox homeostasis.

Chapter VI summarizes the findings of this study and presents future prospects.

Table of Contents

List of Figures

Chapter I: Review of Literature

Chapter III: Systems-level analysis reveals a differential requirement of electron transport chain for the metabolism of non-fermentable carbon sources

Chapter IV: Long-chain fatty acid metabolism compromises envelope redox homeostasis

Chapter V: Envelope stress response pathways monitor redox imbalance during long-chain fatty acid metabolism

List of Tables

Chapter I: Review of Literature

Chapter II: Materials and Methods

Chapter III: Systems-level analysis reveals a differential requirement of electron transport chain for the metabolism of non-fermentable carbon sources

Abbreviations

1	°C	Degree celsius
2	Acetyl-P	Acetyl-phosphate
3	ADP	Adenosine diphosphate
4	AMS	4-acetamido-4’-maleimidystilbene-2,2’-disulfonicacid
5	AP	Alkaline phosphatase
6	ATP	Adenosine triphosphate
7	Bae	Bacterial adaptive response
8	BAM	β-barrel assembly machinery
9	cAMP	Cyclic AMP
10	$CdCl_2$	Cadmium chloride
11	Cit	Citrate
12	Cm	Centimeter
13	CoA	Co-enzyme A
14	CP	Cytoplasm
15	CRP	cAMP-receptor protein
16	C-terminal	Carboxyl-terminal
17	Cyd	Cytochrome bd
18	Cyo	Cytochrome bo
19	Cys	Cysteine
20	DCPIP	2,6-Dichlorophenolindophenol
21	DMK	Demethylmenaquinone
22	DMSO	Dimethyl sulfoxide
23	DNA	Deoxyribonucleic acid
24	DTT	Dithiothreitol
25	e^-	Electron
26	EDTA	Ethylenediaminetetraacetic acid
27	ESR	Envelope stress response
28	ETC	Electron transport chain
29	ETF	Electron transfer flavoprotein
30	FAD	Flavin adenine dinucleotide
31	FDR	False discovery rate
32	FMN	Flavin mononucleotide
92	Fum	Fumarate
94	Glo	Glyoxylate
33	GSEA	Gene set enrichment analysis
34	GSH	Glutathione
35	H^+	Proton
36	H_2O_2	Hydrogen peroxide
37	HPLC	High-performance liquid chromatography
38	IM	Inner membrane
39	Isocit	Isocitrate

40	kDa	kiloDalton
41	kV	Kilovolts
42	LB	Lysogeny broth
43	LCFA	Long-chain fatty acid
44	LPS	Lipopolysaccharide
45	Mal	Malate
46	MCT	Microcentrifuge tube
47	min	Minutes
48	MK	Menaquinone
49	ml	Milliliter
50	mM	Millimolar
51	mV	Millivolts
52	N- terminal	Amino-terminal
53	NAD	Nicotinamide adenine dinucleotide
54	NADP	Nicotinamide adenine dinucleotide phosphate
55	Ndh	NADH dehydrogenase II
56	nM	Nanomolar
57	Nuo	NADH dehydrogenase I
58	O_2^-	Superoxide ion
59	OAA	Oxaloacetate
60	OD	Optical density
61	OM	Outer membrane
62	OMPs	Outer membrane porins/outer membrane proteins
63	PAGE	Polyacrylamide gel electrophoresis
64	PCR	Polymerase chain reaction
65	PL	Phospholipids
66	PMF	Proton-motive force
67	PP	Periplasm
68	ppGpp	Guanosine 3’,5’-bispyrophosphate
69	Psp	Phage shock protein
70	Rcs	Regulator of capsule synthesis
71	RNA	Ribonucleic acids
72	RNAP	RNA Polymerase
73	ROS	Reactive oxygen species
74	SD	Standard deviation
75	Sdh	Succinate dehydrogenase
76	SDS	Sodium dodecyl sulphate
77	Seq analysis	Sequence analysis
78	SOD	Superoxide dismutases
79	sRNA	Small RNA
80	Suc	Succinate
81	TB	Tryptone broth
82	TBK	TB media using KCl in place of NaCl and buffered to pH7

83	TCA	Tri-carboxylic acid
84	TG	Thioglycerol
90	UQ	Ubiquinone
85	w/v	Weight (of solute) per volume (of solvent)
86	WT	Wild-type
87	α-KG	α-ketoglutarate
88	Bgal	β-D-galactosidase
89	µl	Microliter
90	µM	Micromolar
91	µmol	Micromoles

CHAPTER I

Review of Literature

1.1 Introduction

Escherichia coli is a gram-negative facultative anaerobe, which uses both fermentable (e.g., glucose, maltose, and glucosamine) and non-fermentable (e.g., succinate, fatty acids, and acetate) carbon sources to obtain metabolic energy. Whereas energy from fermentable carbon sources is derived both by substrate-level phosphorylation during glycolysis and by oxidative phosphorylation in the electron transport chain (ETC), the latter process is the sole means of energy production from non-fermentable carbon sources. Different non-fermentable carbon sources enter central metabolism at varied steps, thus even among these carbon sources there could be a difference in the requirement of ETC components. I started my thesis work with the objective to understand whether there is any differential requirement of ETC amongst non-fermentable carbon sources. Interestingly, I observed that whereas the requirement of aerobic ETC components for growth was inversely correlated with the energy yield of non-fermentable carbon sources, the requirement of ubiquinone, an electron carrier in the ETC, was maximal for growth on long-chain fatty acids (LCFAs). My work on the requirement of ETC components during LCFA metabolism and the work of another Ph.D. student from our lab, Shashank Agarwal, on understanding the role of oxidative stress response players in counteracting LCFA-induced reactive oxygen species (ROS) led us to identify ubiquinone as a key antioxidant during LCFA metabolism. The first section of the review of literature describes the **metabolism of fermentable and non-fermentable carbon sources with special emphasis on LCFAs.** This is followed by a detailed description of the **ETC components with a particular focus on aerobic respiratory chain and generation of proton-motive force (PMF)**. And, lastly, this section presents information on **metabolism induced oxidative stress and enzymatic and non-enzymatic antioxidants present in *E. coli.***

Besides the critical role of ubiquinone in transferring electrons derived from the metabolism of carbon sources, it also maintains oxidizing environment in the periplasmic compartment of the cell envelope by re-oxidizing the disulfide bond-forming machinery. The convergence of metabolism and disulfide bond formation at the level of ubiquinone in the ETC led me to investigate the interconnection between LCFA metabolism and envelope redox homeostasis. The second section of the review of literature thus provides information on the **cellular architecture of *E. coli* cell envelope, the role of envelope stress response pathways in maintaining envelope homeostasis and the process of disulfide bond formation in *E. coli*.**

Section-I

1.2 Fermentable and non-fermentable carbon sources

Bacterial growth on carbon sources requires the generation of metabolic intermediates that can serve as precursors for cellular macromolecules, production of metabolic energy and maintenance of redox balance. Growth of *E. coli* on carbon sources such as glucose can be achieved by both fermentative (in the absence of electron acceptor) and respiratory (in the presence of electron acceptor) processes (Lin & Iuchi, 1991). During fermentative growth, two molecules of NADH produced in glycolysis are re-oxidized to NAD^+ to maintain redox balance concomitant with the production of reduced fermentation end products such as acetate, ethanol, lactate, succinate, etc. (Sawers & Clark, 2004). Here energy is generated solely via substrate-level phosphorylation wherein a metabolic intermediate transfers its phosphoryl group to ADP and generates ATP (Sawers & Clark, 2004) (Fig. 1.1). However, when an electron acceptor such as oxygen is present, redox balance is maintained by re-oxidation of reduced cofactors at the ETC, and energy is generated by both substrate-level and oxidative phosphorylation. Oxidative phosphorylation is a process in which the PMF generated by the oxidation of reduced substrate in the ETC is accompanied by

phosphorylation of ADP to ATP by an inner membrane protein complex, ATP synthase (Senior, 1988). Besides oxygen, *E. coli* can use fumarate, trimethylamine N-oxide, dimethyl sulfoxide (DMSO), nitrite, and nitrate as the electron acceptor. Whenever electron acceptors are available, the cell favors respiration over fermentation (Lin & Iuchi, 1991). In contrast to fermentable carbon sources, during growth on non-fermentable carbon sources, the maintenance of redox balance by oxidation of reduced cofactors and generation of energy solely depend on the optimal functioning of the ETC (Berger, 1973) (Fig. 1.1). Considering the essential requirement of ETC for growth on non-fermentable carbon sources, most of the ETC components have been identified by screening for mutants which do not grow on non-fermentable carbon sources but can grow on fermentable carbon sources (Stroobant et al, 1972; Wu et al, 1993).

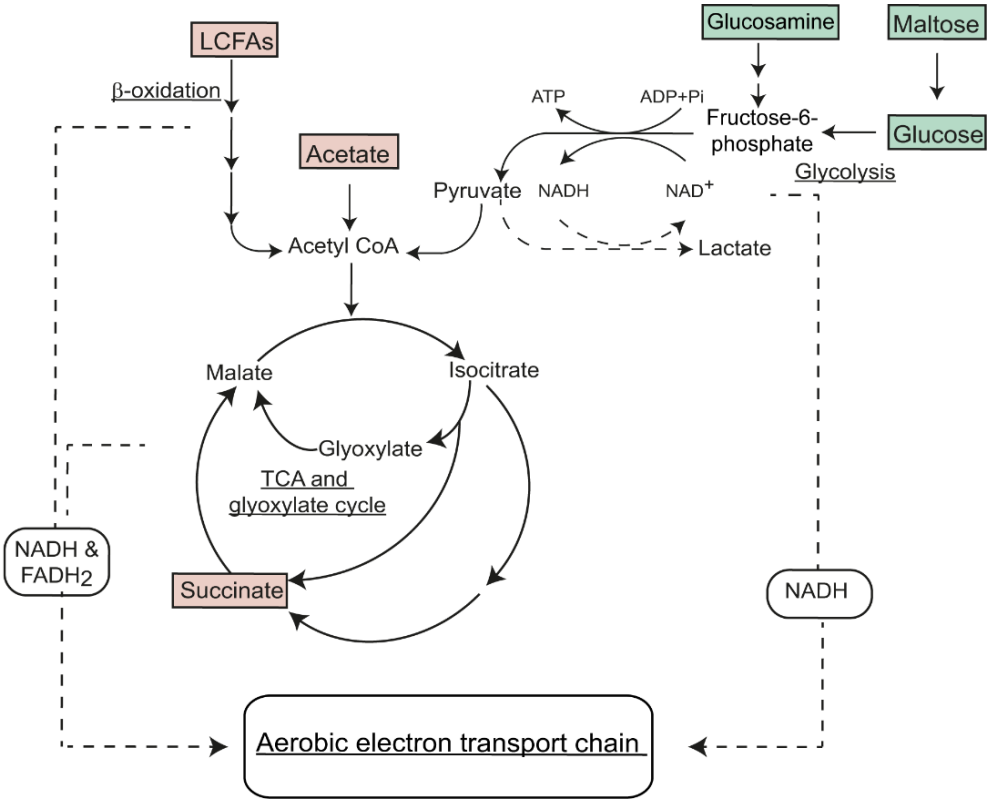

Figure 1.1. Metabolism of fermentable and non-fermentable carbon sources. Fermentable carbon sources such as glucose, maltose, and glucosamine generate ATP both via substrate-level phosphorylation during glycolysis and oxidative phosphorylation at the electron transport chain (ETC). In the absence of terminal electron acceptor, NADH produced during metabolism is re-oxidized to NAD^+ along with the production of

fermentation end products such as lactate. Non-fermentable carbon sources such as acetate, succinate, and long-chain fatty acids (LCFAs) generate energy only via oxidative phosphorylation. The reduced cofactors generated during metabolism are fed into the ETC to maintain redox balance and generate energy.

1.3 Long-chain fatty acids (LCFAs)

Fatty acids are carboxylic acids with an un-branched aliphatic chain and are categorized as short (2 to 4 carbon atoms), medium (5 to 11 carbon atoms), long (12 to 18 carbon atoms) and very long (>18 carbon atoms) chain fatty acids, depending on the number of carbon atoms in the aliphatic chain (Bernal et al, 2016; Mattam & Yazdani, 2013; Nunn et al, 1979). Several gram-negative bacteria, including *E. coli*, can grow on minimal medium containing LCFAs as a sole carbon source (Giles et al, 2011; Iram & Cronan, 2006; Kang et al, 2010). LCFAs are non-fermentable carbon sources, and thus for the generation of energy, cells are dependent on the optimal functioning of the ETC (Fig. 1.1) (Berger, 1973; Campbell et al, 2003). Besides being energy-rich molecules, LCFAs also help in generating precursors for cellular components such as membrane phospholipids (Iram & Cronan, 2006). LCFA metabolism has been implicated in the survival and virulence of several bacterial pathogens. For example, *Mycobacterium tuberculosis*, *Pseudomonas aeruginosa* and *Vibrio cholerae* mutants defective in LCFA utilization exhibit reduced virulence; in *Salmonella* Typhimurium, the LCFA pathway is up-regulated during infection and contributes to the metabolism of pro-inflammatory host LCFAs thereby suppressing the innate immune response; and LCFA degradation enzymes are induced in *P. aeruginosa* during lung infection in cystic fibrosis patients (Kang et al, 2010; Mahan et al, 1995; Pace et al, 1993; Ray et al, 2011; Son et al, 2007). Recently, in *V. cholerae*, cholera toxin dependent remodeling of the host metabolism has been shown to cause lipolysis in the target cells, thereby accumulating LCFAs in the intestinal niche. These LCFAs are acquired by the pathogen resulting in enhanced growth (Rivera-Chavez & Mekalanos, 2019).

1.3.1 Aerobic metabolism of long-chain fatty acids

LCFAs are transported and degraded with the help of proteins encoded by *fad* (fatty acid degradation) genes resulting in the production of acetyl-CoA, which is then fed into the tri-carboxylic acid (TCA) and glyoxylate cycles (Fig. 1.2). NADH and $FADH_2$ produced during LCFA metabolism are oxidized at the ETC. The *fad* genes are transcriptionally controlled by three regulatory systems: 1) negative regulation by a fatty-acid specific transcriptional regulator, FadR, 2) negative regulation by the anoxic redox control ArcA-ArcB two-component system, and 3) positive regulation by the global cyclic AMP (cAMP) receptor protein-cAMP (CRP-cAMP) complex (Clark & Cronan, 2005; Cronan & Laporte, 2006). *E. coli* K12 can utilize LCFAs, but not medium-chain fatty acids (Overath et al, 1969), because the derepression of the fatty-acid specific transcriptional regulator, FadR from *fad* genes occurs via specific binding of the repressor to long-chain fatty acyl-CoA, an intermediate in the LCFA degradation pathway (DiRusso et al, 1992). The *fad* genes are scattered throughout the chromosome except for *fadBA*, which are co-transcribed. However, all *fad* genes are co-ordinately induced in the presence of LCFAs because of the deregulation of FadR in the presence of acyl-CoA (Clark & Cronan, 2005).

1.3.1.1 Long-chain fatty acid transport inside the cell

The short- and medium-chain fatty acids can readily diffuse across the outer membrane without requiring any carrier protein. However, the transport of exogenous LCFAs across the outer membrane requires a β-barrel outer membrane protein, FadL, which delivers the long hydrophobic tails of LCFAs into the periplasm (Clark & Cronan, 2005) (Fig. 1.2). FadL acts as a ligand-gated diffusion channel as revealed by two distinct crystal structures of the protein (van den Berg et al, 2004). LCFAs first bind FadL at the low-affinity binding site and then move to the high-affinity binding site, which causes conformational changes in the periplasmic side hatch region, thereby opening an LCFA-specific diffusion channel.

The binding of LCFAs to FadL is dependent on specific hydrophobic interactions between the long acyl chain and the protein. As oleoyl alcohol and methyl oleate are unable to bind the transporter, carboxylate of the LCFA is also thought to be required for the binding; the charged amino acid residues of FadL are proposed to contact the carboxylate ion (Dirusso & Black, 2004; van den Berg et al, 2004).

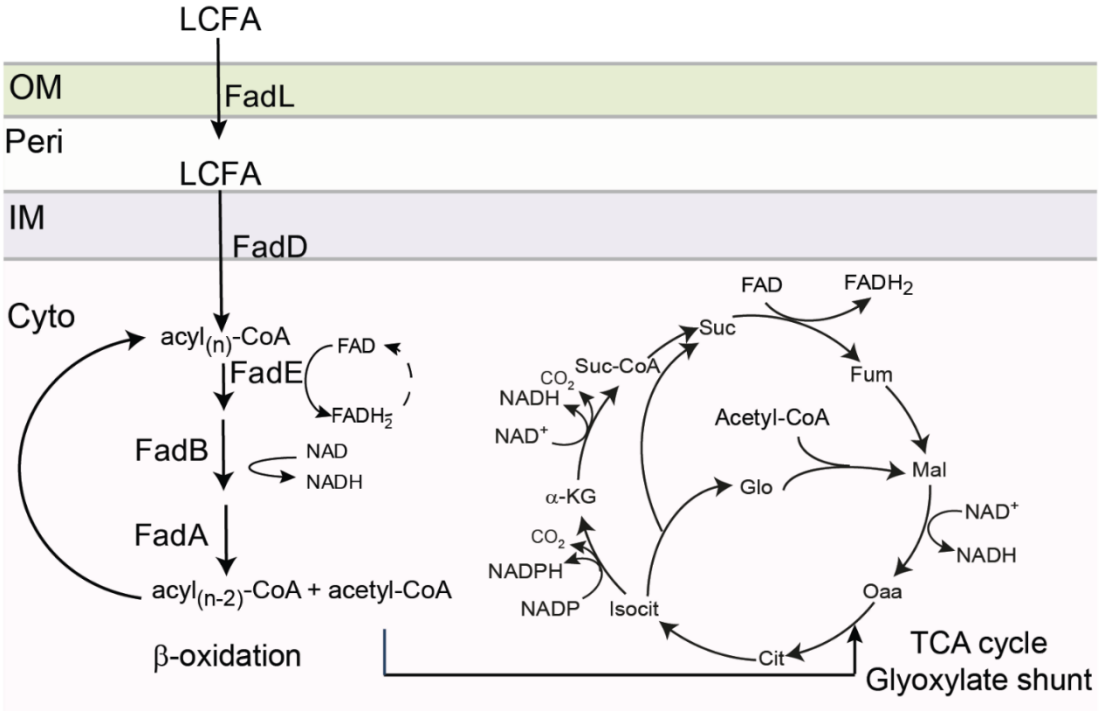

Figure 1.2. Long-chain fatty acid transport and degradation. LCFAs, when present in the medium, are transported inside the cells by an outer membrane transporter, FadL. The LCFAs then partition into the inner membrane and flip towards the cytoplasmic face. The acyl-CoA synthetase, FadD, extracts LCFAs from the inner membrane concomitant with activation of LCFAs to acyl-CoA. Acyl-CoA enters the β-oxidation pathway, which is catalyzed by FadE, FadB, and FadA enzymes. Each round of the β-oxidation pathway releases acetyl-CoA reducing the length of acyl-CoA by two carbon atoms. The acyl-CoA shortened by two carbon atoms again enters the β-oxidation pathway. Acetyl-CoA enters the TCA and glyoxylate cycle for further degradation. Most of the intermediates of the TCA cycle lead to the formation of important precursors such as amino acids, or porphyrins. During the glyoxylate cycle, the decarboxylation step of the TCA cycle is by-passed and therefore, it prevents the loss of carbon from acetyl-CoA as CO_2. Abbreviations: OM, outer membrane; Peri, periplasm; IM, inner membrane; Cyto, cytoplasm; Oaa, oxaloacetate; Cit, citrate; Isocit, isocitrate; α-KG, α-ketoglutarate; Suc-CoA, succinyl-CoA; Suc, succinate; Fum, fumarate; Mal, malate; Glo, glyoxylate.

LCFAs upon entering the periplasmic space, get protonated because of the acidic nature of the periplasm. The protonated LCFAs then partition into the inner membrane and flip towards the cytoplasmic face. The acyl-CoA synthetase, FadD, is involved in the conversion of LCFAs to long-chain fatty acyl-CoA (Fig. 1.2). Importantly, this enzyme was found to be present in both the inner membrane and the cytosol and thus has been proposed to extract LCFAs from the inner membrane along with the activation of LCFAs, thus making LCFA transport unidirectional. This process is known as the vectorial esterification mechanism of transport. The long-chain fatty acyl-CoA formed by the synthetase activity of FadD, binds to FadR and derepresses the *fad* genes including *fadL*; therefore, deletion of *fadD* results in inhibition of transport of LCFAs across the outer membrane (Dirusso & Black, 2004; Hill & Angelmaier, 1972). Collectively, the transport of exogenous LCFAs across the cell envelope requires both FadL and FadD.

1.3.1.2 Long-chain fatty acid degradation (β-oxidation) pathway

After being transported inside the cell, LCFAs get converted to acyl-CoA, which enters the β-oxidation cycle. The first step of the cycle is catalyzed by acyl-CoA dehydrogenase, which converts acyl-CoA to enoyl-CoA (Fig. 1.2). In 1973, Klein identified several *E. coli* mutants that did not have any detectable acyl-CoA dehydrogenase activity (Klein, 1973). Later in 2002, based on the sequence corresponding to dehydrogenase motif along with genetic analysis, acyl-CoA dehydrogenase activity was assigned to the *yafH* gene, which was renamed as *fadE* in *E. coli* and *S. enterica* serovar Typhimurium (Campbell & Cronan, 2002). FadE contains FAD as a cofactor, and two electrons are transferred from its substrate to FAD generating $FADH_2$. The $FADH_2$ molecule needs to be re-oxidized for the dehydrogenase activity of the enzyme. In mitochondrial β-oxidation, electron transfer flavoprotein (ETF) has been reported to mediate the re-oxidation of $FADH_2$ to FAD, transferring electrons to ubiquinone in the ETC (Roberts et al, 1996). Even in bacteria such

as *Bacillus subtilis*¸ ETF proteins have been identified (Barabesi et al, 2007); however, no ETF homologue has been found in *E. coli* (Campbell & Cronan, 2002). *E. coli* FadE is over twice the size of the mammalian homologue, and the extra amino acid residues have been found to be conserved in many bacterial species. These regions seem to play an essential role in FadE function as the truncation of this region leads to loss of activity. Therefore, it has been proposed that the extra region in FadE might perform the function of ETF in *E. coli* (Campbell & Cronan, 2002).

The enoyl-CoA generated by the activity of FadE serves as a substrate for the multienzyme complex, FadBA (Fig. 1.2). The complex is a heterotetramer composed of two copies each of FadA and FadB and is cotranscribed from the operon *fadBA*. There are five enzyme activities present in this complex: 3-ketoacyl-CoA thiolase, enoyl-CoA hydratase, 3-hydroxyacyl-CoA dehydrogenase, cis-Δ3-trans-Δ2-enoyl-CoA isomerase, and 3-hydroxyacyl-CoA epimerase (Clark & Cronan, 2005; Pramanik et al, 1979). The smaller subunit FadA performs the thiolase activity, whereas the rest of the activities are performed by the FadB subunit. During the oxidation of saturated fatty acids, enoyl-CoA hydratase, 3-hydroxyacyl-CoA dehydrogenase, and 3-ketoacyl-CoA thiolase activity of the complex are needed. On the other hand, for the degradation of unsaturated fatty acids, two additional activities mentioned above are also performed by the complex. The activity of the FadBA complex releases acetyl-CoA reducing the length of acyl-CoA by two carbon atoms. The acyl-CoA shortened by two carbon atoms again enters the β-oxidation cycle (Clark & Cronan, 2005) (Fig. 1.2).

1.3.2 Tri-carboxylic acid and glyoxylate cycles

The acetyl-CoA released during β-oxidation or by the degradation of substrates such as acetoacetate, ethanol, or acetate is metabolized by the TCA cycle. Acetyl-CoA enters the TCA cycle by combining with oxaloacetate (OAA). Citrate, hence formed, undergoes

hydration, decarboxylation, phosphorylation and dehydrogenation to regenerate OAA and release two molecules of CO_2. In each round of TCA cycle, two molecules of NADH, one molecule of NADPH and one molecule of $FADH_2$ are produced (Cronan & Laporte, 2006) (Fig. 1.2). The NADH and $FADH_2$ are re-oxidized at the ETC, resulting in the generation of energy, whereas NADPH is consumed in several cellular processes such as fatty acid biosynthesis, proline biosynthesis (Csonka & Fraenkel, 1977; Li et al, 2018). When NADPH production increases in the cell, e.g., during acetate metabolism, the transhydrogenase, UdhA, reoxidizes NADPH by converting NAD^+ to NADH (Sauer et al, 2004).

Several of the TCA cycle intermediates are required for the biosynthesis of cellular precursors, e.g., α-ketoglutarate synthesizes serine and tyrosine, succinyl-CoA is required for cytochrome synthesis, OAA is converted to aspartate which is important for nucleotide synthesis (Layer et al, 2010; Romano & Nickerson, 1958). Since anabolic reactions consume TCA cycle intermediates, it is essential for the cell to have mechanisms to replenish these intermediates to continue the operation of TCA cycle. For example, growth in glucose provides a 3-carbon intermediate such as phosphoenolpyruvate, which undergoes carboxylation to form OAA (Perry et al, 2007). Growth on acetate and fatty acids, however, requires the functioning of glyoxylate shunt to regenerate OAA. During glyoxylate cycle, isocitrate formed by hydration of citrate, is cleaved to generate succinate and glyoxylate. The glyoxylate molecule then reacts with another acetyl-CoA to form malate, which is further oxidized to OAA (Fig. 1.2). In addition, since glyoxylate shunt bypasses the decarboxylation steps of the TCA cycle, it prevents the loss of carbon from acetyl-CoA as CO_2 (Cronan & Laporte, 2006).

1.4 Electron Transport Chain

ETC carries out two important functions, ATP production and maintenance of redox balance. The components of the ETC are located at the inner membrane and consist of dehydrogenases and terminal oxidases, which are linked by quinones. Dehydrogenases transfer electrons from various substrates (NADH, succinate, formate, lactate, etc.) to quinones (menaquinone, ubiquinone, and demethylmenaquinone). Electrons are then transferred from reduced quinones to the terminal electron acceptors (molecular oxygen, dimethyl sulfoxide, nitrate, nitrite, fumarate, and trimethylamine N-oxide) by terminal oxidases (Fig. 1.3). In *E. coli*, there are around 15 primary dehydrogenases, 3 quinones, 14 terminal oxidases, and 8 electron acceptors (Unden et al, 2014). Therefore, the large variability of the ETC can be established by combining the available dehydrogenases, quinones and oxidases if the dehydrogenase and the oxidase can transfer and accept electrons from the same quinone, respectively, and are both expressed under a given growth condition (Unden et al, 2014).

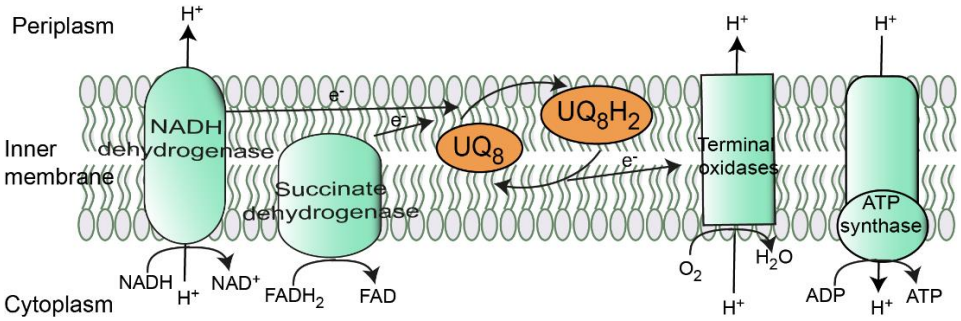

Figure 1.3. Aerobic electron transport chain (ETC) in *E. coli*. NADH dehydrogenase and succinate dehydrogenase transfer electrons from NADH and $FADH_2$, respectively, to ubiquinone. Electrons are then transferred from reduced ubiquinone, ubiquinol, to terminal oxidases, where ubiquinol is oxidized back to ubiquinone. Molecular oxygen finally takes electrons from terminal oxidases and gets converted to water. During this flow of electrons in ETC, NADH dehydrogenase and terminal oxidase can couple electron transfer to generate proton motive force (PMF) by translocating protons from the cytoplasmic side to the periplasmic side of the membrane. The PMF generated is used by the ATP synthase for the synthesis of adenosine 5' triphosphate (ATP). Abbreviations: UQ_8, ubiquinone-8; UQ_8H_2, ubiquinol; H^+, proton; e^-, electron.

1.4.1 Electron Transport Chain components

In this section, I have described the ETC components involved in aerobic metabolism. The aerobic ETC of *E. coli* contains three main dehydrogenases: (i) succinate dehydrogenase (Kasahara & Anraku, 1974), (ii) NADH dehydrogenase I (Nuo) (Calhoun & Gennis, 1993; Meinhardt et al, 1989) and (iii) NADH dehydrogenase II (Ndh) (Bragg & Hou, 1967); three terminal oxidases: (i) cytochrome *bo* (Cyo) (Kita et al, 1984), (ii) cytochrome *bd* I (Cyd) (Kita et al, 1984) and (iii) cytochrome *bd* II (App) (Sturr et al, 1996; Unden & Bongaerts, 1997); and ubiquinone as the major quinone (Unden et al, 2014). During aerobic conditions, the terminal electron acceptor is molecular oxygen (Fig. 1.3).

1.4.1.1 NADH dehydrogenase

During aerobic respiration, NADH is re-oxidized by two major respiratory dehydrogenases, NADH dehydrogenase I (Nuo) and NADH dehydrogenase II (Ndh). Nuo is made up of 13 subunits, has flavin mononucleotide (FMN) and iron-sulfur clusters, and can couple electron transfer with proton translocation (Unden et al, 2014). The enzyme can also drive Na^+ translocation (Steuber et al, 2000). Nuo complex is similar to the mitochondrial NADH dehydrogenase and is often referred to as Complex I. The 13 subunits of Nuo complex from NuoA to NuoN are arranged in an operon. Unlike other bacteria where *nuoC* and *nuoD* genes are separate, *E. coli* contains a fused *nuoCD* gene in the operon (Friedrich & Pohl, 2007). The deletion of any of the genes of the Nuo complex prevents the assembly of Complex I (Erhardt et al, 2012). The Nuo subunits NuoA, H, J, K, L, M, and N form the hydrophobic segment of the complex and are embedded in the membrane. The other subunits form the “peripheral arm” which extends into the cytoplasm. The subunits NuoB, CD, and I form the connecting part of the arm, whereas NuoE, F, and G subunits form the soluble part, and contain iron-sulfur clusters and cofactor (Friedrich & Pohl, 2007). Nuo mutants show poor growth on some amino acids or minimal medium with acetate as a

carbon source. It has been proposed that this phenotype is due to higher NADH/NAD^+ ratio, which likely inhibits citrate synthase and malate dehydrogenase enzymes of the TCA cycle (Falk-Krzesinski & Wolfe, 1998; Pruss et al, 1994).

The NADH dehydrogenase II (Ndh) is a single subunit NADH dehydrogenase and contains FAD. Unlike Nuo, Ndh cannot translocate protons (Friedrich & Pohl, 2007). The major function of Ndh is likely to maintain the NADH/NAD^+ ratio by oxidizing NADH (Neijssel & Teixeira de Mattos, 1994). During the growth of cells in the presence of glucose, the rate of aerobic respiration largely decreases in *ndh* deletion strain but not in *nuo* deletion strain. Therefore, Ndh is considered to be more important during aerobic respiration. The remaining oxygen consumption in *ndh* deletion strain indicates that Nuo also participates in aerobic ETC. Under anaerobic (fumarate and DMSO respiration) conditions, whereas Nuo is expressed, Ndh is repressed, and the rate of fumarate respiration decreases in *nuo* deletion strain but is not affected in *ndh* mutant. Altogether, during aerobic metabolism Ndh is the major NADH dehydrogenase whereas Nuo works under both aerobic and anaerobic conditions (Green & Guest, 1994; Tran et al, 1997; Unden & Bongaerts, 1997).

1.4.1.2 Succinate dehydrogenase

Succinate dehydrogenase (Sdh) is an essential component of the TCA cycle where it converts succinate to fumarate. During this process, quinone is reduced; therefore, Sdh also constitutes a part of the ETC. The enzyme complex is a hetero-tetrameric protein encoded by *sdhCDAB* operon. SdhA is a flavoprotein subunit whereas SdhB contains three iron-sulfur clusters. The other two subunits form an integral membrane domain of the complex (Tomasiak et al, 2007). SdhE, a small protein, which is encoded from a locus distinct from the *sdh* operon, helps in the covalent linkage of flavin to SdhA subunit, facilitating the assembly of the complex (Maher et al, 2018; McNeil et al, 2012). Succinate oxidation takes

place at SdhA converting the covalently bound FAD to $FADH_2$. The electrons are then transferred to quinone, the binding site of which is formed by SdhB, SdhC, and SdhD (Tomasiak et al, 2007).

1.4.1.3 Quinones

The electrons are transferred from dehydrogenases to terminal oxidases by a lipid-soluble electron carrier, quinone. They can be broadly divided into benzoquinones (ubiquinone, UQ) and naphthoquinones (menaquinone, MK, and demethylmenaquinone, DMK). Because DMK (+36 mV) and MK (−74 mV) have low midpoint potential, they are involved in anaerobic respiration, whereas UQ has a higher midpoint potential (+100 mV) and is therefore involved in aerobic respiration (Alvarez et al, 2013). The midpoint potential decides the electron donor or acceptor for quinones e.g. the redox potential of succinate (~ +30 mV) does not allow it to reduce MK but enables reduction of UQ; thus succinate uses UQ as an electron carrier in the ETC (Butler et al, 2006; Unden et al, 2014). During aerobic growth, UQ is the major quinone, and its content is considerably higher (~ 1 μmol/g dry weight) than DMK and MK (<0.1 μmol/g dry weight) (Sharma et al, 2013).

Ubiquinone has a conserved aromatic ring and an isoprenoid chain of varying length. The number of isoprenoid units varies among species; in humans, the number of isoprenoid units is ten, while *E. coli* has eight isoprenoid units. Therefore, *E. coli* ubiquinone is designated as UQ_8 or Q_8 (Aussel et al, 2014). The aromatic ring of ubiquinone is hydrophilic and helps in its interaction with several membrane proteins, whereas the isoprenoid chain is hydrophobic and provides lipid solubility to quinones (Fujimoto et al, 2012).

Ubiquinone is important for several physiological processes. Ubiquinone being an electron carrier in the ETC, generates PMF, which is used by antibiotics such as aminoglycosides to enter inside the cell. Therefore, *ubi* mutants are resistant to

aminoglycosides (Muir et al, 1981; Shan et al, 2015). Besides its role as an electron carrier in ETC, the redox state of ubiquinone can also modulate the phosphorylation of Arc two-component system, which allows *E. coli* to sense respiratory growth conditions (Georgellis et al, 2001). In addition, ubiquinone is important for the catalytic activity and intramolecular electron transfer of membrane-bound glucose dehydrogenase (Fujimoto et al, 2012). Although ubiquinone is a well-known antioxidant in eukaryotes, prior to our work, there was only one report in prokaryotes (in *E. coli*) where it was suggested to be a part of the defense against oxidative stress (Soballe & Poole, 2000) (details in Section 1.6). Ubiquinone also plays a critical role in disulfide bond formation in extracytoplasmic proteins (Kobayashi et al, 1997). Since a major part of my thesis deals with the interconnection between LCFA metabolism and disulfide bond formation, the role of ubiquinone in disulfide bond formation is discussed in detail later in this review.

1.4.1.4 Terminal oxidases

Transfer of electrons from ubiquinol to molecular oxygen is performed by oxidases which are either quinol oxidases, that can directly take electrons from ubiquinol, or cytochrome *c* oxidases, which require an additional middle component, cytochrome *bc*1 complex. *E. coli* lacks the cytochrome *c* oxidase and cytochrome *bc*1 complex, thus has only quinol oxidases as terminal oxidases. The two major quinol oxidases are cytochrome *bo* and cytochrome *bd* I. In recent years, the contribution of another *bd*-type oxidase, cytochrome *bd* II in electron transfer and membrane potential generation has been evidenced (Borisov & Verkhovsky, 2015).

Cytochrome *bo* consists of four different subunits, encoded by the *cyoABCDE* operon. The main catalytic subunits are CyoA and CyoB, where CyoB contains redox groups like heme *a*, heme *o3* and copper ion. These redox groups are required for the electron transfer, oxygen reduction, and proton pumping function of the complex (Borisov

& Verkhovsky, 2015). The subunits CyoC and CyoD are not involved in catalysis (Kita et al, 1984). These subunits are proposed to be required for the assembly of metal cofactors in the complex (Saiki et al, 1996). The *cyoE* gene does not encode any subunit of the complex but is required for the production of heme *o,* which is involved in the reduction of oxygen (Saiki et al, 1992; Saiki et al, 1993). Phylogenetic analysis revealed that cytochrome *bo* oxidases evolved from the same ancestor as cytochrome *c* oxidases; however, cytochrome *bd* oxidases are evolutionarily different and structurally divergent from other oxidases (Castresana et al, 1994; Chepuri et al, 1990). Cytochrome *bd* I is a three subunit enzyme encoded by the operon *cydABX* (Borisov & Verkhovsky, 2015). CydX is a small protein that helps in the stabilization of heme and the other two major subunits of the complex (VanOrsdel et al, 2013). Recently, the fourth subunit of the complex, CydY, has been identified. CydY has a molecular mass of ~3 kDa and is important to block the dioxygen channel providing substrate specificity over other gaseous substrates (Thesseling et al, 2019). The two other genes of the operon *cydCD* are required for the assembly of the cytochrome *bd* I complex but do not form the subunits of the complex. Cytochrome *bd* II is encoded by *appBCX* genes where the amino acid sequence of *appB* and *appC* gene products show homology to CydA (60%) and CydB (57%) subunits of cytochrome *bd* I, respectively (Borisov & Verkhovsky, 2015).

Cytochrome *bo* is expressed under aerobic conditions, whereas cytochrome *bd* I is expressed under microaerobic conditions. Interestingly, under aerobic conditions, there is 150-fold increase in cytochrome *bo* levels whereas there is only 3-fold decrease in cytochrome *bd* I levels. Thus, the change in response to oxygen is more for cytochrome *bo* than cytochrome *bd* I (Borisov & Verkhovsky, 2015). Interestingly, the affinity of cytochrome *bd* I for oxygen is 1000-fold higher than cytochrome *bo,* which is speculated as the reason for the bacteria to switch from Cyo to Cyd terminal oxidase under

microaerobic conditions (D'Mello et al, 1996). The levels of cytochrome *bd* I also increase in response to alkaline pH, high temperature, and low concentrations of cyanide in growth media (Borisov & Verkhovsky, 2015).

Cytochrome *bd* I, apart from generating PMF and helping in ATP synthesis, has many other physiological functions that lead to pleiotropic effects of its deletion. Cytochrome *bd* I acts as an oxygen scavenger and has quinol peroxidase activity (Al-Attar et al, 2016). Interestingly, in a study determining the contribution of respiratory metabolism for the colonization of bacteria in the gut, cytochrome *bd* I mutants failed to colonize, whereas mutation in cytochrome *bo* had no effect (Jones-Carson et al, 2016). Mutants of cytochrome *bd* I also show stationary phase exit defect. The stationary phase is considered as a microaerobic condition and is thus suggested to require cytochrome *bd* I as the terminal oxidase. When cells are re-inoculated from the stationary phase, Cyd functions as the major terminal oxidase till the time Cyo is expressed which explains the stationary phase exit defect phenotype of *cyd* mutant (Siegele et al, 1996; Siegele & Kolter, 1993).

1.4.2 Generation of proton motive force

Most of the ETC complexes are organized such that they can generate a PMF across the inner membrane (positive on the periplasmic side) (Ingledew & Poole, 1984) (Fig. 1.3). This PMF can be generated either by (i) directly pumping the protons towards the periplasm, e.g., NADH dehydrogenase I and cytochrome *bo*, or by (ii) redox-loop or vectorial transfer method where proton translocation is an inevitable consequence of electron transport, e.g., cytochrome *bd* (Unden et al, 2014). In the case of direct pumping, the same proton translocates from cytoplasm to periplasm, and this process is either redox driven (Cytochrome *bo*) or conformationally driven (NADH dehydrogenase I). NADH dehydrogenase I complex involves coordinated conformational changes in the structural elements of the complex which causes proton translocation (Efremov & Sazanov, 2011),

whereas in case of Cytochrome *bo* the electrostatic coupling between electron and proton drives proton across the hydrophobic barrier, the proton is then expelled out of the membrane by electrostatic repulsion from the proton that converts oxygen to water molecule (Borisov & Verkhovsky, 2015; Wikstrom & Verkhovsky, 2007). However, during the vectorial charge transfer, the arrangement of the terminal oxidase is such that quinol oxidation releases proton towards the periplasmic side and the conversion of oxygen to water takes up a proton from the cytoplasmic side. Therefore, the same proton is not translocated from cytoplasm to periplasm during vectorial transfer. Cytochrome *bo* not only generates PMF by direct redox-dependent proton pumping but can also do so by vectorial chemistry like cytochrome *bd* (Borisov et al, 2011; Borisov & Verkhovsky, 2015). Some enzymes consume and release proton at the same side, often referred to as scalar transfer, but this does not contribute to PMF e.g., succinate dehydrogenase, fumarate reductase, and NADH dehydrogenase II. These enzymes have to depend on other enzymes of the redox loop and proton pump category to generate PMF (Unden et al, 2014). The PMF generated can then be used to drive processes such as ATP synthesis by ATP synthase, solute transport, and flagellar motion (Elferink et al, 1985; Manson et al, 1977; Senior, 1988).

The versatility of ETC to generate PMF is possible because a particular quinone can couple different dehydrogenases to different oxidases. Different dehydrogenases can be combined with different oxidases in aerobic ETC to generate $H^+/2e^-$ ratio from $2H^+/2e^-$ to $8H^+/2e^-$ (Calhoun & Gennis, 1993). Amongst the three major dehydrogenases present in aerobic ETC, only Nuo can couple electron transfer to PMF generation with bioenergetic efficiency of $4H^+/2e^-$. The arrangement of the Sdh complex and Ndh is such that proton uptake and release occur on the same side of the membrane; thus, there is no generation of PMF (Unden et al, 2014). All three quinol oxidases generate PMF; however, they differ in their bioenergetic efficiency: $H^+/2e^-$ ratio is 4 for cytochrome *bo* and 2 for cytochrome *bd*

I and cytochrome *bd* II (Borisov & Verkhovsky, 2015). Therefore, when Nuo dehydrogenase is combined with Cyo terminal oxidase, it results in a maximum theoretical ratio of $8H^+/2e^-$ for the aerobic respiratory chain of *E. coli* whereas when Ndh dehydrogenase is used the ratio decreases to $4H^+/2e^-$ (Unden et al, 2014). Table 1.1 shows the bioenergetics of the coupling of different dehydrogenases with different oxidases.

Notably, the combination of dehydrogenases to oxidases is such that the dehydrogenase (e.g. Ndh) which is unable to couple electron transfer with PMF generation (non-coupler) is never linked with non-coupling oxidases. This also explains why Nuo, and not Ndh, plays a role in fumarate and DMSO respiration. The combination of Nuo with the non-coupling oxidases, Fumarate reductase (Frd) or DMSO reductase (DmsABC) under anaerobic conditions leads to $H^+/2e^-$ ratio of $4H^+/2e^-$ (Unden et al, 2014).

Table. 1.1. The table shows the theoretical bioenergetics when different dehydrogenases are combined with different oxidases.

Electron transfer	Dehydrogenase ($H^+/2e^-$)	Terminal oxidase ($H^+/2e^-$)	Theoretical bioenergetic efficiency ($H^+/2e^-$)
From NADH (aerobic)	Nuo (4)	Cyo (4)	8
	Ndh (0)	Cyo (4)	4
From NADH (microaerobic)	Nuo (4)	Cyd (2)	6
	Ndh (0)	Cyd (2)	2
From succinate	Sdh (0)	Cyo (4)	4
From NADH (DMSO respiration)	Nuo (4)	Dimethyl sulfoxide reductase (0)	4
From NADH (fumarate respiration)	Nuo (4)	Fumarate reductase (0)	4

1.4.3 ATP synthesis

The PMF generated by the oxidation of substrates is used by F1F0 ATP synthase for the synthesis of ATP, and the process is called oxidative phosphorylation (Fig. 1.3). Oxidative phosphorylation occurs under both aerobic and anaerobic conditions. The ATP synthase is formed of eight polypeptides, αβγδεabc encoded by *atp* operon. ATP synthase requires two subunits for its assembly, F1 and F0. F1 is a water-soluble ATP hydrolase and comprises of α_3, β_3, γ, δ, and ε subunits whereas F0 is a proton channel formed by a, b_2 and c_{10} subunits. The ATP synthase functions as a rotary motor where it follows the "Binding Change Mechanism" for subunit rotation (Vik, 2007). The proton transport through the interface of a and c subunits drives rotation of the εγc subunits. This induces a conformational change in the β subunits, which catalyze ATP synthesis (Nakanishi-Matsui et al, 2016; Vik, 2007). One complete rotation of the enzyme requires 10 to 11 $H^{+,}$ which are coupled to form 3 ATP molecules (Vik, 2007).

1.4.4 Regulation of aerobic electron transport chain components

In *E. coli*, the expression of ETC is highly regulated under aerobic, anaerobic, and micro-aerobic conditions. Most of the regulation has been studied at the transcriptional level. The global transcriptional regulators, FNR and ArcA, regulate various ETC components in response to oxygen availability (Iuchi & Lin, 1991). Cytochrome *bo* is highly expressed under high oxygen tension, i.e., aerobic conditions. Under microaerobic conditions (when the oxygen tension reaches to 2 to 15% of air saturation), ArcA represses *cyoABCDE* and activates *cydAB*; the peak activation of *cydAB* is dependent on both Arc and FNR (Borisov & Verkhovsky, 2015; Fu et al, 1991). However, under anaerobic conditions (when oxygen tension is less than 2% of air saturation), FNR represses both *cyoABCDE* and *cydAB* (Borisov & Verkhovsky, 2015). Besides downregulating ETC components, ArcA also downregulates β-oxidation and TCA cycle components such as acyl-CoA dehydrogenase,

citrate synthase, and isocitrate dehydrogenase (Cho et al, 2006; Perrenoud & Sauer, 2005). The transcriptional regulator, NarL, controls the expression of respiratory genes in response to nitrate and nitrite (Constantinidou et al, 2006). The expression of *nuo* operon is positively regulated, whereas the expression of *ubiCA* is negatively regulated by NarL (Bongaerts et al, 1995; Kwon et al, 2005). The DNA-binding protein Fis regulates the growth phase-dependent coordinated expression of ETC components, NADH dehydrogenase and terminal oxidases. The expression of NADH dehydrogenases, Nuo and Ndh, and cytochrome *bo* is induced by Fis in the exponential phase, whereas the expression of cytochrome *bd* is repressed (Bradley et al, 2007). The catabolite repression regulator CRP upregulates several ETC components (Shimada et al, 2011). The C4-dicarboxylates such as succinate, acetate, and fumarate stimulate expression of *nuo*; however, these carbon sources do not affect the expression of *ndh* (Bongaerts et al, 1995). The global regulatory protein IHF, integration host factor, weakly represses the NADH dehydrogenases (Bongaerts et al, 1995; Green et al, 1997). Besides global regulators, some specific regulators such as PdhR, CpxR, and Arr also regulate ETC components (Table. 1.2).

Several ETC components are also regulated at the post-transcriptional level. The *sdh* operon is downregulated by the small RNA, RyhB, in response to iron availability (Masse & Gottesman, 2002). The expression of *atp* operon is controlled at the posttranscriptional level by the stability of the transcript and the rate of translation initiation (Vik, 2007). The ubiquinone content of the cell increases ~2 to 3-fold in response to vigorous aeration. In these conditions, the translation inhibitor, chloramphenicol, does not affect these changes in ubiquinone levels, suggesting post-translational regulation of ubiquinone levels (Shestopalov et al, 1997).

Table. 1.2. The table shows the transcriptional regulation of ETC components by different regulators.

Regulators	**ETC components**
Anoxic redox control ArcA-ArcB two-component system	*nuo* (-) (Bongaerts et al, 1995), *sdh* (-) (Iuchi & Lin, 1988), *cyo* (-), *cyd* (+) (Cotter & Gunsalus, 1992), *app* (-) (Borisov & Verkhovsky, 2015), *ubiCA* (-) (Kwon et al, 2005), *ubiD* (-) and *ubiX* (-) (Zhang & Javor, 2003)
Fumarate and nitrate reduction regulatory protein, FNR	*nuo* (-) (Bongaerts et al, 1995), *ndh* (-) (Green et al, 1997), *cyo* (-) (Cotter & Gunsalus, 1992), *cyd* (-/+) (Cotter & Gunsalus, 1992; Govantes et al, 2000), *ubiCA* (-) (Kwon et al, 2005), *ubiD* (-) and *ubiX* (-) (Zhang & Javor, 2003)
cAMP receptor protein, CRP	*nuo* (+), *ndh* (+) (Shimada et al, 2011), *sdh* (+) (Nam et al, 2005), *cyo* (+) , *atp* (+), *ubiCA* (+) and *ubiG* (+) (Shimada et al, 2011)
nitrate/nitrite response regulator, NarL	*nuo* (+) (Bongaerts et al, 1995) and *ubiCA* (-) (Kwon et al, 2005)
Integration host factor, IHF	*nuo* (-) (Bongaerts et al, 1995) and *ndh* (-) (Green et al, 1997)
DNA binding protein, Fis	*ndh* (+), *nuo* (+), *cyo* (+) and *cyd* (-) (Bradley et al, 2007)
Enzyme involved in heme synthesis, HemA	*ubiD* (-) and *ubiX* (-) (Zhang & Javor, 2003)
Pyruvate dehydrogenase complex regulator, PdhR	*ndh* (-) *and cyo* (-) (Ogasawara et al, 2007)
Amino acid response regulator, ARR	*ndh* (+) (Green et al, 1997)
CpxAR ESR pathway	*nuo* (-), *cyo* (-) (Guest et al, 2017) and *sdh* (-) (Raivio et al, 2013)

(-) and (+) indicate negative and positive regulation, respectively

1.5 Metabolism and oxidative stress

The generation of ROS is an inevitable consequence of metabolism. Different types of ROS molecules produced during metabolism are superoxide (O_2^-), hydrogen peroxide (H_2O_2), and hydroxyl radical (·OH). The adventitious collision of molecular oxygen with a single

electron leads to the production of superoxide ions, which is further converted to other ROS molecules, H_2O_2 and ·OH, by taking up second and third electrons, respectively (Imlay, 2013). Due to the reactive nature of ROS, these cause oxidative damage to proteins, lipids, DNA, and other biomolecules (Farr & Kogoma, 1991). Although ROS has been considered harmful, these also play a role in cellular physiology by participating in various signaling cascades (Cap et al, 2012; D'Autreaux & Toledano, 2007).

The endogenous source of ROS are flavins, metal centers and menaquinone (Imlay, 2013). Amongst these, flavins represent the major site of ROS formation (Imlay, 2013; Messner & Imlay, 1999) (Fig. 1.4). The flavoproteins and metal centers, e.g., Fe-S cluster containing proteins are present in the metabolic pathways, specifically in ETC and TCA cycle. In the aerobic ETC, Ndh is the primary source of H_2O_2 during aerobic growth conditions. Mutants of *ndh* have been shown to produce less H_2O_2 *in vitro* in inverted membrane vesicles (Messner & Imlay, 1999), and overexpression of *ndh* has been reported to increase H_2O_2 levels both *in vitro* and *in vivo* (Messner & Imlay, 1999; Seaver & Imlay, 2004). It has been proposed that the adventitious collision of oxygen with solvent-exposed reduced flavins is the source of ROS (Fig. 1.4). The auto-oxidation rate is even higher if there is a backlog of electrons at Ndh, for example, under conditions where quinones are unavailable (Seaver & Imlay, 2004). Although Nuo also contains flavins in the form of FMN, it possesses a feed-back loop to prevent further ROS formation. It has been suggested that when the quinone pool is unavailable, Nuo prevents NAD removal from the complex and inhibits the further binding of NADH to the complex. The bound NAD blocks the NADH binding site and prevents the reduction of FMN, thereby preventing further ROS formation (Schulte et al, 2019). Sdh also contributes to ROS formation by forming superoxide from the reduced flavins. Although terminal oxidases contain metal centers, studies have reported that they do not generate ROS (Messner & Imlay, 1999). The rate of

H_2O_2 production is not significantly diminished in ETC mutants, indicating that the contribution of ETC complexes to overall endogenous ROS production is not substantial (Seaver & Imlay, 2004). The non-respiratory flavoproteins are therefore proposed to contribute primarily to the overall ROS production in the cell. The flavoproteins which lead to the production of endogenous ROS are aspartate oxidase NadB, glutathione reductase, D- amino oxidase, and lipoamide dehydrogenase (Farr & Kogoma, 1991; Imlay, 2013; Korshunov & Imlay, 2010).

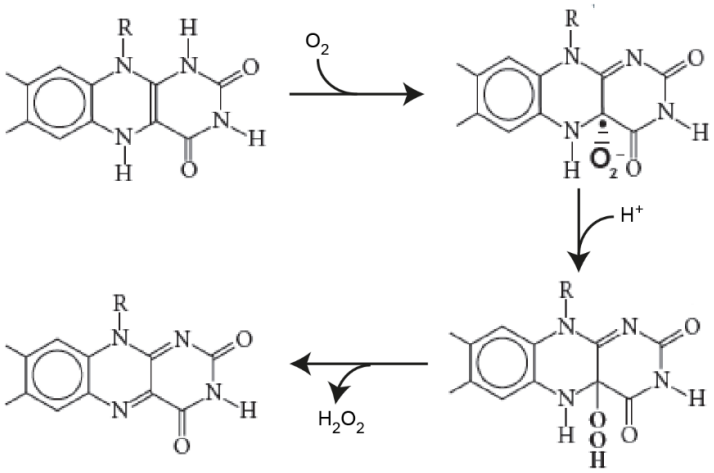

Figure 1.4. Schematic representation of reactive oxygen species (ROS) formation by flavoproteins. Flavin reacts with oxygen and undergoes autooxidation. This results in the formation of flavosemiquinone adduct which finally releases H_2O_2 molecule. The representation was modified from (Imlay, 2013).

A couple of studies have reported the production of ROS by carbon metabolism. Proline metabolism increases ROS production in *E. coli*, which upregulates the enzymatic ROS scavengers, catalases and peroxidases, thereby increasing bacterial resistance to exogenous oxidative stress agents (Zhang et al, 2015). *E. coli* grown in LCFAs is reported to accumulate higher levels of ROS compared with cultures grown in glucose (Doi et al, 2014). In addition, few global studies have also suggested the interconnection between LCFA metabolism and oxidative stress in bacteria. Microarray and proteomics studies revealed the induction of genes involved in defense against oxidative stress in fatty acid

overproducing *E. coli* strains (Lennen et al, 2011). A transcriptomics study in *M. tuberculosis* cultured in medium supplemented with a mixture of even-chain-length LCFAs, revealed the upregulation of genes involved in maintaining redox balance (Rodriguez et al, 2014).

1.6 Antioxidants in *E. coli*

Bacteria employ several players to defend themselves against the harmful effects of ROS. These include both enzymatic scavengers and non-enzymatic antioxidants. Enzymatic scavengers are superoxide dismutases (SOD), catalases and peroxidases. SODs convert superoxide into hydrogen peroxide, which is then decomposed by catalases and peroxidases into H_2O and O_2 (Imlay, 2013). Non-enzymatic antioxidants include glutathione and ubiquinone (Carmel-Harel & Storz, 2000; Dwyer et al, 2014; Goswami et al, 2006; Soballe & Poole, 2000).

There are three SODs present in *E. coli*: SodA (Manganese-containing SOD), SodB (iron-containing SOD), and SodC (Copper-zinc-containing SOD) (Benov & Fridovich, 1994; Fridovich, 1978; McCord et al, 1971). Since superoxide cannot cross the membrane, SODs are located in both cytoplasmic and envelope compartments. SodA and SodB are cytoplasmic dismutases, whereas SodC is a periplasmic enzyme (Imlay, 2013). The expression of SodA is induced by the SoxRS system, which becomes highly active when cells are exposed to redox-cycling compounds (Gu & Imlay, 2011). SoxR is a transcriptional regulator containing sensory iron-sulfur (2Fe-2S) clusters (Hidalgo & Demple, 1994). SoxR remains bound to the *cis*-acting element of *soxS* gene (Nunoshiba et al, 1992). In the presence of redox-active drugs, the Fe-S cluster of SoxR is oxidized, enabling it to activate the transcription of *soxS* (Gu & Imlay, 2011). SoxS act as a secondary transcription factor inducing the expression of several genes, including *sodA* (Pomposiello et al, 2001).

Catalases and peroxidases are the scavengers that detoxify H_2O_2. In *E. coli*, there are two catalases and one peroxidase, which are known to be important during *in vivo* conditions: catalase G (KatG), catalase E (KatE), and alkyl hydroperoxidase (AhpCF). Catalases and peroxidases detoxify H_2O_2 via different mechanisms. Catalases use two molecules of H_2O_2, where one molecule acts as an electron donor, and the other acts as an electron acceptor to convert H_2O_2 to water. In contrast, peroxidases utilize specific compounds such as thioredoxin and NADH as electron donor and produce water and oxygen (Imlay, 2013). During oxidative stress, catalases and peroxidases are regulated by the transcriptional regulator, OxyR. OxyR is a transcriptional regulator with active-site cysteine (Cys) residues that react rapidly with H_2O_2 when the intracellular H_2O_2 concentration reaches ~200 nM. Disulfide bonds are directly formed between Cys residues of OxyR, thereby activating OxyR, which in turn activates the transcription of several genes, including *katG* and *ahpCF* (Choi et al, 2001; Christman et al, 1989). In the absence of oxidative stress, OxyR is maintaind in the reduced form with the help of thioredoxin and glutaredoxin systems. In most aerobic organisms, thioredoxins are also involved in peroxide catabolism by providing the reducing power to the peroxiredoxins and glutathione peroxidases, but in *E. coli*, glutathione peroxidase enzymes are not present (Toledano et al, 2007). Because one of the thioredoxins in *E. coli*, Trx2, is regulated by OxyR, it was suggested to be involved in oxidative stress response (Ritz et al, 2000). However, the deletion of thioredoxins make *E. coli* more resistant to oxidative stress (Aslund et al, 1999; Ritz et al, 2000). This phenotype has been attributed to the loss of reduction of disulfide bonds in OxyR, which will lead to continuous activation of OxyR and hence increased expression of antioxidant enzymes such as catalases and peroxidases. Therefore, in *E. coli*, thioredoxin system is not considered to be involved in combating oxidative stress (Lu & Holmgren, 2014). One of the terminal oxidases, cytochrome *bd*, also confers protection

from oxidative stress through its quinol peroxidase activity by using quinol as an electron donor and H_2O_2 as the electron acceptor (Al-Attar et al, 2016).

Glutathione is a tripeptide thiol that can accumulate up to 10 mM in *E. coli* (Ferguson & Booth, 1998). Glutathione is synthesized by glutamylcysteine synthetase (GshA) and glutathione synthetase (GshB) and exists in both oxidized (GSSG) and reduced (GSH) forms. During oxidative stress, ROS molecules can damage proteins by inducing undesired disulfide bond formation. Reduced glutathione combats oxidative stress by restoring the thiol groups in proteins and has been used widely as an antioxidant in *E. coli* (Toledano et al, 2007).

Although the role of ubiquinone as an antioxidant is well-established in eukaryotes, its antioxidant function in bacteria has remained under-appreciated. Prior to our work, there was only report which suggested ubiquinone as an oxidative stress combat player in bacteria (Soballe & Poole, 2000); however, the physiological condition under which ubiquinone works as an antioxidant and the relative contribution of ubiquinone to the overall oxidative stress defense had not been investigated. It was shown that mutants of *E. coli* defective in ubiquinone biosynthesis exhibit several oxidative stress phenotypes, such as accumulation of ROS in membranes, hypersensitivity to oxidative stress-causing agents ($CuSO_4$ and H_2O_2) and induction of *katG*. Two mechanisms were proposed to explain the anti-oxidant role of ubiquinone. First, ubiquinone limits ROS formation by rapidly transferring electrons from upstream respiratory dehydrogenases to terminal oxidases, thereby decreasing the adventitious collision of electrons with molecular oxygen. Second, the reduced form of ubiquinone (ubiquinol) scavenges ROS (Soballe & Poole, 2000). From a more recent study, the antioxidant role of ubiquinone can also be explained by the ability of quinol to serve as an electron donor for the peroxidase activity of cytochrome *bd (Al-Attar et al, 2016)*.

Section-II

1.7 Architecture of the gram-negative bacterial cell envelope

Based on the architecture of the cell envelope, bacteria are divided into two main groups: gram-positive and gram-negative. The cytoplasm of gram-positive bacteria is surrounded by a single cell membrane. Outside the cytoplasmic membrane is a thick and compact peptidoglycan layer with the perpendicular long anionic polymer of teichoic acids (Malanovic & Lohner, 2016). In contrast, the cytoplasm of gram-negative bacteria is surrounded by two membranes, outer and inner membrane. The peptidoglycan layer in gram-negative bacteria is thin and is present in the periplasmic compartment, which is the space between the inner and outer membrane layers (Costerton et al, 1974; Silhavy et al, 2010) (Fig. 1.5).

The multi-layered structure of gram-negative bacterial envelope protects the bacteria from different environmental stresses, gives bacteria its shape, maintains turgor pressure, provides a site for energy generation, offers an environment for disulfide bond formation, and plays an important role in host-bacterial interactions. Usually, bacteria face more harsh and extreme conditions than higher organisms, which have resulted in the evolution of this sophisticated envelope (Kleanthous & Armitage, 2015; Silhavy et al, 2010) (Fig. 1.5).

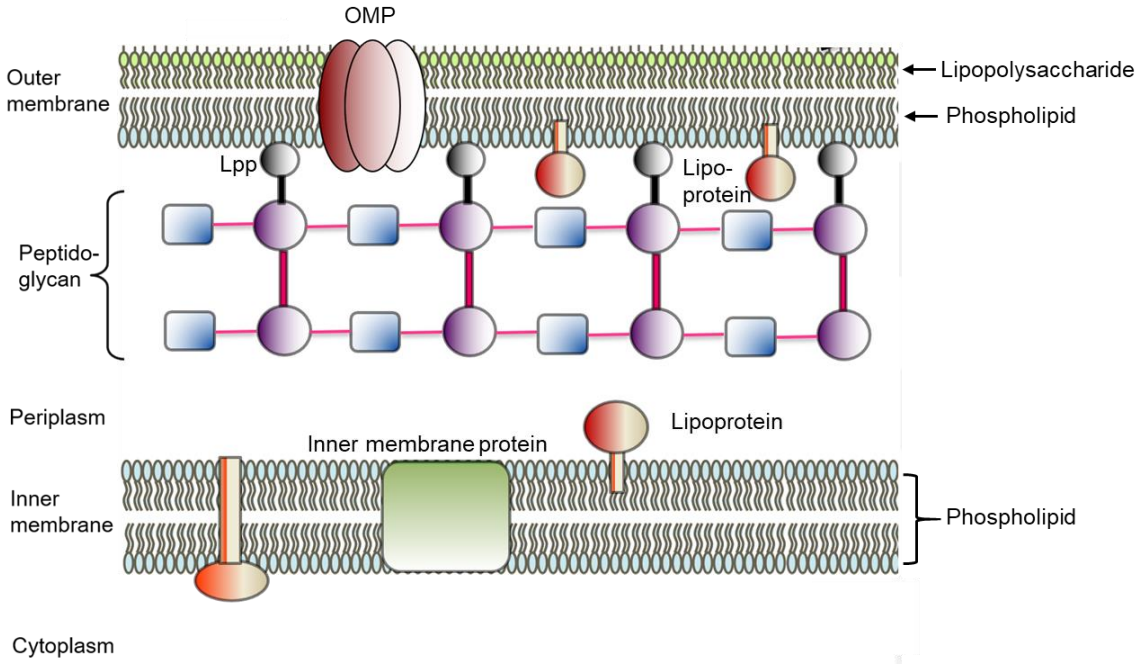

Figure 1.5. Architecture of the gram-negative bacterial cell envelope. The gram-negative bacterial envelope consists of outer membrane, inner membrane, peptidoglycan layer and the periplasmic space. The outer membrane is asymmetric and composed of phospholipids in the inner leaflet and lipopolysaccharide (LPS) in the outer leaflet whereas the inner membrane is a symmetrical phospholipid bilayer. There are two classes of proteins present in the outer membrane: OMPs and lipoproteins. The space between the inner and outer membranes layers is the periplasmic space. Within the periplasmic space is a meshwork of crosslinked sugars and amino acids, called as peptidoglycan layer. The peptidoglycan layer is linked with the outer membrane layer by a lipoprotein, Lpp.

1.7.1 The Outer Membrane

The outer membrane is asymmetric. The inner leaflet is composed of phospholipids, in particular, phosphatidylethanolamine and phosphatidylglycerol, and cardiolipin, whereas the outer leaflet is composed of glycolipids, which are principally lipopolysaccharide (LPS) (Delcour, 2009; Kamio & Nikaido, 1976). This lipid-protein bilayer mostly contains two classes of proteins, lipoproteins and β-barrel proteins (Fig. 1.5). Lipoproteins are covalently modified with lipids at the amino-terminal of cysteine residue (Sankaran & Wu, 1994) whereas β-barrel proteins often referred to as outer membrane porins/outer membrane proteins (OMPs) are oligomeric proteins that have β–sheets arranged to form an aqueous

channel (Duong et al, 1997). Some lipoproteins are also linked with the peptidoglycan mesh of the envelope (Braun & Sieglin, 1970) (Fig. 1.5). Unlike β-barrel proteins, lipoproteins are non-transmembranous; however, they embed in the inner leaflet of the outer membrane via their lipid moieties (Silhavy et al, 2010).

LPS forms a tight seal in the outer membrane as its saturated acyl chains help in dense packaging, and its negative charge allows intermolecular lateral interactions through binding of divalent cations. This rigid continuum formed by LPS slows the passive diffusion of hydrophobic molecules. The aqueous channel formed by OMPs allows the passage of hydrophilic compounds with a size of less than 700 kDa, limiting the size for the penetration of hydrophilic compounds. Therefore, LPS and OMPs together provide a selective permeability barrier to the outer membrane, which limits the entry of harmful agents inside the cell (May & Grabowicz, 2018; Nikaido, 2003; Silhavy et al, 2010). In a recent study, it has been shown that both LPS and OMPs contribute to the stiffness of the outer membrane, which can even be stiffer than the cell wall. Importantly, the mechanical loads are often balanced between the peptidoglycan layer and the outer membrane (Rojas et al, 2018).

LPS and OMPs play an important role in host-bacterial interactions. LPS causes endotoxic shock during septicemia and is recognized by the human innate immune system (Silhavy et al, 2010). Some bacterial pathogens use OMPs to attach to the host cells to induce virulence factors and gain entry inside host cells (Vila-Farres et al, 2017). The presence of an outer membrane protease, OmpT in clinical isolates of *E. coli* has been associated with complicated urinary tract diseases, owing to the ability of the OmpT protease to cleave the antimicrobial peptide, protamine, excreted by epithelial cells of the urinary tract (Vandeputte-Rutten et al, 2001).

1.7.2 Peptidoglycan cell wall

The peptidoglycan cell wall has a rigid skeleton and provides shape to the cell. Peptidoglycan meshwork is a repeat of N-acetyl glucosamine - N-acetyl muramic acid disaccharide, which is cross-linked by pentapeptide side chains (Vollmer et al, 2008). A lipoprotein, Lpp, also known as Braun's lipoprotein, attaches the outer membrane to the peptidoglycan layer (Braun & Sieglin, 1970) (Fig. 1.5).

1.7.3 The Periplasm

Periplasm is an aqueous and viscous area between the outer membrane and the inner membrane (Fig. 1.5). The oxidizing environment of the periplasm allows oxidative protein folding and quality control similar to the eukaryotic endoplasmic reticulum (explained in detail in Section 1.9) (Messens & Collet, 2006). The periplasm harbors enzymes such as ribonucleases and phosphatases, which are otherwise toxic if present in the cytoplasm. Periplasm also contains molecules involved in sensing environmental stresses, periplasmic binding proteins that are involved in sugar and amino acid transport, and chaperone-like molecules that help in envelope biogenesis (Miller & Salama, 2018; Silhavy et al, 2010). Recent studies indicate that the periplasmic size, *i.e.*, the distance between the outer membrane and inner membrane is critical for sensing the outer membrane damage and is controlled by lipoproteins (Miller & Salama, 2018).

1.7.4 The Inner membrane

The inner membrane is a phospholipid bilayer surrounding the cytoplasm (Fig. 1.5). Like the outer membrane, major phospholipids are phosphatidylethanolamine and phosphatidylglycerol. The inner membrane is unique as it has the semi-permeable properties of eukaryotic plasma membrane, protein translocation function of endoplasmic reticulum, and can perform oxidative phosphorylation like the mitochondrial membrane. In contrast to OMPs, inner membrane proteins are largely α-helical in structure (Duong et al,

1997). Proteins can diffuse freely in the inner membrane, unlike the outer membrane, where the motion is relatively constrained (Rojas et al, 2018).

1.8 Envelope stress response

Because a myriad of critical cellular functions are performed in the envelope, its integrity must be continuously monitored and maintained. *E. coli* has six ESR systems dedicated for this purpose. These ESR systems include σ^E response, the CpxAR and BaeSR two-component systems, the PSP response, the Rcs phosphorelay system, and the outer membrane vesicle formation (Macritchie & Raivio, 2009; McBroom & Kuehn, 2007; Mitchell & Silhavy, 2019). These ESR pathways are explained in detail below.

1.8.1 The σ^E envelope stress response

σ^E is an alternative extracytoplasmic sigma factor which responds to disturbances in the envelope biogenesis. The molecular signals for σ^E activation are unfolded OMPs and altered LPS. Under normal/ unstressed conditions, σ^E remains bound to an inner membrane protein RseA and is thus less available to bind RNA polymerase. Accumulation of unfolded OMPs in the periplasm activates DegS, an inner membrane protease which then cleaves the periplasmic domain of RseA. RseA is further cleaved on the cytoplasmic side of the inner membrane by an inner membrane protease RseP. The cytoplasmic domain of RseA bound to σ^E is released into the cytoplasm, which is finally degraded by cytoplasmic ATP-dependent proteases, mainly ClpXP protease. Once released from RseA, σ^E binds RNA polymerase and initiates transcription of its regulon members (Ades et al, 1999; Barchinger & Ades, 2013; Chaba et al, 2011; Walsh et al, 2003) (Fig. 1.6).

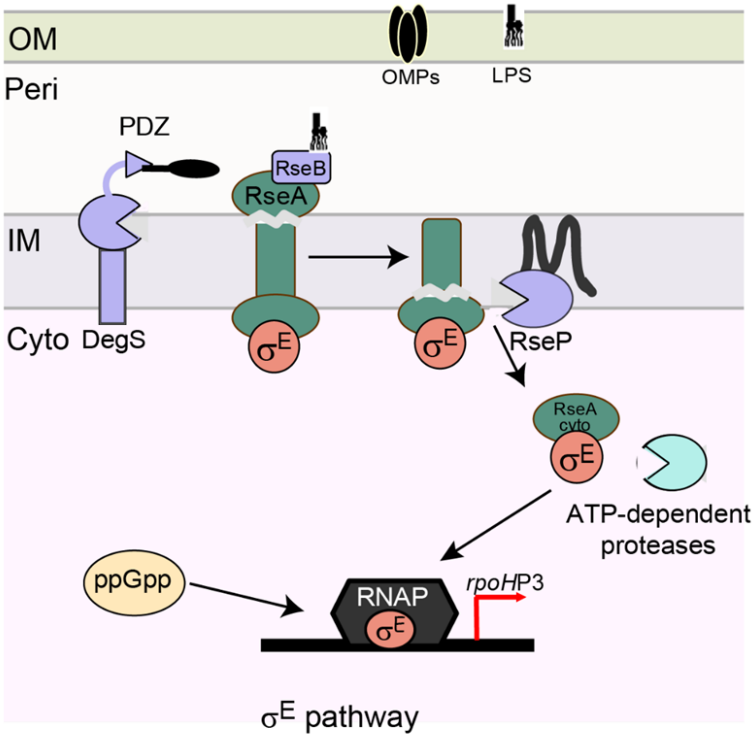

Figure 1.6. Organization of the σ^E pathway. Under unstressed conditions, σ^E remains bound to RseA and is thus less available to bind RNA polymerase. Unfolded OMPs activate DegS by binding to its PDZ domain. A periplasmic protein, RseB, binds RseA and prevents its cleavage by DegS. LPS displaces RseB from RseA enabling activated DegS to cleave RseA in its periplasmic domain. The membrane-embedded RseP further cleaves the RseA fragment near the inner-membrane. The cytoplasmic RseA fragment is finally degraded by ATP-dependent proteases releasing free σ^E, which binds RNA polymerase and initiates transcription of its regulon members. The cytoplasmic alarmone ppGpp upregulates σ^E-dependent transcription. Abbreviations: Cyto, cytoplasm; IM, inner membrane; Peri, periplasm; OM, outer membrane; LPS, lipopolysaccharide; OMPs, outer membrane proteins; RNAP, RNA Polymerase.

The PDZ domain of DegS maintains the protease in an inactive state. The inhibition is relieved when the C-terminal YXF motif of OMPs binds to the PDZ domain. The YXF motif is inaccessible in a properly folded OMP but becomes available in an unfolded OMP which can thus activate DegS (Walsh et al, 2003; Wilken et al, 2004). The first cleavage of the periplasmic domain of RseA by DegS is the rate-limiting step of σ^E activation (Chaba et al, 2007). Notably, the cleavage of RseA by DegS is also inhibited by another periplasmic protein, RseB, which binds to the periplasmic domain of RseA. The

displacement of RseB by LPS when LPS transport is defective constitutes the second signal required for σ^E activation (Lima et al, 2013). Therefore, the full activation of σ^E requires activation of DegS (by sensing of unfolded OMPs) and displacement of RseB away from RseA (via periplasmic LPS) (Fig. 1.6).

Consistent with the nature of stress signals that activate σ^E (unfolded OMPs and accumulation of LPS), a majority of the σ^E regulon members include chaperones, proteases and their modulators, peptidyl-prolyl isomerases (PPIases), components of β-barrel assembly machinery (Bam complex) involved in OMP assembly and LPS transport, and sRNAs involved in decreasing OMP synthesis, which serve to restore outer membrane homeostasis (Grabowicz & Silhavy, 2017; Rowley et al, 2006).

Besides envelope signals, σ^E is also activated by a cytoplasmic signal, the global stress alarmone guanosine 3',5'-bispyrophosphate (ppGpp). ppGpp activates transcription by the σ^E -RNA polymerase holoenzyme (Fig. 1.6). The level of ppGpp increases during the stationary phase when nutrients get depleted, thus the activity of σ^E increases in the stationary phase in a ppGpp-dependent manner (Costanzo & Ades, 2006).

1.8.2 The Cpx envelope stress response

The **c**onjugative **p**ilus e**x**pression (Cpx) ESR pathway is a typical two-component system where CpxA is the inner membrane sensor histidine kinase, and CpxR is the DNA-binding response regulator. Like most histidine kinases of two-component systems, CpxA can act as autokinase, kinase, and phosphatase. CpxA transduces stress signal, and the structural change in the periplasmic loop/ sensor domain of CpxA leads to autophosphorylation of its cytoplasmic domain. CpxA trans-phosphorylates the receiver domain of CpxR, which then acts as a transcriptional regulator by binding to a specific site with consensus sequence: 5′-GTAAA-N5- GTAAA-3′ (Grabowicz & Silhavy, 2017; Raivio & Silhavy, 1997; Rowley et al, 2006). CpxR is also phosphorylated by acetyl-phosphate (acetyl-P), a high-energy

intermediate of the phosphotransacetylase (Pta)- acetate kinase (AckA) pathway. Pta leads to the synthesis of acetyl-P and CoA from acetyl-CoA and Pi, and AckA generates ATP and acetate from acetyl-P. Therefore, the steady-state concentration of acetyl-P depends on the rate of its formation and degradation. Acetyl-P serves as a global signal by transferring its phosphate group to response regulators such as CpxR and activate their regulon members independent of the histidine kinase component (Wolfe et al, 2008) (Fig. 1.7).

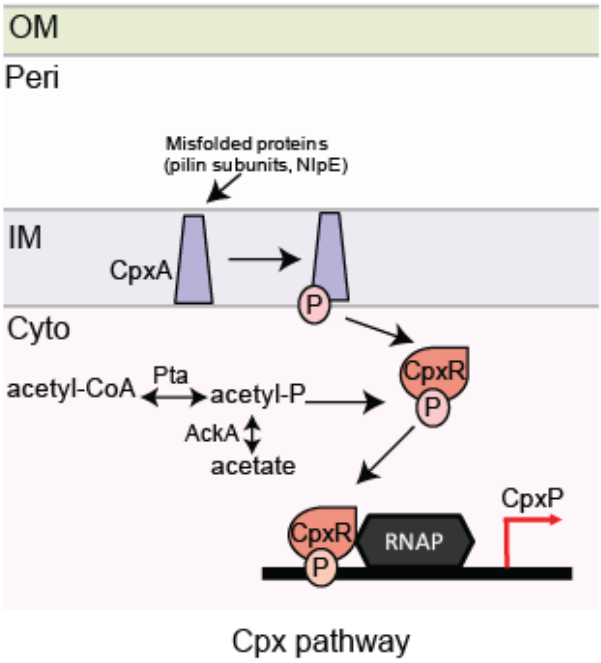

Figure 1.7. Organization of the Cpx pathway. The CpxAR two-component system comprises of an inner-membrane sensor histidine kinase, CpxA and a cytoplasmic response regulator, CpxR. In the presence of envelope signals, such as misfolded proteins, CpxA acts as a kinase and phosphorylates CpxR. Acetyl-phosphate, an intermediate of the Pta-AckA pathway, acts as the cytoplasmic signal for Cpx activation by directly transferring its phosphoryl group to CpxR. Phosphorylated CpxR directs the transcription of genes involved in mitigating stress. Abbreviations: Cyto, cytoplasm; IM, inner membrane; Peri, periplasm; OM, outer membrane; acetyl-P, acetyl-phosphate; RNAP, RNA Polymerase.

In a study on the characterization of *cpxA* gain-of-function mutants, Ravio and Silhavy isolated a *cpxA24* mutant, which has a deletion of 32 amino acids causing the removal of the sensory domain from the periplasmic region. The *cpxA24* mutant has increased Cpx activity even under non-inducing conditions suggesting that this domain

interacts with an inhibitor in the absence of stress (Raivio & Silhavy, 1997). This inhibitor is now a well characterized third component of the Cpx pathway, CpxP. CpxP is a small periplasmic protein and is also a member of the Cpx regulon. Importantly, whereas overexpression of CpxP decreases the Cpx response, its deletion does not have any effect on sensing the inducing stimuli, suggesting that additional components are involved in sensing envelope stress (Danese & Silhavy, 1998; Raivio et al, 1999).

1.8.2.1 Activating cues for Cpx pathway

In *E. coli*, the Cpx system is induced by a variety of conditions such as alkaline pH, presence of copper and EDTA, and changes in composition and perturbation in the trafficking of cellular components such as altered inner membrane lipid composition, problems in peptidoglycan biosynthesis and lipoprotein trafficking, and defects in protein translocation (Delhaye et al, 2016; DiGiuseppe & Silhavy, 2003; May et al, 2019; Mileykovskaya & Dowhan, 1997; Miyadai et al, 2004; Raivio, 2014). However, in a majority of conditions, the molecular nature of Cpx- inducing signal remains elusive. Below I provide current information available on the signaling mechanisms that induce the Cpx pathway.

NlpE was the first signal identified for Cpx activation, which gets induced upon adhesion of the cell to abiotic and hydrophobic surfaces (Danese et al, 1995; Otto & Silhavy, 2002). NlpE was identified as a Cpx activating signal based on the observation that its overexpression limited the toxicity caused by misfolded proteins in the periplasm in a Cpx-dependent manner (Danese et al, 1995). In the same year, another study showed NlpE to be involved in copper resistance in *E. coli* (Gupta et al, 1995). This was later attributed to the ability of NlpE to activate Cpx, which is known to provide copper tolerance (Price & Raivio, 2009). Further, to investigate whether, besides NlpE, other lipoproteins also induce Cpx, 90 lipoproteins were overexpressed in a study and the induction of *degP*,

a regulon member of Cpx, was monitored. It was found that an inner membrane lipoprotein, YafY can activate Cpx when overexpressed, and the effect on Cpx induction is even more remarkable than NlpE. Besides this, several other lipoproteins also induced *degP*, although the activation was less compared to NlpE (Miyadai et al, 2004). Since besides Cpx, *degP* is also a regulon member of σ^E, to specifically determine whether additional lipoproteins induce the Cpx pathway, a regulon member exclusive to Cpx, such as *cpxP*, should be used in such studies.

For decades, NlpE overexpression has served as an artificial trigger for Cpx pathway; however, the physiological relevance of Cpx activation by NlpE was not known. Two recent studies have investigated this issue (Delhaye et al, 2019; May et al, 2019). It was shown that a mutant of LolA (a periplasmic chaperone involved in lipoprotein extraction from the inner membrane), defective in releasing lipoproteins into the periplasm, activates Cpx in a NlpE-dependent manner (Delhaye et al, 2019). In addition, the deletion of LolB (an outer membrane lipoprotein that receives lipoproteins from LolA and anchors them in the outer membrane) requires expression of Cpx and NlpE for its viability. Further, the N-terminal domain of NlpE is sufficient for Cpx activation and viability in a *lolB* deletion strain (May et al, 2019). Collectively, these data suggest NlpE as the inducing cue for Cpx activation when lipoprotein trafficking is perturbed. These studies also provide important details on how NlpE might transmit signals to Cpx. A NlpE mutant retained at the inner membrane (because of avoidance by Lol trafficking pathway) induces the Cpx pathway to a higher extent compared to the WT protein, and this Cpx activation also requires the N-terminal domain of NlpE. Further, using pulldown and bacterial two-hybrid assays, NlpE was found to physically interact with the periplasmic domain of CpxA. Taken together, it is now clear that NlpE accumulates at the inner membrane due to defects in lipoprotein trafficking and activates Cpx by interacting with CpxA periplasmic domain via

its N-terminal domain (Delhaye et al, 2019; May et al, 2019). Copper exposure hinders lipoprotein maturation and thus their trafficking to the outer membrane. It has now been shown that Cpx activation by copper requires NlpE, again reiterating the role of NlpE in sensing lipoprotein trafficking defects (May et al, 2019).

Besides lipoprotein trafficking defects, defect in oxidative protein folding also leads to Cpx activation in a NlpE-dependent manner. NlpE is a DsbA substrate, and its C-terminal domain contains a disulfide bond. The NlpE mutant lacking the C-terminal disulfide bond turns on Cpx, and Cpx activation in Δ*dsbA* is NlpE-dependent, thus suggesting NlpE to be a sensor of redox imbalance in the envelope (Delhaye et al, 2019).

In addition to lipoproteins, other inducing cues for Cpx activation are pilin subunits and ETC complexes (Guest et al, 2017; Lee et al, 2004). Although some information on the molecular mechanism of Cpx activation by pilin subunits is available, nothing is known about ETC complexes. Misfolded pilin subunits, PapE and PapG, of uropathogenic *E. coli*, titrate CpxP away from CpxA and deliver it to the periplasmic protease, DegP. In this process, both pilin subunits and CpxP are degraded by DegP, thereby activating the Cpx pathway. However, CpxP displacement is not the sensing mechanism since pilin subunits activate Cpx even in its absence (Isaac et al, 2005). CpxP is therefore proposed to fine-tune Cpx response by preventing inappropriate activation of CpxA and enabling rapid Cpx downregulation once the envelope stress is mitigated (Danese & Silhavy, 1998; DiGiuseppe & Silhavy, 2003; Isaac et al, 2005).

A comparison of the inducing cues of Cpx and σ^E pathways suggests that whereas σ^E response is mainly activated by OMP assembly and LPS transport defects, Cpx two-component system is induced in response to the inner membrane and periplasmic stress.

1.8.2.2 Diverse Cpx regulon and the underlying physiological role

Cpx regulon consists of more than 100 members that encompass diverse functions. Cpx strongly upregulates several protein folding and degrading factors, which include the disulfide oxidoreductase DsbA, the protease and chaperone DegP, the peptidylprolyl isomerase PpiA, and the periplasmic chaperone Spy (Rowley et al, 2006). Besides, Cpx also downregulates several genes that encode components of inner membrane respiratory complexes, pili and flagella, TCA cycle, oxidative phosphorylation, transporters, and iron-binding proteins (Raivio, 2014; Raivio et al, 2013). The Cpx system counteracts inner membrane and periplasmic stress caused by the accumulation of misfolded proteins, such as the pilin subunits and NlpE, towards the periplasmic face of the inner membrane. Therefore, it has been suggested that the downregulation of envelope- localized protein complexes such as ETC complexes, and pili and flagella, might reduce traffic in the inner membrane and lighten the load on chaperones and proteases to assemble essential protein complexes in the envelope. Taken together, the regulon of the Cpx pathway suggests that this ESR system helps in the adaptation of the cell to stress at the inner membrane by modulating the expression of genes involved in diverse functions, especially energy metabolism and transport (Raivio, 2014). Besides, Cpx also modulates the expression of genes involved in cell wall remodeling, antibiotic resistance, biofilm formation, and metal homeostasis (De Wulf et al, 2002; Price & Raivio, 2009).

The Cpx pathway appears to act antagonistically to σ^E. CpxR directly negatively regulates the transcription of σ^E, and the sRNA, CpxQ, a Cpx regulon member, inhibits translation of the σ^E -induced chaperone Skp (De Wulf et al, 2002; Grabowicz et al, 2016; Price & Raivio, 2009). During defects in the primary OMP insertion pathway, σ^E activates Skp to maintain OMPs in the folding state. However, since Skp directly inserts OMPs into the membrane, it could mislocalize OMPs into the inner membrane. The insertion of OMPs

into the inner membrane disrupts PMF. Therefore, Cpx response maintains the integrity of the inner membrane by inhibiting Skp synthesis. Collectively, whereas the σ^E response restores OMP biogenesis defects by inducing chaperone and Bam machinery, the Cpx response protects against prolonged σ^E response in order to relieve inner membrane stress (Grabowicz & Silhavy, 2017).

1.8.3 The BaeSR two-component system

The **b**acterial **a**daptive r**e**sponse (Bae) consists of BaeS, the sensor histidine kinase, and the response regulator, BaeR (Fig. 1.8). The BaeSR system is activated by exposure to indole, ethanol, nickel chloride, zinc and sodium, and by overexpression of pilin subunit, PapG (Macritchie & Raivio, 2009; Mitchell & Silhavy, 2019). Overexpression of the Bae system increases the resistance of *E. coli* to novobiocin and bile salts. Bae- mediated resistance is due to the upregulation of genes involved in multidrug resistance, *mdtABC* and *acrD*. CpxR promotes the binding of BaeR to these loci and cooperatively combat drug-induced envelope stress. Bae induces the expression of *spy* (a periplasmic chaperone) and several proteins of unknown function (Macritchie & Raivio, 2009).

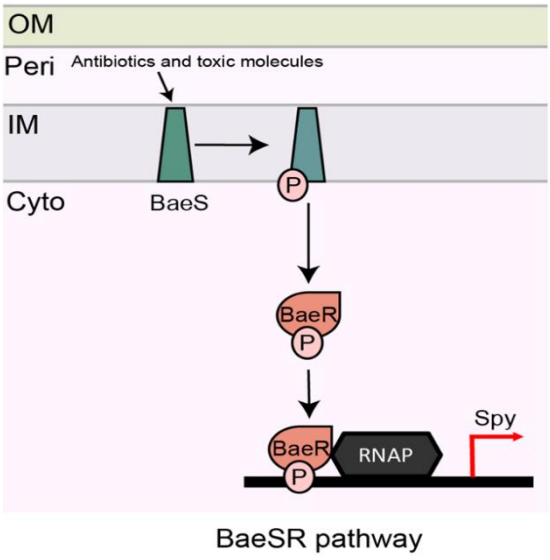

Figure 1.8 Organization of the BaeSR pathway. The BaeSR two-component system comprises of an inner-membrane sensor histidine kinase, BaeS and a cytoplasmic response

regulator, BaeR. In the presence of toxic molecules and antibiotics, BaeS autophosphorylates and transfers the phosphate group to BaeR. Phosphorylated BaeR directs the transcription of genes, including chaperones, efflux pumps, and several genes of unknown function. Abbreviations: Cyto, cytoplasm; IM, inner membrane; Peri, periplasm; OM, outer membrane; RNAP, RNA Polymerase.

1.8.4 The Phage shock protein stress response

The **p**hage **s**hock **p**rotein (PSP) ESR pathway responds to disturbances of the inner membrane that result in the loss of PMF. These disruptions are generally more severe than those required for Cpx activation and include infection with filamentous phage, ethanol and other organic solvent toxicity, heat and osmotic shock, and accumulation of OMPs at the inner membrane. However, the inducing signal for Psp activation seems to be complex (Macritchie & Raivio, 2009; Mitchell & Silhavy, 2019).

The PSP response represents an ESR signal transduction pathway that is regulated through protein-protein interactions. It involves proteins PspABCDE expressed from an operon and a transcriptional enhancer, PspF. Under non-inducing conditions, PspF is inhibited by PspA by directly interacting with it. In the presence of activating conditions, the inner membrane proteins, PspB and PspC, interact with PspA and releases PspF, which then increases the transcription of *psp* operon (Fig. 1.9). The function of PspD and PspG is not fully characterized (Dworkin et al, 2000; Jovanovic et al, 1996; Yamaguchi et al, 2013). Psp response leads to activation of ArcAB system (Jovanovic et al, 2006).

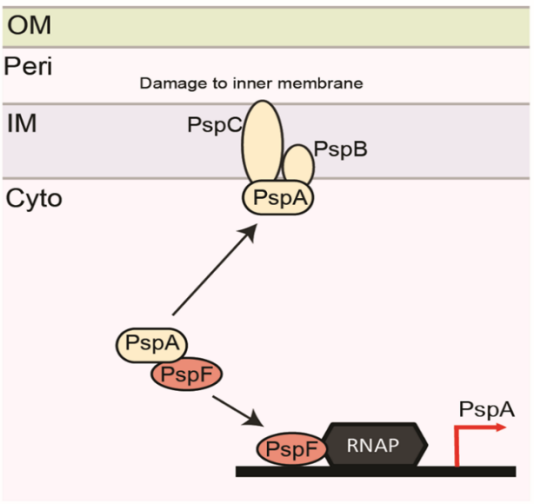

Figure 1.9. Organization of the Psp pathway. Under unstressed conditions, the transcriptional enhancer, PspF, is inhibited by PspA by directly interacting with it. In the presence of severe inner membrane stress, PspB and PspC, interact with PspA and release PspF, which then increases the transcription of *psp* operon. Abbreviations: Cyto, cytoplasm; IM, inner membrane; Peri, periplasm; OM, outer membrane; RNAP, RNA Polymerase.

1.8.5 The Rcs phosphorelay system

The **r**egulator of **c**apsule **s**ynthesis (Rcs) response is a complex phosphorelay system which responds to membrane perturbations such as alteration in LPS charge and fluidity, peptidoglycan stress, and mislocalization of lipoproteins (Mitchell & Silhavy, 2019). Most of these stresses are transduced by a stress sensor protein RcsF, which is an outer membrane lipoprotein. Under non- activating conditions, an inner membrane protein, IgaA represses Rcs activation by interacting with the inner membrane histidine kinase RcsC or the inner membrane phosphotransferase RcsD to prevent RcsD from trans-phosphorylating the cytoplasmic response regulator RcsB. RcsF on receiving the activating signal physically interacts with IgaA and prevents the repression on Rcs signaling. RcsC then autophosphorylates, transphosphorylates RcsD, which in turn phosphorylates RcsB, activating it for transcriptional regulation (Hussein et al, 2018; Konovalova et al, 2014; Mitchell & Silhavy, 2019) (Fig. 1.10). RcsB regulon members include sRNA *rprA*, which

increases the levels of RpoS, the stationary phase sigma factor, and genes involved in biofilm formation, production of the colanic acid capsule, and regulation of flagellar motility (Mitchell & Silhavy, 2019).

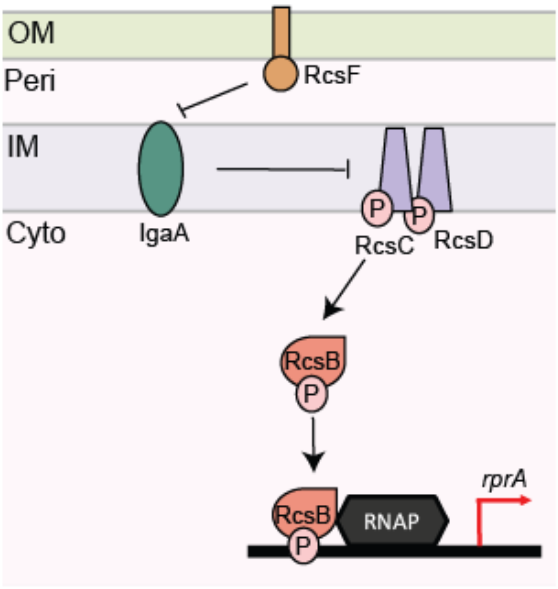

Rcs pathway

Figure 1.10. Organization of the Rcs pathway. Under unstressed conditions, an inner membrane protein, IgaA represses Rcs activation by interacting with the inner membrane histidine kinase RcsC or the inner membrane phosphotransferase RcsD. In the presence of stresses such as LPS or peptidoglycan stress, an outer membrane lipoprotein, RcsF, interacts with IgaA and relieves the repression on RcsC and RcsD. RcsC autophosphorylates, which in turn phosphorylates RcsD. Activated RcsD phosphorylates RcsB and induces the transcription of its regulon members. Abbreviations: Cyto, cytoplasm; IM, inner membrane; Peri, periplasm; OM, outer membrane; RNAP, RNA Polymerase.

1.8.6 The release of outer membrane vesicles

The outer membrane vesicle release is the ESR system that alleviates envelope stress by removing unwanted soluble and insoluble envelope components from the cell. These vesicles are formed by budding of the outer membrane and carry periplasmic content (Fig. 1.11) (Schwechheimer & Kuehn, 2015). The release of outer membrane vesicles is regulated wherein the amount of its release is directly correlated with protein accumulation in the envelope. Importantly, vesiculation increases when either the σ^E or Cpx stress

response pathways are impaired, or these ESR pathways are activated. In either situation, outer membrane vesicle release aids in alleviating envelope stress. For example, in *P. aeruginosa*, the outer membrane vesicle formation increases with an increase in σ^E (AlgU) levels, and these bacteria also show a hypervesiculation phenotype when *algU*, an ortholog of *E. coli rpoE* (gene encoding σ^E) is deleted (Macdonald & Kuehn, 2013). In *E. coli*, the deletion of *degP* increases vesicle formation likely due to the accumulation of misfolded proteins in the periplasm. However, DegP overexpression also leads to hypervesiculation, suggesting that increased vesiculation is due to the increased amount of DegP protein in the envelope (McBroom et al, 2006; McBroom & Kuehn, 2007).

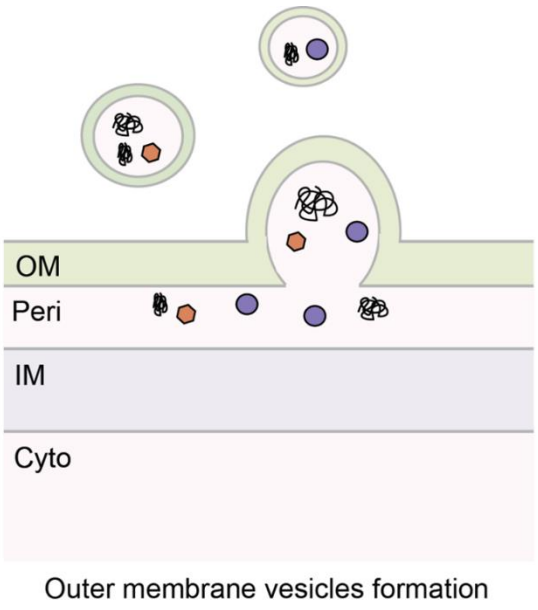

Figure 1.11. The release of outer membrane vesicles. The outer membrane vesicles remove unwanted soluble and insoluble periplasmic components from the cell by budding of the outer membrane. They act in conjuction with Cpx and σ^E pathways. Abbreviations: Cyto, cytoplasm; IM, inner membrane; Peri, periplasm; OM, outer membrane.

1.9 Disulfide bond formation

Besides being a major line of defense, gram-negative bacterial cell envelope also helps in the maturation of extracytoplasmic proteins. Many secreted proteins require disulfide bonds for their folding and stability. Disulfide bonds are formed during the folding of the

polypeptide via a process known as “oxidative folding.” This process requires an oxidizing environment; in gram-negative bacteria, such an environment is provided by the periplasmic space. The enzymes required for disulfide bond formation are present in all domains of life and include a thioredoxin family protein, which directly catalyzes the formation of disulfide bonds in substrate proteins. In *E. coli*, this oxidoreductase is DsbA, a soluble protein present in the bacterial periplasm. In most organisms, a second enzyme serves as a disulfide generator of the oxidoreductase. In *E. coli*, DsbB, an inner membrane disulfide oxidoreductase, reoxidizes DsbA, restoring the latter’s ability to catalyze disulfide bonds (Fig. 1.12). Some Actinobacteria and Cyanobacteria have human vitamin K epoxide reductase homologue in place of DsbB. DsbA is a non-specific oxidant and can form non-native disulfide bonds in proteins with more than two cysteine residues, which have to be corrected for proper folding. For this purpose, *E. coli* contains a disulfide isomerization system, which involves a membrane protein, DsbD, and two protein disulfide isomerases, DsbC and DsbG (Kadokura et al, 2003; Landeta et al, 2018; Manta et al, 2019).

1.9.1 Enzymes involved in disulfide bond formation: DsbA

Until the 1990s, disulfide bonds were thought to be formed spontaneously in the oxidizing environment of the periplasm by molecular oxygen. The discovery that disulfide bond formation is a catalytic process started by the fortuitous identification of DsbA protein (Bardwell et al, 1991). DsbA is a primary disulfide introducer protein located in the periplasm and is a member of the thioredoxin superfamily of proteins. It contains a pair of cysteine residues separated by two amino acids, i.e., Cys30-Cys33, typical of thioredoxin oxidoreductases (Atkinson & Babbitt, 2009; Manta et al, 2019). DsbA interacts with varied protein substrates and forms disulfide bonds indiscriminately between cysteines consecutively present in the polypeptides. However, despite the presence of non-consecutive disulfide bonds in RNase I, DsbA can fold it under appropriate redox

conditions, indicating that disulfide bond formation by DsbA is more specific than presumed (Messens et al, 2007). It has been proposed that disulfide bond formation is in kinetic competition with folding as more oxidizing conditions increase dependency on the disulfide isomerase system to correct non-native disulfides (Ito & Inaba, 2008; Messens et al, 2007).

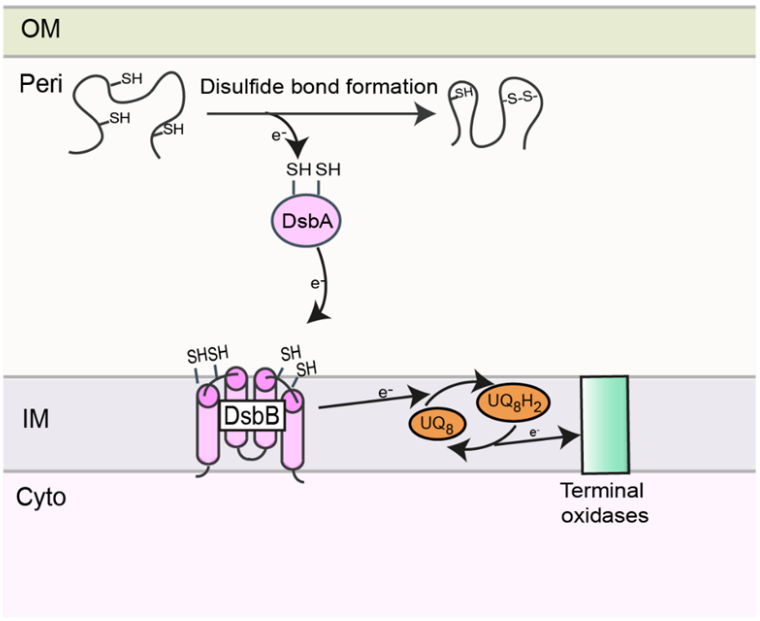

Figure 1.12. Disulfide bond formation in *E. coli*. Disulfide bond formation involves two main enzymes, the periplasmic oxidoreductase DsbA and the inner membrane disulfide oxidoreductase DsbB. DsbA gets reduced after catalyzing the formation of disulfide bonds in substrate proteins and must be re-oxidized. DsbB performs the re-oxidation of DsbA by transferring the electrons to ETC at the level of quinones. Abbreviations: Cyto, cytoplasm; IM, inner membrane; Peri, periplasm; OM, outer membrane.

DsbA forms disulfide bonds in secreted substrate proteins via thiol-disulfide exchange reaction, and the interaction with substrates occurs both co- and post-translocationally (Kadokura & Beckwith, 2009). DsbA has the second-highest redox potential (Redox potential = -120mV) amongst thioredoxin superfamily proteins (Ito & Inaba, 2008). Importantly, the Cys30 residue in the active site has a very low pKa and is thus present in the thiolate anion state at physiological pH, which makes the oxidized form of protein less stable and more reactive than its reduced form (Kadokura et al, 2003). In

addition, the sulfur of Cys30 is exposed in the oxidized state, making it accessible to the substrate proteins (Manta et al, 2019). These conditions promote the transfer of disulfide from DsbA to the substrate proteins. In addition, the oxidized form of DsbA has great mobility, which might facilitate the accommodation of various substrates. In contrast, its reduced form is rigid and helps in the release of oxidized substrates (Vinci et al, 2002).

In *E. coli*, the expression of DsbA is positively regulated by the Cpx ESR system. Under standard laboratory growth conditions, ~850 molecules of DsbA per cell are present, which increases further in response to cell envelope protein folding defects (Akiyama et al, 1992; Manta et al, 2019).

1.9.2 Enzymes involved in disulfide bond formation: DsbB

DsbB, the oxidizer of DsbA, is located in the inner membrane. The Cys30-Cys33 residues of DsbA get reduced after catalyzing the formation of disulfide bonds and need to be re-oxidized. The oxidoreductase, DsbB, performs the re-oxidation of DsbA by transferring electrons to the ETC at the level of quinones. DsbB has two pairs of cysteine residues in the active site, i.e., Cys41-Cys44 and Cys104-Cys130. Although Cys41-Cys44 residues of DsbB are arranged in a CXXC format, it might not have a thioredoxin-like fold as the periplasmic domain where these residues reside is very short and the protein has no sequence homology with other thioredoxins. DsbB uses quinones as the cofactor, which lies around the Cys41-Cys44 motif (Hatahet et al, 2014; Kadokura et al, 2003). The substitution mutation in DsbA, Cys33 to tyrosine or serine, leads to a decrease in the disulfide bond forming capacity of the mutant. These mutants accumulate a mixed-disulfide adduct between DsbA and DsbB, which represents an intermediate in the DsbA oxidation process. Thus, it has been suggested that DsbA Cys33 attacks the mixed disulfide between Cys30 of DsbA and Cys104 of DsbB and resolves the intermediate. Therefore, the electron flow is from reduced Cys30-Cys33 of DsbA to Cys104–Cys130 of DsbB, then to Cys41–

Cys44 pair of DsbB and finally to oxidized quinones (Guilhot et al, 1995; Hatahet et al, 2014; Kishigami et al, 1995).

The redox potential of both cysteine pairs, Cys41-Cys44 (280mV) and Cys104-Cys130 (-250mV), in DsbB is lower than the redox potential of DsbA cysteine pair, Cys Cys30-Cys33 (-120mV). Therefore, the redox gradient opposes the observed direction of electron flow among DsbA and DsbB proteins. However, it has been shown that a DsbA mutant with redox potential lower than the wild-type (WT) protein is oxidized at the same rate by DsbB, which indicates that the redox potential of DsbA is not important for its oxidation by DsbB. Importantly, even among DsbB cysteine pairs, the redox potential of Cys104-Cys130 (-250mV) is higher than Cys41-Cys44 (-280mV) which again opposes the actual flow of electrons. It has been shown that the redox potential of Cys41-Cys44 pair of DsbB decreases in the presence of ubiquinone (redox potential -210mV), making the cysteine pair more oxidizing, thereby facilitating the electron flow. Therefore, it has been proposed than when the re-oxidation of DsbA leads to the formation of DsbA-DsbB intermediate complex, the reduced Cys130 of DsbB is free to interact with Cys41-Cys44, and the high redox potential of ubiquinone in conjunction with Cys130-Cys41 complex facilitates electron flow from DsbA to DsbB (Inaba & Ito, 2002; Kadokura & Beckwith, 2002; Kadokura et al, 2003).

1.9.3 Essentiality of the disulfide bond forming pathway

In *E. coli*, ~300 proteins are predicted to be disulfide-bonded in the periplasm (Dutton et al, 2008). Several of these periplasmic proteins have been experimentally shown to be dependent on DsbA for disulfide bond formation. These include Agp, AppA, ArtJ, Bla, DegP, DppA, FlgI, FtsN, GltI, GltX, HisJ, LivJ, LivK, LptD, MepA, NlpE, OmpA, OppA, PhoA, RcsF, Rna, UgpB, YbeJ, YbjP, YcdO, YedD, YebF, YggN, YodA, YtfQ and ZnuA (Delhaye et al, 2019; Kadokura et al, 2004). Consistent with the role of DsbA in the folding

of several cell envelope and secretory proteins involved in diverse biological processes, *dsbA* mutants show pleiotropic phenotypes. The *dsbA* mutants have decreased levels of the outer membrane proteins, OmpA and β-lactamase (Bla), and decreased alkaline phosphatase (PhoA) activity due to the absence of disulfide bonds required for its stability (Bardwell et al, 1991). The *dsbA* mutants exhibit loss of motility as disulfide bond formation is essential for the assembly of FlgI, a flagellar motor component (Dailey & Berg, 1993). Finally, *dsbA* mutants are hypersensitive to reductants such as dithiothreitol, thioglycerol, drugs such as benzylpenicillin, and heavy metals such as cadmium and zinc (Missiakas et al, 1993; Rensing et al, 1997; Skorko-Glonek et al, 2008; Stafford et al, 1999; Zeng et al, 1998). It has been seen that mutations in *dsbB* lead to the accumulation of DsbA in its reduced form, and *dsbB* mutants show the same pleiotropic phenotypes as *dsbA* mutants (Bardwell et al, 1993; Dailey & Berg, 1993; Kadokura et al, 2003; Missiakas et al, 1993).

Amongst the substrates of the DsbA-DsbB machinery are a few proteins, which are essential for cellular viability. These include FtsN, a protein involved in cell division and LptD, a protein involved in LPS assembly (Meehan et al, 2017a; Meehan et al, 2017b). Despite this, *dsbA* and *dsbB* mutants are viable under aerobic conditions; however, they show growth defects in anaerobic conditions. It has been suggested that in aerobic conditions, background oxidation is sufficient to provide a significant pool of active proteins required for cellular functions (Meehan et al, 2017b). This is evident from a comparison of FtsN levels in a *dsbA* mutant under aerobic and anaerobic conditions. The reduced form of FtsN is unstable and is degraded in the periplasm. In a *dsbA* mutant, under aerobic conditions, there is ~4-fold decrease in the levels of FtsN, which drops further under anaerobic conditions. This result indicates that background oxidation, although less

efficient, can maintain a pool of active, stable FtsN, and prevents any major defects in cell division (Meehan et al, 2017b).

1.9.4 Role of ETC in disulfide bond formation

ETC provides the ultimate oxidizing power for disulfide bond formation by reoxidizing DsbB. DsbB uses quinones as cofactors, which further transfers electrons to terminal oxidases and then to the terminal electron acceptor (Fig. 1.12). This link between ETC and disulfide bond formation was demonstrated in earlier *in vivo* studies. It was shown that DsbA remains in a reduced form in mutants defective in the respiratory chain components, i.e., in mutants defective in heme biosynthesis (*hemA* mutant) or defective in ubiquinone and menaquinone biosynthesis (*ubiA-menA* mutant) (Kobayashi et al, 1997). Further, disulfide bond formation was compromised under conditions of non-operational ETC; a strain grown anaerobically without any electron acceptor on glucose (in a fermentative manner), accumulated β-lactamase in a reduced form (Bader et al, 1999). In addition, similar to the *dsb* mutants, ubiquinone biosynthesis mutants also exhibit thiol hypersensitivity. This is suggested to be due to the inability of the suboptimal respiratory chain to re-oxidize Dsb enzymes reduced in the presence of excess thiol agents (Zeng et al, 1998).

1.9.5 Disulfide bond formation and pathogenesis

Several pathogenic bacteria contain DsbA homologue, and its mutation affects their survival and virulence due to defects in the folding and assembly of virulence determinants. For example, in *V. cholerae*, TcpG, a homologue of disulfide bond-forming DsbA oxidoreductase, allows a group of virulence-associated proteins to attain a functionally competent state. Importantly, the secretion and activity of cholera toxin A (which contains disulfide bonds) is reduced in *V. cholerae tcpG* mutant (Peek & Taylor, 1992; Yu et al, 1992). In *S. enterica* serovar Typhimurium, DsbA is required for disulfide bond formation

in SpiA, an outer membrane protein of *Salmonella* Pathogenicity Island 2 Type III secretion system, and *dsbA* mutants exhibit attenuated virulence (Miki et al, 2004). *Francisella tularensis* encodes an ortholog of DsbA, which functions both as oxidoreductase and isomerase, and several of its substrates are virulence factors (Ren et al, 2014). In addition, the *dsbA* gene in *Shigella flexneri, P. aeruginosa, Haemophilus influenzae*, and *E. coli* O157:H7 is required for intracellular survival and virulence upon infection (Ha et al, 2003; Lee et al, 2008; Rosadini et al, 2008; Yu, 1998).

1.10 Thesis objective

The important functions of the electron transport chain (ETC) are maintenance of redox balance and production of ATP. ETC plays a critical role for the growth of organisms on non-fermentable carbon sources because these carbon sources can generate energy solely by oxidative phosphorylation in the ETC, and the reduced cofactors generated by carbon metabolism can also be re-oxidized only at the ETC. Although this fundamental information is available for decades, there has not been any investigation on whether amongst non-fermentable carbon sources, there is a differential requirement of ETC. This question seems logical given that different non-fermentable carbon sources enter into the TCA cycle at different steps (Fig. 1.1) and theoretically generate different amounts of reduced cofactors. Therefore, in the first objective of my thesis (presented in Chapter III) by analyzing data from high-throughput genetic screens of the single-gene deletion library of *E. coli* (covering ~4000 genes) on various carbon sources followed by detailed genetic and biochemical analysis, I have compared the requirement of ETC components on different non-fermentable carbon sources. The results from this objective established that the requirement of aerobic ETC components for growth is inversely correlated with the energy yield of non-fermentable carbon sources, however, the requirement of ubiquinone is maximal for growth on LCFAs to counteract oxidative stress. We propose that high

$NADH/NAD^+$ and $FADH_2/FAD$ ratios during LCFA catabolism increase electron flow in the ETC, thereby increasing ROS formation, and ubiquinone decreases ROS by rapidly transferring electrons from the site of ROS formation to the ETC.

Besides transferring electrons generated by the metabolism of carbon sources from respiratory dehydrogenases to the terminal oxidases in the ETC, ubiquinone plays a pivotal role in transferring electrons from the disulfide bond forming machinery. Considering the large flow of electrons in the ETC during LCFA metabolism, I was tempted to ask if during LCFA metabolism, ubiquinone is limiting to handle electrons from the disulfide bond forming machinery and whether this makes the environment of the periplasm less oxidizing. I have investigated this issue in the second objective of my thesis (presented in Chapter IV). Results from this objective establish that indeed increased electron flow in the ETC during LCFA metabolism renders ubiquinone limiting for disulfide bond formation, thereby compromising redox balance in the envelope. Finally, in the third objective of my thesis (presented in Chapter V), I have identified the stress response systems that monitor redox imbalance in the envelope during LCFA metabolism.

CHAPTER II

Materials and Methods

2.1 Strains, plasmids, and primers:

Strains and plasmids are listed in Table 2.1. Primers used in this study are listed in Table 2.2. For deletion strains obtained from the Keio collection (Baba et al, 2006), either both independent clones from the library and/or their fresh transductants were made by P1 transduction and verified by colony PCR to rule out genetic errors. The derivatives of *degS*ΔPDZ strain were unstable as glycerol stocks and thus were always freshly made before use.

The transcriptional reporter fusion for the Psp ESR pathway, RC15106, was constructed as follows. P1 lysate from AM1247 was used to infect MG1655 Δ*lac* strain. Transductants were screened for Lac^+ phenotype on LB agar containing 10 mM citrate and 0.1 mg/ml X-gal. Colonies were re-streaked to obtain pure blue colonies. Blue colonies were further screened for the presence of *nadA* based on tetracycline sensitivity.

The $ppGpp^0$ strain was always freshly made before use. Briefly, RC15105 was constructed by transducing *relA::kan* from the Keio collection into CAG45114. The *spoT::cam* allele from CAG55907 was then transduced into RC15105. The $ppGpp^0$ phenotype was confirmed by the inability of the strain to grow on M9 minimal medium lacking amino acids (Costanzo & Ades, 2006). Construction of $ppGpp^0$ strain and experiments involving this strain were performed at 30°C.

Table 2.1 List of strains and plasmids used in this study.

Strain/Plasmid	**Relevant genotype**	**Source (reference)**
Strains		
BW25113	F^- Δ(*araD-araB*)*567* Δ*lacZ4787*(::rrnB-3) λ^- *rph-1* Δ(*rhaD-rhaB*)*568 hsdR514*	*E. coli* Genetic Stock Center
BEFB05	MG1655 *nuo*::*nptI*, Kan^r	Frédéric Barras (Ezraty et al, 2013)
GS022	MC4100 λRS45 Φ(*katG-lacZ*)	Gisela Storz (Seaver & Imlay, 2001)
MC4100 *ahpC-lacZ*	MC4100 λRS45 Φ(*ahpC-lacZ*)	Gisela Storz

RI89	F^- Δ*araBAD714* (*araD139*)$_{B/r}$ Δ(*codB-lacI*)*3 phoR82 galK16 galE15* λ^- *e14*$^-$ *relA1 rpsL150 spoT1 mcrB1*	Sardesai lab (Rietsch et al, 1996)
MG1655	F^- λ^- *rph-1*	*E. coli* Genetic Stock Center
MG1655 Δ*lac*	MG1655 Δ*lacX74*	Gross lab
SEA4170	MG1655 Δ*lacX74* λ*RS88* [P_{spy}-*lacZ*]	Ades Lab
SEA4166	MG1655 Δ*lacX74* λ*RS88* [P_{cpxP}-*lacZ*]	Ades Lab
AM1247	MG1655 *lacIZYA*::*frt nadA*::*Tn10 att*λ [P_{pspA}-*lacZ*], Tet^r	Reddy Lab (Mychack et al, 2019)
DH300	MG1655 Δ(*argF-lac*)*U169* [$P_{rprA142}$-*lacZ*]	Ades Lab (Majdalani et al, 2002)
CAG45114	MG1655 Δ*lacX74* λ[P_{rpoHP3}-*lacZ*]	Gross Lab (Ades et al, 2003)
CAG53524	MC1061 [ϕλ*rpoH*P3::*lacZ*] *degS*ΔPDZ::*kan*, Kan^r	Gross lab (Chaba et al, 2011)
CAG55907	CAG45114 Δ*relA* Δ*spoT*::*cam*, Cam^r	Gross lab (Mutalik et al, 2009)
BW25113 Δ*ahpC*	BW25113 *ahpC*::*kan*, Kan^r	Keio collection (Baba et al, 2006)
BW25113 Δ*cyoA*	BW25113 *cyoA*::*kan*, Kan^r	Keio collection (Baba et al, 2006)
BW25113 Δ*fadL*	BW25113 *fadL*::*kan*, Kan^r	Keio collection (Baba et al, 2006)
BW25113 Δ*dsbA*	BW25113 *dsbA*::*kan*, Kan^r	Keio collection (Baba et al, 2006)
BW25113 Δ*dsbB*	BW25113 *dsbB*::*kan*, Kan^r	Keio collection (Baba et al, 2006)
BW25113 Δ*katG*	BW25113 *katG*::*kan*, Kan^r	Keio collection (Baba et al, 2006)
BW25113 Δ*ndh*	BW25113 *ndh*::*kan*, Kan^r	Keio collection (Baba et al, 2006)
BW25113 Δ*nuoK*	BW25113 *nuoK*::*kan*, Kan^r	Keio collection (Baba et al, 2006)
BW25113 Δ*oxyR*	BW25113 *oxyR*::*kan*, Kan^r	Keio collection (Baba et al, 2006)
BW25113 Δ*sdhB*	BW25113 *sdhB*::*kan*, Kan^r	Keio collection (Baba et al, 2006)
BW25113 Δ*ubiI*	BW25113 *ubiI*::*kan*, Kan^r	Keio collection (Baba et al, 2006)

BW25113 Δ*ubiH*	BW25113 *ubiH*::*kan*, Kan^r	Keio collection (Baba et al, 2006)
RC5157	P1 (BEFB05) x BW25113, Kan^r	This work
RC8007	BW25113 *ubiI*::*kan*, kan cassette flipped out	Chaba lab
RC5263	P1 (BW25113 *ahpC*::*kan*) x RC8007, Kan^r	This work
RC5261	P1 (BW25113 *katG*::*kan*) x RC8007, Kan^r	This work
RC5258	P1 (BW25113 *oxyR*::*kan*) x RC8007, Kan^r	This work
RC15082	BW25113 *attλ*::[Kan P_{fadE} -*lacZ oriR6K*], Kan^r	Chaba Lab
RC5167	P1 (BW25113 *ubiI*::*kan*) x GS022, Kan^r	This work
RC5171	RC5167; *kan* cassette flipped out	This work
RC5172	P1 (BW25113 *fadL*::*kan*) x RC5171, Kan^r	This work
RC5163	P1 (BW25113 *ubiI*::*kan*) x MC4100 *ahpC-lacZ*, Kan^r	This work
RC5221	RC5163; *kan* cassette flipped out	This work
RC5215	P1 (BW25113 *fadL*::*kan*) x RC5221, Kan^r	This work
RC5264	P1 (BW25113 *fadL*::*kan*) X RI89, Kan^r	This work
RC15062	P1 (BW25113 *fadE*::*kan*) X RI89, Kan^r	Chaba Lab
RC5327	P1 (BW25113 *dsbA*::*kan*) X RI89, Kan^r	This work
RC5328	P1 (BW25113 *dsbB*::*kan*) X RI89, Kan^r	This work
RC5337	P1 (BW25113 *dsbA*::*kan*) X MG1655, Kan^r	This work
RC5338	P1 (BW25113 *dsbB*::*kan*) X MG1655, Kan^r	This work
RC15106	P1 (AM1247) X MG1655 Δ*lacX74 nadA*$^+$	Chaba Lab
RC15020	P1 (BW25113 *fadL*::*kan*) X SEA4166, Kan^r	Chaba Lab
RC15019	P1 (BW25113 *fadE*::*kan*) X SEA4166, Kan^r	Chaba Lab
RC15043	P1 (BW25113 *ackA*::*kan*) X SEA4166, Kan^r	Chaba Lab
RC5320	RC15043, *kan* cassette flipped out	This work
RC5322	P1 (BW25113 *pta*::*kan*) X RC5320, Kan^r	This work
RC5302	P1 (BW25113 *cpxA*::*kan*) X SEA4166, Kan^r	This work
RC15096	P1 (BW25113 *cydD*::*kan*) X SEA4166, Kan^r	Chaba Lab
RC15006	P1 (BW25113 *fadL*::*kan*) X CAG45114, Kan^r	Chaba Lab
RC15005	P1 (BW25113 *fadE*::*kan*) X CAG45114, Kan^r	Chaba Lab
RC15104	P1 (BW25113 *rseB*::*kan*) X CAG45114, Kan^r	Chaba Lab
RC15103	RC15104, *kan* cassette flipped out	Chaba Lab
RC5317	P1 (CAG53524) X CAG45114, Kan^r	This work
RC15105	P1 (BW25113 *relA*::*kan*) X CAG45114, Kan^r	Chaba Lab
RC15095	P1 (BW25113 *cydD*::*kan*) X CAG45114, Kan^r	Chaba Lab
Plasmids		
pBAD24	Vector, f1 ori, pBR322 ori, Amp^r	(Guzman et al, 1995)
pKJ7	*ubiI*-6XHis in pBAD24, Amp^r	This work

pCP20	pSC101 *ori cI857* λ-P_R *flp* ts Amp^r Cam^r	(Datsenko & Wanner, 2000)

Table 2.2 List of primers used in this study.

Primers	**Sequence (from 5' to 3')**	**Purpose**
Primers used for cloning		
SA49	ACCGGAATTCGAAGGAGATATACATATGC AAAGTGTTGATGTAGCCATTGTTGGCGG	Forward primer for cloning *ubiI*-6XHis in pBAD24
KJ60	CGTAAGCTTTTAGTGATGATGATGATGATG ACGCAGCCATTCAGGCAAATCGTTTAATCC	Reverse primer for cloning *ubiI*-6XHis in pBAD24
Primers used for strain confirmation		
KJ104	AAATGTCGGTGTCATCATGCG	Forward primer used to verify *ackA* transductants
KJ105	ATCACGCCAAGGCTGACGC	Reverse primer used to verify *ackA* transductants
KJ77	ATTACACGGTCACCTGGAAAGG	Forward primer used to verify *ahpC* transductants
KJ78	GCTATGGCGTGAAAGACGAAGG	Reverse primer used to verify *ahpC* transductants
MS19	TTCCCGTGAACATTTAAGCCAGG	Forward primer used to verify *cpxA* transductants
MS20	AGATCGAAGATTTTTCCCGCC	Reverse primer used to verify *cpxA* transductants
MS54	TTTCCCCGTTGTAACATTGCTCTGC	Forward primer used to verify *cydD* transductants
MS55	CATATAGTTGAAGCTGTACAGTCCGGC	Reverse primer used to verify *cydD* transductants
KJ79	ACCTTCCCGTAAAATGCCCAC	Forward primer used to verify *cyoA* transductants
KJ80	TTCATGGAACGGGACTGCATC	Reverse primer used to verify *cyoA* transductants
MS25	GACGGCGACTTTTATAGAACAGGC	Forward primer used to verify *dsbA* transductants
MS26	TGAAATAATGTCCAGCGGCAGG	Reverse primer used to verify *dsbA* transductants
MS27	AACGCTTTGATAACAACTTACCGGG	Forward primer used to verify *dsbB* transductants
MS28	AGGAACACTCTATTTTGCCGGG	Reverse primer used to verify *dsbB* transductants
KJ67	CACTACAACCATATCATCACAAGTGG	Forward primer used to verify *fadE* transductants
KJ68	TAGCGGATAAAGAAACGGAGCC	Reverse primer used to verify *fadE* transductants

KJ63	TCGCCACTGGTCTGATTTCTAAG	Forward primer used to verify *fadL* transductants
KJ64	AGGACACTACTTTCGGTGAAGTGG	Reverse primer used to verify *fadL* transductants
KJ75	ATCTCAACTATCGCATCCGTGG	Forward primer used to verify *katG* transductants
KJ76	AACTCCAGATAAGTGTGAGCACAACC	Reverse primer used to verify *katG* transductants
MS78	GGTAACGAAAGAGGATAAACC	Forward primer used to verify *pta* transductants
MS79	TATTTCCGGTTCAGATATCC	Reverse primer used to verify *pta* transductants
MS58	GCGAAGCGTTATTAAAAGCAGGATA	Forward primer used to verify *relA* transductants
MS59	CGGTGAATTTCCCCAACGCTTTA	Reverse primer used to verify *relA* transductants
MS68	TTCAAACTTTAGGAACGCAATCG	Forward primer used to verify *rseB* transductants
MS69	ACAATGGTATGCGTGGTTTGC	Reverse primer used to verify *rseB* transductants
SA36	GCTGATGACGATGGAATTATTC	Forward primer used to verify *ubiI* transductants
SA37	GAGATGAAAGTGTGATGGGTATC	Reverse primer used to verify *ubiI* transductants
GA18	ATGCAGAAGTGCCAGAACAATATCG	Forward primer used to verify *ubiH* transductants
GA19	AATGGCTACATCAACACTTTG	Reverse primer used to verify *ubiH* transductants
SAK1	GAGGCTATTCGGCTATGACTG	Forward primer specific to kanamycin cassette
SAK2	TTCCATCCGAGTACGTGCTC	Reverse primer specific to kanamycin cassette

2.2 Media composition and growth conditions:

Media had the following composition: lysogeny broth (LB) was 5 g/liter Bacto yeast extract, 10 g/liter Bacto tryptone, and 5 g/liter NaCl; tryptone broth (TB) was 10 g/liter Bacto tryptone, and 5 g/liter NaCl; tryptone broth K (TBK) was 10 g/liter Bacto tryptone, and 5 g/liter KCl; M9 minimal medium was 5.3 g/liter Na_2HPO_4, 3 g/liter KH_2PO_4, 0.5 g/liter NaCl, 1 g/liter NH_4Cl, 0.12 g/liter $MgSO_4$, 2 mg/liter biotin, 2 mg/liter nicotinamide,

0.2 mg/liter riboflavin, and 2 mg/liter thiamine. TBK media was buffered at pH 7.0 using 100 mM potassium phosphate buffer. Where required, media were supplemented with either glucose or sodium salt of acetate, succinate or oleate, at a final concentration of 5 mM. Stock of oleate (50 mM) was prepared in 5.0% Brij-58. Media were solidified using 1.5% (w/v) Difco agar. When required, ampicillin (100 μg/ml), chloramphenicol (20 μg/ml), kanamycin (30 μg/ml) and tetracycline (25 μg/ml) were used. For specific experiments, glutathione, thiourea, urea, $CdCl_2$, DTT and 1-thioglycerol at desired concentrations and ubiquinone-8 at 20 μM concentration were added to the medium. A 10 mM stock of ubiquinone-8 (Avanti Polar Lipids) was prepared in 50% ethanol.

Primary cultures were grown in 3 ml LB. Secondary cultures were set-up either in TB, TBK or in M9 minimal medium containing the desired carbon source and grown for defined time periods. The optical density was measured at 450 nm (for cultures grown in M9 Minimal medium) or 600 nm (for cultures grown in LB, TB and TBK). Except for $ppGpp^0$, all cultures were incubated at 37°C.

2.3 Comparative analysis of chemical genomic screens

In a previous study in our laboratory where data from high-throughput genetic screens of the Keio deletion library (Baba et al., xx) on minimal media supplemented with oleate and glucose were compared (Agrawal, 2018; Agrawal et al, 2017), the colony sizes of the mutants from the screens were filtered and normalized using established methods for chemical genomics in *E. coli* K-12 (Shiver et al, 2016). To account for the possible effect of the detergent Brij-58 on growth, the colony sizes of the oleate condition were directly compared with that of glucose-Brij-58 control to generate the fitness scores for the oleate condition, using the same statistical test as the S-score (Agrawal, 2018; Agrawal et al, 2017). In this thesis, to facilitate comparison of the chemical genomic profile of oleate to other fermentable and non-fermentable carbon sources, raw data from minimal media

conditions of a previous large-scale chemical genomic screen (Nichols et al., 2011) were reanalyzed using the same workflow above and M9 minimal medium with 0.2% glucose as a normalization. Finally, fitness score distributions for each condition were scaled to have a standard inter-quartile range of 1.35 (Nichols et al, 2011) to minimize bias in any downstream analysis from conditions with a large variance. The MATLAB code and raw data for this analysis are available online at https://github.com/AnthonyShiverMicrobes/fitness_lcfa.

2.4 Recombinant DNA work and gel electrophoresis

Protocols for cloning, colony PCR, agarose gel electrophoresis, and SDS-PAGE were adapted from 'Sambrook Molecular cloning: A Laboratory manual'. Plasmid isolation, PCR product purification and gel extraction of DNA was performed using kits purchased from Thermo scientific and Promega and protocols were followed as per manufacturer's instruction manual. Transformation was done by electroporation at 1.8kV in 1mm electro cuvettes.

2.5 P1 Lysate preparation and transduction

2.5.1 P1 lysate preparation

P1 lysate was prepared according to the protocol mentioned in (Miller, 1972) with slight modifications. The overnight culture was reinoculated in 2 ml LB medium containing 5 mM $CaCl_2$ in 1:100 ratio in a 15 ml falcon tube and incubated at 37°C for 1 hour 30 minutes. 20 µl of P1 lysate was added and the culture was again incubated at 37°C for 3-4 hours to allow lysis. 50 µl of chloroform was added and the lysed culture was vortexed for 30 seconds. Cell debris was pelleted by centrifugation at 8000 rpm for 10 minutes and the clear supernatant (lysate) was transferred in a fresh MCT containing 50 µl chloroform. The lysate was stored at 4°C until use.

2.5.2 P1 transduction

P1 transduction was done according to the protocol mentioned in (Miller, 1972) with slight modifications. 1 ml of the overnight culture was pelleted and resuspended in 1 ml of P1 salt solution containing 5 mM $MgSO_4$ and 10 mM $CaCl_2$ in water. 100 µl of the re-suspended cells were transferred into the MCTs containing 0 µl, 20 µl and 60 µl of P1 lysate and incubated at 37°C for 30 minutes in a water bath. 1 ml LB containing 10 mM sodium citrate was added and the samples were again incubated at 37°C for 1 hour. Samples were washed twice with 1 ml LB and suspended in 100 µl LB. The resuspended cells were plated on LB-agar plates supplemented with 10 mM sodium citrate and appropriate antibiotic and incubated at 30°C for 16-18 hours. Transductants obtained were re-streaked twice on LB-agar plates supplemented with 10 mM sodium citrate and appropriate antibiotic followed by incubation at 37°C. Transductants were confirmed by colony PCR and preserved as glycerol stocks.

2.6 Growth curves in 96-well plates and shake flasks

Growth curves in M9 minimal medium were performed in 96-well plates. Cells washed and re-suspended in M9 minimal medium were re-inoculated in 200 µl of minimal medium containing the desired carbon source to an initial OD_{450} of ~0.03, using a robotic liquid handling system (Tecan). Plates were incubated at 37°C in a shaker, and OD_{450} of the cultures was measured at regular time intervals in a Tecan Infinite M200 monochromator-based microplate reader. The microplate reader and incubator shaker were integrated with the liquid handling system where the transfer of plates between the shaker and reader was automated.

Growth curves in TBK medium were performed in shake flasks. Primary cultures were pelleted, washed, and re-suspended in TBK medium. Cells were re-inoculated in 15

ml medium in 125 ml flasks to an initial OD_{600} of ~0.01. Cultures were grown at 37°C, and OD_{600} was measured at definite time intervals.

2.7 Generation time calculation

The generation time of the cultures was calculated when there was steady rate of growth i.e., when cells entered the exponential phase of growth. Generation time (G) was calculated as the time in minutes or hours (t) / number of generations (n).

The number of generations (n) is the number of times the cell population doubles during a given time interval (t). If B is the OD at the beginning of a time interval and b is the OD at the end of the time interval, then:

$b = B \times 2^n$
$\log b = \log B + n \log 2$
$n = (\log b - \log B)/\log 2$
$n = 3.3 \log b/B$
Thus, generation time, $G = t/ 3.3 \log b/B$

2.8 β-galactosidase assay

Secondary cultures (15 ml) were grown in 125-ml flasks for 14–16 h. Cells were pelleted, washed at least 4 times with Z-buffer (8.52 g/liter Na_2HPO_4, 5.5 g/liter $NaH_2PO_4.H_2O$, 0.75 g/liter NaCl, 0.246g/liter $MgSO_4.7H_2O$; pH 7.0), and normalized in the same buffer to OD_{450} ~0.5. Several washings of the culture were critical to remove Brij-58 because the detergent interferes with β-gal assay. In 0.5 ml of the resuspended culture, 0.5 ml of Z-buffer containing 2.7 ml/liter β-mercaptoethanol, 1 drop of 0.1% SDS and 2 drops of chloroform were added. The samples were vortexted. The assay was performed at 30°C. The reaction was initiated by the addition of 200 µl of 4 mg/ml o-nitrophenyl-β-galactoside and was stopped by the addition of 500 µl of 1 M Na_2CO_3. Miller Units were calculated as described in (Miller, 1972).

2.9 NADH and NAD^+ quantitation

The extraction of NAD^+ and NADH was carried out using the protocol described in (San et al, 2002), with slight modifications. Briefly, 6 ml cultures were pelleted, washed three times with 1 ml cold 1X PBS (8 g/liter NaCl, 0.2 g/liter KCl, 1.44 g/liter Na_2HPO_4 and 0.24 g/liter KH_2PO_4; pH 7.4), and normalized to OD_{450} ~1. Immediately, 1 ml of each sample was taken in two MCTs, pelleted and re-suspended in 300 µl of 0.2 M NaOH (for NADH) or 0.2 M HCl (for NAD^+). The samples were incubated at 50°C in a water bath for 10 min and then immediately transferred to ice for 5 min. Following this, 300 µl of 0.1 M HCl (for NADH) or 0.1 M NaOH (for NAD^+) was added drop-wise to the samples with vortexing. Samples were centrifuged at 18,400 X g for 5 min at 4°C to remove cell debris. The supernatant was transferred to a fresh MCT and kept in ice. Samples were deproteinized using a 10 kDa cut-off filter by centrifugation at 6,900 X g for 15 min at 4°C and kept in ice. The amount of NADH and NAD^+ in samples was quantitated using the NAD/NADH quantitation kit (Sigma). Briefly, 150 µl reaction mix was prepared in 96-well plates (transparent with clear bottom) where each reaction mix contained 50 µl of the extracted sample, 98 µl cycling buffer, and 2 µl cycling enzyme mix. The reaction mixture was kept at room temperature for 10 min followed by the addition of 10 µl NADH developer in the dark. Samples were incubated further for one hour. Absorbance was measured at 450 nm (Thermo Scientific Multiskan Go). A standard curve was obtained using the NADH standard provided in the kit, and the amount of NADH and NAD^+ in the samples was quantified.

2.10 Respiratory dehydrogenase activity assays

2.10.1 Preparation of cell extract

Secondary cultures were washed at least three times with assay buffer. ~10^{10} cells were resuspended and sonicated. Samples were centrifuged at 18,400 X g for 40 min at 4°C. The supernatant was collected and kept in ice. Protein was quantified using Bradford assay.

2.10.2 NADH dehydrogenase assay

The NADH dehydrogenase assay was performed as described in (Wang & Maier, 2004), with slight modifications. 1 ml reaction mixture contained 50 mM Tris-Cl (pH 8.0), 250 µM menadione, and 1 µg protein. The reaction was started by adding 250 µM NADH. The decrease in absorbance of NADH (extinction coefficient: 6.22 mM^{-1} cm^{-1}) at 340 nm over a period of 5 min was monitored. The reaction mixture without NADH was taken as blank. Enzyme activity was expressed as NADH oxidized (in nmoles) per min per mg protein.

2.10.3 Succinate dehydrogenase assay

The succinate dehydrogenase assay was performed as described in (McNeil et al, 2012), with slight modifications. 1 ml reaction mixture containing 150 mM $NaPO_4$ (pH 7.0), 100 mM sodium succinate (pH 7.5), 20 mM sodium azide, 100 µM ubiquinone-2 (Sigma; 10 mM stock was prepared in ethanol) and 50 µg protein. The reaction was started by adding 50 µM DCPIP (2,6-Dichlorophenolindophenol). The decrease in absorbance of DCPIP (extinction coefficient: 22 mM^{-1} cm^{-1}) at 600 nm over a period of 15 min was monitored. The reaction mixture without DCPIP was taken as blank. Enzyme activity was expressed as DCPIP reduced (in nmoles) per min per mg protein.

2.11 Alkaline phosphatase assay

Alkaline phosphatase (AP) activity was determined as described in (Pathania et al, 2016), with modifications. 1 mM of freshly prepared iodoacetamide was added directly to the cultures and the samples were kept on ice for 15 min. Cells were pelleted and washed three

times with a buffer containing 10 mM Tris (pH 8.0), 10 mM $MgSO_4$, and 1 mM iodoacetamide. Cells were then resuspended in a buffer containing 1 M Tris (pH 8.0), 0.1 mM $ZnCl_2$, 0.002% SDS and 20 µl chloroform. The assay was performed at 37°C, and initiated by the addition of 200 µl of 4 mg/ml *p*-nitrophenyl phosphate and was stopped by the addition of 120 µl of a buffer containing 165 mM K_2HPO_4 and 80 mM EDTA. Units of AP activity were calculated as described in (Brickman & Beckwith, 1975).

2.12 Dilution spotting

The overnight primary culture was pelleted, washed, and re-suspended in M9 minimal medium. OD_{450} of the culture was taken and normalized to OD_{450} ~ 9. Serial dilutions of the cultures were made in minimal medium. 5 µl of 10^{-4}, 10^{-5}, and 10^{-6} dilutions of cultures were spotted on TBK-Brij and TBK-Ole plates supplemented with different concentrations of DTT. Plates were incubated and imaged (Gel Doc XR+ imaging system, Bio-Rad) at different time intervals. A representative image (at 21 hours) is shown in the figure.

2.13 Determination of the redox state of DsbA protein

The redox state of DsbA was determined as described in (Kumar et al, 2011), with slight modifications. Cells were treated with tri-chloroacetic acid (final concentration 20%), which prevents aerial oxidation and traps thiols of DsbA in their original state. Protein precipitates were collected by centrifugation, washed with acetone, dried, and dissolved in a buffer containing 100 mM Tris-Cl (pH 8.8), 10 mM EDTA, 1% SDS and 30 mM AMS. The samples were incubated at 37°C for 1 hour in a thermomixer set at 1400 revolutions/min. Proteins were separated on a 15% non-reducing SDS-PAGE, transferred to nitrocellulose membrane and processed for Western blotting.

2.14 Western Blotting

The redox state of DsbA and expression of AP was monitored by Western blot analysis. Samples separated on SDS-PAGE were transferred to a nitrocellulose membrane. The

membrane was blocked overnight with 5% (w/v) skimmed milk at 4°C and probed with anti-DsbA (1:1000, Thermo Fisher Scientific) or anti-AP (1:5000, Millipore) primary antibody and HRP-conjugated anti-mouse (1:5000, Sigma) secondary antibody. Blots were developed using the SuperSignal West Dura Extended Duration Substrate (Pierce). Signal was captured on an X-ray film.

CHAPTER III

Systems-level analysis reveals a differential requirement of electron transport chain for the metabolism of non-fermentable carbon sources

3.1 Introduction

In gram-negative bacteria, the electron transport chain **(**ETC), located in the inner membrane, transfers electrons from electron donors to electron acceptors and translocates protons from cytoplasm to periplasm. In this process, the ETC performs two important functions: ATP production and maintenance of redox balance. The ETC comprises two major classes of enzymes: dehydrogenases, which function as quinone reductases, and terminal oxidases, which function as quinol oxidases. In *E. coli*, during aerobic metabolism, dehydrogenases include NADH dehydrogenases (Ndh and Nuo) and succinate dehydrogenase (Sdh), which oxidize NADH and $FADH_2$, respectively, and transfer electrons to the lipid-soluble electron carrier, ubiquinone (UQ_8). The reduced form of ubiquinone, ubiquinol (UQ_8H_2), in turn, transfers electrons to the quinol oxidases, cytochrome *bo* (Cyo) and cytochrome *bd* (Cyd). Terminal oxidases further transfer electrons to molecular oxygen, reducing it to water. Nuo, Cyo, and Cyd couple redox energy to generate proton motive force (PMF) that drives ATP synthesis through ATP synthase (Unden et al, 2014).

In the presence of electron acceptors, fermentable carbon sources such as glucose re-oxidize reduced cofactors in the ETC, whereas, in the absence of electron acceptors, they can undergo fermentation to reoxidize reduced cofactors. Further, fermentable carbon sources produce ATP through both substrate-level phosphorylation in glycolysis and oxidative-phosphorylation in the ETC. However, during growth on non-fermentable carbon sources, cells are totally dependent on ETC for the re-oxidation of reduced cofactors and generation of energy (Berger, 1973; Lin & Iuchi, 1991). This difference in the requirement of ETC amongst fermentable and non-fermentable carbon sources has traditionally been used as a rationale for identifying novel ETC players (Au & Gennis, 1987; Aussel et al, 2014; Falk-Krzesinski & Wolfe, 1998; McNeil et al, 2012). In contrast to growth on

glucose, mutants of several ETC components exhibit severe growth defect on non-fermentable carbon sources. For example, NADH dehydrogenase I (Nuo) is essential for growth on acetate whereas *nuo* deletion strains show growth similar to wild-type (WT) on glucose (Falk-Krzesinski & Wolfe, 1998), and the active complex of succinate dehydrogenase is required for growth on acetate and succinate, however, the mutant with the inactive complex can grow in glucose (Creaghan & Guest, 1978; McNeil et al, 2012).

Different non-fermentable carbon sources enter into the tri-carboxylic acid (TCA) cycle at varied steps (Fig. 1.1, Chapter I) and are theoretically expected to generate different amounts of reduced cofactors, thus even amongst non-fermentable carbon sources, there could be a difference in the requirement of ETC components. However, this scenario has not been investigated. Besides a fundamental perspective, these studies can help identify ETC components that can be targeted to influence the growth of commensal/ pathogenic *E. coli* strains on non-fermentable carbon sources.

In this study, we compared the existing high-throughput datasets wherein the Keio deletion library (single-gene deletion library of *E. coli* K12 covering ~4000 genes) was screened on minimal media supplemented with fermentable (glucose, glucosamine, N-acetyl glucosamine, and maltose) and non-fermentable carbon sources (acetate, glycerol, oleate, and succinate) (Agrawal et al, 2017; Nichols et al, 2011). This large-scale analysis revealed the differential requirement of ETC components on non-fermentable carbon sources. The requirement of ETC components was inversely correlated with the energy yield of non-fermentable carbon sources; however, the requirement of ubiquinone was maximal for growth in oleate, a long-chain fatty acid (LCFA) with eighteen carbon atoms. Importantly, the work of another Ph.D. student from the lab, Shashank Agrawal, showed that LCFA transport and degradation results in oxidative stress in *E. coli* (Agrawal, 2018; Agrawal et al, 2017). Following up on these observations that ubiquinone is maximally

required for growth on LCFAs amongst all tested non-fermentable carbon sources and LCFA degradation generates oxidative stress, we showed that the increased requirement of ubiquinone on LCFAs is to mitigate oxidative stress.

3.2 Results

3.2.1 ETC is differentially required for growth on non-fermentable carbon sources

To understand the requirement of ETC components in *E. coli* for growth on various non-fermentable carbon sources, we re-analyzed data from a previous screen of the Keio deletion library on various fermentable (glucose, glucosamine, N-acetyl glucosamine, and maltose) and non-fermentable carbon sources (acetate, glycerol, and succinate) (Nichols et al, 2011). In addition, in our lab, a genetic screen was performed by Dr. Rachna Chaba where the growth profile of the Keio deletion library on a non-fermentable carbon source, oleate, was compared to that on the fermentable carbon source, glucose (Agrawal et al, 2017). In all these screens, the Keio deletion library was arrayed in 1536- format and pinned onto solid minimal medium plates containing the desired carbon source and colony size was used as a parameter to assign fitness score to the mutants (Agrawal et al, 2017; Shiver et al, 2016). Therefore, collectively, we compared high-throughput screens of the *E. coli* deletion library on eight different carbon sources to understand the differential requirement of ETC components for growth.

3.2.1.1 Comparative analysis of the growth of mutants from the Keio deletion library on fermentable and non-fermentable carbon sources

In the LCFA dataset, fitness-score to mutants in the oleate condition was assigned by computing the statistical significance of the difference in colony size between oleate and glucose control (Agrawal, 2018; Agrawal et al, 2017). To facilitate the comparison of datasets from two separate studies (Agrawal, 2018; Agrawal et al, 2017; Nichols et al, 2011), the datasets from high-throughput screens performed by (Nichols et al, 2011) were

re-analysed by comparing the growth of mutants on both fermentable (glucosamine, N-acetyl glucosamine, and maltose) and non-fermentable (acetate, glycerol, and succinate) carbon sources to glucose control (done in collaboration with Dr. Anthony Shiver). The fitness scores reported thus represent the statistical significance of a change in colony size on a particular carbon source as compared with growth on glucose with positive and negative fitness scores representing increased and decreased colony size, respectively. A full list of fitness scores of Keio library strains in different carbon sources (normalized to a glucose control) is available as "Supplemental Dataset" at https://www.jbc.org/content/292/49/20086/suppl/DC1.

3.2.1.2 GSEA analysis reveals the critical requirement of ETC and TCA and glyoxylate cycles for growth on non-fermentable carbon sources

The requirement of ETC is more for growth on non-fermentable carbon sources as compared to fermentable carbon sources (as described in the introduction to this chapter). Besides this, TCA and glyoxylate cycles are also important for growth on non-fermentable carbon sources. This is because non-fermentable carbon sources generate several metabolic intermediates for growth only in TCA and glyoxylate cycles, whereas these metabolic intermediates can be generated through glycolysis during growth in fermentable carbon sources (Cronan & Laporte, 2006; Layer et al, 2010; Romano & Nickerson, 1958). Before further probing the requirement of ETC on different non-fermentable carbon sources, we first verified the accuracy of our statistical approach by ensuring that as reported in the literature in our comparative analysis genes encoding components of ETC and TCA and glyoxylate cycles are required more on non-fermentable carbon sources compared to fermentable carbon sources.

To understand whether the given phenotype of a mutant is physiologically relevant, we carried out analysis that uses gene sets of a pathway or a complex to associate with its

phenotype. We performed a global analysis using Gene Set Enrichment Analysis (GSEA) and gold standard biological pathways (Keseler et al, 2013; Mootha et al, 2003; Subramanian et al, 2005) to find pathways that have a substantial role in growth on the tested carbon sources (Appendix 1). Importantly, β-oxidation pathway (FDR q-value: 1.1%) was critical only for the utilization of oleate, emphasizing the accuracy of our analysis. Oleate, acetate, and succinate showed significant enrichment in TCA and glyoxylate cycles (FDR q-value <5%). This result was expected as TCA and glyoxylate cycles are critical for the generation of reduced cofactors and metabolites for growth on non-fermentable carbon sources (Cronan & Laporte, 2006). Oleate, acetate, and succinate utilization also displayed enrichment in multiple pathways for respiratory chain activity (FDR q-value <5%), emphasizing the role of ETC in energy generation during growth on non-fermentable carbon sources (Appendix 1). The requirement of gluconeogenesis is expected to be more on carbon sources which do not enter directly into glycolysis since gluconeogenesis provides several critical cellular precursors during growth on these carbon sources. Importantly, the GSEA analysis shows significant enrichment of gluconeogenesis in LCFAs (FDR q-value: 1.3%; Appendix 1). We subsequently performed GSEA analysis for protein complexes containing three or more proteins (Keseler et al, 2013; Subramanian et al, 2005). Oleate, acetate, and succinate utilization exhibited enrichment for ETC complexes, NADH dehydrogenase I (Nuo) (FDR q-value <1%) and succinate dehydrogenase (FDR q-value <7%) (Appendix 2).

Although glycerol is considered to be a non-fermentable carbon source, this substrate did not show significant enrichment of any of the ETC pathways or complexes in our GSEA analysis. We speculate that because there is ATP generation (by substrate-level phosphorylation) after the entry of glycerol in the later part of glycolysis (Booth, 2005), this ATP might allow for growth on glycerol. Moreover, the fermentative utilization of

glycerol has also been suggested (Dharmadi et al, 2006). Thus, for detailed studies on the requirement of ETC components for growth on non-fermentable carbon sources, we further focused on oleate, acetate, and succinate.

3.2.1.3 Differential requirement of ETC components for growth on non-fermentable carbon sources

A comparison of high-throughput genetic screens on different carbon sources clearly showed that ETC is critical for the growth of *E. coli* on non-fermentable carbon sources. Figure 3.1 shows a heatmap of the fitness scores of strains deleted for various ETC components. It is evident that even amongst non-fermentable carbon sources, there is a difference in the requirement of various ETC components. NADH dehydrogenase I (Nuo) and terminal oxidase (Cyo) shows more requirement for growth in acetate compared to other non-fermentable carbon sources. In contrast, genes involved in ubiquinone biosynthesis are required more for growth in oleate. Succinate dehydrogenase seems to be equally important for growth in all non-fermentable carbon sources.

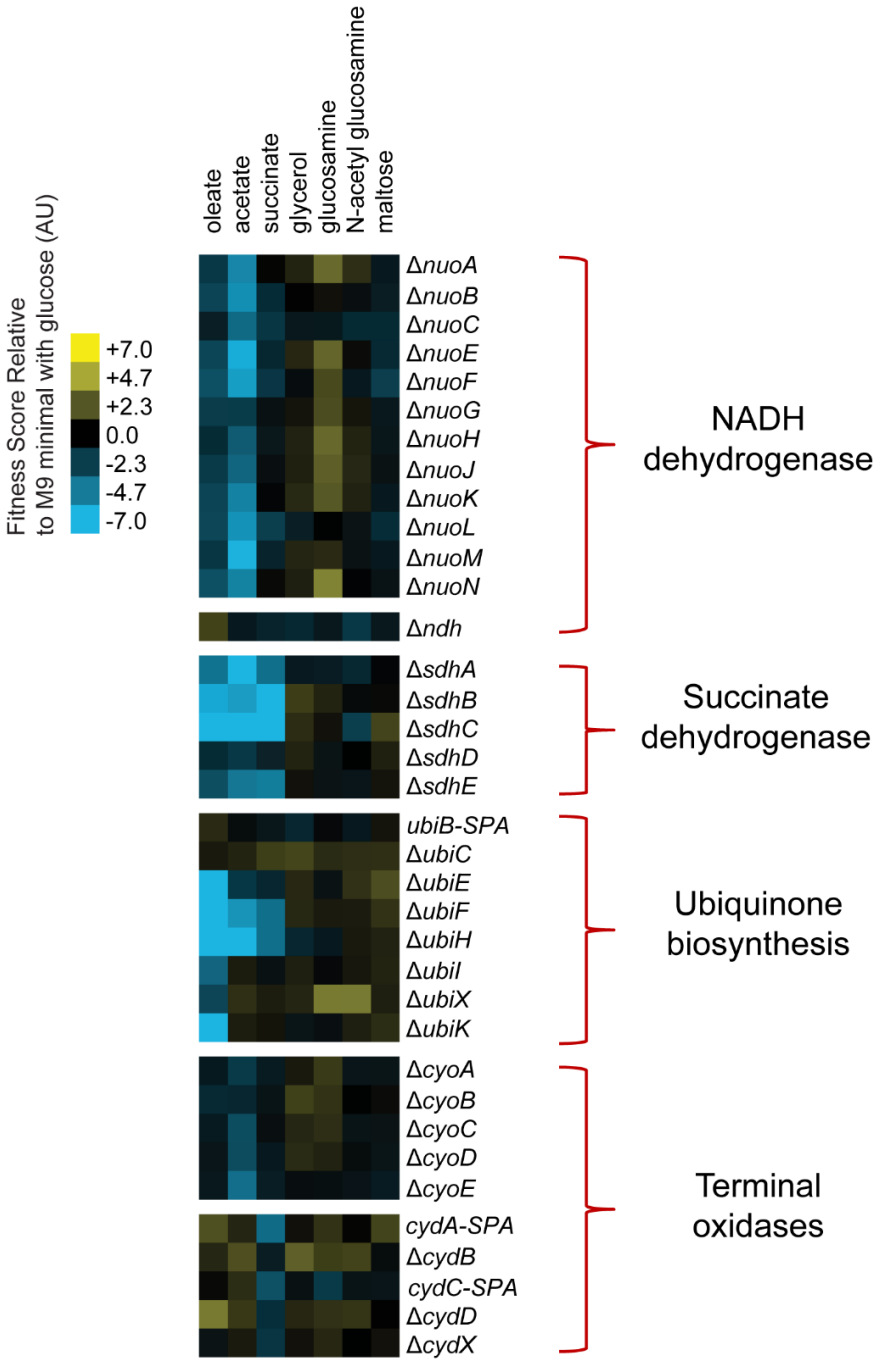

Figure 3.1. Comparative analysis of high-throughput genetic screens of the Keio deletion library on various carbon sources reveals the differential requirement of ETC components for growth on non-fermentable carbon sources. Fitness scores were calculated for all carbon sources as compared to glucose control, as described in Materials and Methods. A heat map of the fitness scores of strains deleted for genes encoding ETC components is shown. Positive and negative fitness scores represent growth advantage and growth defect in the specified carbon source, respectively. The Keio deletion library has SPA-tagged derivatives of some essential genes, and these were also included in the analysis.

3.2.2 Requirement of ETC components correlates with the energy yield of non-fermentable carbon sources

High-throughput genetic screens enable the study of a large set of strains/conditions at a time; however, issues such as incorrect strains in the library, suppressors, and cross-contamination have to be considered before deriving conclusions about the phenotypes of mutants. Considering these limitations of high-throughput datasets, I verified the growth phenotype of ETC components at a candidate level. Furthermore, because oxygen availability to cells in a colony varies with the size of the colony (Pipe & Grimson, 2008), I validated the requirement of ETC components in aerobic metabolism by assessing their phenotypes in the liquid medium. I made fresh transductants of deletion strains of various ETC components and compared their growth on glucose, acetate, succinate, and oleate.

3.2.2.1 Amongst non-fermentable carbon sources, NADH dehydrogenase I (Nuo) is maximally required for growth in acetate

Of the two NADH dehydrogenases involved in ETC, Ndh is known to be more important during aerobic respiration, whereas Nuo is essential for dimethyl sulfoxide and fumarate (anaerobic) respiration (Friedrich & Pohl, 2007; Tran et al, 1997). However, our comparative analysis showed that for aerobic metabolism of oleate, acetate, and succinate, Nuo was important, whereas Ndh was dispensable (Fig. 3.1). The growth defect of *nuo* mutants for growth on acetate as well as on a few amino acids has previously been reported (Falk-Krzesinski & Wolfe, 1998; Pruss et al, 1994); however, the relative requirement of Ndh and Nuo has not been assessed. To compare the requirement of NADH dehydrogenases on different non-fermentable carbon sources, we used fresh transductants of Δ*nuo* and Δ*ndh* strains. Δ*nuo* strain carries a deletion of all 13 genes required for the synthesis of different subunits of NADH dehydrogenase I and Δ*ndh* is the deletion in the single subunit dehydrogenase, NADH dehydrogenase II. We compared the growth profile

of Δ*nuo* and Δ*ndh* in the liquid minimal medium supplemented with glucose, acetate, succinate, or oleate. Whereas Δ*ndh* did not show growth defect in any carbon source, Δ*nuo* showed a significant growth defect in all three non-fermentable carbon sources (Fig. 3.2). We suggest that because Nuo can couple NADH oxidation to proton translocation ($H^+/2e^-$ = 4) whereas Ndh cannot ($H^+/2e^-$ = 0) (Friedrich & Pohl, 2007; Unden et al, 2014), it is likely that Nuo is required for ATP production during growth on non-fermentable carbon sources.

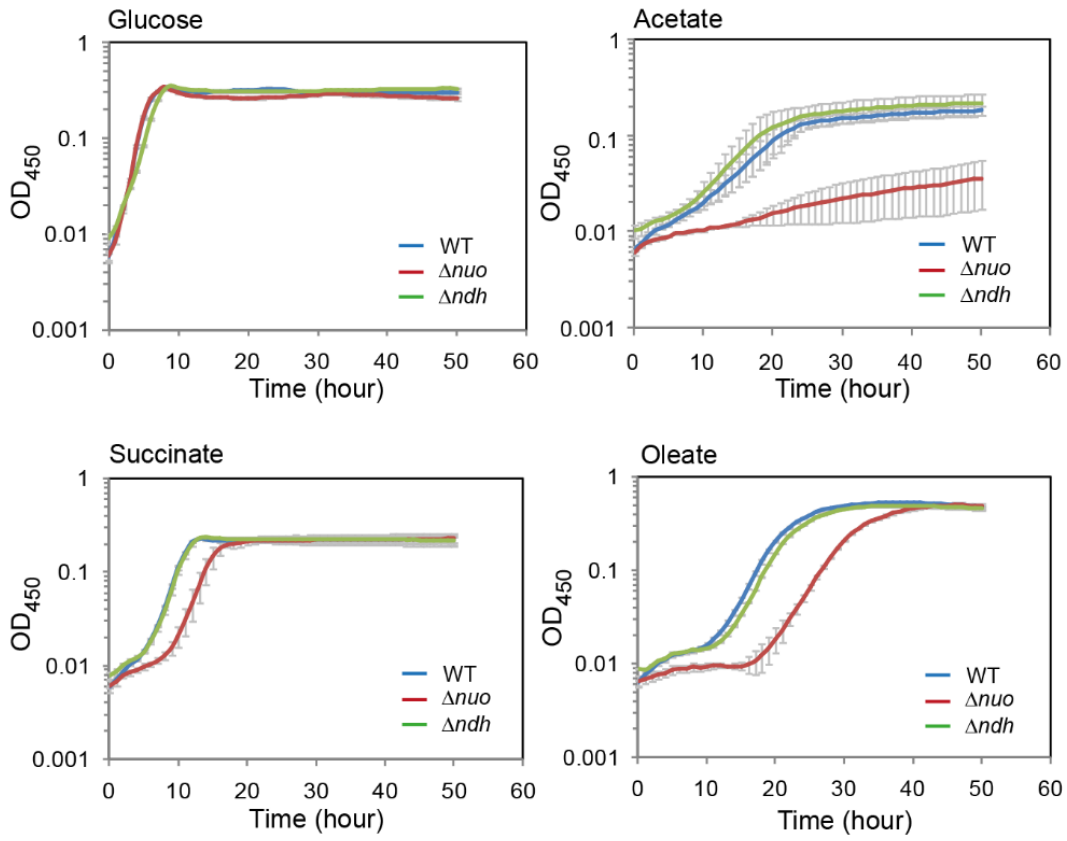

Figure 3.2. Among NADH dehydrogenases, only Nuo complex is required for growth on non-fermentable carbon sources. WT, Δ*nuo*, and Δ*ndh* strains were grown in minimal medium containing glucose, acetate, succinate, or oleate, and OD_{450} was measured. Each medium condition had Brij-58. The experiment was repeated 4 times; each experiment had 2 technical replicates. A representative dataset with average and SD of technical replicates is shown.

Amongst non-fermentable carbon sources, the requirement of Nuo for growth was maximal in acetate (Fig. 3.2). Whereas Δ*nuo* did not grow in acetate, the strain showed an

extended lag in oleate and succinate but grew at the same growth rate and to the same yield as the WT strain (Fig. 3.2). To exclude the possibility of Δ*nuo* strain picking-up suppressors in oleate and succinate, we sub-cultured cells from the stationary phase. The Δ*nuo* strain again showed the same phenotype of extended lag in succinate and oleate. Importantly, acetate has the worst net ATP yield amongst the three tested non-fermentable carbon sources (Clark & Cronan, 2005). Our results thus suggest that the quantitative contribution of Nuo to growth on non-fermentable carbon sources is inversely correlated with the energy yield of these substrates.

3.2.2.2 Amongst non-fermentable carbon sources, requirement of Cyo is highest during growth in acetate

Our comparative analysis showed that Cyo, the major terminal oxidase during aerobic metabolism, is maximally required for growth in acetate (Fig. 3.1). To verify the requirement of Cyo on different non-fermentable carbon sources, we used fresh transductants of Δ*cyoA* strain, which carries a deletion in one of the catalytic subunits of the Cyo terminal oxidase. Δ*cyoA* showed growth defect in acetate, oleate, and succinate (Fig. 3.3). However, amongst these non-fermentable carbon sources, the generation time of Δ*cyoA* strain was severely affected in acetate (Table. 3.1). Similar to NADH dehydrogenase I (Nuo), Cyo also generates proton motive force in the ETC ($H^+/2e^-$ = 4) (Unden et al, 2014), thereby suggesting the inverse correlation between the requirement of this terminal oxidase and the energy yield of non-fermentable carbon sources.

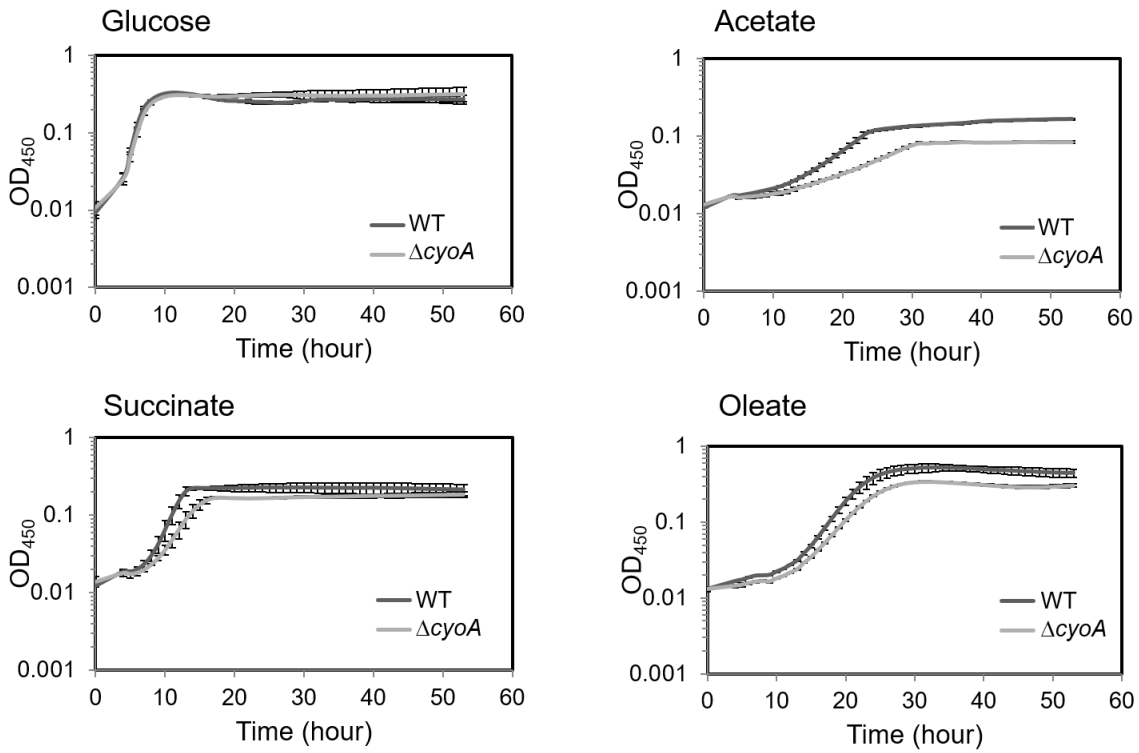

Figure 3.3. Requirement of Cyo is higher in acetate in comparison to other non-fermentable carbon sources. WT and Δ*cyoA* strains were grown in minimal medium containing glucose, acetate, succinate, or oleate, and OD_{450} was measured. Each medium condition contained Brij-58. The experiment was repeated 2 times; each experiment had 3 technical replicates. A representative dataset with average and SD of technical replicates is shown.

Table. 3.1. Generation time (in hour) of Δ*cyoA* strain on different non-fermentable carbon sources (calculated from the above semi-log plot). The p-values were calculated using the unpaired two-tailed Student's t test (***, P<0.0005; **, P<0.005; *, P<0.05 ns, P>0.05).

C- Source	WT	Δ*cyoA*	p-value
Glucose	1.29±0.12	1.32±0.07	0.7723 (NS)
Acetate	4.16±0.15	8.17±0.19	0.0001 (***)
Succinate	1.63±0.08	2.63±0.58	0.0403 (*)
Oleate	2.58±0.11	3.11±0.01	0.0013 (**)

3.2.2.3 Succinate dehydrogenase is essential for growth in all non-fermentable carbon sources

Succinate dehydrogenase (Sdh) is an essential component of the TCA cycle as well as ETC, so the deletion of genes encoding components of Sdh complex disrupts the functioning of both processes. To check for the requirement of succinate dehydrogenase, we used Δ*sdhB* strain deleted for one of the components of this respiratory complex. Contrary to normal growth in glucose, Δ*sdhB* strain did not grow at all in any of the tested non-fermentable carbon sources. This result is consistent with the requirement of optimal functioning of ETC and TCA cycle for growth on non-fermentable carbon sources because these are the only processes that generate energy and metabolic intermediates, respectively, on these substrates (Fig. 3.4).

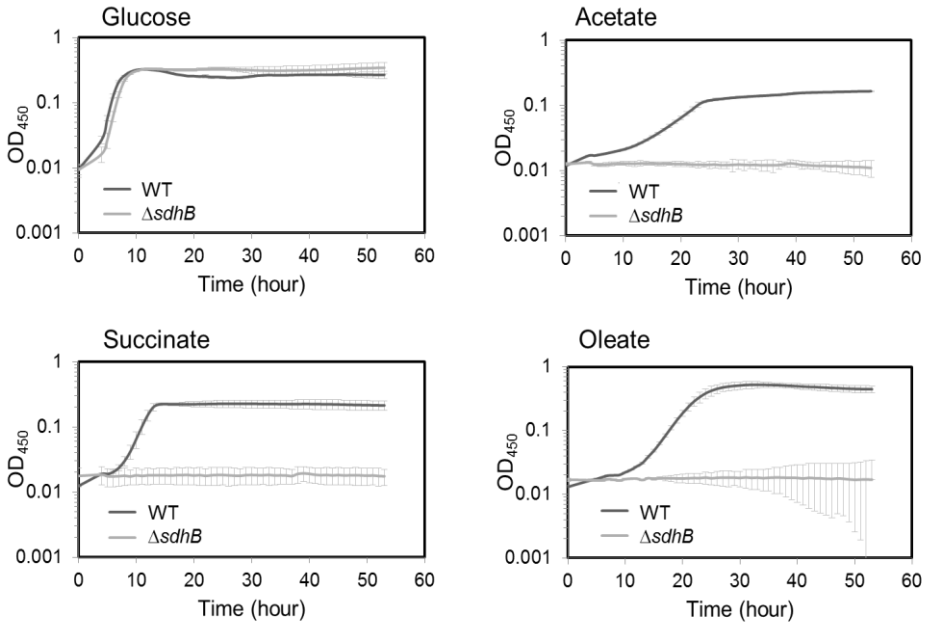

Figure 3.4. Succinate dehydrogenase is essential for growth in all non-fermentable carbon sources. WT and Δ*sdhB* strains were grown in minimal medium containing glucose, acetate, succinate, or oleate, and OD_{450} was measured. Each medium condition contained Brij-58. The experiment was done once and had 3 technical replicates. The dataset with average and SD of technical replicates is shown.

Collectively, our results emphasize that the requirement of ETC complexes on non-fermentable carbon sources inversely correlates with the ATP yield of these substrates.

3.2.3 Requirement of ubiquinone does not correlate with the energy yield of non-fermentable carbon sources

In our comparative analysis, we observed that in contrast to other ETC components, the requirement of ubiquinone was maximal in oleate amongst all tested non-fermentable carbon sources (Fig. 3.1). In *E. coli*, the biosynthesis of ubiquinone is known to involve at least 13 *ubi* genes (Aussel et al, 2014; Hajj Chehade et al, 2019; Loiseau et al, 2017). In the high-throughput datasets that were used for comparative analysis, the fitness scores on non-fermentable carbon sources were available for only eight *ubi* deletion strains (Nichols et al, 2011) (Fig. 3.1). Amongst these eight *ubi* genes, prior to this comparative analysis, the growth phenotype of null mutants of only five *ubi* genes (*ubiE*, *ubiF*, *ubiH*, *ubiI*, and *ubiX*) was reported in succinate: *ubiE*, *ubiF*, and *ubiH* mutants exhibited no growth (Lee et al, 1997; Pelosi et al, 2016), *ubiX* mutant showed a growth defect (Gulmezian et al, 2007), and the *ubiI* mutant displayed WT growth (Hajj Chehade et al, 2013; Pelosi et al, 2016). In another study in our lab (Agrawal, 2018; Agrawal et al, 2017), the growth phenotype of these five *ubi* mutants was compared at a candidate level on solid minimal medium containing succinate or oleate as the carbon source. The phenotype of all *ubi* mutants corroborated with their known phenotypes in succinate. In oleate, *ubi* mutants either did not grow at all (*ubiE*, *ubiF*, and *ubiH*) or showed a significant growth defect (*ubiI* and *ubiX*) in comparison to WT (Agrawal, 2018; Agrawal et al, 2017). Collectively, the requirement of *ubi* genes for growth was significantly higher in oleate in comparison to succinate.

In our comparative analysis, in addition to succinate and oleate, the growth of ETC components was also compared on acetate. As shown above, the requirement of respiratory complexes, Nuo and Cyo, was more in acetate in comparison to oleate and succinate,

suggesting that the requirement of these ETC components inversely correlates with the energy yield of non-fermentable carbon sources (Fig. 3.1, 3.2 & 3.3; Table. 3.1). Because in the comparative analysis, the requirement of ubiquinone did not follow this trend, it was necessary to validate the requirement of *ubi* genes at a candidate level on non-fermentable carbon sources, including acetate. Further, because on the solid medium, oxygen availability depends on the size of the colony (Pipe & Grimson, 2008), it was important to confirm the requirement of *ubi* genes in aerobic metabolism of non-fermentable carbon sources by assessing their phenotypes in the liquid medium. We selected two *ubi* genes (*ubiI* and *ubiH*) and assessed the growth phenotype of their mutants on glucose, acetate, succinate, and oleate in liquid minimal medium. As shown in Fig. 3.5 A, Δ*ubiH* strain showed a growth reduction in glucose and no growth in acetate, oleate, and succinate. On the other hand, Δ*ubiI* strain showed a significant growth defect only in oleate. The growth defect of the Δ*ubiI* strain was complemented by *ubiI* cloned on plasmid (Fig. 3.5 B). Upon relating the growth profile of *ubi* deletion strains observed in our study with their ubiquinone levels reported in literature, we find that the *ubiH* mutant with no detectable ubiquinone (Pelosi et al, 2016) does not grow in any of the three non-fermentable carbon sources, whereas the *ubiI* mutant, which produces reduced levels of ubiquinone (Hajj Chehade et al, 2013), exhibits significant growth defect only in oleate. UbiI catalyzes C5-hydroxylation of the 3-octaprenylphenol intermediate in the ubiquinone biosynthesis pathway, and the residual level of ubiquinone in a Δ*ubiI* strain is attributed to the suboptimal C5-hydroxylase activity of a C6-monooxygenase, UbiF (Hajj Chehade et al, 2013).

For the last several decades, the higher requirement of ubiquinone for energy generation during growth with succinate compared to glucose has been used as the basis for identifying genes involved in ubiquinone biosynthesis (Stroobant et al, 1972; Wu et al,

1993). Despite this, it was surprising that a study showed that Δ*ubiI*, where the ubiquinone level is reduced to only ~10–15% of WT level, exhibited normal growth in succinate (Hajj Chehade et al, 2013; Pelosi et al, 2016). Work presented here on comparison of the growth phenotype of Δ*ubiI* strain in liquid minimal medium containing acetate, oleate, or succinate and the phenotype reported earlier in our lab on solid minimal medium supplemented with oleate or succinate emphasize that whereas 10% ubiquinone is sufficient for growth on acetate and succinate, this ubiquinone level is clearly sub-optimal for growth in oleate.

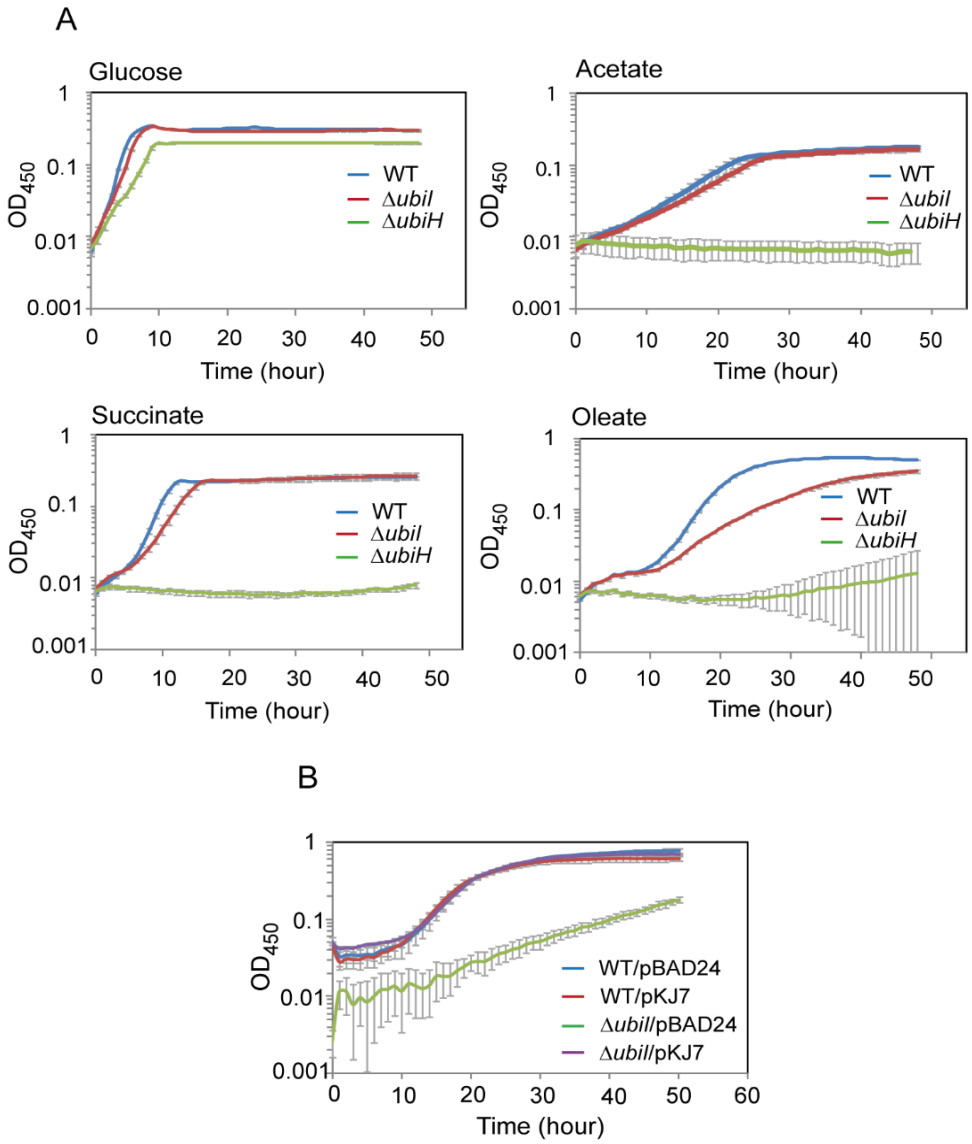

Figure 3.5. Δ*ubiI* shows a significant growth defect in oleate in comparison to other non-fermentable carbon sources. (A) WT, Δ*ubiH*, and Δ*ubiI* strains were grown in minimal medium containing glucose, acetate, succinate or oleate, and OD_{450} was measured.

Each medium condition contained Brij-58. The experiment was repeated 3 times; each experiment had 3 technical replicates. A representative dataset with average and SD of technical replicates is shown. (B) *ubiI* cloned in plasmid complements the growth phenotype of Δ*ubiI* strain in oleate. WT and Δ*ubiI* strains containing vector (pBAD24) and *ubiI* cloned in pBAD24 (pKJ7) were grown in minimal medium containing oleate, and OD_{450} was measured. Each medium condition had Brij-58. The experiment was repeated 3 times; each experiment had 3 technical replicates. A representative dataset with average and SD of technical replicates is shown.

In our lab, oleate transport and degradation have been shown to induce oxidative stress in *E. coli*, and chemical antioxidants, thiourea and vitamin C (ascorbate) have been shown to partially recover the growth defect of *ubiI* mutant on solid minimal medium supplemented with oleate (Agrawal, 2018; Agrawal et al, 2017). Here, we validated the recovery of the growth of *ubiI* mutant in liquid minimal medium using glutathione and thiourea, widely used chemical antioxidants in *E. coli* (Dwyer et al, 2014; Erental et al, 2014; Goswami et al, 2006). Interestingly, WT strain also grew better in the presence of antioxidants emphasizing that indeed cells are under oxidative stress during growth in oleate (Fig. 3.6). We did not observe a complete growth recovery of Δ*ubiI* in oleate supplemented with antioxidants because another factor responsible for the growth defect would be decreased energy generation due to hampered ETC function.

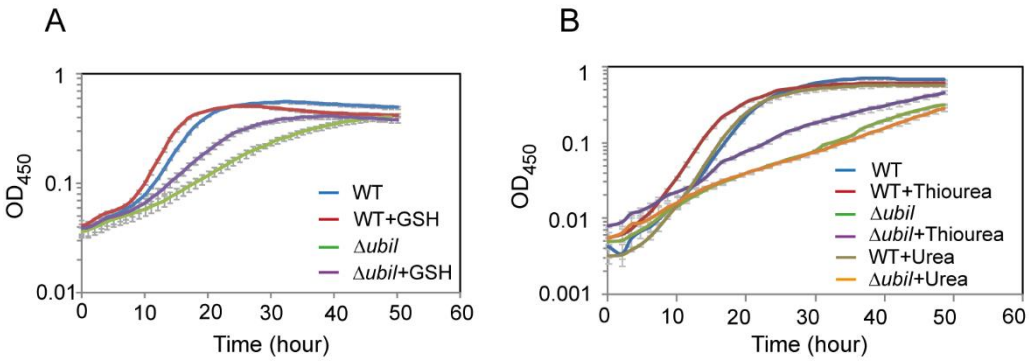

Figure 3.6. Growth defect of Δ*ubiI* in oleate is partially recovered by antioxidants, glutathione (A) and thiourea (B). WT and Δ*ubiI* were grown in minimal medium containing oleate with or without 1 mM glutathione (GSH) or 1 mM thiourea, and OD_{450} was measured. Urea (1 mM) was added as a control for the thiourea experiment. The

experiment was repeated 3 times; each experiment had 3 technical replicates. A representative dataset with average and SD of technical replicates is shown.

Our results that amongst the three tested non-fermentable carbon sources, acetate, oleate and succinate, Δ*ubiI* showed significant growth defect only in oleate and that this growth defect could be partially recovered by chemical antioxidants, suggested that metabolism of oleate generates maximum ROS levels amongst the above non-fermentable carbon sources and the requirement of ubiquinone is maximal during oleate metabolism to counteract oxidative stress. To test this proposal, another Ph.D. student from the lab, Shashank Agrawal, investigated ROS levels in *E. coli* cultured in acetate, oleate and succinate. WT had the highest ROS levels in basal medium supplemented with oleate; ~1.5-fold higher than basal medium. Moreover, ROS levels further increased in Δ*ubiI* in all media conditions with maximal ROS levels again in oleate supplemented cells (Agrawal et al, 2017).

Taken together, amongst all ETC components, the requirement of ubiquinone for growth does not correlate with the energy yield of non-fermentable carbon sources. The requirement of ubiquinone is maximal during oleate metabolism to counteract oxidative stress.

3.2.4 Ubiquinone is the first line of defense against LCFA-induced oxidative stress

In *E. coli*, the ROS scavenging enzymes, superoxide dismutases (SodA, SodB, and SodC), catalases (KatG and KatE) and peroxidases (AhpC-AhpF), and their transcriptional regulators, OxyR, SoxRS, and RpoS, are known to be the major oxidative stress combat players (Chiang & Schellhorn, 2012; Imlay, 2013). However, previous work from our lab suggested that during LCFA metabolism, ubiquinone plays a major role in relieving oxidative stress compared to other oxidative stress response players: *i)* in contrast to strains deleted for genes involved in ubiquinone biosynthesis, strains deleted for genes encoding

other oxidative stress combat players did not show significant fitness defects in the LCFA dataset, and *ii)* whereas in basal medium, ROS levels increase in strains deleted for genes involved in ubiquinone biosynthesis, genes encoding enzymatic scavengers (AhpC, SodA, and KatE) or genes encoding regulators of enzymatic scavengers (SoxR), in basal medium supplemented with oleate, ROS levels further increase only in *ubi* deletion strains (Agrawal, 2018; Agrawal et al, 2017). In the data presented below, by assessing the growth phenotype of strains deleted for genes encoding enzymatic scavengers or their regulators, at a candidate level, and by determining the induction of enzymatic scavengers in oleate-grown cells in WT and *ubi* deletion strains, in this study, we established that as long as the optimal level of ubiquinone is produced in the cell, it does not allow ROS to build-up further in oleate-utilizing cells, thereby reducing dependency on other oxidative stress players.

3.2.4.1 Requirement of ubiquinone is higher for growth in oleate in comparison to ROS scavengers

OxyR is a transcriptional regulator that directly senses H_2O_2 and regulates the transcription of *katG* and *ahpC*. We checked the growth phenotype of *katG*, *ahpC,* and *oxyR* deletion strains in minimal medium containing oleate and compared with the growth phenotype of the *ubiI* mutant. In oleate, Δ*katG* and Δ*ahpC* showed increased lag; however, they exhibited doubling time similar to the WT. The Δ*oxyR* strain showed slower growth in the early phase; however, it grew better later in the exponential phase. The Δ*ubiI* strain showed slower growth in oleate, all throughout. Therefore, whereas Δ*katG*, Δ*ahpC,* and Δ*oxyR* strains reached stationary phase optical density similar to WT, Δ*ubiI* strain had a considerably reduced stationary phase growth. In glucose, none of these strains exhibited any growth defect (Fig. 3.7; Table. 3.2).

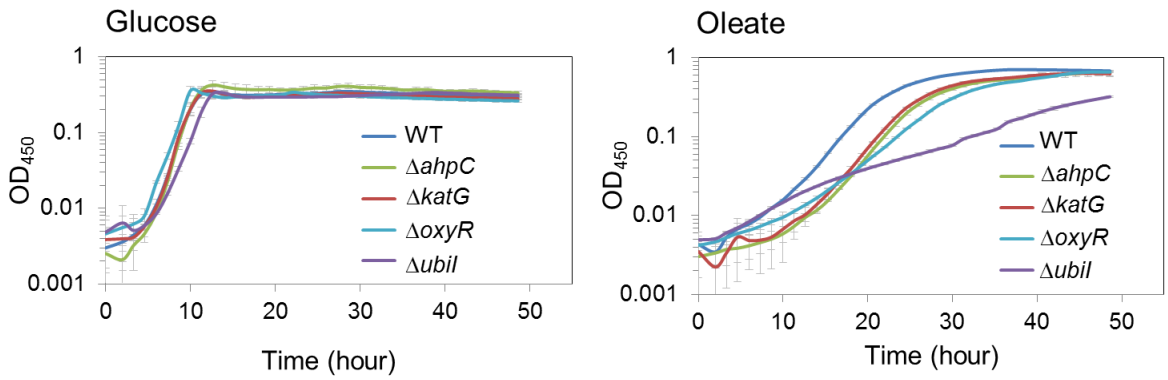

Figure 3.7. Ubiquinone deficient strain shows significant growth defect in oleate in comparison to strains deleted for genes encoding enzymatic scavengers or their regulator. WT, Δ*ubiI*, Δ*oxyR*, Δ*katG*, and Δ*ahpC* strains were grown in minimal medium containing either glucose or oleate, and OD_{450} was measured. Each medium condition had Brij-58. Experiment was done 2 times; each experiment had 3 technical replicates. A representative dataset, with average (± SD) of technical replicates, is shown.

Table. 3.2 Generation time (in hour) of strains deleted either for *ubiI*, *oxyR* or its regulon members (*katG* and *ahpC*) in glucose and oleate (calculated from the above semi-log plot).

C- source / Strains	Glucose	Oleate
WT	0.97±0.07	2.57±.026
Δ*ahpC*	0.91±.04	2.62±0.11
Δ*katG*	0.94±.033	2.54±0.26
Δ*oxyR*	1.27±.066	3.81±0.07
Δ*ubiI*	1.13±.045	7.73±0.88

Our above results suggested that in Δ*katG*, Δ*ahpC*, and Δ*oxyR* strains, since ubiquinone is present, bacteria are able to manage oxidative stress generated by LCFA metabolism, however, when cells are deprived of ubiquinone (as in Δ*ubiI* strain), enzymatic players are able to combat ROS but not to the same extent. To test this, we made double deletion strains of *katG ubiI*, *ahpC ubiI*, and *oxyR ubiI* and checked their growth phenotype. Compared to the single deletion strains, the double mutants showed severe growth defect in oleate (Fig. 3.8).

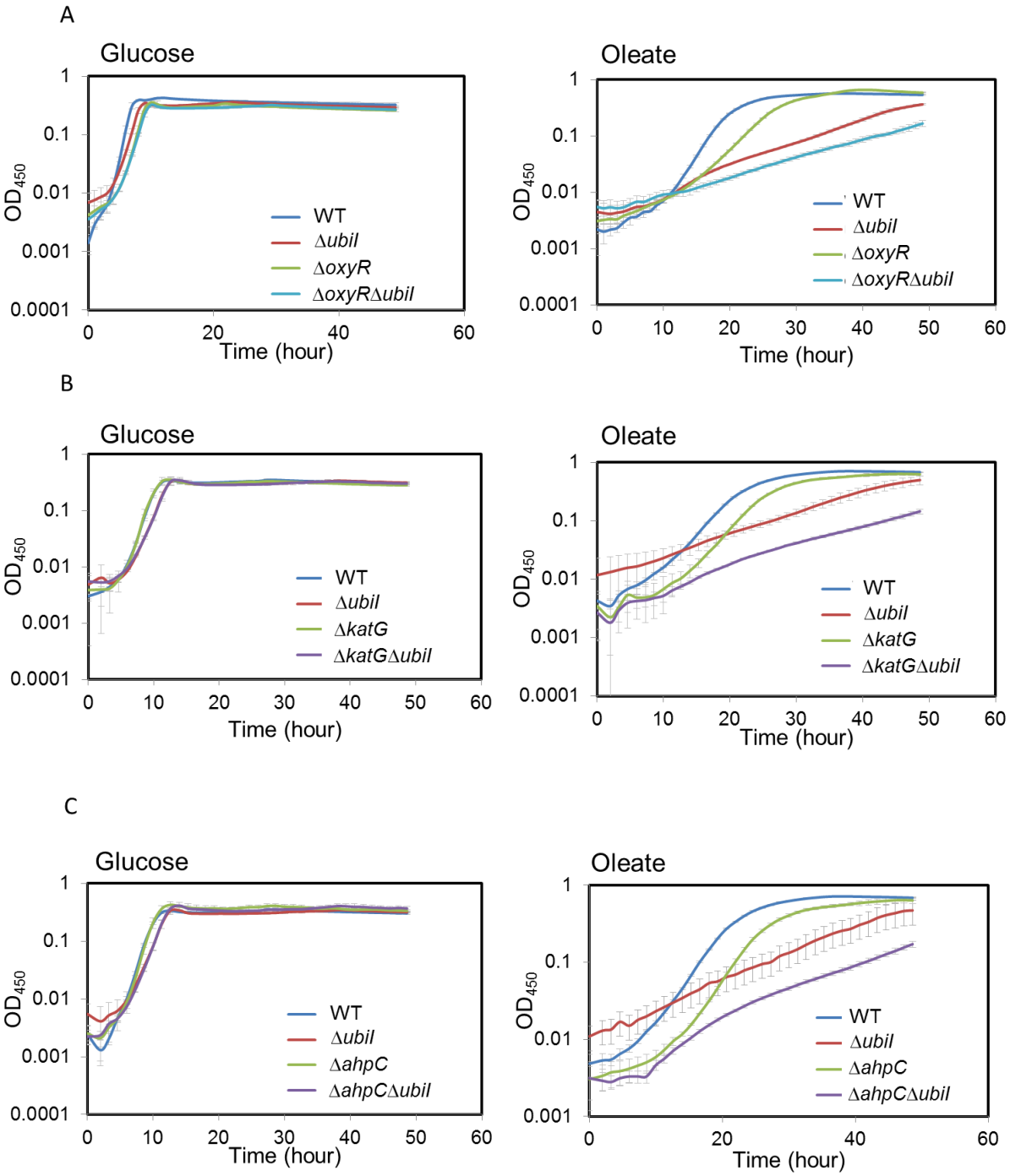

Figure 3.8. Δ*ubiI* strain carrying additional deletion of *oxyR* or its regulon members (*katG* and *ahpC*) shows severe growth defect in oleate. WT, Δ*ubiI*, Δ*oxyR* and Δ*ubiI*Δ*oxyR* strains (A), WT, Δ*ubiI*, Δ*katG*, and Δ*ubiI*Δ*katG* strains (B), and WT, Δ*ubiI*, Δ*ahpC*, and Δ*ubiI*Δ*ahpC* strains (C) were grown in minimal medium containing either glucose or oleate, and OD_{450} was measured. Each medium condition had Brij-58. Experiment was done 2 times (A & B) and once (C); each experiment had at least 2 technical replicates. A representative dataset is shown.

3.2.4.2 Enzymatic scavengers are induced in ubiquinone deficient strains grown in oleate

To further investigate whether enzymatic scavengers play a secondary role in managing ROS during LCFA metabolism, we examined their induction in *E. coli* cultured in oleate. For these experiments, we had to use Δ*ubiI*, Δ*fadL*, and Δ*fadL*Δ*ubiI* strains which either show growth defect or do not grow at all in minimal medium containing oleate as the sole carbon source. Therefore, we used tryptone broth (TB) medium, which besides allowing the growth of the above mutants, enables co-utilization of oleate. We monitored the induction of β-galactosidase (β-gal) from the promoter of *katG* and *ahpC*. Although we did not observe the induction of enzymatic scavengers in WT strain grown in TB supplemented with oleate (TB-Ole), both the enzymatic scavengers were induced (~2-fold) by oleate in a Δ*ubiI* strain. Importantly, the induction of *katG* and *ahpC* in Δ*ubiI* was dependent on oleate-utilization; no induction was observed in a Δ*fadL*Δ*ubiI* strain (Fig. 3.9 A & B). Importantly, the increased expression of scavengers in Δ*ubiI* strain was reduced by ~25% upon exogenous supplementation of ubiquinone-8 (Fig. 3.9 C).

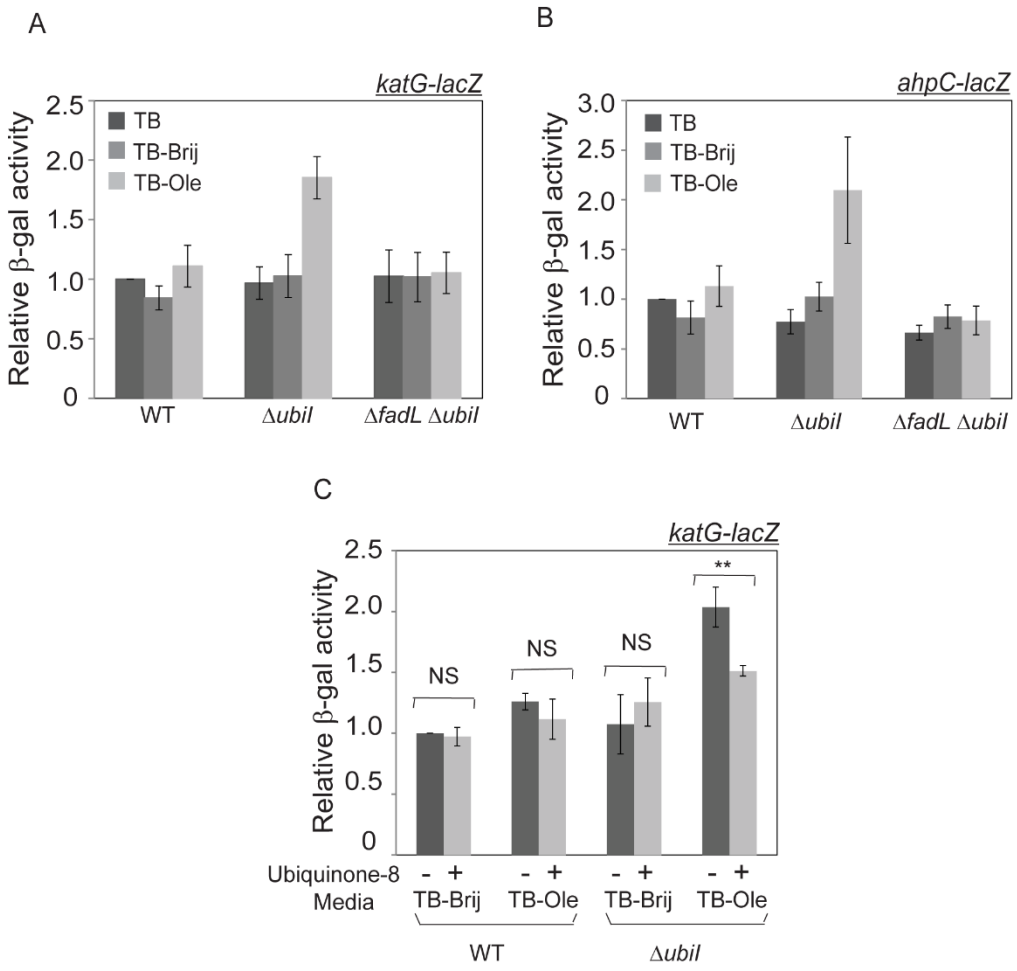

Figure 3.9. Enzymatic scavengers KatG and AhpC are induced during LCFA metabolism when ubiquinone levels are low. WT, Δ*ubiI*, and Δ*fadL*Δ*ubiI* strains carrying either *katG-lacZ* (A) or *ahpC-lacZ* (B) (*lacZ* placed under the H_2O_2 responsive promoter of *katG* or *ahpC*) in MC4100 background were grown in TB, TB-Brij or TB-Ole, and β-gal activity was measured. Data were normalized with the β -gal activity of WT in TB medium and represent average (± SD) of at least 4 independent experiments. The average β-gal activity of WT carrying *katG-lacZ* and *ahpC-lacZ* in TB medium was 166 ± 45 Miller units and 38 ± 15 Miller units, respectively. (C) Supplementation of ubiquinone-8 decreases the induction of *katG-lacZ* in a Δ*ubiI* strain grown in the presence of oleate. WT and Δ*ubiI* strains carrying *katG-lacZ* reporter construct in the MC4100 background were grown either in TB-Brij or TB-Ole medium. Media contained either 0.1% ethanol or 20 µM ubiquinone-8. β-gal activity was measured. Data were normalized with the β-gal activity of WT in TB-Brij with 0.1% ethanol and represent average (± SD) of 3 independent experiments. The average β-gal activity of WT in TB-Brij with 0.1% ethanol was 257 ± 88 Miller units. **, p 0.0058; NS, not significant (unpaired two-tailed Student's t-test).

Taken together, the mild growth defect of strains deleted for genes encoding KatG, AhpC, or OxyR in oleate medium and the induction of *katG* and *ahpC* only in ubiquinone deficient strains grown in oleate validates ubiquinone as the first line of defense against LCFA-induced oxidative stress.

3.3 Discussion

3.3.1 Quantitative contribution of Nuo and Cyo to growth is inversely correlated with the energy yield of non-fermentable carbon sources

E. coli has a versatile respiratory chain which functions to generate ATP and maintain redox balance by reoxidizing reduced cofactors produced by metabolism. The enzyme complexes, Nuo and Cyo couple redox energy to proton translocation by directly pumping protons towards the periplasm, whereas Cyd translocates protons by vectorial transfer method. Besides proton pumping, Cyo also generates PMF by vectorial chemistry like Cyd. However, the bioenergetic efficiency of these respiratory complexes varies: $H^+/2e^-$ ratio is 4 for Nuo, 4 for Cyo, and 2 for Cyd. Considering this, for the aerobic respiratory chain, the maximum theoretical ratio of $8H^+/2e^-$ is achieved when Nuo dehydrogenase is coupled with Cyo terminal oxidase (Unden et al, 2014). The enzyme complexes, Sdh and Ndh, cannot translocate protons and thus do not contribute to PMF.

From the present work, we find that of the two NADH dehydrogenases, Nuo and Ndh, Nuo is the major NADH dehydrogenase for aerobic growth on acetate, oleate, and succinate (Figs. 3.1 & 3.2; Appendix 2). It has been suggested that increased $NADH/NAD^+$ ratio inhibits enzymes involved in TCA and glyoxylate cycles. Because *nuo* mutants would be unable to oxidize NADH efficiently, this would increase the $NADH/NAD^+$ ratio, which would inhibit TCA and glyoxylate cycle enzymes, thereby resulting in a decrease in cellular metabolites (Pruss et al, 1994). Besides, because Nuo is a proton pump ($4H^+/2e^-$) (Unden et al, 2014), its deletion would result in a decrease in ATP synthesis in the cell. Therefore,

in *nuo* mutants grown on non-fermentable carbon sources, ATP would be produced mainly from $FADH_2$ oxidation.

The *nuo* deletion strain exhibited no growth in acetate (Fig. 3.2). We speculate that during acetate metabolism, in addition to the decrease in cellular metabolites caused by increased NADH/NAD^+ ratio, the *nuo* mutant cannot produce energy to support growth. The PMF generated across the inner membrane is used by F_oF_1 ATP synthase for the synthesis of ATP. F_oF_1 ATP synthase functions as a rotary motor and one complete rotation of the enzyme requires 10 to 11 H^+, which are coupled to form 3 ATP molecules, resulting in an H^+/ATP stoichiometry of ~3.5 H^+/ATP (Vik, 2007). For *nuo* mutant, as explained above, ATP can be produced only from $FADH_2$ oxidation and that too when coupled with Cyo terminal oxidase ($4H^+/2e^-$), because coupling with Cyd will lead to $2H^+/2e^-$ ratio, which is not sufficient for ATP generation (Cronan & Laporte, 2006; Unden et al, 2014). Thus, during acetate metabolism, since only 1 $FADH_2$ is produced in one round of the TCA cycle (Cronan & Laporte, 2006), only 1 molecule of ATP will be generated per acetate molecule. However, activation of acetate to acetyl-CoA also requires 1 molecule of ATP (Clark & Cronan, 2005), resulting in no net ATP gain in *nuo* mutant. Unlike acetate, the *nuo* mutant could grow in succinate and oleate, although with an increased lag phase duration. We suggest that because *nuo* mutant can generate energy from the oxidation of $FADH_2$ produced during β-oxidation of oleate and in the first step of succinate utilization (Clark & Cronan, 2005; Unden & Kleefeld, 2004), this allows cells to re-adjust its metabolism to maintain redox balance resulting in the same growth rate and growth yield as WT cells. Furthermore, unlike acetate, activation of succinate is not required for its metabolism, and although the conversion of oleate to oleoyl-CoA is required for oleate metabolism, only 1 molecule of ATP is consumed per 18 carbon atoms (Clark & Cronan, 2005; Unden & Kleefeld, 2004).

The terminal oxidase Cyo also showed maximum growth defect in acetate amongst the three non-fermentable carbon sources (Fig. 3.1 & 3.3; Table. 3.1). Because Cyo, the major terminal oxidase during aerobic metabolism, generates PMF ($4H^+/2e^-$) (Unden et al, 2014), disruption of the Cyo complex would be expected to result in a more compromised growth on carbon sources such as acetate that have poor net ATP yield.

3.3.2 Ubiquinone is the first line of defense against LCFA-induced oxidative stress

In bacteria, the enzymes, peroxidases, catalases, and superoxide dismutases, and the non-enzymatic compound, glutathione, are well-established oxidative stress combat players (Chiang & Schellhorn, 2012; Dwyer et al, 2014; Erental et al, 2014; Goswami et al, 2006; Imlay, 2013). Although the function of ubiquinone as an electron carrier in bacterial ETC is known from the last several decades (Cox et al, 1970), its antioxidant function in bacteria was first suggested by Soballe and Poole in 2000 (Soballe & Poole, 2000). In this study, an *ubiCA* knockout of *E. coli*, which produces no detectable ubiquinone (Sharma et al, 2013), was shown to exhibit several oxidative stress phenotypes in LB: accumulation of superoxide and H_2O_2 in membranes, hypersensitivity to oxidative stress-inducing agents, and up-regulation of catalase (Soballe & Poole, 2000). However, the relative contribution of ubiquinone to the overall oxidative stress defense had not been investigated. Earlier observations from our lab (Agrawal, 2018; Agrawal et al, 2017) and the work presented in this thesis chapter provide evidence that ubiquinone is the major antioxidant during LCFA metabolism. Our following observations collectively suggest that as long as ubiquinone is present in the cell, bacteria can manage LCFA-induced oxidative stress, however, when cells are deprived of ubiquinone, other players are induced and are able to combat ROS but not to the same extent: *i)* compared to the significant growth defect of strain defective in ubiquinone biosynthesis (Δ*ubiI*) in oleate, strains individually deleted for genes encoding catalase, KatG and alkyl hydroperoxide reductase subunit, AhpC or their regulator OxyR

exhibit increased lag or slower growth in the initial phase but are able to grow later at a normal growth rate (Fig. 3.7; Table. 3.2). Thus unlike Δ*ubiI,* strains Δ*katG*, Δ*ahpC* and Δ*oxyR* are able to adapt to LCFA-mediated oxidative stress; *ii)* whereas in basal medium, ROS levels are ~1.3 to 1.7-fold higher when strains lack either the *ubi* genes or other players (alkyl hydroperoxide reductase subunit, AhpC; oxidative stress regulator, SoxR; superoxide dismutase, SodA; catalase, KatE; and an enzyme involved in glutathione biosynthesis, GshB), in medium supplemented with oleate, ROS levels further increase only in *ubi* deletion strains (Agrawal, 2018; Agrawal et al, 2017); *iii)* KatG and AhpC are induced during LCFA metabolism only when ubiquinone levels are decreased suggesting that ubiquinone does not allow ROS to build-up thereby reducing dependency on other oxidative stress combat players (Fig. 3.9); and *iv)* the transport and degradation of LCFAs generates ROS and also results in ubiquinone accumulation, thus the major defense player involved in combating oxidative stress is induced during LCFA metabolism (Agrawal, 2018; Agrawal et al, 2017).

The leakage of electrons in the ETC and autoxidation of reduced respiratory dehydrogenases have been suggested to lead to ROS formation (Imlay, 2013; Messner & Imlay, 1999; Seaver & Imlay, 2004; Soballe & Poole, 2000). Several mechanisms have been proposed to explain the antioxidant role of ubiquinone. The reduced form of ubiquinone (ubiquinol) has been suggested to directly scavenge ROS (Soballe & Poole, 2000). In addition, a study has demonstrated the *in vitro* quinol peroxidase activity of Cyd, where quinol serves as a substrate for the peroxidase to detoxify H_2O_2 (Al-Attar et al, 2016). Thus, during LCFA catabolism, ubiquinol might promote the peroxidase activity of terminal oxidase to clear ROS. One might argue that if the above mechanism holds during LCFA metabolism, then similar to ubiquinone, the requirement of Cyd should be maximal for growth in LCFAs. However, in our comparative analysis, Cyd did not show any specific

requirement in oleate. Besides generating PMF and helping in ATP synthesis, Cyd has other physiological functions, and thus *cyd* deletion results in pleiotropic phenotypes (Green & Gennis, 1983; Jones-Carson et al, 2016; Siegele et al, 1996; Siegele & Kolter, 1993). Therefore, either the quinol peroxidase activity of Cyd is not the mechanism of action of ubiquinone during LCFA metabolism, or it cannot be explained solely on the basis of the growth phenotype of *cyd* deletion strains.

Ubiquinone being an electron carrier, transfers electrons from upstream respiratory dehydrogenases to terminal oxidases in the ETC. The rapid transfer of electrons by ubiquinone has been suggested to decrease the probability of adventitious collision of oxygen with electrons, thereby reducing ROS formation (Soballe & Poole, 2000). Based on LCFA metabolic pathway, LCFA utilization produces a large amount of reduced cofactors. Thus during growth in LCFAs, there would be an increased flow of electrons in the ETC, which would increase the probability of electron leakage and autoxidation of reduced respiratory dehydrogenases, thereby resulting in elevated levels of ROS (Agrawal et al, 2017). Given that ubiquinone accumulates during LCFA metabolism, it might rapidly transfer the large flow of electrons in the ETC, decreasing the residence time of electrons at the sites of ROS formation. However, the comparative analysis of ETC components suggests that the antioxidant role of ubiquinone cannot be explained by its known electron carrier function in the ETC, i.e., transferring electrons from NADH and succinate dehydrogenases to terminal oxidases. Because if that was the case, then similar to ubiquinone, dehydrogenases and/or terminal oxidases would also be more important on LCFAs compared to other non-fermentable carbon sources (Fig. 3.1). Besides NADH and succinate dehydrogenases, an acyl-CoA dehydrogenase FadE also participates in LCFA metabolism. FadE is suggested to catalyze the first step of β-oxidation with concomitant reduction of FAD to $FADH_2$. This $FADH_2$ needs to be reoxidized but whether FadE itself

reoxidizes $FADH_2$ and directly transfers electrons to ubiquinone or requires the involvement of an electron transfer flavoprotein is unclear (Campbell & Cronan, 2002). Nevertheless, if FadE is the predominant dehydrogenase where ROS is formed during LCFA metabolism, ubiquinone might function to rapidly transfer electrons from FadE to quinol oxidases, thereby decreasing ROS formation.

CHAPTER IV

Long-chain fatty acid metabolism compromises envelope redox homeostasis

4.1 Introduction

The multilayered envelope of gram-negative bacteria comprised of the inner membrane, the outer membrane, and the peptidoglycan layer within the periplasm is the site for a myriad of functions critical for cellular growth and viability (reviewed in (Silhavy et al, 2010)). A critical function performed in the envelope is oxidative protein folding. Many secreted proteins require disulfide bonds for their maturation and stability. In *E. coli*, ~300 proteins are predicted to be disulfide-bonded in the periplasm (Dutton et al, 2008). The formation of disulfide bonds in *E. coli* takes place with the help of a periplasmic oxidoreductase, DsbA, which gets reduced after catalyzing the formation of disulfide bonds in substrate proteins. DsbB, an inner membrane disulfide oxidoreductase, performs the re-oxidation of DsbA (Denoncin & Collet, 2013; Manta et al, 2019). Due to the requirement of disulfide bond formation in proteins involved in diverse biological processes, mutants of disulfide bond-forming machinery show pleiotropic phenotypes. For example, *dsbA* and *dsbB* mutants of *E. coli* exhibit dramatic reductions in motility and alkaline phosphatase (AP) activity, and sensitivity to thiol agents such as dithiothreitol (DTT), heavy metals such as cadmium and zinc, and drugs such as benzylpenicillin (Bardwell et al, 1993; Bardwell et al, 1991; Missiakas et al, 1993; Rensing et al, 1997; Stafford et al, 1999). Furthermore, mutants of several pathogenic bacteria defective in disulfide bond formation are attenuated for virulence [Section 1.9.5; (Landeta et al, 2018)].

The ultimate oxidizing power for disulfide bond formation is provided by the electron transport chain (ETC). The reduced form of DsbB is re-oxidized by transferring electrons to the quinones, ubiquinone and menaquinone, under aerobic and anaerobic conditions, respectively. The terminal oxidases finally shuttle electrons from reduced quinones (quinol) to the terminal electron acceptors. For example, cytochrome *bo* transfers electrons from reduced ubiquinone (ubiquinol) to molecular oxygen under aerobic

conditions (Denoncin & Collet, 2013; Manta et al, 2019). This link between ETC and envelope redox homeostasis was demonstrated in earlier *in vivo* studies where the status of disulfide bond formation was examined under conditions of non-operational or defective ETC. For example, *E. coli* grown in a purely fermentative manner, without any terminal electron acceptor, i.e., non-operational ETC, was compromised for disulfide bond formation, and mutants defective in the biosynthesis of the respiratory chain components, heme and quinones accumulated DsbA in a reduced form (Bader et al, 1999; Kobayashi et al, 1997).

In the presence of terminal electron acceptors, i.e., operational ETC, besides transferring electrons from the disulfide bond-forming machinery, quinones play a pivotal role in transferring electrons generated by the metabolism of carbon sources from respiratory dehydrogenases to the terminal oxidases (Unden et al, 2014). The convergence of metabolism and disulfide bond formation at the level of quinones in the ETC tempted us to speculate that metabolic conditions that increase electron flow in the ETC might limit quinones from taking up electrons from the disulfide bond-forming machinery, thereby compromising envelope redox homeostasis. So far, this scenario has not been investigated. Besides a fundamental perspective, because disulfide bonds are required for the activity of several virulence factors, these studies are of tremendous importance to envision how carbon metabolism impacts bacterial pathogenesis.

Long-chain fatty acids (LCFAs) are used as a rich source of metabolic energy by *E. coli* and several other bacterial pathogens (Fang et al, 2005; Rivera-Chavez & Mekalanos, 2019; Son et al, 2007). The metabolic pathway of LCFAs suggests that its degradation generates a large number of reduced cofactors, which might increase electron flow in the ETC (Clark & Cronan, 2005). Thus, LCFAs represent a suitable carbon source to examine the interconnection between cellular metabolism and the redox status of the envelope.

Here, in this chapter, we investigated the relation between LCFA metabolism and disulfide bond formation in *E. coli*. We show that LCFA metabolism increases electron flow in the ETC. We find that LCFA-utilizing cells exhibit several hallmarks of insufficient disulfide bond formation, and these are prevented in cells exogenously provided with ubiquinone. Collectively, these data establish that during LCFA metabolism, ubiquinone is limiting for disulfide bond formation.

4.2 Results

4.2.1 LCFA metabolism increases electron flow in the ETC

Based on the metabolic pathway, LCFA degradation theoretically generates a large number of reduced cofactors. One round of β-oxidation produces one molecule, each of NADH and $FADH_2$, and releases two carbon atoms as acetyl-CoA. The metabolism of acetyl-CoA in the tricarboxylic acid (TCA) cycle further generates two NADH and one $FADH_2$ (Fig. 1.2; Chapter I) (Clark & Cronan, 2005). Thus, during degradation of oleate (C18:1 cis-9), a representative LCFA used in this study, β-oxidation will produce eight molecules each of NADH and $FADH_2$, and the TCA cycle will further generate more reduced cofactors from nine molecules of acetyl-CoA. We tested whether LCFA metabolism indeed increases electron flow in the ETC by determining the $NADH/NAD^+$ ratio and measuring the activity of aerobic respiratory dehydrogenases. For this, WT BW25113 was grown in buffered tryptone broth (TBK) supplemented either with oleate (TBK-Ole) or with the detergent Brij-58 used for solubilizing oleate (TBK-Brij) (Fig. 4.1).

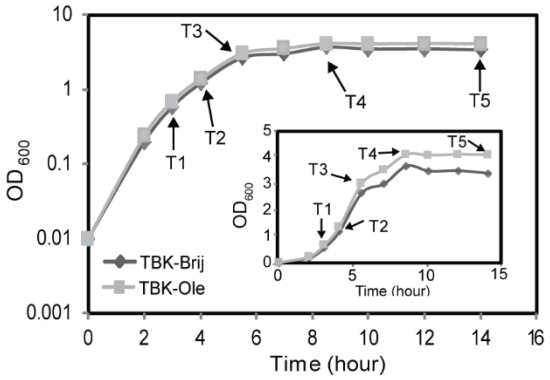

Figure 4.1. Growth curve of WT BW25113 in TBK-Brij and TBK-Ole. WT was grown either in TBK-Brij or TBK-Ole. OD_{600} of the cultures was measured, and growth curves were plotted on a semi-logarithmic scale. The experiment was done three times. A representative dataset is shown. T1, T2, T3, T4, and T5 indicate time points where cultures were harvested for various assays. *Inset*: The above growth curves were also plotted on a linear scale.

In the previous chapter, we explained the rationale of using tryptone broth (TB) medium to study aspects of LCFA metabolism, i.e., low catabolite repression enables co-utilization of oleate with carbon components of TB, and unlike minimal medium supplemented with oleate where *ubi* and *fad* mutants show growth defect/ no growth, TB supplemented with oleate allows normal growth of these mutants. Stress response pathways that monitor and maintain envelope integrity are known to be affected by the pH of the medium. For example, in *E. coli*, the Cpx envelope stress response (ESR) pathway is induced by alkaline pH, and another ESR, σ^E pathway, is induced in *S. enterica* serovar Typhimurium by acid stress (Muller et al, 2009; Wolfe et al, 2008). Importantly, the consumption of amino acids from the TB medium produces ammonia, which is suggested to increase the pH of the culture medium (Wolfe et al, 2008). Because in the work presented in this chapter, our objective was to determine the redox status of the envelope during LCFA metabolism, to avoid any confounding effect of change in pH of the medium (e.g., induction of ESR pathways because of altered pH), we used buffered TB medium (TBK) for our experiments.

4.2.1.1 LCFA metabolism increases NADH/NAD$^+$ ratio

The steady-state levels of intracellular NADH and NAD$^+$ were measured in the exponential phase (time point T1, Fig. 4.1) using a colorimetric assay (Sigma). Intracellular NADH and NAD$^+$ were quantified using the NADH standard curve (Fig. 4.2 A). We observed ~2.5-fold increase in NADH in WT cells grown in TBK-Ole compared to TBK-Brij; however, there was no significant change in NAD$^+$ levels (Figs. 4.2 B & C). Together, this resulted in ~2.5-fold higher NADH/NAD$^+$ ratio in TBK-Ole (0.363 ± 0.017) compared to TBK-Brij (0.135 ± 0.007) (Fig. 4.2 D). This higher NADH level and NADH/NAD$^+$ ratio in TBK-Ole were due to oleate utilization; in contrast to WT, a Δ*fadL* strain has similar NADH level and NADH/NAD$^+$ ratio in TBK-Ole and TBK-Brij (Figs. 4.2 B-D).

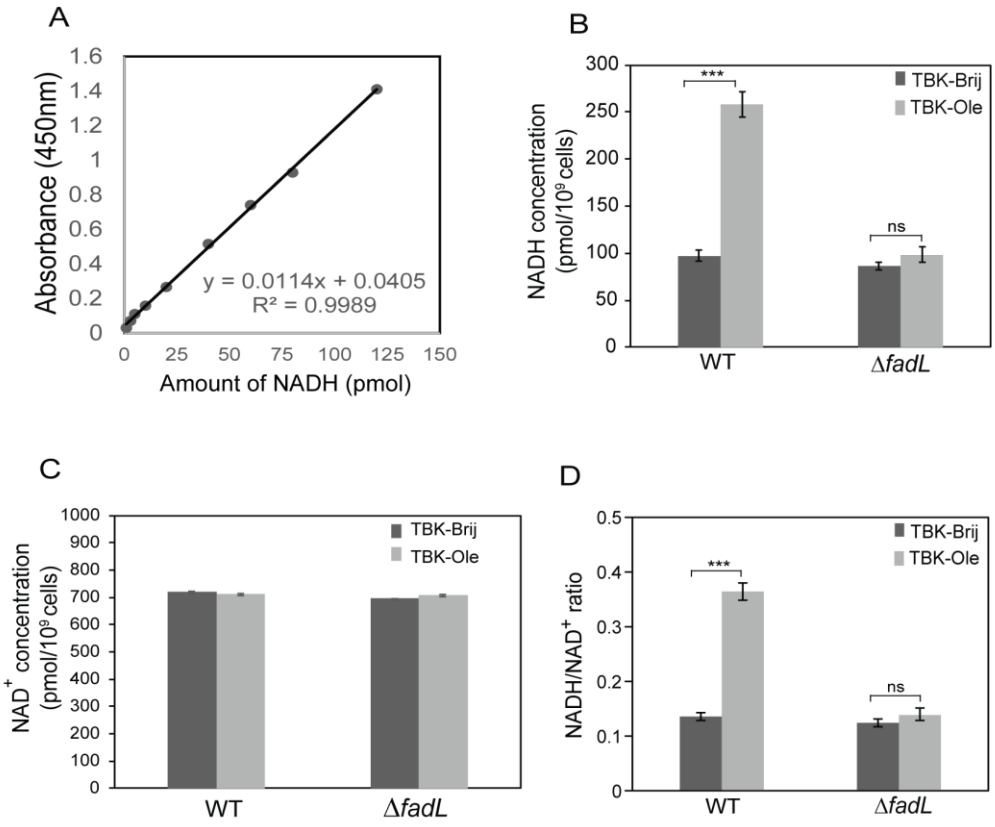

Figure 4.2. NADH/NAD$^+$ ratio is higher in LCFA-utilizing cells. (A) A standard curve was plotted for NADH based on the colorimetric detection, as mentioned in the kit (Sigma). The absorbance at 450 nm increases linearly with an increasing amount of NADH. (B-D) Strains were grown either in TBK-Brij or TBK-Ole. Cultures were harvested at time point T1 indicated in Fig. 4.1, and NADH (B) and NAD$^+$ (C) concentration, and NADH/NAD$^+$ ratio (D) were determined. Data represent the average (± SD) of three independent

experiments. For panels B, C, and D, the p-values were calculated using the unpaired two-tailed Student's t test (***, P<0.001; ns, P>0.03).

4.2.1.2 Activity of NADH and succinate dehydrogenases increases in LCFA-metabolizing cells

During aerobic metabolism, NADH and $FADH_2$ are oxidized at the ETC by NADH dehydrogenases and succinate dehydrogenase, respectively, and the electrons are transferred to the lipid-soluble electron carrier, ubiquinone (Fig. 1.3; Chapter I) (Unden et al, 2014). We investigated whether a large amount of reduced cofactors produced during LCFA metabolism increases electron flow in the ETC by determining the activity of NADH and succinate dehydrogenases. The NADH dehydrogenase activity was determined by measuring the rate of decay of NADH at 340 nm. The activity of NADH dehydrogenase was higher in WT cultured in TBK-Ole compared to cells grown in TBK-Brij, and this increase was dependent on oleate utilization; the increase in activity was abolished in a Δ*fadL* strain (Fig. 4.3 A). The succinate dehydrogenase activity was determined using a blue-colored dye, 2,6-dichlorophenolindophenol (DCPIP), as an electron acceptor. DCPIP decolorizes upon reduction by taking up electrons from $FADH_2$, thus the succinate dehydrogenase activity can be measured by quantifying the rate of decay of DCPIP absorbance at 600 nm. Similar to NADH dehydrogenase, the activity of succinate dehydrogenase was higher in WT cultured in TBK-Ole compared to cells grown in TBK-Brij, and this increase was dependent on oleate utilization (Fig. 4.3 B). Strains individually deleted for gene encoding the NADH dehydrogenase I subunit, NuoK (Erhardt et al, 2012) and succinate dehydrogenase subunit, SdhB (Cheng et al, 2006) were used as controls in the activity assays. As expected, the activity of NADH and succinate dehydrogenases was considerably lower in Δ*nuoK* and Δ*sdhB* strains, respectively, in both TBK-Brij and TBK-Ole (Figs. 4.3 A & B).

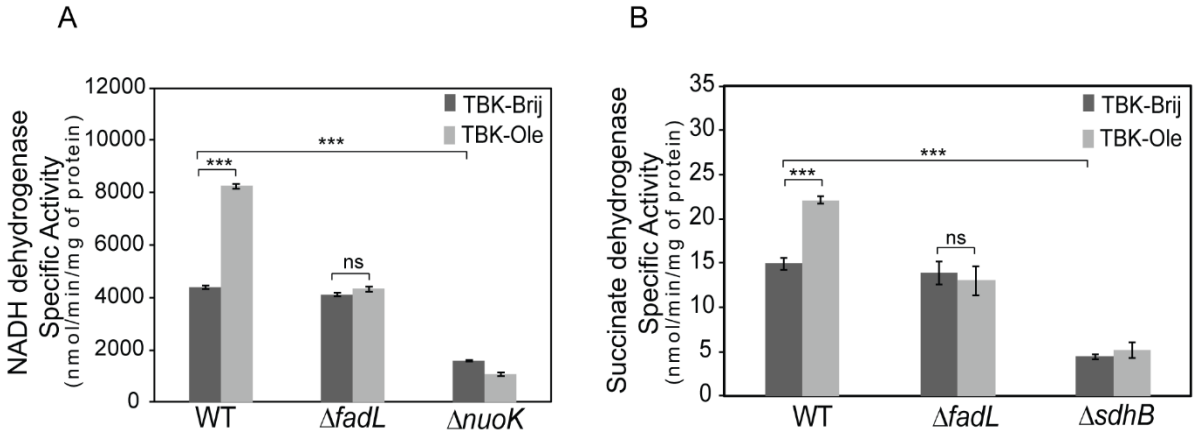

Figure 4.3. The activity of NADH dehydrogenase (A) and succinate dehydrogenase (B) increases in cells utilizing LCFAs. Strains were grown either in TBK-Brij or TBK-Ole. Cultures were harvested at time point T1 indicated in Fig. 4.1, and the activity of the respiratory dehydrogenases was measured. Data represent the average (± SD) of three independent experiments. The p-values were calculated using the unpaired two-tailed Student's t test (***, $P<0.001$; ns, $P>0.03$).

4.2.1.3 Induction of *fadE* in LCFA-metabolizing cells

During β-oxidation, the acyl-CoA dehydrogenase, FadE, catalyzes the oxidation of acyl-CoA (an intermediate in LCFA metabolism) to enoyl-CoA concomitant with reduction of FAD to $FADH_2$ (Fig. 1.2; Chapter I). FadE has also been speculated to re-oxidize $FADH_2$ to FAD by transferring electrons from its dehydrogenase domain to quinones (Section 1.3.1.2; Chapter I) (Campbell & Cronan, 2002), which can thus lead to increased electron flow in the ETC. We checked the induction of *fadE* in TBK-Ole at the exponential phase by assaying the β-gal activity of chromosomal *lacZ* fused to the promoter of *fadE*. We observed ~4 fold induction of *fadE* in cells grown in TBK-Ole in comparison to TBK-Brij (Fig. 4.4). This data suggests an increased flow of electrons from FadE to the ETC during LCFA metabolism.

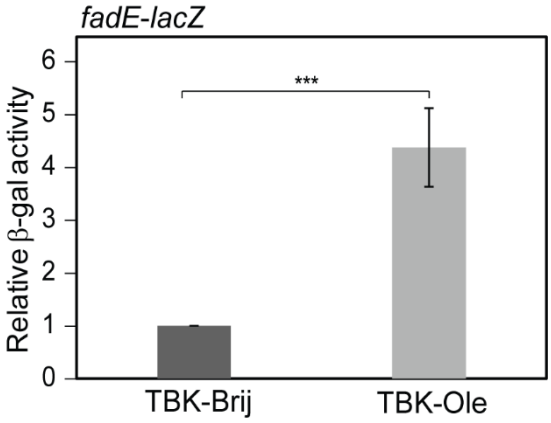

Figure 4.4. FadE is induced in LCFA-utilizing cells. WT carrying chromosomal fusion of *lacZ* with the promoter of *fadE* was grown either in TBK-Brij or TBK-Ole. Cultures were harvested at time point T1 indicated in Fig. 4.1, and β-gal activity was measured. Data were normalized to the β-gal activity of WT in TBK-Brij. Data represent the average (± SD) of four independent experiments. The average β-gal activity of the reporter strain in TBK-Brij was 54 (± 9) Miller units. The p-values were calculated using the unpaired two-tailed Student's t test (***, P<0.001).

4.2.2 Disulfide bond formation is hampered during LCFA metabolism

Our above results indicate an increase in electron flow into the ETC during LCFA metabolism. Because electrons from aerobic metabolism of carbon sources and disulfide bond-forming machinery converge at the level of ubiquinone in the ETC, we suggested that a large flow of electrons during LCFA metabolism would make ubiquinone less available to handle electrons from the disulfide bond-forming machinery. To test this proposal, we investigated whether oleate-grown cells exhibit characteristics of insufficient disulfide bond formation.

4.2.2.1 Decrease in alkaline phosphatase activity during LCFA metabolism

AP is a periplasmic enzyme that requires the formation of intramolecular disulfide bonds for its activity (Sone et al, 1997). Therefore, AP activity is routinely used to determine the redox state of the periplasm (Rietsch et al, 1996). The *phoA* gene that encodes AP is inducible in *E. coli* and is positively regulated by PhoRB two-component signal transduction pathway. PhoR is the sensor kinase that indirectly senses the level of

extracellular inorganic phosphate (Pi) and phosphorylates its cognate response regulator, PhoB. Thus, in wild-type *E. coli*, *phoA* is induced when the level of inorganic phosphate (Pi) is limiting in the culture medium (Carmany et al, 2003; Yamada et al, 1989).

As a test for our proposal that LCFA metabolism results in a less oxidizing environment in the periplasm, we determined AP activity in LCFA-metabolising cells. For this purpose, we used RI89 strain, a *phoR* mutant that produces AP enzyme constitutively (Rietsch et al, 1996). The strain was cultured in TBK-Ole and TBK-Brij media (Fig. 4.5 A), and AP activity was measured in the exponential phase. In line with our hypothesis, compared to TBK-Brij, in TBK-Ole, there was ~40% reduction in AP activity (Fig. 4.5 B). This decrease in AP activity was not due to a decrease in AP protein levels in TBK-Ole grown cells (*Inset* Fig. 4.5 B). The reduction in AP activity was due to oleate utilization; compared to RI89, the AP activity did not exhibit any decrease in TBK-Ole in the isogenic Δ*fadL* and Δ*fadE* strains (Fig. 4.5 B). Due to insufficient disulfide bond formation, the AP activity is considerably reduced in a Δ*dsbA* strain (Rietsch et al, 1996). Interestingly, we find that although the AP activity in TBK-Brij decreased to ~30% and ~60% in Δ*dsbA* and Δ*dsbB* strains, respectively, the activity did not drop further in TBK-Ole (Fig. 4.5 C). These data validate our proposal that insufficient disulfide bond formation in the periplasmic enzyme in TBK-Ole is due to problems in the DsbA-DsbB oxidative pathway.

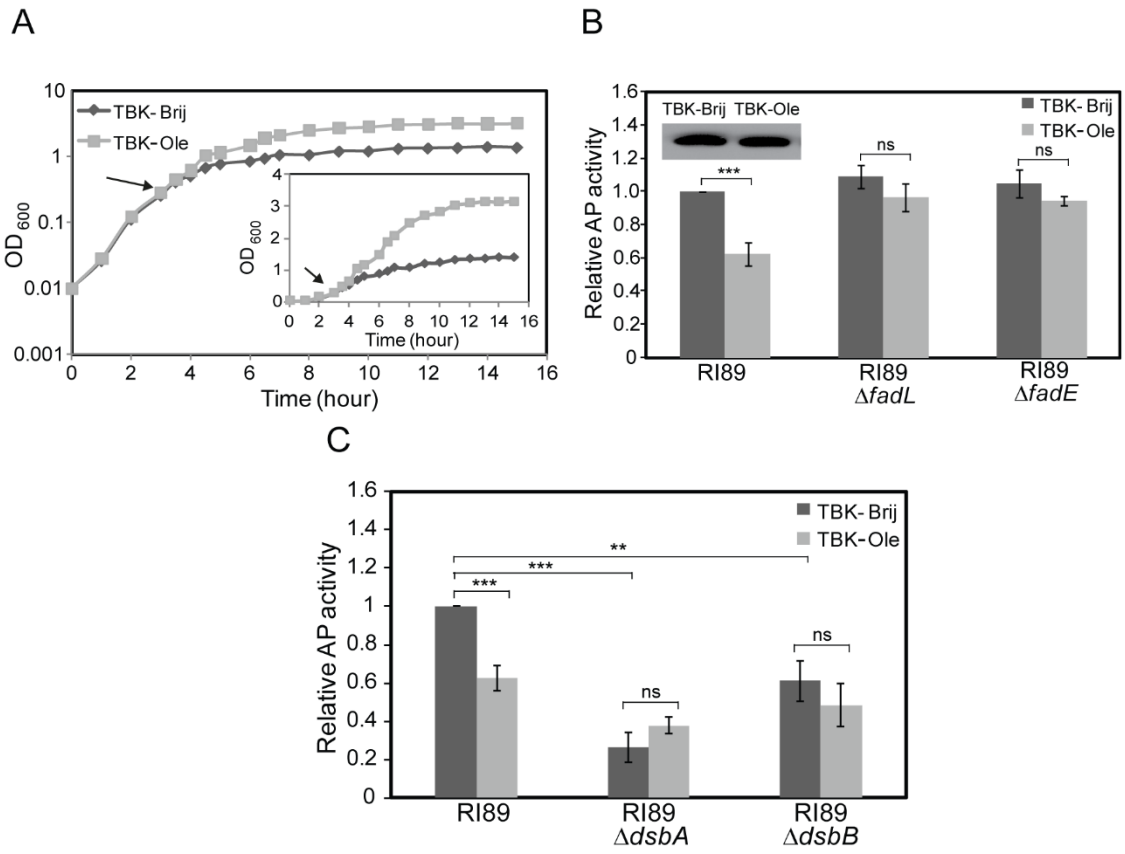

Figure 4.5. Insufficient disulfide bond formation results in a decrease in alkaline phosphatase activity in LCFA-utilizing cells. (A) Growth curve of RI89 in TBK-Brij and TBK-Ole. RI89 was grown either in TBK-Brij or TBK-Ole. OD_{600} of the cultures was measured, and growth curves were plotted on a semi-logarithmic scale. The experiment was done three times. A representative dataset is shown. Arrow indicates the time point where the cultures were harvested for determining AP activity and AP levels. *Inset*: The above growth curves were also plotted on a linear scale. (B) Oleate utilization results in a decrease in alkaline phosphatase activity. Cultures grown either in TBK-Brij or TBK-Ole were harvested in the exponential phase and processed for AP assay. Data were normalized to the AP activity of RI89 in TBK-Brij and represent average (± SD) of three independent experiments. The average AP activity of RI89 in TBK-Brij was 1384 (± 73) units. *Inset*: AP levels are similar in RI89 grown in TBK-Brij and TBK-Ole. Cultures were harvested, lysates were prepared, samples were run on 15% SDS-PAGE, and processed for Western blotting. Blots were probed with an anti-AP antibody. The band corresponding to AP is shown (Mol. wt. ~52 kDa). (C) Compromised DsbA-DsbB machinery is responsible for the decrease in alkaline phosphatase activity in cells utilizing oleate. Cultures grown either in TBK-Brij or TBK-Ole were harvested in the exponential phase and processed for AP assay. Data were normalized to the AP activity of RI89 in TBK-Brij and represent average (± SD) of three independent experiments. The average AP activity of RI89 in TBK-Brij was 1245 (± 357) units. For panels B and C, the p-values were calculated using the unpaired two-tailed Student's t test (**, $P<0.01$; ***, $P<0.001$; ns, $P>0.03$).

4.2.2.3 LCFA-utilizing cells exhibit thiol hypersensitivity

Another hallmark of impaired disulfide bond formation is the hypersensitivity to thiol agents. For example, the *dsbA* and *dsbB* mutants show either growth defect or no growth on LB agar containing millimolar concentrations of DTT, which otherwise do not affect the growth of WT strain (Missiakas et al, 1993; Sardesai et al, 2003; Skorko-Glonek et al, 2008). Further, the growth of these strains is also inhibited by millimolar concentrations of 1-thioglycerol in liquid minimal medium containing glucose as a carbon source (Zeng et al, 1998). We examined whether cells grown in oleate are also sensitive to thiol agents by comparing the growth of WT BW25113 strain on TBK-Brij and TBK-Ole agar containing different concentrations of DTT. Whereas growth was observed in TBK-Brij even at 8 mM DTT, in TBK-Ole, 7 mM DTT resulted in a considerable growth defect and almost no growth was observed in 8 mM DTT (Fig. 4.6 A). We also profiled the growth of WT strain in liquid minimal medium containing oleate as a sole carbon source in the presence of either DTT or 1-thioglycerol and compared it with growth in minimal medium containing acetate. We chose acetate for comparison because i) acetate and oleate follow a common metabolic route; they are both non-fermentable carbon sources that directly enter the TCA cycle after conversion to acetyl-CoA, and ii) acetate metabolism theoretically generates less amount of reduced cofactors than oleate; hence the load of electrons on ETC from metabolism would be less during growth in this carbon source (Clark & Cronan, 2005). Consistent with our proposal, whereas 0.5 mM DTT resulted in a substantial delay in the growth of cells in oleate, it did not have an adverse effect on growth in acetate. Similarly, whereas 1 mM 1-thioglycerol completely inhibited growth in oleate, it only had a mild effect on growth in acetate (Fig. 4.6 B).

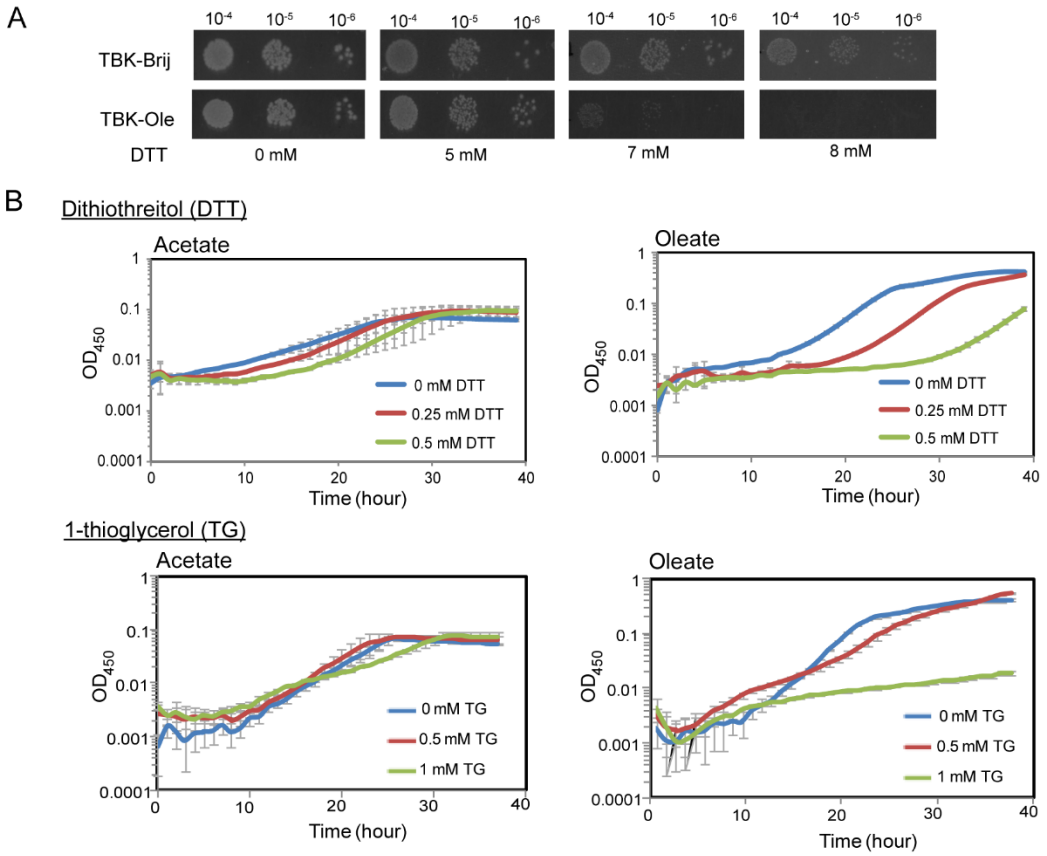

Figure 4.6. LCFA-utilizing cells exhibit thiol hypersensitivity. (A) WT cells grown in TBK-Ole are hypersensitive to DTT. WT BW25113 was spotted on TBK-Brij or TBK-Ole with or without indicated concentrations of DTT. The experiment was performed two times. A representative dataset is shown. (B) Amongst acetate and oleate, oleate utilization renders cells more sensitive to thiol agents. WT BW25113 was grown in minimal medium containing either acetate or oleate, with or without indicated concentrations of DTT or 1-thioglycerol. Acetate medium was also supplemented with Brij-58. OD_{450} of the cultures was measured, and growth curves were plotted on a semi-logarithmic scale. The experiment was done at least two times; each experiment had three technical replicates. A representative dataset, with average (± SD) of technical replicates, is shown.

4.2.2.4 LCFA-utilizing cells exhibit cadmium sensitivity

Problems in disulfide bond formation lead to the accumulation of proteins in their thiol form. It has been reported that the Δ*dsbA* strain shows sensitivity to heavy metals such as cadmium (Cd^{2+}) and zinc (Zn^{2+}), due to the binding of these metals with free thiols of

proteins (Rensing et al, 1997; Stafford et al, 1999). To investigate whether disulfide bond formation is impaired during LCFA metabolism and leads to the accumulation of proteins in their thiol state, we determined Cd^{2+} sensitivity of TBK-Brij and TBK-Ole grown WT BW25113 by adding different concentrations of cadmium chloride ($CdCl_2$) to the cultures at T1, T2 and T3 time points (Fig. 4.1). There was no effect of $CdCl_2$ on the growth of WT in TBK-Brij whether $CdCl_2$ was added at time point T1, T2, or T3. On the other hand, in cells grown in TBK-Ole, whereas the addition of 2 mM $CdCl_2$ at time point T1 resulted in a ~15% decrease in growth, its addition at time points T2 and T3 led to ~25% and ~30% decrease in growth, respectively. These data suggest that the amount of thiol-containing proteins increases with an increase in cell density of oleate-grown cultures. As expected, the Δ*dsbA* strain grown in TBK-Brij was highly sensitive to cadmium (~35 to 40% decrease in growth upon treatment with 2 mM $CdCl_2$) irrespective of the time point of $CdCl_2$ addition (Fig. 4.7). This result was expected since disulfide bond formation is compromised in a Δ*dsbA* strain from the initial stage of growth. In another set of experiments conducted in our lab where the redox state of DegP, a substrate of DsbA (Skorko-Glonek et al, 2006), was determined, it was observed that the reduced form of DegP accumulates significantly in oleate-grown cells and gradually increases from exponential phase (time point T1) to entry into stationary phase (time point T3) (Deeptodeep Roy, Ph.D. student). Collectively, the above experiments convincingly demonstrate that there is a gradual build-up of free thiol-containing proteins during LCFA metabolism.

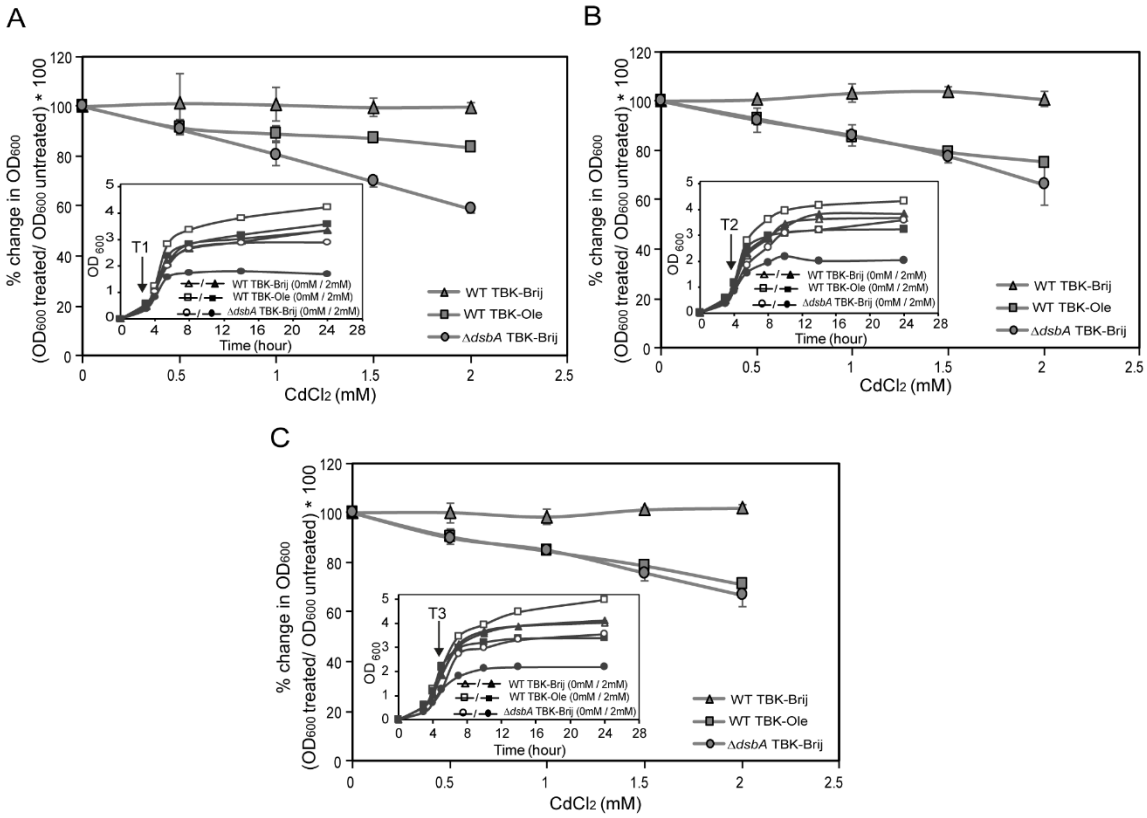

Figure 4.7. LCFA-utilizing cells exhibit cadmium sensitivity. WT grown either in TBK-Brij or TBK-Ole and Δ*dsbA* grown in TBK-Brij were treated with different concentrations of $CdCl_2$ at time points T1 (A), T2 (B), or T3 (C). OD_{600} of the cultures was measured after 24 hours of growth. Percent change in OD_{600} of the cultures treated with $CdCl_2$ in comparison to their untreated controls was calculated and plotted against $CdCl_2$ concentration. Data represent the average (± SD) of three independent experiments. *Insets*: Growth curves of WT in TBK-Brij or TBK-Ole and Δ*dsbA* in TBK-Brij either without $CdCl_2$ treatment (open symbols) or treated with 2 mM $CdCl_2$ (filled symbols), is shown. Arrow indicates the time points T1(A), T2 (B), or T3 (C) at which $CdCl_2$ was added. Data is shown for one of the three biological replicates.

Taken together, the phenotypes of decreased AP activity, thiol hypersensitivity, and cadmium sensitivity exhibited by oleate-utilizing cells establish that disulfide bond formation is inadequate during growth in LCFAs.

4.2.3 During LCFA metabolism ETC is limiting to take up electrons from the disulfide bond-forming machinery

From our experiments above, we showed that during LCFA metabolism, there is an increased flow of electrons towards ETC, and there is a problem in disulfide bond formation

in proteins. Importantly, some of the phenotypes of insufficient disulfide bond formation that we observe for oleate-utilizing cells are also shown by *ubi* mutants. For example, *ubi* mutants that contain low levels of ubiquinone are compromised for growth in minimal medium (glucose as carbon source) supplemented either with DTT or 1-thioglycerol, due to the inability of the suboptimal respiratory chain to re-oxidize Dsb enzymes reduced in the presence of excess thiol agents (Zeng et al, 1998). Therefore, we next investigated whether hampered disulfide bond formation in oleate-utilizing cells is because ubiquinone is limiting to take up electrons from the disulfide bond-forming machinery.

4.2.3.1 Increasing the oxidizing power of ETC restores alkaline phosphatase activity in LCFA-utilizing cells

To determine whether, during LCFA metabolism, ubiquinone is limiting to handle electrons from DsbA-DsbB machinery, we increased the oxidizing power of ETC by exogenously supplementing the cells with ubiquinone-8. We determined AP activity of RI89 strain grown in TBK-Brij and TBK-Ole. The exogenous supplementation of ubiquinone prevented a decrease in AP activity of RI89 grown in TBK-Ole (Fig. 4.8). This result emphasizes that ubiquinone is indeed limiting for disulfide bond formation in oleate-utilizing cells.

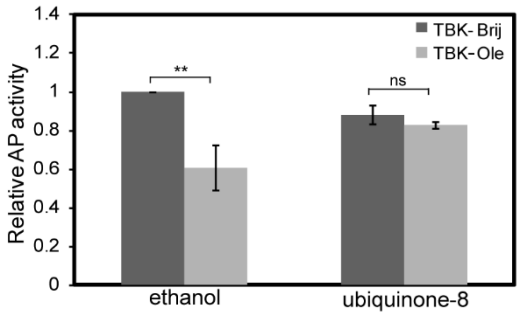

Figure 4.8. Supplementation of ubiquinone-8 prevents a decrease in alkaline phosphatase activity in LCFA-utilizing cells. RI89 cells were grown either in TBK-Brij or TBK-Ole. Media contained either 20 µM ubiquinone-8 or 0.1% ethanol (solvent for ubiquinone-8). Cultures were harvested in the exponential phase, AP activity was measured, and the data were normalized to the AP activity of RI89 in TBK-Brij containing

0.1% ethanol. Data represent the average (± SD) of three independent experiments. The average AP activity of RI89 in TBK-Brij supplemented with 0.1% ethanol was 1192 (± 341) units. The p-values were calculated using the unpaired two-tailed Student's t test (**, $P<0.01$; ns, $P>0.03$).

4.2.3.2 DsbA accumulates in a reduced form in LCFA-utilizing cells

DsbA transfers disulfide bonds in secreted substrate proteins via thiol-disulfide exchange reaction. The cysteine residues of DsbA get reduced after catalyzing the formation of disulfide bonds and need to be re-oxidized by the oxidoreductase, DsbB, which in turn transfers electrons to the ETC at the level of ubiquinone (Manta et al, 2019). Because of the obstruction of electron flow from the DsbA-DsbB machinery to the ETC, strains defective in quinone biosynthesis accumulate DsbA in a reduced form (Kobayashi et al, 1997). We reasoned that if there is limited availability of ubiquinone for disulfide bond formation during oleate metabolism, then cells might accumulate reduced form of DsbA. To test this, we harvested WT BW25113 grown in TBK-Brij and TBK-Ole at T1, T2, and T3 time points (Fig. 4.1), denatured and precipitated proteins, and treated samples with 4-acetamido-4'-maleimidystilbene-2,2'-disulfonicacid (AMS), a maleimide derivative that results in a specific, rapid and irreversible alkylation of free thiols adding ~0.5 kDa moiety per thiol group (Kobayashi et al, 1997). AMS modification enabled differentiation of the oxidized and reduced forms of the thiol-containing DsbA protein on non-reducing SDS-PAGE gels. Whereas DsbA was present in the oxidized form in TBK-Brij at all phases of growth, TBK-Ole grown cells accumulated DsbA in a completely reduced form at time point T3 (corresponding to entry into stationary phase) (Figs. 4.1 & 4.9).

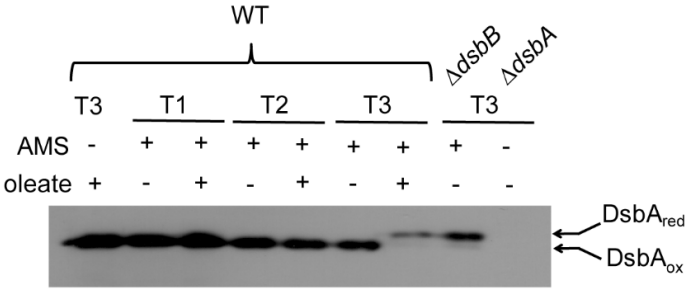

Figure 4.9. DsbA accumulates in a reduced form in LCFA-grown cells. WT BW25113 was grown either in TBK-Brij or TBK-Ole, and cultures were harvested at time points, T1, T2, and T3, as indicated in Fig. 4.1. Proteins were denatured and precipitated using trichloroacetic acid, followed by treatment with AMS. Oxidized and reduced forms of DsbA were identified by running the AMS-treated samples on non-reducing SDS-PAGE gels, followed by Western blot using an anti-DsbA antibody. Δ*dsbA* and Δ*dsbB* cultured in TBK-Brij served as controls. DsbA is re-oxidized by DsbB; hence DsbA accumulates in a reduced form in a Δ*dsbB* strain. $DsbA_{ox}$ and $DsbA_{red}$ indicate oxidized and reduced forms of DsbA, respectively.

The accumulation of reduced form of DsbA at the T3 time point was due to oleate utilization (Figs. 4.10 A & B); DsbA is present in its oxidized form in the isogenic Δ*fadL* strain grown in TBK-Ole.

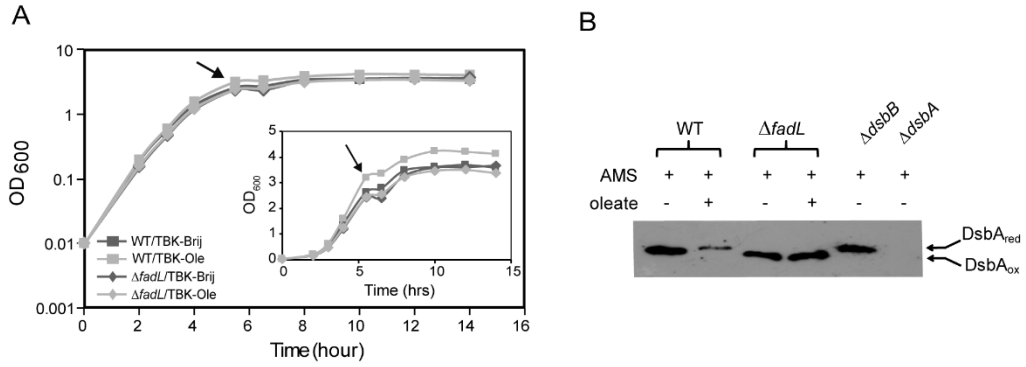

Figure 4.10. Accumulation of the reduced form of DsbA in LCFA-grown cells is due to the utilization of this carbon source. (A) Growth curve of WT BW25113 and the isogenic Δ*fadL* strain in TBK-Brij and TBK-Ole. Strains were grown either in TBK-Brij or TBK-Ole. OD_{600} of the cultures was measured, and growth curves were plotted on a semi-logarithmic scale. The experiment was done two times. A representative dataset is shown. Arrow indicates the T3 time point where the cultures were harvested to check the redox state of DsbA protein. *Inset*: The above growth curves were also plotted on a linear scale. (B) Accumulation of the reduced form of DsbA is oleate-utilization dependent. WT BW25113 and its isogenic Δ*fadL* strain were grown either in TBK-Brij or TBK-Ole. Cultures were harvested at time point T3 (indicated in Fig. 4.10 A) and processed as

mentioned in the legend to Fig. 4.9. Δ*dsbA* and Δ*dsbB* cultured in TBK-Brij served as controls. $DsbA_{ox}$ and $DsbA_{red}$ indicate oxidized and reduced forms of DsbA, respectively.

4.2.3.3 Ubiquinone supplementation prevents the accumulation of reduced form of DsbA in LCFA-utilizing cells

To examine whether the accumulation of reduced form of DsbA in LCFA-utilizing cells is indeed because of a decrease in the rate of electron transfer from DsbA-DsbB machinery to ubiquinone, we exogenously supplemented WT BW25113 grown in TBK-Brij and TBK-Ole with ubiquinone-8 and determined the redox state of DsbA. Importantly, DsbA was present in its oxidized form at time point T3 when the TBK-Ole medium was supplemented with ubiquinone-8, reiterating that ubiquinone is limiting for disulfide bond formation in oleate-utilizing cells (Fig. 4.11).

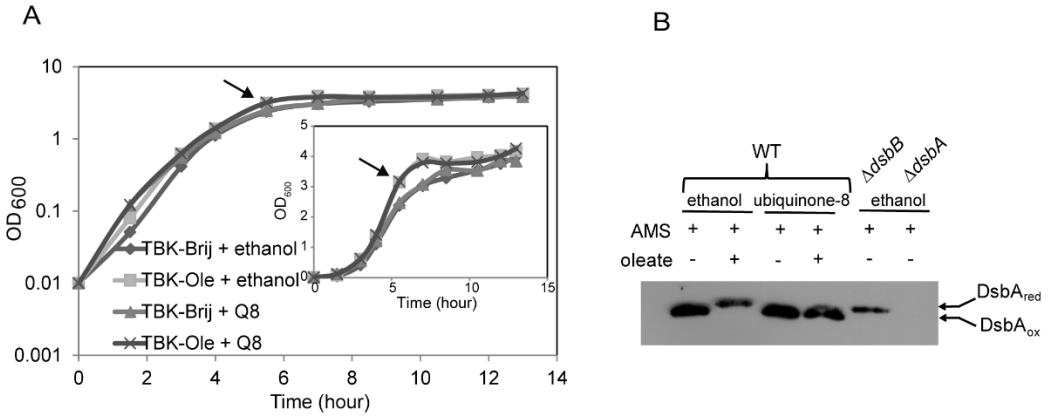

Figure 4.11. Supplementation of ubiquinone-8 prevents the accumulation of reduced form of DsbA in LCFA-utilizing cells. (A) Growth curve of WT BW25113 in TBK-Brij and TBK-Ole with or without ubiquinone-8 supplementation. Strains were grown in TBK-Brij and TBK-Ole either alone or with 20 µM ubiquinone-8 or 0.1% ethanol. OD_{600} of the cultures was measured, and growth curves were plotted on a semi-logarithmic scale. The experiment was done two times. A representative dataset is shown. Arrow indicates the T3 time point where the cultures were harvested to check the redox state of DsbA protein. *Inset*: The above growth curves were also plotted on a linear scale. (B) Ubiquinone-8 prevents the accumulation of reduced form of DsbA in oleate-utilizing cells. WT BW25113 was grown either in TBK-Brij or TBK-Ole. The media contained either 20 µM ubiquinone-8 or 0.1% ethanol. Cultures were harvested at time point T3 (indicated in Fig. 4.11 A) and processed as mentioned in the legend to Fig. 4.9. Δ*dsbA* and Δ*dsbB* cultured in TBK-Brij containing 0.1% ethanol served as controls. $DsbA_{ox}$ and $DsbA_{red}$ indicate oxidized and reduced forms of DsbA, respectively.

4.3 Discussion

Here we investigated the interconnection between LCFA metabolism and disulfide bond formation in *E. coli*. We demonstrated that during LCFA metabolism increased electron flow in the ETC renders ubiquinone limiting for disulfide bond formation, thereby compromising redox balance in the envelope.

Ubiquinone has been considered non-limiting for its electron transfer function based on an earlier observation that during aerobic growth of *E. coli* (in minimal medium supplemented with glucose), it is present in ~15 to 20-fold excess over flavins and cytochromes (Cox et al, 1970). However, work from our lab suggested that ubiquinone is limiting during aerobic metabolism of LCFAs (Agrawal, 2018; Agrawal et al, 2017). Briefly, comparing *E. coli* grown in basal TB medium and TB supplemented with LCFAs, it was shown that LCFA degradation generates high levels of ROS. It was proposed that high $NADH/NAD^+$ and $FADH_2/FAD$ ratios during LCFA catabolism increase electron flow in the ETC, thereby increasing ROS formation. Further, it was observed that ubiquinone upregulates ~1.8-fold in LCFA-utilizing cells and decreases ROS, which is likely achieved by rapidly transferring electrons from the site of ROS formation to the ETC. Despite endogenous accumulation, exogenous supplementation of ubiquinone was required to further decrease ROS in LCFA-utilizing cells. On the contrary, the addition of ubiquinone did not decrease ROS in cells metabolizing basal components of TB. These data strongly suggested that ubiquinone is limiting under metabolic conditions that feed a large number of electron donors in the ETC (Agrawal, 2018; Agrawal et al, 2017).

Here we show that electron flow in the ETC is indeed high during LCFA metabolism (Figs. 4.2, 4.3 & 4.4), and in addition to being insufficient for the transfer of electrons derived from metabolism, ubiquinone is also limiting for electron transfer from the disulfide bond-forming machinery. The latter is evident from several hallmarks of

inadequate disulfide bond formation exhibited by LCFA-utilizing cells: decreased AP activity, hypersensitivity to thiol agents, cadmium sensitivity, and accumulation of the reduced form of DsbA, which could be prevented upon ubiquinone supplementation (Figs. 4.5–4.11). Although compromised disulfide bond formation has been observed earlier in a mutant with defective ETC (mutant defective in the biosynthesis of heme and quinones) or in a condition where ETC is non-operational (during fermentative growth on glucose) (Bader et al, 1999; Kobayashi et al, 1997), aerobic growth on LCFAs represents the first instance where in an otherwise operational ETC, increased electron flow from carbon metabolism significantly hampers disulfide bond formation.

A previous study showed that during aerobic growth of *E. coli* (in minimal medium supplemented with glucose), an increase in cell density increases the ubiquinol/ubiquinone ratio due to a decrease in the availability of dissolved oxygen (Sharma et al, 2013). Because LCFA metabolism produces a large number of electron donors, this would lead to a much larger increase in ubiquinol/ubiquinone ratio with an increase in cell density, thereby making ubiquinone less available for the oxidation of the disulfide bond-forming machinery. This gradual increase in load on the disulfide bond forming machinery during LCFA metabolism is evident from our experiments: *i)* oleate-grown cells entering into stationary phase are more sensitive to $CdCl_2$ treatment compared to cells in the exponential phase (Fig. 4.7), *ii)* the reduced form of DegP, a DsbA substrate, accumulates significantly in oleate-utilizing cells and gradually increases from exponential phase to entry into stationary phase (Deeptodeep Roy, Ph.D. student), and *iii)* the reduced form of DsbA is observed when oleate-grown cells enter the stationary phase, *i.e.*, T3 time point (Fig. 4.9). We note that whereas thiol-containing proteins accumulate in oleate-grown cells even in the exponential phase (as revealed from the cadmium sensitivity data and the accumulation of reduced form of DegP), we did not observe the reduced form of DsbA in this phase of

growth (compare Figs. 4.7 & 4.9). We repeatedly observed lower levels of AMS conjugated form of reduced DsbA compared to its unconjugated form in TBK-Ole-grown cells at time point T3, although both the samples were same except AMS treatment (compare lanes 1 and 7; Fig. 4.9). We suggest that due to the lower stability of AMS conjugated DsbA, we are unable to capture its gradual accumulation in oleate-utilizing cells. Importantly, the accumulation of DsbA in its reduced form at time point T3 in TBK-Ole is not due to the difference in growth between TBK-Brij and TBK-Ole at this time point. This is because although WT cells grown in TBK-Ole with or without ubiquinone-8 supplementation have a similar growth profile, DsbA is present in its oxidized form upon ubiquinone supplementation (similar to TBK-Brij grown cells) and present in its reduced form without ubiquinone supplementation (Fig. 4.11). Further, whereas there was a gradual increase in load on the disulfide bond-forming machinery in WT BW25113 grown in LCFAs, the AP activity was compromised in RI89 in TBK-Ole even in the exponential phase (Figs. 4.5 & 4.8), (Figs. 4.7 & 4.9). We suggest that this difference is due to the constitutive expression of AP in RI89 that likely overburdens the DsbA-DsbB machinery in TBK-Ole from the initial stages of growth.

The above study, which reported an increase in ubiquinol/ubiquinone ratio with an increase in cell density, also showed that the ubiquinol/ubiquinone ratio decreases later in the stationary phase, and this was suggested to be due to lowered metabolism (Sharma et al, 2013). In the next chapter, we present results that DsbA, which accumulates in a reduced form when cells enter stationary phase, resumes to its oxidized state later in the stationary phase (Fig. 5.1; Chapter V). Our work identifies envelope stress response (ESR) systems that are induced during LCFA metabolism to monitor envelope redox status, and one of the mechanisms by which these pathways likely maintain redox homeostasis is by lowering LCFA metabolism (Chapter V).

CHAPTER V

Envelope stress response pathways monitor redox imbalance during long-chain fatty acid metabolism

5.1 Introduction

The cell envelope of gram-negative bacteria is a protective barrier at the forefront of interaction with the extracellular environment and represents a site for a multitude of functions critical for growth and viability. For example, the outer membrane provides a selective permeability barrier to external agents where lipopolysaccharide (LPS) forms a tight seal that prevents entry of large hydrophobic and hydrophilic molecules, while the outer membrane proteins (OMPs) allow passage of small hydrophilic compounds (May & Grabowicz, 2018; Nikaido, 2003; Silhavy et al, 2010). The peptidoglycan layer shares the mechanical load with the outer membrane and protects cells against osmotic stress (Rojas et al, 2018; Silhavy et al, 2010). The periplasm harbors proteins involved in sensing environmental stresses, enzymes involved in transport and envelope biogenesis, and its oxidizing environment allows oxidative protein folding and quality control (Messens & Collet, 2006; Miller & Salama, 2018; Silhavy et al, 2010). The inner membrane presents a final barrier to external agents and is the site for cellular functions such as protein translocation and oxidative phosphorylation (Silhavy et al, 2010) (Section 1.7; Chapter I).

Given the essential role of the envelope in maintaining cellular homeostasis and protection against fluctuating environmental conditions, its integrity must be continuously monitored and maintained. In *E. coli,* this task is accomplished by at least five dedicated envelope stress response (ESR) systems which sense problems in the envelope and change the transcriptional program to combat stress (Section in 1.8; Chapter I) [reviewed in (Macritchie & Raivio, 2009; Mitchell & Silhavy, 2019)]. These ESR systems include σ^E response, the CpxAR and BaeSR two-component systems, the PSP response and the Rcs phosphorelay system. The σ^E pathway senses and responds to defects in the transport and assembly of OMPs and LPS (Grabowicz & Silhavy, 2017; Kim, 2015). The Cpx pathway predominantly deals with misfolded inner membrane and periplasmic proteins, and defects

in inner membrane protein translocation, peptidoglycan biosynthesis, and lipoprotein trafficking (Grabowicz & Silhavy, 2017; Raivio, 2014). The BaeSR system is activated by exposure to antibiotics and toxic molecules; however, the inducing signal is unknown. The PSP pathway responds to disturbances of the inner membrane that result in loss of proton motive force (PMF) (Macritchie & Raivio, 2009; Mitchell & Silhavy, 2019). The Rcs pathway responds to membrane perturbations such as alteration in LPS charge and fluidity, peptidoglycan stress, and mislocalization of lipoproteins (Mitchell & Silhavy, 2019). In addition to the above ESR systems, outer membrane vesicles are formed in response to protein accumulation in the envelope and relieve envelope stress by removing unwanted envelope components from the cell (Schwechheimer & Kuehn, 2015).

From the results presented in Chapter IV, we know that LCFA-metabolising cells exhibit problems in disulfide bond formation due to the unavailability of ubiquinone to handle electrons from the disulfide bond-forming machinery. In *E. coli*, ~300 proteins are predicted to be disulfide-bonded in the periplasm (Dutton et al, 2008). Of these, more than two dozen proteins have been shown to be dependent on DsbA for their correct folding and are involved in diverse cellular processes. These include FlgI, a flagellum component required for cellular motility; the outer membrane lipoproteins RcsF and NlpE, which sense stress in the envelope; DegP, a periplasmic chaperone and protease; FtsN, a protein involved in cell division; and LptD, a protein involved in LPS assembly (Delhaye et al, 2019; Kadokura et al, 2004). Because insufficient disulfide bond formation can compromise the function of DsbA substrates and can therefore affect the integrity of the envelope, it is likely that the ESR pathways that monitor envelope status are activated as a combat strategy in cells grown in LCFAs.

In this chapter, we investigated the activation of various ESR pathways during LCFA metabolism. Our results show that the envelope signals generated during growth in

LCFAs activate Cpx and σ^E. Amongst the two ESR systems, only Cpx senses redox-dependent signal and is induced to a greater extent by LCFAs. Therefore, we argue that Cpx is the primary ESR that senses envelope redox homeostasis during LCFA metabolism.

5.2 Results

5.2.1 Reduced form of DsbA that accumulates during LCFA metabolism resumes to its oxidized form later in the stationary phase

In our experiment presented in the previous chapter, where we monitored the redox state of DsbA, we observed that cells grown in oleate accumulate DsbA in a completely reduced form during entry into the stationary phase (time point T3) (Figs. 4.1 & 4.9; Chapter IV). However, when we determined the redox state of DsbA later in the stationary phase (time points T4 and T5), we found that DsbA resumes to its oxidized form (Fig. 4.1; Chapter IV & Fig. 5.1). This data suggests that defense mechanisms are induced in oleate-grown cells to deal with the hypo-oxidizing environment of the periplasm.

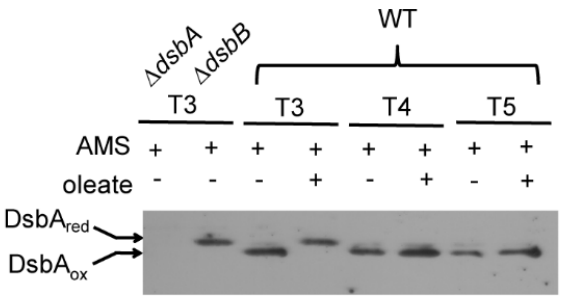

Figure 5.1. **DsbA resumes to its oxidized form later in the stationary phase in LCFA-utilizing cells.** WT BW25113 was grown in buffered tryptone broth (TBK) supplemented either with oleate (TBK-Ole) or with the detergent Brij-58 (TBK-Brij), and cultures were harvested at time points, T3, T4, and T5 as indicated in Fig. 4.1; Chapter IV and processed, as mentioned in the legend to Fig. 4.9; Chapter IV. Δ*dsbA* and Δ*dsbB* cultured in TBK-Brij served as controls. $DsbA_{ox}$ and $DsbA_{red}$ indicate oxidized and reduced forms of DsbA, respectively.

5.2.2 Cpx and σ^E pathways are activated in LCFA-utilizing cells

To identify the defense mechanisms that restore redox homeostasis during LCFA metabolism, we checked the induction of the five well-characterized ESR pathways in *E.*

coli by assaying the β-gal activity of chromosomal *lacZ* fusions to the promoters of their known regulon members. Since the reporter fusions were in MG1655 background, we first ensured that similar to BW25113, MG1655 cultured in oleate also exhibits inadequate disulfide bond formation. For this, we cultured WT MG1655 in TBK-Ole and TBK-Brij, and checked the redox state of DsbA at T1, T2, T3, T4, and T5 time points (Fig. 5.2 A). Similar to BW25113, MG1655 cultured in TBK-Ole accumulated a completely reduced form of DsbA at time point T3 (corresponding to entry into stationary phase) (Figs. 5.2 A & B).

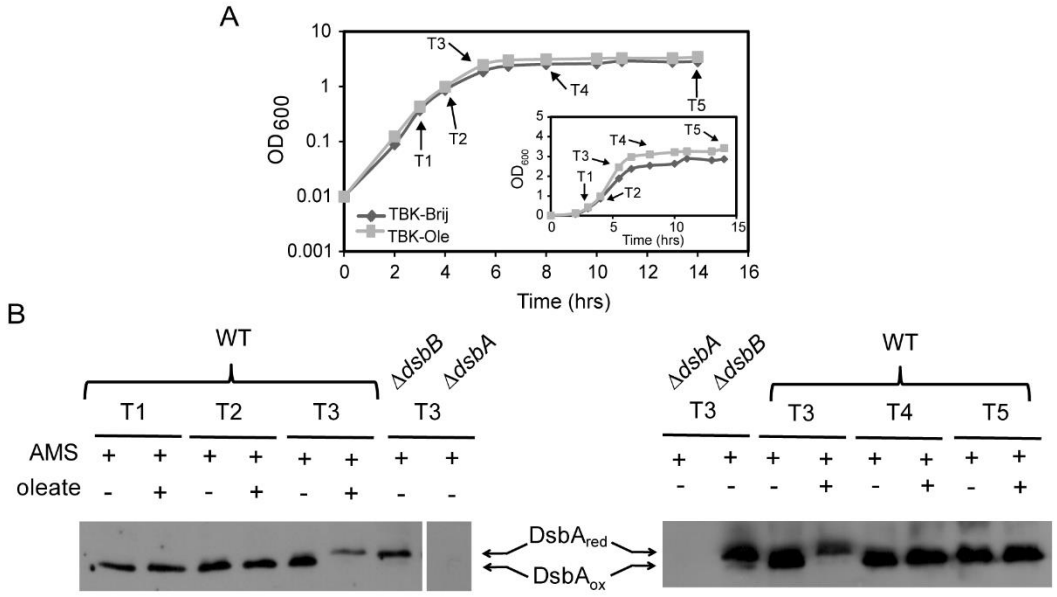

Figure 5.2. DsbA accumulates in a reduced form in WT MG1655 grown in LCFAs. (A) Growth curve of WT MG1655 in TBK-Brij and TBK-Ole. Cells were grown either in TBK-Brij or TBK-Ole. OD_{600} of the cultures was measured, and growth curves were plotted on a semi-logarithmic scale. The experiment was done two times. A representative dataset is shown. T1, T2, T3, T4, and T5 indicate time points where cultures were harvested to check the redox state of DsbA protein. *Inset*: The above growth curves were also plotted on a linear scale. (B) Accumulation of DsbA in a reduced form in WT MG1655 in LCFA-utilizing cells. WT MG1655 was grown either in TBK-Brij or TBK-Ole. Cultures were harvested at different time points, as indicated in Fig. 5.2 A, and processed as mentioned in the legend to Fig. 4.9; Chapter IV. Δ*dsbA* and Δ*dsbB* cultured in TBK-Brij served as controls. $DsbA_{ox}$ and $DsbA_{red}$ indicate oxidized and reduced forms of DsbA, respectively.

5.2.2.1 Cpx and σ^E ESR pathways are upregulated during LCFA metabolism

To check the induction of ESR pathways during LCFA metabolism, β-gal activity of chromosomal *lacZ* fusions to the promoters of their known regulon members (*spy* for Bae, *cpxP* for Cpx, *pspA* for Psp, *rprA* for Rcs and *rpoH*P3 for σ^E) (Macritchie & Raivio, 2009; Mitchell & Silhavy, 2019) at different phases of growth (Fig. 5.3 A) was determined in TBK-Brij amd TBK-Ole media. Of the five ESR pathways, only Cpx and σ^E were upregulated in TBK-Ole grown cells, with Cpx being activated to a greater extent (Figs. 5.3 B-F). Importantly, the upregulation of these systems was observed only in the stationary phase (Figs. 5.3 C & F). Further, the induction of these pathways was oleate utilization-dependent; in contrast to WT strain, Δ*fadL* and Δ*fadE* strains did not show significant induction of Cpx and σ^E pathways in TBK-Ole medium (Figs. 5.3 G & H). Collectively, these data indicate that Cpx and σ^E induction in oleate-utilizing cells might be a combat strategy to maintain redox homeostasis in the envelope.

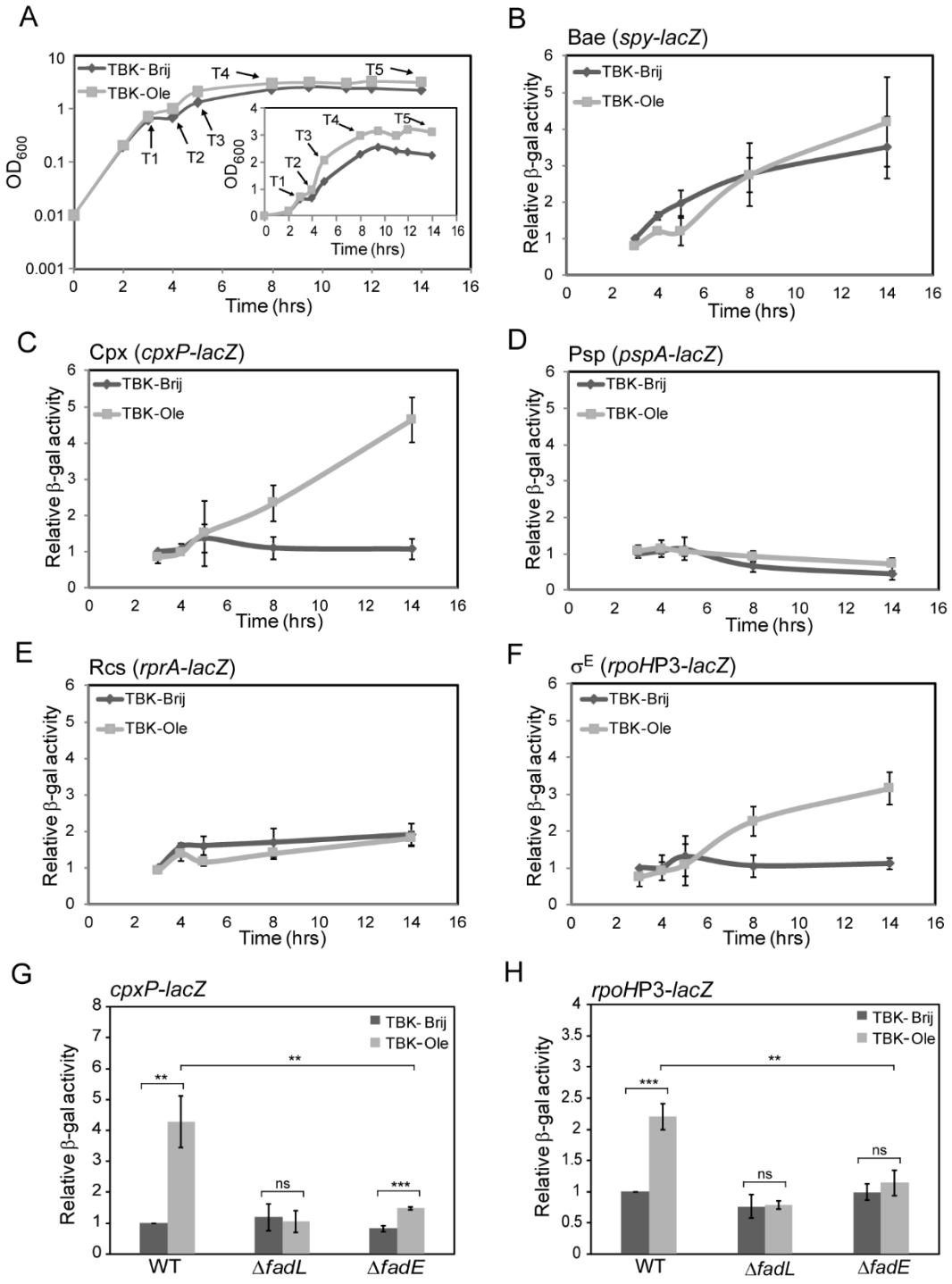

Figure 5.3. Amongst the various envelope stress response systems in *E. coli*, only Cpx and σ^E are induced during LCFA metabolism. (A) Growth curve of WT MG1655 carrying *cpxP-lacZ* reporter fusion in TBK-Brij and TBK-Ole. Cells were grown either in TBK-Brij or TBK-Ole. OD_{600} of the cultures was measured, and growth curves were plotted on a semi-logarithmic scale. The experiment was done three times. A representative dataset is shown. T1, T2, T3, T4, and T5 indicate time points where cultures were harvested for β-gal assays. The growth pattern of other reporter strains in MG1655 was similar, and thus, samples for β-gal assays were collected at the analogous time points. *Inset*: The above

growth curves were also plotted on a linear scale. (B-F) Cpx and σ^E responses are induced in the stationary phase in *E. coli* cultured in oleate. WT MG1655 carrying chromosomal fusion of *lacZ* with the promoters of known regulon members of Bae (*spy-lacZ*) (B), Cpx (*cpxP-lacZ*) (C), Psp (*pspA-lacZ*) (D), Rcs (*rprA-lacZ*) (E), and σ^E (*rpoH*P3-*lacZ*) (F) response systems were grown either in TBK-Brij or TBK-Ole. Cultures were harvested at different phases of growth corresponding to the time points indicated in Fig. 5.3 A and β-gal activity was measured. Data were normalized to the β-gal activity of WT in TBK-Brij at time point T1. Data represent the average (± SD) of at least three independent experiments. The average β-gal activity of the various reporter strains in TBK-Brij at time point T1 was: 34 (± 4) Miller units for *spy-lacZ*, 41 (± 8) Miller units for *cpxP-lacZ*, 150 (± 75) Miller units for *pspA-lacZ*, 43 (± 2) Miller units for *rprA-lacZ* and 33 (± 15) Miller units for *rpoH*P3-*lacZ*. (G-H) Activation of Cpx and σ^E responses in *E. coli* cultured in oleate is dependent on oleate utilization. Strains carrying *cpxP-lacZ* (G) or *rpoH*P3-*lacZ* (H) reporter fusions were grown either in TBK-Brij or TBK-Ole. Cultures were harvested in the stationary phase corresponding to the time point T5 indicated in Fig. 5.3 A and β-gal activity was measured. Data were normalized to the β-gal activity of WT in TBK-Brij. Data represent the average (± SD) of three independent experiments. The average β-gal activity of the WT *cpxP-lacZ* reporter strain in TBK-Brij was 51 (± 9) Miller units, and that of the WT *rpoH*P3-*lacZ* was 87 (± 31) Miller units. For figures F and G, the p-values were calculated using the unpaired two-tailed Student's t test (**, $P<0.01$; ***, $P<0.001$; ns, $P>0.03$).

5.2.3 Envelope signals generated by LCFA metabolism activate Cpx and σ^E

In *E. coli*, the Cpx and σ^E systems are induced by a vast array of stressors, including both cytoplasmic and envelope signals. We investigated whether during LCFA metabolism, the inducing signals for Cpx and σ^E originate in the cytoplasm or in the envelope.

5.2.3.1 Activation of Cpx pathway is majorly in response to envelope signal(s)

Misfolded proteins, such as the pilin subunits (PapE and PapG) of uropathogenic *E. coli* and the outer-membrane lipoprotein NlpE, constitute the envelope signals for Cpx activation. These signals mediate phosphorylation of an inner-membrane sensor histidine kinase CpxA, which in turn phosphorylates the cytoplasmic response regulator CpxR (Fig. 5.4 A, left panel) (Buelow & Raivio, 2005; Isaac et al, 2005; Raivio & Silhavy, 1997; Snyder et al, 1995). On the other hand, the low-molecular-weight phosphodonor, acetyl phosphate, a product of the phosphotransacetylase (Pta)- acetate kinase (AckA) pathway, constitutes the cytoplasmic signal for Cpx response. In cells grown in glucose, high levels

of acetyl phosphate phosphorylate CpxR in a CpxA-independent manner (Fig. 5.4 A, right panel) (Wolfe et al, 2008) (Section 1.8.2; Chapter I).

To determine whether the signal for Cpx activation in LCFA-utilizing cells is cytoplasmic or envelope in nature, we checked Cpx induction in Δ*pta*Δ*ackA* (where the cytoplasmic Cpx signal is eliminated) and Δ*cpxA* (where Cpx signaling from the envelope is eliminated) mutants, grown in basal and oleate- supplemented media (at time point T5; Figs. 5.4 B & C). We used glucose- supplemented medium as a control. We observed that in contrast to glucose-grown cells where Cpx induction was majorly in response to the cytoplasmic signal, in oleate-grown cells, Cpx induction was mainly in response to envelope signal. In glucose, Cpx induction decreased from ~6-fold in WT to ~2-fold in a Δ*pta*Δ*ackA* mutant (~30% residual induction); however, it decreased to only ~4-fold in a Δ*cpxA* mutant (~70% residual induction) (Figs. 5.4 B & C). On the other hand, in oleate, Cpx induction reduced from ~7-fold in WT to ~2-fold in a Δ*cpxA* mutant (~30% residual induction); however, it decreased to only ~4-fold in a Δ*pta*Δ*ackA* mutant (~70% residual induction) (Figs. 5.4 B & C). The Δ*pta*Δ*ackA* strain exhibited lower Cpx induction compared to WT in TBK-Brij, likely due to the elimination of signaling from acetyl-phosphate generated during growth in this medium (Fig. 5.4 B). On the other hand, the Δ*cpxA* strain showed higher Cpx induction in basal medium, likely due to the high steady-state levels of phosphorylated CpxR (phosphorylated by acetyl phosphate) resulting from the loss of phosphatase activity of CpxA (Fig. 5.4 C) (Vogt et al, 2014; Wolfe et al, 2008).

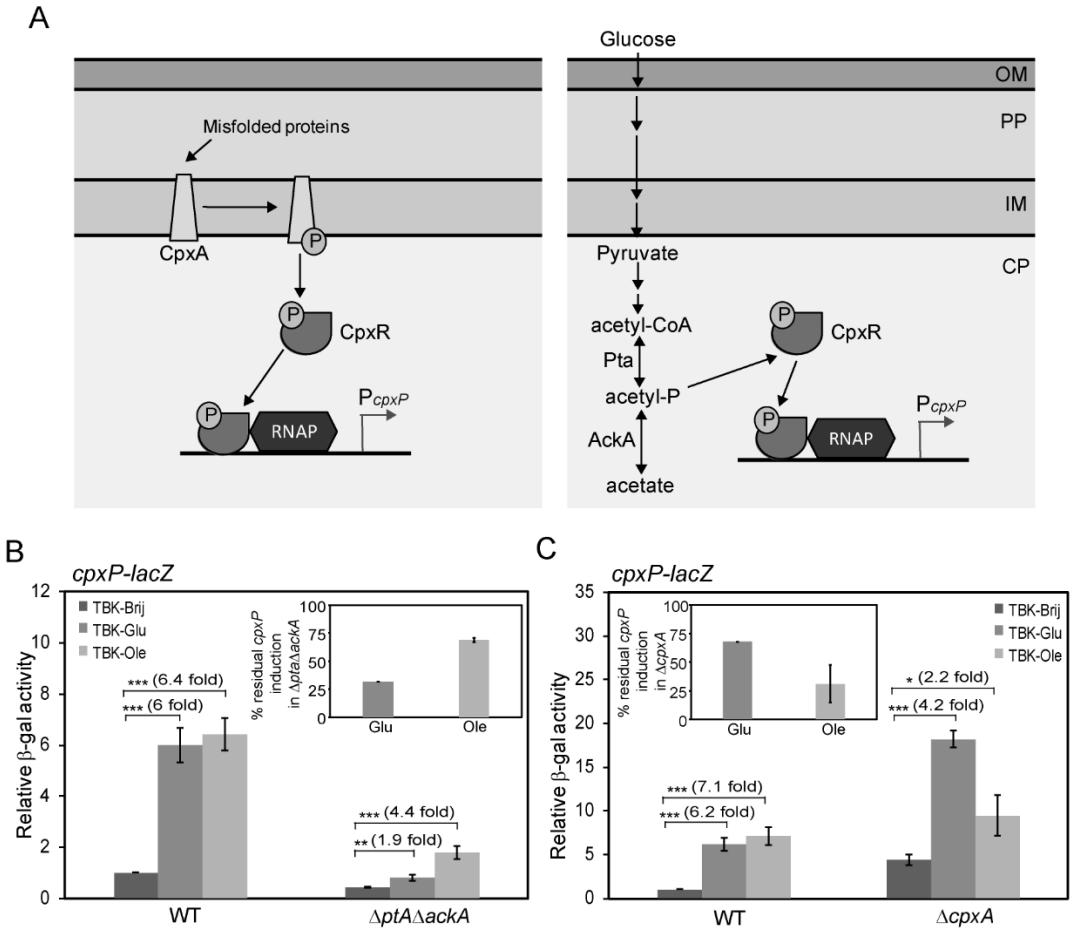

Figure 5.4. Cpx pathway is activated in response to envelope signals generated by LCFA metabolism. (A) Organization of the Cpx pathway. The CpxAR two-component system comprises of an inner-membrane sensor histidine kinase, CpxA, and a cytoplasmic response regulator, CpxR. Left panel: In the presence of envelope signals, such as misfolded proteins, CpxA acts as a kinase and phosphorylates CpxR. Right panel: Acetyl-phosphate, an intermediate of the Pta-AckA pathway, acts as the cytoplasmic signal for Cpx activation in cells grown in glucose, by directly transferring its phosphoryl group to CpxR. Phosphorylated CpxR directs the transcription of genes involved in mitigating stress. Abbreviations: CP, cytoplasm; IM, inner membrane; PP, periplasm; OM, outer membrane; acetyl-P, acetyl-phosphate; RNAP, RNA Polymerase. (B and C) Induction of the Cpx pathway in oleate-grown cells is majorly in response to envelope signal(s). Strains carrying *cpxP-lacZ* reporter fusion were grown in TBK-Brij, TBK-Brij supplemented with glucose (TBK-Glu) or TBK-Ole. Cultures were harvested in the stationary phase (time point T5, as indicated in Fig. 5.3 A), and β-gal activity was measured. Data were normalized to the β-gal activity of WT in TBK-Brij and represent the average (± SD) of three independent experiments. *Insets*: The data from the main figures 5.4 B and C are plotted as percent residual CpxP induction in the deletion strain, which is calculated as (fold CpxP induction in deletion strain in TBK-Glu or TBK-Ole with respect to its TBK-Brij control / fold CpxP induction in WT in TBK-Glu or TBK-Ole with respect to its TBK-Brij control)) × 100. The average β-gal activity of the WT *cpxP-lacZ* reporter strain in TBK-

Brij was 37 (± 5) Miller units (B) and 26 (± 3) Miller units (C). For figures B and C, the p-values were calculated using the unpaired two-tailed Student's t test (*, P<0.03; **, P<0.01; ***, P<0.001; ns, P>0.03).

5.2.3.2 Activation of σ^E pathway is in response to unfolded outer membrane protein(s)

The two major components of the outer membrane, OMPs and LPS, constitute the envelope signals for σ^E induction. Unfolded OMPs activate the inner membrane-anchored periplasmic protease DegS by binding to its PDZ domain. Activated DegS initiates cleavage of the anti-σ^E factor RseA, which normally sequesters σ^E at the inner membrane and prevents it from binding RNA polymerase (Walsh et al, 2003). LPS activates σ^E by displacing the periplasmic protein, RseB away from RseA, enabling OMP-activated DegS to cleave RseA (Lima et al, 2013). The σ^E response is also activated independent of the envelope signals. Under nutritional stress, a cytoplasmic alarmone factor, guanosine 3',5'-bispyrophosphate (ppGpp), upregulates σ^E-dependent transcription (Costanzo et al, 2008) (Fig. 5.5 A) (Section 1.8.1; Chapter I).

To determine whether during LCFA metabolism, the signal for σ^E activation is cytoplasmic or envelope in nature, we checked σ^E induction in *degS*ΔPDZ (where OMP-signaling is eliminated), Δ*rseB* (where LPS-signaling is eliminated) and $ppGpp^0$ (which lacks enzymes, RelA and SpoT, involved in ppGpp synthesis) strains, grown in basal and oleate- supplemented media (at time point T5; Figs. 5.5 B & C). We observed that in oleate-grown cells, σ^E induction was completely abolished in a *degS*ΔPDZ strain; however, σ^E activation was not affected either in a Δ*rseB* strain or a $ppGpp^0$ strain (Figs. 5.5 B & C). The requirement of the DegS PDZ domain strongly suggests that the signal for σ^E induction during oleate metabolism is an unfolded OMP.

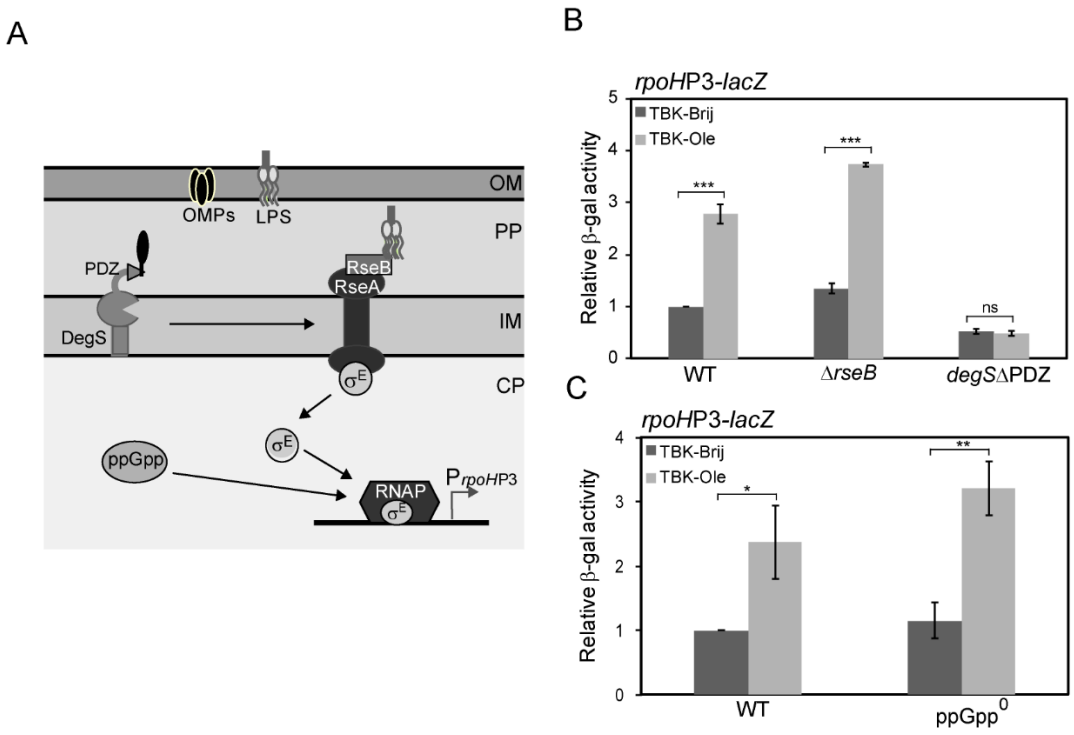

Figure 5.5. σ^E pathway is activated in response to envelope signals generated by LCFA metabolism. (A) Organization of the σ^E pathway. Under unstressed conditions, σ^E remains bound to RseA and is thus less available to bind RNA polymerase. Unfolded OMPs activate DegS by binding to its PDZ domain. LPS displaces RseB from RseA, enabling activated DegS to cleave RseA in its periplasmic domain. RseA is finally degraded by additional proteases to release σ^E, which binds RNA polymerase and initiates transcription of its regulon members. The cytoplasmic alarmone ppGpp upregulates σ^E-dependent transcription. Abbreviations: CP, cytoplasm; IM, inner membrane; PP, periplasm; OM, outer membrane; LPS, lipopolysaccharide; OMPs, outer membrane proteins; RNAP, RNA Polymerase. (B and C) Induction of the σ^E pathway in oleate-grown cells is in response to envelope signal(s). Strains carrying *rpoH*P3-*lacZ* were grown either in TBK-Brij or TBK-Ole. Cultures were harvested in the stationary phase (time point T5, as indicated in Fig. 5.3A), and β-gal activity was measured. Data were normalized to the β-gal activity of WT in TBK-Brij and represent the average (± SD) of three independent experiments. The average β-gal activity of the WT *rpoH*P3-*lacZ* in TBK-Brij was 29 (± 3) Miller units (B) and 71 (± 9) Miller units (C). For figures B and C, the p-values were calculated using the unpaired two-tailed Student's t test (*, P<0.03; **, P<0.01; ***, P<0.001; ns, P>0.03).

Taken together, our data indicate that both Cpx and σ^E pathways are activated in response to envelope signals generated by LCFA metabolism.

5.2.4 Hypo-oxidizing environment of the envelope is one of the reasons for Cpx induction during LCFA metabolism

Our results presented in the previous chapter showed that LCFA metabolism results in insufficient disulfide bond formation in the periplasm, i.e., a hypo-oxidizing envelope. In our results above, we showed that LCFA metabolism generates envelope signals for the activation of Cpx and σ^E pathways. We next investigated whether the signals for Cpx and σ^E activation are generated because of the hypo-oxidizing environment of the envelope.

5.2.4.1 LCFA-utilizing cells exogenously supplemented with ubiquinone exhibit only a partial induction of Cpx

We measured Cpx and σ^E induction in oleate-grown cells upon exogenous supplementation of ubiquinone, which would make the environment of the periplasm oxidizing by taking up electrons from the disulfide bond-forming machinery. We find that Cpx induction decreased by ~40% in TBK-Ole grown cells, however, there was no effect on σ^E induction (Fig. 5.6 A & B). The solvent used for ubiquinone, 0.1% ethanol, itself had no effect on either Cpx or σ^E induction (Fig. 5.6 C & D). These data indicate that during LCFA metabolism, the hypo-oxidizing environment of the envelope generates a stressor for Cpx activation, whereas the signal for σ^E induction is likely redox-independent.

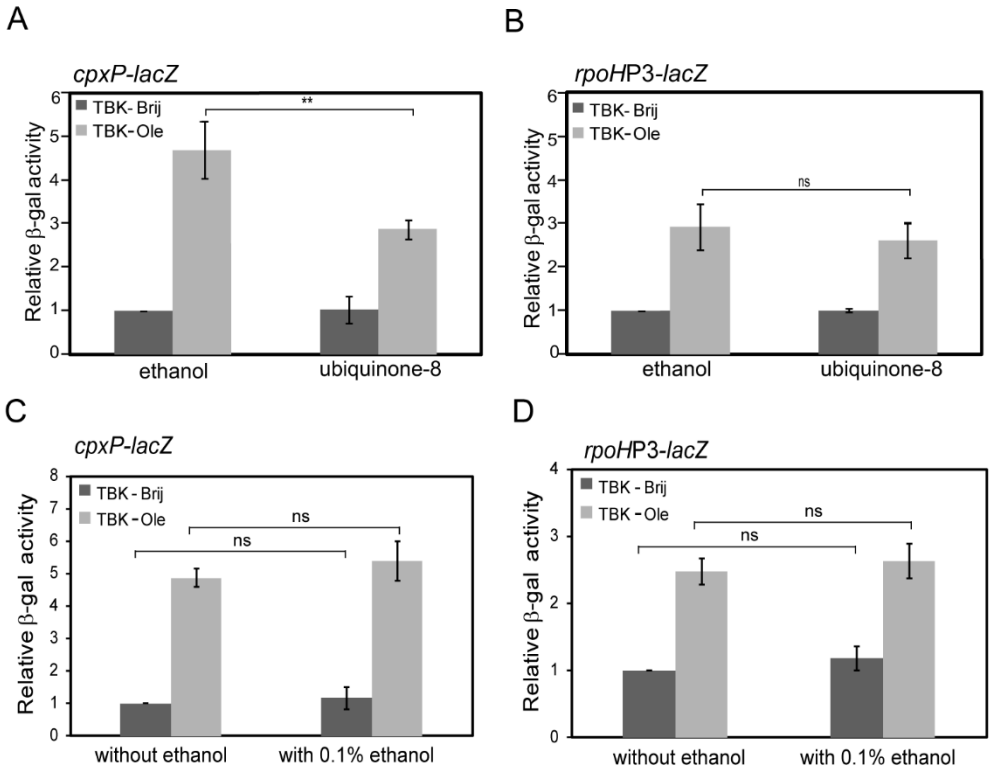

Figure 5.6. Ubiquinone supplementation decreases Cpx induction in LCFA-utilizing cells. (A and B) Supplementation of ubiquinone-8 decreases Cpx induction in oleate-utilizing cells. WT carrying either *cpxP-lacZ* (A) or *rpoH*P3-*lacZ* (B) reporter fusion was grown either in TBK-Brij or TBK-Ole. The media contained either 20 µM ubiquinone-8 or 0.1% ethanol. Cultures were harvested in the stationary phase (time point T5, as indicated in Fig. 5.3A), and β-gal activity was measured. Data were normalized to the β-gal activity of WT in TBK-Brij supplemented with 0.1% ethanol and represent the average (± SD) of three independent experiments. The average β-gal activity of the *cpxP-lacZ* reporter strain in TBK-Brij supplemented with 0.1% ethanol was 30 (± 13) Miller units, and that of the *rpoH*P3-*lacZ* was 57 (± 17) Miller units. (C and D) Ethanol supplementation does not affect the induction of Cpx and σ^E. WT carrying either *cpxP-lacZ* (C) or *rpoH*P3-*lacZ* (D) reporter fusion was grown either in TBK-Brij or TBK-Ole with or without 0.1% ethanol supplementation. Cultures were harvested in the stationary phase (time point T5, as indicated in Fig. 5.3 A), and β-gal activity was measured. Data were normalized to the β-gal activity of WT in TBK-Brij without ethanol supplementation and represent average (± SD) of three independent experiments. The average β-gal activity of the *cpxP-lacZ* reporter strain in TBK-Brij without ethanol supplementation was 34 (± 4) Miller units, and that of *rpoH*P3-*lacZ* was 45 (± 9) Miller units. The p-values were calculated using the unpaired two-tailed Student's t test (**, $P<0.01$; ns, $P>0.03$).

5.2.4.2 Cpx pathway responds to the altered redox state of the envelope

As a separate test that the Cpx pathway is activated in response to the altered redox state of the envelope, we used the Δ*cydD* strain, which is defective in exporting reduced glutathione

and cysteine to the periplasm and thus results in a hyper-oxidizing envelope (the redox potential of the periplasm in WT is -165 mV and in Δ*cydD* strain is -125 mV) (Messens et al, 2007; Pittman et al, 2002; Pittman et al, 2005). The Cpx response was downregulated ~2-fold in the Δ*cydD* strain in both basal and oleate supplemented media; however, there was no effect on σ^E induction (Fig. 5.7), indicating that only the Cpx pathway responds to the altered redox state of the periplasm.

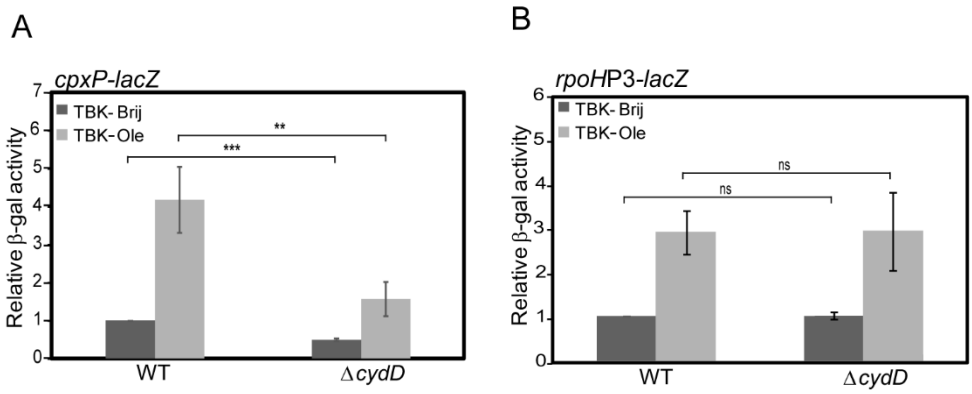

Figure 5.7. Cpx response is downregulated in a Δ*cydD* strain. Strains carrying either *cpxP-lacZ* (A) or *rpoH*P3-*lacZ* (B) reporter fusion were grown either in TBK-Brij or TBK-Ole. Cultures were harvested in the stationary phase (time point T5, as indicated in Fig. 5.3 A), and β-gal activity was measured. Data were normalized to the β-gal activity of WT in TBK-Brij and represent the average (± SD) of three independent experiments. The average β-gal activity of the WT *cpxP-lacZ* reporter strain in TBK-Brij was 53 (± 12) Miller units, and that of the WT *rpoH*P3-*lacZ* was 51 (± 16) Miller units. The p-values were calculated using the unpaired two-tailed Student's t test (**, P<0.01; ***, P<0.001; ns, P>0.03).

5.2.4.3 Cpx pathway is induced by the thiol agent, DTT

As another test that the Cpx pathway is activated by the altered redox state of the envelope, we determined Cpx induction upon supplementation of TBK-Brij medium with DTT, which would outcompete the oxidation of periplasmic proteins by DsbA, resulting in accumulation of reduced proteins in the periplasm (Zeng et al, 1998). Whereas there was ~6 fold induction of the Cpx response at 3 mM DTT, σ^E was induced only ~2-fold (Fig. 5.8). We also checked the induction of Rcs as a control since DTT is a strong reductant and

might induce ESR pathways globally. We did not find any induction of the Rcs ESR pathway on DTT supplementation.

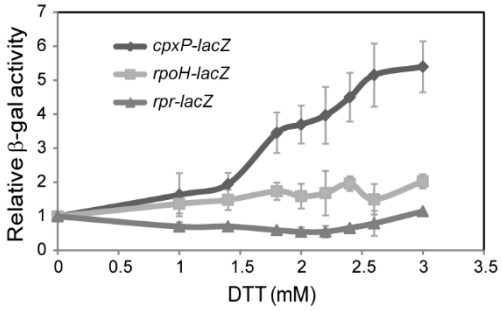

Figure 5.8. Cpx pathway is considerably induced in the presence of DTT. WT carrying *cpxP-lacZ, rpoH*P3-*lacZ,* or *rpr-lacZ* reporter fusion was grown in TBK-Brij supplemented with increasing concentrations of DTT, as indicated. Cultures were harvested in the exponential phase, and β-gal activity was measured. Data were normalized to the β-gal activity of WT in TBK-Brij without DTT and represent average (± SD) of atleast two independent experiments. The average β-gal activity of the *cpxP-lacZ* reporter strain in TBK-Brij without DTT was 13 (± 5) Miller units, and that of *rpoH*P3-*lacZ* and *rpr-lacZ* were 45 (± 17) Miller units and 99 (± 57) Miller units, respectively.

Collectively, our data emphasize that Cpx is the major pathway that gets activated in response to the altered redox state of the envelope.

5.3 Discussion

In this chapter, we demonstrated that signals generated during growth in LCFAs activate Cpx and σ^E ESR systems. Importantly, our work suggests that of the two ESR systems, Cpx plays a primary role during LCFA metabolism: i) amongst Cpx and σ^E, Cpx is induced to a greater extent by LCFAs, and ii) only the Cpx pathway senses redox-dependent signal. The work presented in chapters IV and V collectively emphasizes that ETC and ESR systems govern the interconnection between cellular metabolism and envelope redox homeostasis.

5.3.1 Possible mechanisms by which Cpx and σ^E sense envelope stress during LCFA metabolism

Several lipoproteins, misfolded pilin subunits of uropathogenic *E. coli*, and inner membrane respiratory complexes are known inducers of the Cpx pathway (Guest et al, 2017; Isaac et al, 2005; Miyadai et al, 2004; Snyder et al, 1995). Although the details of Cpx activation by these envelope components remains largely elusive, there are two suggested mechanisms. One mechanism involves direct interaction of the molecular signal with the sensor kinase, CpxA. An outer membrane lipoprotein, NlpE, accumulates at the inner membrane due to defects in lipoprotein trafficking and physically interacts with CpxA. Since NlpE is also a DsbA substrate, its mutant lacking the C-terminal disulfide bond turns on Cpx and Cpx activation in Δ*dsbA* is NlpE-dependent, this lipoprotein has been proposed to sense redox imbalance in the envelope (Delhaye et al, 2019; May et al, 2019). Another mechanism of Cpx activation involves titration of CpxP, a periplasmic inhibitor of CpxA. Misfolded pilin subunits sequester CpxP and deliver it to the periplasmic protease DegP. In this process, DegP degrades both CpxP and the pilin subunits (Isaac et al, 2005). However, CpxP displacement itself is not a sensing mechanism since pilin subunits activate Cpx even in its absence. CpxP is therefore proposed to fine-tune Cpx response by preventing inappropriate activation of CpxA and enabling rapid Cpx downregulation once the envelope stress is mitigated (DiGiuseppe & Silhavy, 2003).

The utilization of LCFAs generates envelope signals for Cpx activation, which are likely both redox-dependent and redox-independent. The presence of two types of signals is supported by the observation that upon providing ubiquinone to oleate-grown cells, whereas DsbA is present in its oxidized form and there is no decrease in AP activity, Cpx response is only partially downregulated (Figs. 4.8 & 4.11; Chapter IV and Fig. 5.6). Because NlpE is a well-recognized molecular signal for Cpx and can also sense redox

imbalance, we tested if it is the molecular cue during LCFA metabolism. However, we find that Cpx is fully induced in a Δ*nlpE* strain grown in oleate (Fig. 5.9).

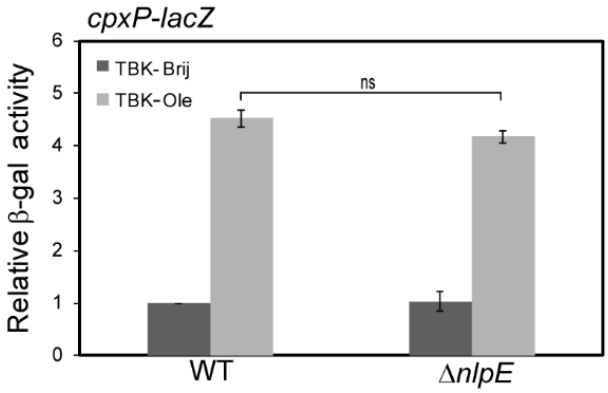

Figure 5.9. NlpE is not the signal for Cpx induction during LCFA metabolism. WT and Δ*nlpE* strains carrying *cpxP-lacZ* reporter fusion were grown either in TBK-Brij or TBK-Ole. Cultures were harvested in the stationary phase (time point T5, as indicated in Fig. 5.3 A), and β-gal activity was measured. Data were normalized to the β-gal activity of WT in TBK-Brij and represent average (± SD) of three independent experiments. The average β-gal activity of the WT *cpxP-lac*Z reporter strain in TBK-Brij was 28 (± 5) Miller units. The p-values were calculated using the unpaired two-tailed Student's t test (ns, P>0.03).

Because DegP is also a DsbA substrate that has been shown to accumulate significantly in its reduced form in LCFA-utilizing cells (Deeptodeep Roy, Ph.D. student) and functions as a protease in the thiol state (Skorko-Glonek et al, 2008), it is plausible that during LCFA metabolism, the reduced form of DegP degrades CpxP. However, since CpxP titration only fine-tunes the Cpx response, the additional redox-independent signal likely interacts directly with CpxA, resulting in robust activation of Cpx. Alternatively, both redox-dependent and redox-independent signals might induce Cpx exclusively via CpxA, without involving CpxP. It will be worth testing whether respiratory complexes or lipoproteins other than NlpE constitute signal(s) for Cpx activation during growth in LCFAs.

The σ^E pathway senses perturbations in the biogenesis of the outer membrane components, OMPs and LPS, via the DegS PDZ domain and RseB, respectively (Kim,

2015; Lima et al, 2013; Walsh et al, 2003). In a Δ*dsbA* strain, σ^E activation does not require the DegS PDZ domain and is suggested to be via RseB inhibition. An outer membrane component of the LPS transport machinery, LptD, is a DsbA substrate. Therefore, it is suggested that a decrease in the level of properly disulfide-bonded LptD in a Δ*dsbA* strain results in LPS accumulation, which then inhibits RseB to activate σ^E (Lima et al, 2013). Although LCFA metabolism also causes redox imbalance, σ^E induction is likely in response to the redox-independent envelope signal (Fig. 5.6). Further, the complete abolishment of σ^E induction in a *degS*ΔPDZ strain, but not in a Δ*rseB* strain, strongly indicates that an unfolded OMP, and not LPS, is the molecular signal for σ^E activation (Fig. 5.5 B). The probable candidate is FadL, the outer membrane LCFA transporter, which is upregulated during growth in LCFAs (Agrawal et al, 2017), and activates σ^E when overexpressed (Chaba et al, 2011). Taken together, multiple cues induce Cpx and σ^E pathways, which differ in their mode of activation. We suggest that even for conditions that ultimately impact the redox status of the envelope, i.e., deletion of *dsbA* and LCFA metabolism, the molecular signals which activate these stress responses are distinct.

5.3.2 Probable feedback exerted by Cpx and σ^E to maintain envelope redox homeostasis during growth in LCFAs

The Cpx and σ^E responses mediate adaptation to damaged proteins by upregulating envelope-localized protein folding and degrading factors (Raivio, 2014; Raivio et al, 2013; Rhodius et al, 2006). Because insufficient disulfide bond formation in LCFA-grown cells will result in the accumulation of unfolded/ misfolded proteins, the induction of Cpx and σ^E might restore envelope homeostasis by repairing/ clearing out damaged proteins. DsbA, a Cpx regulon member, maintains redox homeostasis by forming disulfide bonds in thiol proteins (Bardwell et al, 1991; Pogliano et al, 1997). However, during growth in LCFAs, DsbA upregulation might exacerbate the situation because newly synthesized DsbA would

itself require disulfide bond formation for its activity. A more effective mechanism for restoring redox homeostasis would be to downregulate components of the metabolic pathway that feed electrons into the ETC and upregulate components that increase the oxidizing power of the ETC. In fact, a combination of the following observations suggests that the Cpx pathway can maintain redox homeostasis by modulating LCFA metabolism: i) Cpx strongly downregulates NADH dehydrogenase I and succinate dehydrogenase, which transfer electrons into the ETC (Guest et al, 2017; Raivio et al, 2013), ii) in the Δ*cydD* strain, which has a hyper-oxidizing envelope, Cpx is downregulated (Fig. 5.7; this study), whereas *fad* genes involved in β-oxidation are upregulated (Holyoake et al, 2016), and iii) preliminary work from our lab shows that ubiquinone is downregulated in a Δ*cpxR* strain grown in LCFAs suggesting that Cpx upregulation during LCFA metabolism increases the oxidizing power of ETC by increasing ubiquinone levels (Megha Shrivastava, Ph.D. student). Future studies are required for a detailed investigation of the regulation exerted by Cpx on the LCFA metabolic pathway. Figure 5.10 summarizes the findings from chapters IV and V, and presents model for Cpx and σ^E activation during LCFA metabolism and the feedback provided by these systems to maintain envelope redox homeostasis.

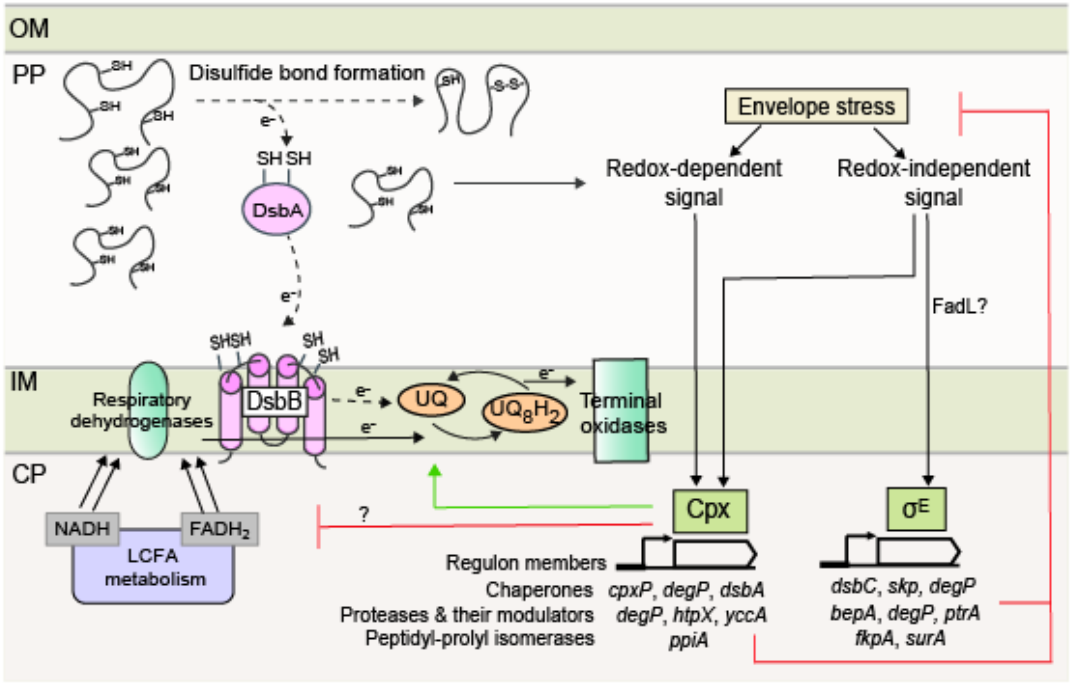

Figure 5.10. Model depicting the interconnection between LCFA metabolism, envelope redox status, and ESR pathways. LCFA degradation produces a large number of NADH and $FADH_2$, which are oxidized by respiratory dehydrogenases in the ETC. The increased flow of electrons in the ETC makes ubiquinone insufficient for taking up electrons from DsbA-DsbB, resulting in the accumulation of unfolded/ misfolded proteins. Cpx and σ^E ESR systems are activated, which restore envelope homeostasis. Cpx is partly induced by a redox-dependent signal, which is likely a DsbA substrate. Some redox-independent signal also activates Cpx. σ^E is activated in response to the accumulation of an unfolded OMP, likely FadL, and this constitutes its redox-independent signal. Cpx and σ^E responses decrease envelope stress by upregulating chaperones, proteases and their modulators, and peptidyl-prolyl isomerases, which repair damaged proteins. Besides, Cpx increases the oxidizing power of ETC by upregulating ubiquinone levels and might also decrease the load on ETC by downregulating LCFA metabolism. Arrows with e^- labeled on the line denote the direction of electron flow. The dotted arrows indicate decreased electron flow at these steps. Abbreviations: CP, cytoplasm; IM, inner membrane; PP, periplasm; OM, outer membrane; Ub, ubiquinone; UbH_2, ubiquinol.

Several gram-negative bacterial pathogens such as *Pseudomonas aeruginosa*, *Salmonella typhimurium*, and *Vibrio cholerae* use LCFAs acquired from host tissues as their source of energy (Fang et al, 2005; Rivera-Chavez & Mekalanos, 2019; Son et al, 2007). The present study provides a rationale for examining whether LCFA metabolism induces redox stress in these pathogens and whether activation of ESR pathways equivalent

of Cpx and σ^E represents their combat strategy. In addition to LCFA metabolism, disulfide bond formation and ESR systems have also been associated with bacterial pathogenesis (Acosta et al, 2015; Fang et al, 2005; Ha et al, 2003; Humphreys et al, 2004; Humphreys et al, 1999; Kovacikova & Skorupski, 2002; Miki et al, 2004; Peek & Taylor, 1992; Rivera-Chavez & Mekalanos, 2019; Son et al, 2007; Wu et al, 2004). Therefore, it will be important to determine whether LCFA metabolism impacts pathogenesis by influencing the redox status of the envelope and activation of ESR pathways.

CHAPTER VI

Summary and Future Prospects

In the first part of the thesis, we investigated the differential requirement of ETC components on non-fermentable carbon sources. We established that the requirement of aerobic ETC components for growth is inversely correlated with the energy yield of non-fermentable carbon sources; however, the requirement of ubiquinone is maximal for growth on LCFAs to counteract oxidative stress. The detailed genetic and biochemical analysis revealed ubiquinone as the first line of defense to manage oxidative stress-induced during LCFA metabolism.

Although we identified ubiquinone to be a major player during LCFA metabolism the mechanism that ubiquinone employs to counteract oxidative stress during LCFA metabolism is not known. The mechanism would depend on the major site of ROS formation. Based on previous suggestions that auto-oxidation of flavins is a likely source of ROS during aerobic metabolism, a predominant site of ROS formation during LCFA degradation could be the acyl-CoA dehydrogenase, FadE, which catalyzes the oxidation of acyl-CoA to enoyl-CoA concomitant with reduction of FAD to $FADH_2$. FadE has not been biochemically characterized till date; it has been considered to be the acyl-CoA dehydrogenase in *E. coli* based on genetic studies and the presence of characteristic sequence motifs. FadE is almost double the length of its mammalian counterpart, where the N- terminal 150 and C- terminal 400 amino acid residues have no match to the mammalian dehydrogenase. It has been proposed that the extra region in FadE performs the re-oxidation of $FADH_2$, transferring electrons to ubiquinone. In this direction, detailed studies would be required first to establish the dehydrogenase activity of FadE and then assessing whether FadE itself re-oxidizes $FADH_2$ and directly transfers electrons to ubiquinone or requires a separate electron transfer flavoprotein (ETF). Downstream experiments will include determining ROS production in cells upon altering the ratio of dehydrogenase and ETF components.

In the next part of the study, we showed that increased electron flow in the ETC during LCFA metabolism renders ubiquinone limiting for disulfide bond formation, thereby compromising redox balance in the envelope. Importantly, we showed that envelope signals generated during LCFA metabolism induce Cpx and σ^E pathways, with Cpx playing a primary role in monitoring redox homeostasis.

Future investigations are required to understand the mechanism of activation of the Cpx pathway during LCFA metabolism and the nature of feedback exerted by this ESR system to maintain envelope redox homeostasis. The Cpx pathway comprises a transmembrane sensor histidine kinase CpxA, cytoplasmic response regulator CpxR, and a periplasmic inhibitor of CpxA, CpxP. Stress conditions mediate phosphorylation of CpxA, which in turn, phosphorylates CpxR. Phosphorylated CpxR directs the transcription of genes, several of which encode envelope-localized protein folding and degrading factors that serve to combat stress. Studies focused on understanding the details of Cpx activation by its molecular signals have put forth two distinct mechanisms. In uropathogenic *E. coli*, misfolded subunits of P pilus, PapE and PapG, titrate away CpxP, enabling CpxA to autophosphorylate and further phosphorylate CpxR, thereby activating the pathway. On the other hand, the outer-membrane lipoprotein NlpE induces Cpx by directly interacting with CpxA. The present work strongly suggests that the molecular signal for Cpx induction in *E. coli* utilizing LCFAs is distinct from both NlpE and Pap pilin subunits. The periplasmic chaperone-protease DegP is a substrate of the DsbA-DsbB disulfide bond-forming machinery. Its function is redox-dependent; the disulfide-bonded form is a chaperone whereas the thiol form is a protease. Therefore, it is plausible that during LCFA metabolism, DegP accumulates in a reduced form and degrades CpxP, thereby activating Cpx pathway. Importantly, in the ongoing project in our lab, where we are trying to understand the molecular signal for Cpx activation, we find that the reduced form of DegP

is significantly more in cells grown in oleate in comparison to the basal medium (Deeptodeep Roy, PhD student). However, since CpxP titration only fine-tunes the Cpx response, the additional redox-independent signal likely interacts directly with CpxA, resulting in robust activation of Cpx. Therefore, in order to cover the entire repertoire of molecular signals that activate Cpx in LCFA-utilizing cells, we can use an unbiased systems approach. A transposon mutagenesis screen can be used to identify mutants defective in the upregulation of Cpx by LCFAs. We can combine transposon mutagenesis with the screening of the ordered single-deletion library (Keio deletion library) for mutants defective in Cpx induction by LCFAs. Since the signal for Cpx induction by oleate is periplasmic in nature, from the Keio library, only those strains which are deleted for genes encoding envelope proteins (~683 genes) can be selectively used.

Regarding the nature of feedback exerted by Cpx system to maintain envelope redox homeostasis during LCFA metabolism, we suggest that the Cpx pathway not only repairs the damaged proteins in the periplasm but also prevents stress by increasing the oxidizing power of the cell. Preliminary work from our lab shows that ubiquinone is downregulated in a Δ*cpxR* strain grown in LCFAs (Megha Shrivastava, Ph.D. student). Therefore, we suggest that Cpx upregulation during LCFA metabolism might increase the oxidizing power of ETC by increasing ubiquinone levels. In *E. coli*, the biosynthesis of ubiquinone is known to involve at least 13 *ubi* genes. It will be worthwhile to investigate the transcriptional regulation of the genes involved in ubiquinone biosynthesis by Cpx pathway. Recently, sRNA components of the Cpx pathway have also been recognized. Cpx pathway increases the expression of several sRNA genes (*micF, omrA, omrB, rprA* and *cyaR*). Cpx pathway might regulate ubiquinone levels during LCFA metabolism by modulating the levels of these sRNA or might involve novel sRNAs upregulated during LCFA metabolism. The sRNA regulation by the Cpx pathway can be investigated by

comparing the sRNA-Sequence profile of samples from WT and *cpxR* deletion strains cultured in LCFAs.

Bibliography

Acosta N, Pukatzki S, Raivio TL (2015) The Cpx system regulates virulence gene expression in *Vibrio cholerae*. *Infection and immunity* **83:** 2396-2408

Ades SE, Connolly LE, Alba BM, Gross CA (1999) The *Escherichia coli* σ^E-dependent extracytoplasmic stress response is controlled by the regulated proteolysis of an anti-sigma factor. *Genes & development* **13:** 2449-2461

Ades SE, Grigorova IL, Gross CA (2003) Regulation of the alternative sigma factor σ^E during initiation, adaptation, and shutoff of the extracytoplasmic heat shock response in *Escherichia coli*. *J Bacteriol* **185:** 2512-2519

Agrawal S (2018) Ubiquinone is a key antioxidant during long-chain fatty acid metabolism in *Escherichia coli* (Thesis submitted to Indian Institute of Science Education and Research Mohali, India, for Ph.D. degree).

Agrawal S, Jaswal K, Shiver AL, Balecha H, Patra T, Chaba R (2017) A genome-wide screen in *Escherichia coli* reveals that ubiquinone is a key antioxidant for metabolism of long-chain fatty acids. *J Biol Chem* **292:** 20086-20099

Akiyama Y, Kamitani S, Kusukawa N, Ito K (1992) *In vitro* catalysis of oxidative folding of disulfide-bonded proteins by the *Escherichia coli dsbA* (*ppfA*) gene product. *J Biol Chem* **267:** 22440-22445

Al-Attar S, Yu Y, Pinkse M, Hoeser J, Friedrich T, Bald D, de Vries S (2016) Cytochrome *bd* Displays Significant Quinol Peroxidase Activity. *Scientific reports* **6:** 27631

Alvarez AF, Rodriguez C, Georgellis D (2013) Ubiquinone and menaquinone electron carriers represent the yin and yang in the redox regulation of the ArcB sensor kinase. *J Bacteriol* **195:** 3054-3061

Aslund F, Zheng M, Beckwith J, Storz G (1999) Regulation of the OxyR transcription factor by hydrogen peroxide and the cellular thiol-disulfide status. *Proc Natl Acad Sci U S A* **96:** 6161-6165

Atkinson HJ, Babbitt PC (2009) An atlas of the thioredoxin fold class reveals the complexity of function-enabling adaptations. *PLoS computational biology* **5:** e1000541

Au DC, Gennis RB (1987) Cloning of the *cyo* locus encoding the cytochrome *o* terminal oxidase complex of *Escherichia coli*. *J Bacteriol* **169:** 3237-3242

Aussel L, Pierrel F, Loiseau L, Lombard M, Fontecave M, Barras F (2014) Biosynthesis and physiology of coenzyme Q in bacteria. *Biochim Biophys Acta* **1837:** 1004-1011

Baba T, Ara T, Hasegawa M, Takai Y, Okumura Y, Baba M, Datsenko KA, Tomita M, Wanner BL, Mori H (2006) Construction of *Escherichia coli* K-12 in-frame, single-gene knockout mutants: the Keio collection. *Molecular systems biology* **2:** 2006 0008

Bader M, Muse W, Ballou DP, Gassner C, Bardwell JC (1999) Oxidative protein folding is driven by the electron transport system. *Cell* **98:** 217-227

Barabesi C, Galizzi A, Mastromei G, Rossi M, Tamburini E, Perito B (2007) *Bacillus subtilis* gene cluster involved in calcium carbonate biomineralization. *J Bacteriol* **189:** 228-235

Barchinger SE, Ades SE (2013) Regulated proteolysis: control of the *Escherichia coli* σ^E-dependent cell envelope stress response. *Sub-cellular biochemistry* **66:** 129-160

Bardwell JC, Lee JO, Jander G, Martin N, Belin D, Beckwith J (1993) A pathway for disulfide bond formation *in vivo*. *Proc Natl Acad Sci U S A* **90:** 1038-1042

Bardwell JC, McGovern K, Beckwith J (1991) Identification of a protein required for disulfide bond formation *in vivo*. *Cell* **67:** 581-589

Benov LT, Fridovich I (1994) *Escherichia coli* expresses a copper- and zinc-containing superoxide dismutase. *J Biol Chem* **269:** 25310-25314

Berger EA (1973) Different mechanisms of energy coupling for the active transport of proline and glutamine in *Escherichia coli*. *Proc Natl Acad Sci U S A* **70:** 1514-1518

Bernal V, Castano-Cerezo S, Canovas M (2016) Acetate metabolism regulation in *Escherichia coli*: carbon overflow, pathogenicity, and beyond. *Appl Microbiol Biotechnol* **100:** 8985-9001

Bongaerts J, Zoske S, Weidner U, Unden G (1995) Transcriptional regulation of the proton translocating NADH dehydrogenase genes (*nuoA-N*) of *Escherichia coli* by electron acceptors, electron donors and gene regulators. *Mol Microbiol* **16:** 521-534

Booth IR (2005) Glycerol and Methylglyoxal Metabolism. In *EcoSal—Escherichia coli and Salmonella: Cellular and Molecular Biology*. , R. Curtiss III (ed), 3.4.4. http://www.ecosal.org. ASM Press, Washington, DC.

Borisov VB, Gennis RB, Hemp J, Verkhovsky MI (2011) The cytochrome *bd* respiratory oxygen reductases. *Biochim Biophys Acta* **1807:** 1398-1413

Borisov VB, Verkhovsky MI (2015) Oxygen as Acceptor. *EcoSal Plus* **6**

Bradley MD, Beach MB, de Koning APJ, Pratt TS, Osuna R (2007) Effects of Fis on *Escherichia coli* gene expression during different growth stages. *Microbiology* **153:** 2922-2940

Bragg PD, Hou C (1967) Reduced nicotinamide adenine dinucleotide oxidation in *Escherichia coli* particles. II. NADH dehydrogenases. *Archives of biochemistry and biophysics* **119:** 202-208

Braun V, Sieglin U (1970) The covalent murein-lipoprotein structure of the *Escherichia coli* cell wall. The attachment site of the lipoprotein on the murein. *Eur J Biochem* **13:** 336-346

Brickman E, Beckwith J (1975) Analysis of the regulation of *Escherichia coli* alkaline phosphatase synthesis using deletions and *phi*80 transducing phages. *Journal of molecular biology* **96:** 307-316

Buelow DR, Raivio TL (2005) Cpx signal transduction is influenced by a conserved N-terminal domain in the novel inhibitor CpxP and the periplasmic protease DegP. *J Bacteriol* **187:** 6622-6630

Butler JE, Glaven RH, Esteve-Nunez A, Nunez C, Shelobolina ES, Bond DR, Lovley DR (2006) Genetic characterization of a single bifunctional enzyme for fumarate reduction and succinate oxidation in *Geobacter sulfurreducens* and engineering of fumarate reduction in *Geobacter metallireducens*. *J Bacteriol* **188:** 450-455

Calhoun MW, Gennis RB (1993) Demonstration of separate genetic loci encoding distinct membrane-bound respiratory NADH dehydrogenases in *Escherichia coli*. *J Bacteriol* **175:** 3013-3019

Campbell JW, Cronan JE, Jr. (2002) The enigmatic *Escherichia coli fadE* gene is *yafH*. *J Bacteriol* **184:** 3759-3764

Campbell JW, Morgan-Kiss RM, Cronan JE, Jr. (2003) A new *Escherichia coli* metabolic competency: growth on fatty acids by a novel anaerobic beta-oxidation pathway. *Mol Microbiol* **47:** 793-805

Cap M, Vachova L, Palkova Z (2012) Reactive oxygen species in the signaling and adaptation of multicellular microbial communities. *Oxidative medicine and cellular longevity* **2012:** 976753

Carmany DO, Hollingsworth K, McCleary WR (2003) Genetic and biochemical studies of phosphatase activity of PhoR. *J Bacteriol* **185:** 1112-1115

Carmel-Harel O, Storz G (2000) Roles of the glutathione- and thioredoxin-dependent reduction systems in the *Escherichia coli* and *Saccharomyces cerevisiae* responses to oxidative stress. *Annual review of microbiology* **54:** 439-461

Castresana J, Lubben M, Saraste M, Higgins DG (1994) Evolution of cytochrome oxidase, an enzyme older than atmospheric oxygen. *The EMBO journal* **13:** 2516-2525

Chaba R, Alba BM, Guo MS, Sohn J, Ahuja N, Sauer RT, Gross CA (2011) Signal integration by DegS and RseB governs the σ^E-mediated envelope stress response in *Escherichia coli*. *Proc Natl Acad Sci U S A* **108:** 2106-2111

Chaba R, Grigorova IL, Flynn JM, Baker TA, Gross CA (2007) Design principles of the proteolytic cascade governing the σ^E-mediated envelope stress response in *Escherichia coli*: keys to graded, buffered, and rapid signal transduction. *Genes & development* **21:** 124-136

Cheng VW, Ma E, Zhao Z, Rothery RA, Weiner JH (2006) The iron-sulfur clusters in *Escherichia coli* succinate dehydrogenase direct electron flow. *J Biol Chem* **281:** 27662-27668

Chepuri V, Lemieux L, Au DC, Gennis RB (1990) The sequence of the *cyo* operon indicates substantial structural similarities between the cytochrome *o* ubiquinol oxidase of *Escherichia coli* and the aa3-type family of cytochrome *c* oxidases. *J Biol Chem* **265:** 11185-11192

Chiang SM, Schellhorn HE (2012) Regulators of oxidative stress response genes in *Escherichia coli* and their functional conservation in bacteria. *Archives of biochemistry and biophysics* **525:** 161-169

Cho BK, Knight EM, Palsson BO (2006) Transcriptional regulation of the *fad* regulon genes of *Escherichia coli* by ArcA. *Microbiology* **152:** 2207-2219

Choi H, Kim S, Mukhopadhyay P, Cho S, Woo J, Storz G, Ryu SE (2001) Structural basis of the redox switch in the OxyR transcription factor. *Cell* **105:** 103-113

Christman MF, Storz G, Ames BN (1989) OxyR, a positive regulator of hydrogen peroxide-inducible genes in *Escherichia coli* and *Salmonella typhimurium*, is homologous to a family of bacterial regulatory proteins. *Proc Natl Acad Sci U S A* **86:** 3484-3488

Clark DP, Cronan JE (2005) Two-carbon compounds and fatty acids as carbon sources. In *EcoSal—Escherichia coli and Salmonella: Cellular and Molecular Biology.* , R. Curtiss III (ed), 3.4.4. http://www.ecosal.org. ASM Press, Washington, DC.

Constantinidou C, Hobman JL, Griffiths L, Patel MD, Penn CW, Cole JA, Overton TW (2006) A reassessment of the FNR regulon and transcriptomic analysis of the effects of nitrate, nitrite, NarXL, and NarQP as *Escherichia coli* K12 adapts from aerobic to anaerobic growth. *J Biol Chem* **281:** 4802-4815

Costanzo A, Ades SE (2006) Growth phase-dependent regulation of the extracytoplasmic stress factor, σ^E, by guanosine 3',5'-bispyrophosphate (ppGpp). *J Bacteriol* **188:** 4627-4634

Costanzo A, Nicoloff H, Barchinger SE, Banta AB, Gourse RL, Ades SE (2008) ppGpp and DksA likely regulate the activity of the extracytoplasmic stress factor σ^E in *Escherichia coli* by both direct and indirect mechanisms. *Mol Microbiol* **67:** 619-632

Costerton JW, Ingram JM, Cheng KJ (1974) Structure and function of the cell envelope of gram-negative bacteria. *Bacteriological reviews* **38:** 87-110

Cotter PA, Gunsalus RP (1992) Contribution of the *fnr* and *arcA* gene products in coordinate regulation of cytochrome *o* and *d* oxidase (*cyoABCDE* and *cydAB*) genes in *Escherichia coli*. *FEMS microbiology letters* **70:** 31-36

Cox GB, Newton NA, Gibson F, Snoswell AM, Hamilton JA (1970) The function of ubiquinone in *Escherichia coli*. *Biochem J* **117:** 551-562

Creaghan IT, Guest JR (1978) Succinate dehydrogenase-dependent nutritional requirement for succinate in mutants of *Escherichia coli* K12. *J Gen Microbiol* **107:** 1-13

Cronan JE, Laporte D (2006) Tricarboxylic acid cycle and glyoxylate bypass. In *EcoSal—Escherichia coli and Salmonella: Cellular and Molecular Biology.* , R. Curtiss III (ed), 3.4.4. http://www.ecosal.org. ASM Press, Washington, DC.

Csonka LN, Fraenkel DG (1977) Pathways of NADPH formation in *Escherichia coli*. *J Biol Chem* **252:** 3382-3391

D'Autreaux B, Toledano MB (2007) ROS as signalling molecules: mechanisms that generate specificity in ROS homeostasis. *Nature reviews Molecular cell biology* **8:** 813-824

D'Mello R, Hill S, Poole RK (1996) The cytochrome *bd* quinol oxidase in *Escherichia coli* has an extremely high oxygen affinity and two oxygen-binding haems: implications for regulation of activity *in vivo* by oxygen inhibition. *Microbiology* **142 (Pt 4):** 755-763

Dailey FE, Berg HC (1993) Mutants in disulfide bond formation that disrupt flagellar assembly in *Escherichia coli*. *Proc Natl Acad Sci U S A* **90:** 1043-1047

Danese PN, Silhavy TJ (1998) CpxP, a stress-combative member of the Cpx regulon. *J Bacteriol* **180:** 831-839

Danese PN, Snyder WB, Cosma CL, Davis LJ, Silhavy TJ (1995) The Cpx two-component signal transduction pathway of *Escherichia coli* regulates transcription of the gene specifying the stress-inducible periplasmic protease, DegP. *Genes & development* **9:** 387-398

Datsenko KA, Wanner BL (2000) One-step inactivation of chromosomal genes in *Escherichia coli* K-12 using PCR products. *Proc Natl Acad Sci U S A* **97:** 6640-6645

De Wulf P, McGuire AM, Liu X, Lin EC (2002) Genome-wide profiling of promoter recognition by the two-component response regulator CpxR-P in *Escherichia coli*. *J Biol Chem* **277:** 26652-26661

Delcour AH (2009) Outer membrane permeability and antibiotic resistance. *Biochim Biophys Acta* **1794:** 808-816

Delhaye A, Collet JF, Laloux G (2016) Fine-Tuning of the Cpx Envelope Stress Response Is Required for Cell Wall Homeostasis in *Escherichia coli*. *mBio* **7:** e00047-00016

Delhaye A, Laloux G, Collet JF (2019) The Lipoprotein NlpE Is a Cpx Sensor That Serves as a Sentinel for Protein Sorting and Folding Defects in the *Escherichia coli* Envelope. *J Bacteriol* **201**

Denoncin K, Collet JF (2013) Disulfide bond formation in the bacterial periplasm: major achievements and challenges ahead. *Antioxid Redox Signal* **19:** 63-71

Dharmadi Y, Murarka A, Gonzalez R (2006) Anaerobic fermentation of glycerol by *Escherichia coli*: a new platform for metabolic engineering. *Biotechnology and bioengineering* **94:** 821-829

DiGiuseppe PA, Silhavy TJ (2003) Signal detection and target gene induction by the CpxRA two-component system. *J Bacteriol* **185:** 2432-2440

Dirusso CC, Black PN (2004) Bacterial long chain fatty acid transport: gateway to a fatty acid-responsive signaling system. *J Biol Chem* **279:** 49563-49566

DiRusso CC, Heimert TL, Metzger AK (1992) Characterization of FadR, a global transcriptional regulator of fatty acid metabolism in *Escherichia coli*. Interaction with the *fadB* promoter is prevented by long chain fatty acyl coenzyme A. *J Biol Chem* **267:** 8685-8691

Doi H, Hoshino Y, Nakase K, Usuda Y (2014) Reduction of hydrogen peroxide stress derived from fatty acid beta-oxidation improves fatty acid utilization in *Escherichia coli*. *Appl Microbiol Biotechnol* **98:** 629-639

Duong F, Eichler J, Price A, Leonard MR, Wickner W (1997) Biogenesis of the gram-negative bacterial envelope. *Cell* **91:** 567-573

Dutton RJ, Boyd D, Berkmen M, Beckwith J (2008) Bacterial species exhibit diversity in their mechanisms and capacity for protein disulfide bond formation. *Proc Natl Acad Sci U S A* **105:** 11933-11938

Dworkin J, Jovanovic G, Model P (2000) The PspA protein of *Escherichia coli* is a negative regulator of σ^{54}-dependent transcription. *J Bacteriol* **182:** 311-319

Dwyer DJ, Belenky PA, Yang JH, MacDonald IC, Martell JD, Takahashi N, Chan CT, Lobritz MA, Braff D, Schwarz EG, Ye JD, Pati M, Vercruysse M, Ralifo PS, Allison KR, Khalil AS, Ting AY, Walker GC, Collins JJ (2014) Antibiotics induce redox-related physiological alterations as part of their lethality. *Proc Natl Acad Sci U S A* **111:** E2100-2109

Efremov RG, Sazanov LA (2011) Structure of the membrane domain of respiratory complex I. *Nature* **476:** 414-420

Elferink MG, Hellingwerf KJ, Konings WN (1985) The role of the proton motive force and electron flow in solute transport in *Escherichia coli*. *Eur J Biochem* **153:** 161-165

Erental A, Kalderon Z, Saada A, Smith Y, Engelberg-Kulka H (2014) Apoptosis-like death, an extreme SOS response in *Escherichia coli*. *mBio* **5:** e01426-01414

Erhardt H, Steimle S, Muders V, Pohl T, Walter J, Friedrich T (2012) Disruption of individual *nuo*-genes leads to the formation of partially assembled NADH:ubiquinone oxidoreductase (complex I) in *Escherichia coli*. *Biochim Biophys Acta* **1817:** 863-871

Ezraty B, Vergnes A, Banzhaf M, Duverger Y, Huguenot A, Brochado AR, Su SY, Espinosa L, Loiseau L, Py B, Typas A, Barras F (2013) Fe-S cluster biosynthesis controls uptake of aminoglycosides in a ROS-less death pathway. *Science* **340:** 1583-1587

Falk-Krzesinski HJ, Wolfe AJ (1998) Genetic analysis of the *nuo* locus, which encodes the proton-translocating NADH dehydrogenase in *Escherichia coli*. *J Bacteriol* **180:** 1174-1184

Fang FC, Libby SJ, Castor ME, Fung AM (2005) Isocitrate lyase (AceA) is required for *Salmonella* persistence but not for acute lethal infection in mice. *Infection and immunity* **73:** 2547-2549

Farr SB, Kogoma T (1991) Oxidative stress responses in *Escherichia coli* and *Salmonella typhimurium*. *Microbiol Rev* **55:** 561-585

Ferguson GP, Booth IR (1998) Importance of glutathione for growth and survival of *Escherichia coli* cells: detoxification of methylglyoxal and maintenance of intracellular K^+. *J Bacteriol* **180:** 4314-4318

Fridovich I (1978) The biology of oxygen radicals. *Science* **201:** 875-880

Friedrich T, Pohl T (2007) NADH as donor. In *EcoSal—Escherichia coli and Salmonella: Cellular and Molecular Biology.* , R. Curtiss III (ed), 3.4.4. http://www.ecosal.org. ASM Press, Washington, DC.

Fu HA, Iuchi S, Lin EC (1991) The requirement of ArcA and Fnr for peak expression of the *cyd* operon in *Escherichia coli* under microaerobic conditions. *Molecular & general genetics : MGG* **226:** 209-213

Fujimoto N, Kosaka T, Yamada M (2012) Menaquinone as Well as Ubiquinone as a Crucial Component in the *Escherichia coli* Respiratory Chain. *Chemical Biology Book Chapter*

Georgellis D, Kwon O, Lin EC (2001) Quinones as the redox signal for the arc two-component system of bacteria. *Science* **292:** 2314-2316

Giles DK, Hankins JV, Guan Z, Trent MS (2011) Remodelling of the *Vibrio cholerae* membrane by incorporation of exogenous fatty acids from host and aquatic environments. *Mol Microbiol* **79:** 716-728

Goswami M, Mangoli SH, Jawali N (2006) Involvement of reactive oxygen species in the action of ciprofloxacin against *Escherichia coli*. *Antimicrob Agents Chemother* **50:** 949-954

Govantes F, Orjalo AV, Gunsalus RP (2000) Interplay between three global regulatory proteins mediates oxygen regulation of the *Escherichia coli* cytochrome *d* oxidase (*cydAB*) operon. *Mol Microbiol* **38:** 1061-1073

Grabowicz M, Koren D, Silhavy TJ (2016) The CpxQ sRNA Negatively Regulates Skp To Prevent Mistargeting of beta-Barrel Outer Membrane Proteins into the Cytoplasmic Membrane. *mBio* **7:** e00312-00316

Grabowicz M, Silhavy TJ (2017) Envelope Stress Responses: An Interconnected Safety Net. *Trends in biochemical sciences* **42:** 232-242

Green GN, Gennis RB (1983) Isolation and characterization of an *Escherichia coli* mutant lacking cytochrome *d* terminal oxidase. *J Bacteriol* **154:** 1269-1275

Green J, Anjum MF, Guest JR (1997) Regulation of the *ndh* gene of *Escherichia coli* by integration host factor and a novel regulator, Arr. *Microbiology* **143 (Pt 9):** 2865-2875

Green J, Guest JR (1994) Regulation of transcription at the *ndh* promoter of *Escherichia coli* by FNR and novel factors. *Mol Microbiol* **12:** 433-444

Gu M, Imlay JA (2011) The SoxRS response of *Escherichia coli* is directly activated by redox-cycling drugs rather than by superoxide. *Mol Microbiol* **79:** 1136-1150

Guest RL, Wang J, Wong JL, Raivio TL (2017) A Bacterial Stress Response Regulates Respiratory Protein Complexes To Control Envelope Stress Adaptation. *J Bacteriol* **199**

Guilhot C, Jander G, Martin NL, Beckwith J (1995) Evidence that the pathway of disulfide bond formation in *Escherichia coli* involves interactions between the cysteines of DsbB and DsbA. *Proc Natl Acad Sci U S A* **92:** 9895-9899

Gulmezian M, Hyman KR, Marbois BN, Clarke CF, Javor GT (2007) The role of UbiX in *Escherichia coli* coenzyme Q biosynthesis. *Archives of biochemistry and biophysics* **467:** 144-153

Gupta SD, Lee BT, Camakaris J, Wu HC (1995) Identification of *cutC* and *cutF* (*nlpE*) genes involved in copper tolerance in *Escherichia coli*. *J Bacteriol* **177:** 4207-4215

Guzman LM, Belin D, Carson MJ, Beckwith J (1995) Tight regulation, modulation, and high-level expression by vectors containing the arabinose PBAD promoter. *J Bacteriol* **177:** 4121-4130

Ha UH, Wang Y, Jin S (2003) DsbA of *Pseudomonas aeruginosa* is essential for multiple virulence factors. *Infection and immunity* **71:** 1590-1595

Hajj Chehade M, Loiseau L, Lombard M, Pecqueur L, Ismail A, Smadja M, Golinelli-Pimpaneau B, Mellot-Draznieks C, Hamelin O, Aussel L, Kieffer-Jaquinod S, Labessan N, Barras F, Fontecave M, Pierrel F (2013) *ubiI*, a new gene in *Escherichia coli* coenzyme Q biosynthesis, is involved in aerobic C5-hydroxylation. *J Biol Chem* **288:** 20085-20092

Hajj Chehade M, Pelosi L, Fyfe CD, Loiseau L, Rascalou B, Brugiere S, Kazemzadeh K, Vo CD, Ciccone L, Aussel L, Coute Y, Fontecave M, Barras F, Lombard M, Pierrel F (2019) A Soluble Metabolon Synthesizes the Isoprenoid Lipid Ubiquinone. *Cell Chem Biol* **26:** 482-492 e487

Hatahet F, Boyd D, Beckwith J (2014) Disulfide bond formation in prokaryotes: history, diversity and design. *Biochim Biophys Acta* **1844:** 1402-1414

Hidalgo E, Demple B (1994) An iron-sulfur center essential for transcriptional activation by the redox-sensing SoxR protein. *The EMBO journal* **13:** 138-146

Hill FF, Angelmaier D (1972) Specific enrichment of mutants of *Escherichia coli* with an altered acyl CoA synthetase by tritium suicide. *Molecular & general genetics : MGG* **117:** 143-152

Holyoake LV, Hunt S, Sanguinetti G, Cook GM, Howard MJ, Rowe ML, Poole RK, Shepherd M (2016) CydDC-mediated reductant export in *Escherichia coli* controls the transcriptional wiring of energy metabolism and combats nitrosative stress. *Biochem J* **473:** 693-701

Humphreys S, Rowley G, Stevenson A, Anjum MF, Woodward MJ, Gilbert S, Kormanec J, Roberts M (2004) Role of the two-component regulator CpxAR in the virulence of *Salmonella enterica* serotype Typhimurium. *Infection and immunity* **72:** 4654-4661

Humphreys S, Stevenson A, Bacon A, Weinhardt AB, Roberts M (1999) The alternative sigma factor, σ^E, is critically important for the virulence of *Salmonella typhimurium*. *Infection and immunity* **67:** 1560-1568

Hussein NA, Cho SH, Laloux G, Siam R, Collet JF (2018) Distinct domains of *Escherichia coli* IgaA connect envelope stress sensing and down-regulation of the Rcs phosphorelay across subcellular compartments. *PLoS genetics* **14:** e1007398

Imlay JA (2013) The molecular mechanisms and physiological consequences of oxidative stress: lessons from a model bacterium. *Nat Rev Microbiol* **11:** 443-454

Inaba K, Ito K (2002) Paradoxical redox properties of DsbB and DsbA in the protein disulfide-introducing reaction cascade. *The EMBO journal* **21:** 2646-2654

Ingledew WJ, Poole RK (1984) The respiratory chains of *Escherichia coli*. *Microbiol Rev* **48:** 222-271

Iram SH, Cronan JE (2006) The beta-oxidation systems of *Escherichia coli* and *Salmonella enterica* are not functionally equivalent. *J Bacteriol* **188:** 599-608

Isaac DD, Pinkner JS, Hultgren SJ, Silhavy TJ (2005) The extracytoplasmic adaptor protein CpxP is degraded with substrate by DegP. *Proc Natl Acad Sci U S A* **102:** 17775-17779

Ito K, Inaba K (2008) The disulfide bond formation (Dsb) system. *Current opinion in structural biology* **18:** 450-458

Iuchi S, Lin EC (1988) *arcA* (*dye*), a global regulatory gene in *Escherichia coli* mediating repression of enzymes in aerobic pathways. *Proc Natl Acad Sci U S A* **85:** 1888-1892

Iuchi S, Lin EC (1991) Adaptation of *Escherichia coli* to respiratory conditions: regulation of gene expression. *Cell* **66:** 5-7

Jones-Carson J, Husain M, Liu L, Orlicky DJ, Vazquez-Torres A (2016) Cytochrome *bd*-Dependent Bioenergetics and Antinitrosative Defenses in *Salmonella* Pathogenesis. *mBio* **7**

Jovanovic G, Lloyd LJ, Stumpf MP, Mayhew AJ, Buck M (2006) Induction and function of the phage shock protein extracytoplasmic stress response in *Escherichia coli*. *J Biol Chem* **281:** 21147-21161

Jovanovic G, Weiner L, Model P (1996) Identification, nucleotide sequence, and characterization of PspF, the transcriptional activator of the *Escherichia coli* stress-induced *psp* operon. *J Bacteriol* **178:** 1936-1945

Kadokura H, Beckwith J (2002) Four cysteines of the membrane protein DsbB act in concert to oxidize its substrate DsbA. *The EMBO journal* **21:** 2354-2363

Kadokura H, Beckwith J (2009) Detecting folding intermediates of a protein as it passes through the bacterial translocation channel. *Cell* **138:** 1164-1173

Kadokura H, Katzen F, Beckwith J (2003) Protein disulfide bond formation in prokaryotes. *Annual review of biochemistry* **72:** 111-135

Kadokura H, Tian H, Zander T, Bardwell JC, Beckwith J (2004) Snapshots of DsbA in action: detection of proteins in the process of oxidative folding. *Science* **303:** 534-537

Kamio Y, Nikaido H (1976) Outer membrane of *Salmonella typhimurium*: accessibility of phospholipid head groups to phospholipase c and cyanogen bromide activated dextran in the external medium. *Biochemistry* **15:** 2561-2570

Kang Y, Zarzycki-Siek J, Walton CB, Norris MH, Hoang TT (2010) Multiple FadD acyl-CoA synthetases contribute to differential fatty acid degradation and virulence in *Pseudomonas aeruginosa*. *PLoS One* **5:** e13557

Kasahara M, Anraku Y (1974) Succinate dehydrogenase of *Escherichia coli* membrane vesicles. Activation and properties of the enzyme. *Journal of biochemistry* **76:** 959-966

Keseler IM, Mackie A, Peralta-Gil M, Santos-Zavaleta A, Gama-Castro S, Bonavides-Martinez C, Fulcher C, Huerta AM, Kothari A, Krummenacker M, Latendresse M, Muniz-Rascado L, Ong Q, Paley S, Schroder I, Shearer AG, Subhraveti P, Travers M, Weerasinghe D, Weiss V, Collado-Vides J, Gunsalus RP, Paulsen I, Karp PD (2013) EcoCyc: fusing model organism databases with systems biology. *Nucleic acids research* **41:** D605-612

Kim DY (2015) Two stress sensor proteins for the expression of σ^E regulon: DegS and RseB. *J Microbiol* **53:** 306-310

Kishigami S, Kanaya E, Kikuchi M, Ito K (1995) DsbA-DsbB interaction through their active site cysteines. Evidence from an odd cysteine mutant of DsbA. *J Biol Chem* **270:** 17072-17074

Kita K, Konishi K, Anraku Y (1984) Terminal oxidases of *Escherichia coli* aerobic respiratory chain. I. Purification and properties of cytochrome *b*562-*o* complex from cells in the early exponential phase of aerobic growth. *J Biol Chem* **259:** 3368-3374

Kleanthous C, Armitage JP (2015) The bacterial cell envelope. *Philosophical transactions of the Royal Society of London Series B, Biological sciences* **370**

Klein K (1973) AcylCoADehydrogenasen und ETF in *Escherichia coli*: Studien zum Fetts¨aureabbau. Ph.D. thesis. Universit¨at zu K¨oln, Cologne, Germany.

Kobayashi T, Kishigami S, Sone M, Inokuchi H, Mogi T, Ito K (1997) Respiratory chain is required to maintain oxidized states of the DsbA-DsbB disulfide bond formation system in aerobically growing *Escherichia coli* cells. *Proc Natl Acad Sci U S A* **94:** 11857-11862

Konovalova A, Perlman DH, Cowles CE, Silhavy TJ (2014) Transmembrane domain of surface-exposed outer membrane lipoprotein RcsF is threaded through the lumen of beta-barrel proteins. *Proc Natl Acad Sci U S A* **111:** E4350-4358

Korshunov S, Imlay JA (2010) Two sources of endogenous hydrogen peroxide in *Escherichia coli*. *Mol Microbiol* **75:** 1389-1401

Kovacikova G, Skorupski K (2002) The alternative sigma factor σ^E plays an important role in intestinal survival and virulence in *Vibrio cholerae*. *Infection and immunity* **70:** 5355-5362

Kumar C, Igbaria A, D'Autreaux B, Planson AG, Junot C, Godat E, Bachhawat AK, Delaunay-Moisan A, Toledano MB (2011) Glutathione revisited: a vital function in iron metabolism and ancillary role in thiol-redox control. *The EMBO journal* **30:** 2044-2056

Kwon O, Druce-Hoffman M, Meganathan R (2005) Regulation of the ubiquinone (coenzyme Q) biosynthetic genes *ubiCA* in *Escherichia coli*. *Current microbiology* **50:** 180-189

Landeta C, Boyd D, Beckwith J (2018) Disulfide bond formation in prokaryotes. *Nature microbiology* **3:** 270-280

Layer G, Reichelt J, Jahn D, Heinz DW (2010) Structure and function of enzymes in heme biosynthesis. *Protein science : a publication of the Protein Society* **19:** 1137-1161

Lee PT, Hsu AY, Ha HT, Clarke CF (1997) A C-methyltransferase involved in both ubiquinone and menaquinone biosynthesis: isolation and identification of the *Escherichia coli ubiE* gene. *J Bacteriol* **179:** 1748-1754

Lee Y, Kim Y, Yeom S, Kim S, Park S, Jeon CO, Park W (2008) The role of disulfide bond isomerase A (DsbA) of *Escherichia coli* O157:H7 in biofilm formation and virulence. *FEMS microbiology letters* **278:** 213-222

Lee YM, DiGiuseppe PA, Silhavy TJ, Hultgren SJ (2004) P pilus assembly motif necessary for activation of the CpxRA pathway by PapE in *Escherichia coli*. *J Bacteriol* **186:** 4326-4337

Lennen RM, Kruziki MA, Kumar K, Zinkel RA, Burnum KE, Lipton MS, Hoover SW, Ranatunga DR, Wittkopp TM, Marner WD, 2nd, Pfleger BF (2011) Membrane stresses induced by overproduction of free fatty acids in *Escherichia coli*. *Appl Environ Microbiol* **77:** 8114-8128

Li W, Wu H, Li M, San KY (2018) Effect of NADPH availability on free fatty acid production in *Escherichia coli*. *Biotechnology and bioengineering* **115:** 444-452

Lima S, Guo MS, Chaba R, Gross CA, Sauer RT (2013) Dual molecular signals mediate the bacterial response to outer-membrane stress. *Science* **340:** 837-841

Lin EC, Iuchi S (1991) Regulation of gene expression in fermentative and respiratory systems in *Escherichia coli* and related bacteria. *Annual review of genetics* **25:** 361-387

Loiseau L, Fyfe C, Aussel L, Hajj Chehade M, Hernandez SB, Faivre B, Hamdane D, Mellot-Draznieks C, Rascalou B, Pelosi L, Velours C, Cornu D, Lombard M, Casadesus J, Pierrel F, Fontecave M, Barras F (2017) The UbiK protein is an accessory factor necessary for bacterial ubiquinone (UQ) biosynthesis and forms a complex with the UQ biogenesis factor UbiJ. *J Biol Chem* **292:** 11937-11950

Lu J, Holmgren A (2014) The thioredoxin antioxidant system. *Free radical biology & medicine* **66:** 75-87

Macdonald IA, Kuehn MJ (2013) Stress-induced outer membrane vesicle production by *Pseudomonas aeruginosa*. *J Bacteriol* **195:** 2971-2981

Macritchie DM, Raivio TL (2009) Envelope Stress Responses. *EcoSal Plus* **3**

Mahan MJ, Tobias JW, Slauch JM, Hanna PC, Collier RJ, Mekalanos JJ (1995) Antibiotic-based selection for bacterial genes that are specifically induced during infection of a host. *Proc Natl Acad Sci U S A* **92:** 669-673

Maher MJ, Herath AS, Udagedara SR, Dougan DA, Truscott KN (2018) Crystal structure of bacterial succinate:quinone oxidoreductase flavoprotein SdhA in complex with its assembly factor SdhE. *Proc Natl Acad Sci U S A* **115:** 2982-2987

Majdalani N, Hernandez D, Gottesman S (2002) Regulation and mode of action of the second small RNA activator of RpoS translation, RprA. *Mol Microbiol* **46:** 813-826

Malanovic N, Lohner K (2016) Gram-positive bacterial cell envelopes: The impact on the activity of antimicrobial peptides. *Biochim Biophys Acta* **1858:** 936-946

Manson MD, Tedesco P, Berg HC, Harold FM, Van der Drift C (1977) A protonmotive force drives bacterial flagella. *Proc Natl Acad Sci U S A* **74:** 3060-3064

Manta B, Boyd D, Berkmen M (2019) Disulfide Bond Formation in the Periplasm of *Escherichia coli*. *EcoSal Plus* **8**

Masse E, Gottesman S (2002) A small RNA regulates the expression of genes involved in iron metabolism in *Escherichia coli*. *Proc Natl Acad Sci U S A* **99:** 4620-4625

Mattam AJ, Yazdani SS (2013) Engineering *E. coli* strain for conversion of short chain fatty acids to bioalcohols. *Biotechnology for biofuels* **6:** 128

May KL, Grabowicz M (2018) The bacterial outer membrane is an evolving antibiotic barrier. *Proc Natl Acad Sci U S A* **115:** 8852-8854

May KL, Lehman KM, Mitchell AM, Grabowicz M (2019) A Stress Response Monitoring Lipoprotein Trafficking to the Outer Membrane. *mBio* **10**

McBroom AJ, Johnson AP, Vemulapalli S, Kuehn MJ (2006) Outer membrane vesicle production by *Escherichia coli* is independent of membrane instability. *J Bacteriol* **188:** 5385-5392

McBroom AJ, Kuehn MJ (2007) Release of outer membrane vesicles by Gram-negative bacteria is a novel envelope stress response. *Mol Microbiol* **63:** 545-558

McCord JM, Keele BB, Jr., Fridovich I (1971) An enzyme-based theory of obligate anaerobiosis: the physiological function of superoxide dismutase. *Proc Natl Acad Sci U S A* **68:** 1024-1027

McNeil MB, Clulow JS, Wilf NM, Salmond GP, Fineran PC (2012) SdhE is a conserved protein required for flavinylation of succinate dehydrogenase in bacteria. *J Biol Chem* **287:** 18418-18428

Meehan BM, Landeta C, Boyd D, Beckwith J (2017a) The Disulfide Bond Formation Pathway Is Essential for Anaerobic Growth of *Escherichia coli*. *J Bacteriol* **199**

Meehan BM, Landeta C, Boyd D, Beckwith J (2017b) The essential cell division protein FtsN contains a critical disulfide bond in a non-essential domain. *Mol Microbiol* **103:** 413-422

Meinhardt SW, Matsushita K, Kaback HR, Ohnishi T (1989) EPR characterization of the iron-sulfur-containing NADH-ubiquinone oxidoreductase of the *Escherichia coli* aerobic respiratory chain. *Biochemistry* **28:** 2153-2160

Messens J, Collet JF (2006) Pathways of disulfide bond formation in *Escherichia coli*. *The international journal of biochemistry & cell biology* **38:** 1050-1062

Messens J, Collet JF, Van Belle K, Brosens E, Loris R, Wyns L (2007) The oxidase DsbA folds a protein with a nonconsecutive disulfide. *J Biol Chem* **282:** 31302-31307

Messner KR, Imlay JA (1999) The identification of primary sites of superoxide and hydrogen peroxide formation in the aerobic respiratory chain and sulfite reductase complex of *Escherichia coli*. *J Biol Chem* **274:** 10119-10128

Miki T, Okada N, Danbara H (2004) Two periplasmic disulfide oxidoreductases, DsbA and SrgA, target outer membrane protein SpiA, a component of the *Salmonella* pathogenicity island 2 type III secretion system. *J Biol Chem* **279:** 34631-34642

Mileykovskaya E, Dowhan W (1997) The Cpx two-component signal transduction pathway is activated in *Escherichia coli* mutant strains lacking phosphatidylethanolamine. *J Bacteriol* **179:** 1029-1034

Miller JH (1972) *Experiments in molecular genetics* Cold Spring Harbor Laboratory, NY.

Miller SI, Salama NR (2018) The gram-negative bacterial periplasm: Size matters. *PLoS biology* **16:** e2004935

Missiakas D, Georgopoulos C, Raina S (1993) Identification and characterization of the *Escherichia coli* gene *dsbB*, whose product is involved in the formation of disulfide bonds *in vivo*. *Proc Natl Acad Sci U S A* **90:** 7084-7088

Mitchell AM, Silhavy TJ (2019) Envelope stress responses: balancing damage repair and toxicity. *Nat Rev Microbiol* **17:** 417-428

Miyadai H, Tanaka-Masuda K, Matsuyama S, Tokuda H (2004) Effects of lipoprotein overproduction on the induction of DegP (HtrA) involved in quality control in the *Escherichia coli* periplasm. *J Biol Chem* **279:** 39807-39813

Mootha VK, Lindgren CM, Eriksson KF, Subramanian A, Sihag S, Lehar J, Puigserver P, Carlsson E, Ridderstrale M, Laurila E, Houstis N, Daly MJ, Patterson N, Mesirov JP, Golub TR, Tamayo P, Spiegelman B, Lander ES, Hirschhorn JN, Altshuler D, Groop LC (2003) PGC-1alpha-responsive genes involved in oxidative phosphorylation are coordinately downregulated in human diabetes. *Nat Genet* **34:** 267-273

Muir ME, Hanwell DR, Wallace BJ (1981) Characterization of a respiratory mutant of *Escherichia coli* with reduced uptake of aminoglycoside antibiotics. *Biochim Biophys Acta* **638:** 234-241

Muller C, Bang IS, Velayudhan J, Karlinsey J, Papenfort K, Vogel J, Fang FC (2009) Acid stress activation of the σ^E stress response in *Salmonella enterica* serovar Typhimurium. *Mol Microbiol* **71:** 1228-1238

Mutalik VK, Nonaka G, Ades SE, Rhodius VA, Gross CA (2009) Promoter strength properties of the complete σ^E regulon of *Escherichia coli* and *Salmonella enterica*. *J Bacteriol* **191:** 7279-7287

Mychack A, Amrutha RN, Chung C, Cardenas Arevalo K, Reddy M, Janakiraman A (2019) A synergistic role for two predicted inner membrane proteins of *Escherichia coli* in cell envelope integrity. *Mol Microbiol* **111:** 317-337

Nakanishi-Matsui M, Sekiya M, Futai M (2016) ATP synthase from *Escherichia coli*: Mechanism of rotational catalysis, and inhibition with the epsilon subunit and phytopolyphenols. *Biochim Biophys Acta* **1857:** 129-140

Nam TW, Park YH, Jeong HJ, Ryu S, Seok YJ (2005) Glucose repression of the *Escherichia coli sdhCDAB* operon, revisited: regulation by the CRP*cAMP complex. *Nucleic acids research* **33:** 6712-6722

Neijssel OM, Teixeira de Mattos MJ (1994) The energetics of bacterial growth: a reassessment. *Mol Microbiol* **13:** 172-182

Nichols RJ, Sen S, Choo YJ, Beltrao P, Zietek M, Chaba R, Lee S, Kazmierczak KM, Lee KJ, Wong A, Shales M, Lovett S, Winkler ME, Krogan NJ, Typas A, Gross CA (2011) Phenotypic landscape of a bacterial cell. *Cell* **144:** 143-156

Nikaido H (2003) Molecular basis of bacterial outer membrane permeability revisited. *Microbiology and molecular biology reviews : MMBR* **67:** 593-656

Nunn WD, Simons RW, Egan PA, Maloy SR (1979) Kinetics of the utilization of medium and long chain fatty acids by mutant of *Escherichia coli* defective in the *fadL* gene. *J Biol Chem* **254:** 9130-9134

Nunoshiba T, Hidalgo E, Amabile Cuevas CF, Demple B (1992) Two-stage control of an oxidative stress regulon: the *Escherichia coli* SoxR protein triggers redox-inducible expression of the *soxS* regulatory gene. *J Bacteriol* **174:** 6054-6060

Ogasawara H, Ishida Y, Yamada K, Yamamoto K, Ishihama A (2007) PdhR (pyruvate dehydrogenase complex regulator) controls the respiratory electron transport system in *Escherichia coli*. *J Bacteriol* **189:** 5534-5541

Otto K, Silhavy TJ (2002) Surface sensing and adhesion of *Escherichia coli* controlled by the Cpx-signaling pathway. *Proc Natl Acad Sci U S A* **99:** 2287-2292

Overath P, Pauli G, Schairer HU (1969) Fatty acid degradation in *Escherichia coli*. An inducible acyl-CoA synthetase, the mapping of old-mutations, and the isolation of regulatory mutants. *Eur J Biochem* **7:** 559-574

Pace J, Hayman MJ, Galan JE (1993) Signal transduction and invasion of epithelial cells by *S. typhimurium*. *Cell* **72:** 505-514

Pathania A, Gupta AK, Dubey S, Gopal B, Sardesai AA (2016) The Topology of the l-Arginine Exporter ArgO Conforms to an Nin-Cout Configuration in *Escherichia coli*: Requirement for the Cytoplasmic N-Terminal Domain, Functional Helical Interactions, and an Aspartate Pair for ArgO Function. *J Bacteriol* **198:** 3186-3199

Peek JA, Taylor RK (1992) Characterization of a periplasmic thiol:disulfide interchange protein required for the functional maturation of secreted virulence factors of *Vibrio cholerae*. *Proc Natl Acad Sci U S A* **89:** 6210-6214

Pelosi L, Ducluzeau AL, Loiseau L, Barras F, Schneider D, Junier I, Pierrel F (2016) Evolution of ubiquinone biosynthesis: multiple proteobacterial enzymes with various regioselectives to catalyze three contiguous aromatic hydroxylation reactions. *MSystems* **1:** e00091-00016

Perrenoud A, Sauer U (2005) Impact of global transcriptional regulation by ArcA, ArcB, Cra, Crp, Cya, Fnr, and Mlc on glucose catabolism in *Escherichia coli*. *J Bacteriol* **187:** 3171-3179

Perry JJ, Gunsalus RP, Lory S, Staley JT (2007) Microbial Life.

Pipe LZ, Grimson MJ (2008) Spatial-temporal modelling of bacterial colony growth on solid media. *Mol Biosyst* **4:** 192-198

Pittman MS, Corker H, Wu G, Binet MB, Moir AJ, Poole RK (2002) Cysteine is exported from the *Escherichia coli* cytoplasm by CydDC, an ATP-binding cassette-type transporter required for cytochrome assembly. *J Biol Chem* **277:** 49841-49849

Pittman MS, Robinson HC, Poole RK (2005) A bacterial glutathione transporter (*Escherichia coli* CydDC) exports reductant to the periplasm. *J Biol Chem* **280:** 32254-32261

Pogliano J, Lynch AS, Belin D, Lin EC, Beckwith J (1997) Regulation of *Escherichia coli* cell envelope proteins involved in protein folding and degradation by the Cpx two-component system. *Genes & development* **11:** 1169-1182

Pomposiello PJ, Bennik MH, Demple B (2001) Genome-wide transcriptional profiling of the *Escherichia coli* responses to superoxide stress and sodium salicylate. *J Bacteriol* **183:** 3890-3902

Pramanik A, Pawar S, Antonian E, Schulz H (1979) Five different enzymatic activities are associated with the multienzyme complex of fatty acid oxidation from *Escherichia coli*. *J Bacteriol* **137:** 469-473

Price NL, Raivio TL (2009) Characterization of the Cpx regulon in *Escherichia coli* strain MC4100. *J Bacteriol* **191:** 1798-1815

Pruss BM, Nelms JM, Park C, Wolfe AJ (1994) Mutations in NADH:ubiquinone oxidoreductase of *Escherichia coli* affect growth on mixed amino acids. *J Bacteriol* **176:** 2143-2150

Raivio TL (2014) Everything old is new again: an update on current research on the Cpx envelope stress response. *Biochim Biophys Acta* **1843:** 1529-1541

Raivio TL, Leblanc SK, Price NL (2013) The *Escherichia coli* Cpx envelope stress response regulates genes of diverse function that impact antibiotic resistance and membrane integrity. *J Bacteriol* **195:** 2755-2767

Raivio TL, Popkin DL, Silhavy TJ (1999) The Cpx envelope stress response is controlled by amplification and feedback inhibition. *J Bacteriol* **181:** 5263-5272

Raivio TL, Silhavy TJ (1997) Transduction of envelope stress in *Escherichia coli* by the Cpx two-component system. *J Bacteriol* **179:** 7724-7733

Ray S, Chatterjee E, Chatterjee A, Paul K, Chowdhury R (2011) A *fadD* mutant of *Vibrio cholerae* is impaired in the production of virulence factors and membrane localization of the virulence regulatory protein TcpP. *Infection and immunity* **79:** 258-266

Ren G, Champion MM, Huntley JF (2014) Identification of disulfide bond isomerase substrates reveals bacterial virulence factors. *Mol Microbiol* **94:** 926-944

Rensing C, Mitra B, Rosen BP (1997) Insertional inactivation of *dsbA* produces sensitivity to cadmium and zinc in *Escherichia coli*. *J Bacteriol* **179:** 2769-2771

Rhodius VA, Suh WC, Nonaka G, West J, Gross CA (2006) Conserved and variable functions of the σ^E stress response in related genomes. *PLoS biology* **4:** e2

Rietsch A, Belin D, Martin N, Beckwith J (1996) An *in vivo* pathway for disulfide bond isomerization in *Escherichia coli*. *Proc Natl Acad Sci U S A* **93:** 13048-13053

Ritz D, Patel H, Doan B, Zheng M, Aslund F, Storz G, Beckwith J (2000) Thioredoxin 2 is involved in the oxidative stress response in *Escherichia coli*. *J Biol Chem* **275:** 2505-2512

Rivera-Chavez F, Mekalanos JJ (2019) Cholera toxin promotes pathogen acquisition of host-derived nutrients. *Nature* **572:** 244-248

Roberts DL, Frerman FE, Kim JJ (1996) Three-dimensional structure of human electron transfer flavoprotein to 2.1-A resolution. *Proc Natl Acad Sci U S A* **93:** 14355-14360

Rodriguez JG, Hernandez AC, Helguera-Repetto C, Aguilar Ayala D, Guadarrama-Medina R, Anzola JM, Bustos JR, Zambrano MM, Gonzalez YMJ, Garcia MJ, Del Portillo P (2014) Global adaptation to a lipid environment triggers the dormancy-related phenotype of *Mycobacterium tuberculosis*. *mBio* **5:** e01125-01114

Rojas ER, Billings G, Odermatt PD, Auer GK, Zhu L, Miguel A, Chang F, Weibel DB, Theriot JA, Huang KC (2018) The outer membrane is an essential load-bearing element in Gram-negative bacteria. *Nature* **559:** 617-621

Romano AH, Nickerson WJ (1958) Utilization of amino acids as carbon sources by *Streptomyces fradiae*. *J Bacteriol* **75:** 161-166

Rosadini CV, Wong SM, Akerley BJ (2008) The periplasmic disulfide oxidoreductase DsbA contributes to *Haemophilus influenzae* pathogenesis. *Infection and immunity* **76:** 1498-1508

Rowley G, Spector M, Kormanec J, Roberts M (2006) Pushing the envelope: extracytoplasmic stress responses in bacterial pathogens. *Nat Rev Microbiol* **4:** 383-394

Saiki K, Mogi T, Anraku Y (1992) Heme O biosynthesis in *Escherichia coli*: the *cyoE* gene in the cytochrome *bo* operon encodes a protoheme IX farnesyltransferase. *Biochemical and biophysical research communications* **189:** 1491-1497

Saiki K, Mogi T, Ogura K, Anraku Y (1993) *In vitro* heme *O* synthesis by the *cyoE* gene product from *Escherichia coli*. *J Biol Chem* **268:** 26041-26044

Saiki K, Nakamura H, Mogi T, Anraku Y (1996) Probing a role of subunit IV of the *Escherichia coli bo*-type ubiquinol oxidase by deletion and cross-linking analyses. *J Biol Chem* **271:** 15336-15340

San KY, Bennett GN, Berrios-Rivera SJ, Vadali RV, Yang YT, Horton E, Rudolph FB, Sariyar B, Blackwood K (2002) Metabolic engineering through cofactor manipulation and its effects on metabolic flux redistribution in *Escherichia coli*. *Metabolic engineering* **4:** 182-192

Sankaran K, Wu HC (1994) Lipid modification of bacterial prolipoprotein. Transfer of diacylglyceryl moiety from phosphatidylglycerol. *J Biol Chem* **269:** 19701-19706

Sardesai AA, Genevaux P, Schwager F, Ang D, Georgopoulos C (2003) The OmpL porin does not modulate redox potential in the periplasmic space of *Escherichia coli*. *The EMBO journal* **22:** 1461-1466

Sauer U, Canonaco F, Heri S, Perrenoud A, Fischer E (2004) The soluble and membrane-bound transhydrogenases UdhA and PntAB have divergent functions in NADPH metabolism of *Escherichia coli*. *J Biol Chem* **279:** 6613-6619

Sawers RG, Clark DP (2004) Fermentative Pyruvate and Acetyl-Coenzyme A Metabolism. *EcoSal Plus* **1**

Schulte M, Frick K, Gnandt E, Jurkovic S, Burschel S, Labatzke R, Aierstock K, Fiegen D, Wohlwend D, Gerhardt S, Einsle O, Friedrich T (2019) A mechanism to prevent production of reactive oxygen species by *Escherichia coli* respiratory complex I. *Nature communications* **10:** 2551

Schwechheimer C, Kuehn MJ (2015) Outer-membrane vesicles from Gram-negative bacteria: biogenesis and functions. *Nat Rev Microbiol* **13:** 605-619

Seaver LC, Imlay JA (2001) Alkyl hydroperoxide reductase is the primary scavenger of endogenous hydrogen peroxide in *Escherichia coli*. *J Bacteriol* **183:** 7173-7181

Seaver LC, Imlay JA (2004) Are respiratory enzymes the primary sources of intracellular hydrogen peroxide? *J Biol Chem* **279:** 48742-48750

Senior AE (1988) ATP synthesis by oxidative phosphorylation. *Physiological reviews* **68:** 177-231

Shan Y, Lazinski D, Rowe S, Camilli A, Lewis K (2015) Genetic basis of persister tolerance to aminoglycosides in *Escherichia coli*. *mBio* **6**

Sharma P, Stagge S, Bekker M, Bettenbrock K, Hellingwerf KJ (2013) Kinase activity of ArcB from *Escherichia coli* is subject to regulation by both ubiquinone and demethylmenaquinone. *PLoS One* **8:** e75412

Shestopalov AI, Bogachev AV, Murtazina RA, Viryasov MB, Skulachev VP (1997) Aeration-dependent changes in composition of the quinone pool in *Escherichia coli*. Evidence of post-transcriptional regulation of the quinone biosynthesis. *FEBS letters* **404:** 272-274

Shimada T, Fujita N, Yamamoto K, Ishihama A (2011) Novel roles of cAMP receptor protein (CRP) in regulation of transport and metabolism of carbon sources. *PLoS One* **6:** e20081

Shiver AL, Osadnik H, Kritikos G, Li B, Krogan N, Typas A, Gross CA (2016) A Chemical-Genomic Screen of Neglected Antibiotics Reveals Illicit Transport of Kasugamycin and Blasticidin S. *PLoS genetics* **12:** e1006124

Siegele DA, Imlay KR, Imlay JA (1996) The stationary-phase-exit defect of *cydC* (*surB*) mutants is due to the lack of a functional terminal cytochrome oxidase. *J Bacteriol* **178:** 6091-6096

Siegele DA, Kolter R (1993) Isolation and characterization of an *Escherichia coli* mutant defective in resuming growth after starvation. *Genes & development* **7:** 2629-2640

Silhavy TJ, Kahne D, Walker S (2010) The bacterial cell envelope. *Cold Spring Harbor perspectives in biology* **2:** a000414

Skorko-Glonek J, Sobiecka-Szkatula A, Lipinska B (2006) Characterization of disulfide exchange between DsbA and HtrA proteins from *Escherichia coli*. *Acta Biochim Pol* **53:** 585-589

Skorko-Glonek J, Sobiecka-Szkatula A, Narkiewicz J, Lipinska B (2008) The proteolytic activity of the HtrA (DegP) protein from *Escherichia coli* at low temperatures. *Microbiology* **154:** 3649-3658

Snyder WB, Davis LJ, Danese PN, Cosma CL, Silhavy TJ (1995) Overproduction of NlpE, a new outer membrane lipoprotein, suppresses the toxicity of periplasmic LacZ by activation of the Cpx signal transduction pathway. *J Bacteriol* **177:** 4216-4223

Soballe B, Poole RK (2000) Ubiquinone limits oxidative stress in *Escherichia coli*. *Microbiology* **146 (Pt 4):** 787-796

Son MS, Matthews WJ, Jr., Kang Y, Nguyen DT, Hoang TT (2007) *In vivo* evidence of *Pseudomonas aeruginosa* nutrient acquisition and pathogenesis in the lungs of cystic fibrosis patients. *Infection and immunity* **75:** 5313-5324

Sone M, Kishigami S, Yoshihisa T, Ito K (1997) Roles of disulfide bonds in bacterial alkaline phosphatase. *J Biol Chem* **272:** 6174-6178

Stafford SJ, Humphreys DP, Lund PA (1999) Mutations in *dsbA* and *dsbB*, but not *dsbC*, lead to an enhanced sensitivity of *Escherichia coli* to Hg^{2+} and Cd^{2+}. *FEMS microbiology letters* **174:** 179-184

Steuber J, Schmid C, Rufibach M, Dimroth P (2000) Na^+ translocation by complex I (NADH:quinone oxidoreductase) of *Escherichia coli*. *Mol Microbiol* **35:** 428-434

Stroobant P, Young IG, Gibson F (1972) Mutants of *Escherichia coli* K-12 blocked in the final reaction of ubiquinone biosynthesis: characterization and genetic analysis. *J Bacteriol* **109:** 134-139

Sturr MG, Krulwich TA, Hicks DB (1996) Purification of a cytochrome *bd* terminal oxidase encoded by the *Escherichia coli* app locus from a delta *cyo* delta *cyd* strain complemented by genes from *Bacillus firmus* OF4. *J Bacteriol* **178:** 1742-1749

Subramanian A, Tamayo P, Mootha VK, Mukherjee S, Ebert BL, Gillette MA, Paulovich A, Pomeroy SL, Golub TR, Lander ES, Mesirov JP (2005) Gene set enrichment analysis: a knowledge-based approach for interpreting genome-wide expression profiles. *Proc Natl Acad Sci U S A* **102:** 15545-15550

Thesseling A, Rasmussen T, Burschel S, Wohlwend D, Kagi J, Muller R, Bottcher B, Friedrich T (2019) Homologous *bd* oxidases share the same architecture but differ in mechanism. *Nature communications* **10:** 5138

Toledano MB, Kumar C, Le Moan N, Spector D, Tacnet F (2007) The system biology of thiol redox system in *Escherichia coli* and yeast: differential functions in oxidative stress, iron metabolism and DNA synthesis. *FEBS letters* **581:** 3598-3607

Tomasiak TM, Cecchini G, Iverson TM (2007) Succinate as Donor; Fumarate as Acceptor. *EcoSal Plus* **2**

Tran QH, Bongaerts J, Vlad D, Unden G (1997) Requirement for the proton-pumping NADH dehydrogenase I of *Escherichia coli* in respiration of NADH to fumarate and its bioenergetic implications. *Eur J Biochem* **244:** 155-160

Unden G, Bongaerts J (1997) Alternative respiratory pathways of *Escherichia coli*: energetics and transcriptional regulation in response to electron acceptors. *Biochim Biophys Acta* **1320:** 217-234

Unden G, Kleefeld A (2004) C4-dicarboxylate degradation in aerobic and anaerobic growth. In *EcoSal—Escherichia coli and Salmonella: Cellular and Molecular Biology.* , R. Curtiss III (ed), 3.4.4. http://www.ecosal.org. ASM Press, Washington, DC.

Unden G, Steinmetz PA, Degreif-Dunnwald P (2014) The Aerobic and Anaerobic Respiratory Chain of *Escherichia coli* and S*almonella enterica*: Enzymes and Energetics. *EcoSal Plus* **6**

van den Berg B, Black PN, Clemons WM, Jr., Rapoport TA (2004) Crystal structure of the long-chain fatty acid transporter FadL. *Science* **304:** 1506-1509

Vandeputte-Rutten L, Kramer RA, Kroon J, Dekker N, Egmond MR, Gros P (2001) Crystal structure of the outer membrane protease OmpT from *Escherichia coli* suggests a novel catalytic site. *The EMBO journal* **20:** 5033-5039

VanOrsdel CE, Bhatt S, Allen RJ, Brenner EP, Hobson JJ, Jamil A, Haynes BM, Genson AM, Hemm MR (2013) The *Escherichia coli* CydX protein is a member of the CydAB cytochrome *bd* oxidase complex and is required for cytochrome *bd* oxidase activity. *J Bacteriol* **195:** 3640-3650

Vik SB (2007) ATP Synthesis by Oxidative Phosphorylation. *EcoSal Plus* **2**

Vila-Farres X, Parra-Millan R, Sanchez-Encinales V, Varese M, Ayerbe-Algaba R, Bayo N, Guardiola S, Pachon-Ibanez ME, Kotev M, Garcia J, Teixido M, Vila J, Pachon J, Giralt E, Smani Y (2017) Combating virulence of Gram-negative *bacilli* by OmpA inhibition. *Scientific reports* **7:** 14683

Vinci F, Couprie J, Pucci P, Quemeneur E, Moutiez M (2002) Description of the topographical changes associated to the different stages of the DsbA catalytic cycle. *Protein science : a publication of the Protein Society* **11:** 1600-1612

Vogt SL, Evans AD, Guest RL, Raivio TL (2014) The Cpx envelope stress response regulates and is regulated by small noncoding RNAs. *J Bacteriol* **196:** 4229-4238

Vollmer W, Blanot D, de Pedro MA (2008) Peptidoglycan structure and architecture. *FEMS microbiology reviews* **32:** 149-167

Walsh NP, Alba BM, Bose B, Gross CA, Sauer RT (2003) OMP peptide signals initiate the envelope-stress response by activating DegS protease via relief of inhibition mediated by its PDZ domain. *Cell* **113:** 61-71

Wang G, Maier RJ (2004) An NADPH quinone reductase of *Helicobacter pylori* plays an important role in oxidative stress resistance and host colonization. *Infection and immunity* **72:** 1391-1396

Wikstrom M, Verkhovsky MI (2007) Mechanism and energetics of proton translocation by the respiratory heme-copper oxidases. *Biochim Biophys Acta* **1767:** 1200-1214

Wilken C, Kitzing K, Kurzbauer R, Ehrmann M, Clausen T (2004) Crystal structure of the DegS stress sensor: How a PDZ domain recognizes misfolded protein and activates a protease. *Cell* **117:** 483-494

Wolfe AJ, Parikh N, Lima BP, Zemaitaitis B (2008) Signal integration by the two-component signal transduction response regulator CpxR. *J Bacteriol* **190:** 2314-2322

Wu G, Williams HD, Gibson F, Poole RK (1993) Mutants of *Escherichia coli* affected in respiration: the cloning and nucleotide sequence of *ubiA*, encoding the membrane-bound p-hydroxybenzoate:octaprenyltransferase. *J Gen Microbiol* **139:** 1795-1805

Wu W, Badrane H, Arora S, Baker HV, Jin S (2004) MucA-mediated coordination of type III secretion and alginate synthesis in *Pseudomonas aeruginosa*. *J Bacteriol* **186:** 7575-7585

Yamada M, Makino K, Amemura M, Shinagawa H, Nakata A (1989) Regulation of the phosphate regulon of *Escherichia coli*: analysis of mutant *phoB* and *phoR* genes causing different phenotypes. *J Bacteriol* **171:** 5601-5606

Yamaguchi S, Reid DA, Rothenberg E, Darwin AJ (2013) Changes in Psp protein binding partners, localization and behaviour upon activation of the *Yersinia enterocolitica* phage shock protein response. *Mol Microbiol* **87:** 656-671

Yu J (1998) Inactivation of DsbA, but not DsbC and DsbD, affects the intracellular survival and virulence of *Shigella flexneri*. *Infection and immunity* **66:** 3909-3917

Yu J, Webb H, Hirst TR (1992) A homologue of the *Escherichia coli* DsbA protein involved in disulphide bond formation is required for enterotoxin biogenesis in *Vibrio cholerae*. *Mol Microbiol* **6:** 1949-1958

Zeng H, Snavely I, Zamorano P, Javor GT (1998) Low ubiquinone content in *Escherichia coli* causes thiol hypersensitivity. *J Bacteriol* **180:** 3681-3685

Zhang H, Javor GT (2003) Regulation of the isofunctional genes *ubiD* and *ubiX* of the ubiquinone biosynthetic pathway of *Escherichia coli*. *FEMS microbiology letters* **223:** 67-72

Zhang L, Alfano JR, Becker DF (2015) Proline metabolism increases *katG* expression and oxidative stress resistance in *Escherichia coli*. *J Bacteriol* **197:** 431-440

Appendix

Appendix 1: Gene Set Enrichment Analysis of Pathways in *E. coli*

Oleate

NAME (Pathways)	*SIZE*	*NES*	*NOM p-val*	*FDR q-val*
ADENOSINE RIBONUCLEOTIDES <I>DE NOVO</I> BIOSYNTHESIS	10	-2.1666	0	2.71E-04
NADH TO CYTOCHROME <I>BO</I> OXIDASE ELECTRON TRANSFER I	15	-2.1199	0	2.83E-04
SUPERPATHWAY OF GLYCOLYSIS, PYRUVATE DEHYDROGENASE, TCA, AND GLYOXYLATE BYPASS	40	-2.1241	0	3.24E-04
SUPERPATHWAY OF ADENOSINE NUCLEOTIDES <I>DE NOVO</I> BIOSYNTHESIS II	18	-2.1684	0.00208768	3.61E-04
SUPERPATHWAY OF PURINE NUCLEOTIDES <I>DE NOVO</I> BIOSYNTHESIS II	29	-2.0929	0	3.66E-04
NADH TO TRIMETHYLAMINE <I>N</I>-OXIDE ELECTRON TRANSFER	13	-2.1311	0	3.78E-04
TCA CYCLE I (PROKARYOTIC)	16	-2.1334	0	4.53E-04
NADH TO FUMARATE ELECTRON TRANSFER	15	-2.0843	0	5.37E-04
NADH TO DIMETHYL SULFOXIDE ELECTRON TRANSFER	14	-2.1763	0	5.42E-04
SUPERPATHWAY OF GLYOXYLATE BYPASS AND TCA	20	-2.2165	0	0.00108333
NADH TO CYTOCHROME <I>BD</I> OXIDASE ELECTRON TRANSFER I	14	-2.0328	0	0.00142584
NITRATE REDUCTION VIII (DISSIMILATORY)	17	-1.9966	0	0.00256972
FATTY ACID &BETA;-OXIDATION I	6	-1.896	0	0.01091814
SUCCINATE TO CYTOCHROME <I>BO</I> OXIDASE ELECTRON TRANSFER	7	-1.8866	0.0021645	0.01169031
SUPERPATHWAY OF LIPOPOLYSACCHARIDE BIOSYNTHESIS	19	-1.8734	0.00230415	0.01279964
GLUCONEOGENESIS I	16	-1.8633	0.00431035	0.01290186
GLYOXYLATE CYCLE	5	-1.8511	0	0.0147448

SUPERPATHWAY OF UBIQUINOL-8 BIOSYNTHESIS (PROKARYOTIC)	5	-1.8378	0	0.0167636
UBIQUINOL-8 BIOSYNTHESIS (PROKARYOTIC)	4	-1.7842	0	0.029801
LIPID A-CORE BIOSYNTHESIS	8	-1.734	0.02169197	0.0526685
SUCCINATE TO CYTOCHROME <I>BD</I> OXIDASE ELECTRON TRANSFER	6	-1.7145	0.01535088	0.06141216
PANTOTHENATE AND COENZYME A BIOSYNTHESIS I	4	-1.6766	0.00217391	0.08356956

Acetate

NAME (Pathways)	*SIZE*	*NES*	*NOM p-val*	*FDR q-val*
SUPERPATHWAY OF PURINE NUCLEOTIDES <I>DE NOVO</I> BIOSYNTHESIS II	29	-2.5203	0	0
NADH TO CYTOCHROME <I>BO</I> OXIDASE ELECTRON TRANSFER I	15	-2.3925	0	0
NADH TO FUMARATE ELECTRON TRANSFER	15	-2.3291	0	0
SUPERPATHWAY OF ADENOSINE NUCLEOTIDES <I>DE NOVO</I> BIOSYNTHESIS II	18	-2.3289	0	0
NITRATE REDUCTION VIII (DISSIMILATORY)	17	-2.3137	0	0
NADH TO TRIMETHYLAMINE <I>N</I>-OXIDE ELECTRON TRANSFER	13	-2.2995	0	0
NADH TO CYTOCHROME <I>BD</I> OXIDASE ELECTRON TRANSFER I	14	-2.2842	0	0
NADH TO DIMETHYL SULFOXIDE ELECTRON TRANSFER	14	-2.2804	0	0
SUPERPATHWAY OF GLYOXYLATE BYPASS AND TCA	20	-2.2508	0	0
SUPERPATHWAY OF GLYCOLYSIS, PYRUVATE DEHYDROGENASE, TCA, AND GLYOXYLATE BYPASS	40	-2.2302	0	0
ADENOSINE RIBONUCLEOTIDES <I>DE NOVO</I> BIOSYNTHESIS	10	-2.1363	0	8.35E-05
TCA CYCLE I (PROKARYOTIC)	16	-1.9947	0	0.00108545
SUCCINATE TO CYTOCHROME <I>BO</I> OXIDASE ELECTRON TRANSFER	7	-1.9462	0	0.00254514
LIPID A-CORE BIOSYNTHESIS	8	-1.8577	0.00199203	0.01088881

5-AMINOIMIDAZOLE RIBONUCLEOTIDE BIOSYNTHESIS I	4	-1.8229	0	0.01744319
SUCCINATE TO CYTOCHROME <I>BD</I> OXIDASE ELECTRON TRANSFER	6	-1.8096	0	0.01851105
SUPERPATHWAY OF HISTIDINE, PURINE, AND PYRIMIDINE BIOSYNTHESIS	48	-1.7641	0.00185529	0.02771329
SUPERPATHWAY OF L-THREONINE METABOLISM	21	-1.7325	0.01663586	0.03801174
SUPERPATHWAY OF UBIQUINOL-8 BIOSYNTHESIS (PROKARYOTIC)	5	-1.7139	0.00580271	0.04470347
GLYOXYLATE CYCLE	5	-1.7049	0.01004016	0.04786623
NADH TO CYTOCHROME <I>BO</I> OXIDASE ELECTRON TRANSFER II	4	-1.6465	0.00206186	0.08628332
PROLINE TO CYTOCHROME <I>BO</I> OXIDASE ELECTRON TRANSFER	4	-1.6269	0.01796407	0.09391517
GLYCEROL-3-PHOSPHATE TO CYTOCHROME <I>BO</I> OXIDASE ELECTRON TRANSFER	4	-1.6165	0.01181102	0.09514987
PYRUVATE TO CYTOCHROME <I>BO</I> OXIDASE ELECTRON TRANSFER	4	-1.6196	0.00625	0.09622047
D-LACTATE TO CYTOCHROME <I>BO</I> OXIDASE ELECTRON TRANSPORT	4	-1.6272	0.01369863	0.09800983

Succinate

NAME (Pathways)	*SIZE*	*NES*	*NOM p-val*	*FDR q-val*
SUPERPATHWAY OF PURINE NUCLEOTIDES <I>DE NOVO</I> BIOSYNTHESIS II	29	-2.5359	0	0
SUPERPATHWAY OF ADENOSINE NUCLEOTIDES <I>DE NOVO</I> BIOSYNTHESIS II	18	-2.472	0	0
SUPERPATHWAY OF HISTIDINE, PURINE, AND PYRIMIDINE BIOSYNTHESIS	48	-2.3495	0	0
ADENOSINE RIBONUCLEOTIDES <I>DE NOVO</I> BIOSYNTHESIS	10	-2.2922	0	0
NADH TO CYTOCHROME <I>BD</I> OXIDASE ELECTRON TRANSFER I	14	-2.0296	0.00199203	0.00522304
SUPERPATHWAY OF GLYCOLYSIS, PYRUVATE DEHYDROGENASE, TCA, AND GLYOXYLATE BYPASS	40	-1.9749	0.00444444	0.00899359
LIPID A-CORE BIOSYNTHESIS	8	-1.9468	0	0.0119351

SUCCINATE TO CYTOCHROME <I>BO</I> OXIDASE ELECTRON TRANSFER	7	-1.9261	0.00207469	0.01473205
SUCCINATE TO CYTOCHROME <I>BD</I> OXIDASE ELECTRON TRANSFER	6	-1.882	0	0.0241498
SUPERPATHWAY OF GLYOXYLATE BYPASS AND TCA	20	-1.8627	0.00782779	0.02755721
NADH TO TRIMETHYLAMINE <I>N</I>-OXIDE ELECTRON TRANSFER	13	-1.839	0.00445434	0.03391914
TCA CYCLE I (PROKARYOTIC)	16	-1.8227	0.01167315	0.03720384
GLUCONEOGENESIS I	16	-1.783	0.01449275	0.05178795
NADH TO FUMARATE ELECTRON TRANSFER	15	-1.7547	0.01263158	0.06374289
NITRATE REDUCTION VIII (DISSIMILATORY)	17	-1.6991	0.03420523	0.08982711
GALACTOSE DEGRADATION I (LELOIR PATHWAY)	4	-1.7019	0.0040568	0.09290419
NADH TO CYTOCHROME <I>BO</I> OXIDASE ELECTRON TRANSFER I	15	-1.7057	0.024	0.095584

Glycerol

NAME (Pathways)	*SIZE*	*NES*	*NOM p-val*	*FDR q-val*
SUPERPATHWAY OF PURINE NUCLEOTIDES <I>DE NOVO</I> BIOSYNTHESIS II	29	-2.2989	0	0
SUPERPATHWAY OF ADENOSINE NUCLEOTIDES <I>DE NOVO</I> BIOSYNTHESIS II	18	-2.0788	0.00425532	0.01100251
ADENOSINE RIBONUCLEOTIDES <I>DE NOVO</I> BIOSYNTHESIS	10	-1.92	0.00814664	0.02694642
SUPERPATHWAY OF <I>S</I>-ADENOSYL-L-METHIONINE BIOSYNTHESIS	9	-1.9555	0	0.03034521
GLYCOLYSIS II (FROM FRUCTOSE 6-PHOSPHATE)	17	-1.9205	0.00862069	0.03343536
SUPERPATHWAY OF 5-AMINOIMIDAZOLE RIBONUCLEOTIDE BIOSYNTHESIS	5	-1.8751	0	0.0352295
GLUCONEOGENESIS I	16	-1.8588	0.0141129	0.0357606
L-HISTIDINE BIOSYNTHESIS	7	-1.8151	0.00212314	0.05104417
GLYCOLYSIS I (FROM GLUCOSE 6-PHOSPHATE)	17	-1.7883	0.00671141	0.05983547

5-AMINOIMIDAZOLE RIBONUCLEOTIDE BIOSYNTHESIS II	4	-1.7726	0	0.06161615
SUPERPATHWAY OF HEXITOL DEGRADATION (BACTERIA)	24	-1.6911	0.02643172	0.09698947
GALACTOSE DEGRADATION I (LELOIR PATHWAY)	4	-1.6968	0.00612245	0.09946957

Glucosamine

NAME (Pathways)	*SIZE*	*NES*	*NOM p-val*	*FDR q-val*
SUPERPATHWAY OF PURINE NUCLEOTIDES <I>DE NOVO</I> BIOSYNTHESIS II	29	-2.2293	0	8.74E-04
SUPERPATHWAY OF ADENOSINE NUCLEOTIDES <I>DE NOVO</I> BIOSYNTHESIS II	18	-2.0306	0.00191205	0.00406316
ADENOSINE RIBONUCLEOTIDES <I>DE NOVO</I> BIOSYNTHESIS	10	-1.9324	0	0.0114748

N-acetylglucosamine

NAME (Pathways)	*SIZE*	*NES*	*NOM p-val*	*FDR q-val*
SUPERPATHWAY OF PURINE NUCLEOTIDES <I>DE NOVO</I> BIOSYNTHESIS II	29	-2.0675	0	0.00376371
SUPERPATHWAY OF ADENOSINE NUCLEOTIDES <I>DE NOVO</I> BIOSYNTHESIS II	18	-2.0689	0.00222222	0.00752743
ADENOSINE RIBONUCLEOTIDES <I>DE NOVO</I> BIOSYNTHESIS	10	-1.9319	0.00209205	0.01374091
SUPERPATHWAY OF FUCOSE AND RHAMNOSE DEGRADATION	7	-1.7744	0.00210526	0.08500927

Maltose

NAME (Pathways)	*SIZE*	*NES*	*NOM p-val*	*FDR q-val*
SUPERPATHWAY OF PURINE NUCLEOTIDES <I>DE NOVO</I> BIOSYNTHESIS II	29	-2.1888	0	0.00513311
NADH TO CYTOCHROME <I>BO</I> OXIDASE ELECTRON TRANSFER I	15	-1.8992	0.01037344	0.07809221
SUPERPATHWAY OF ADENOSINE NUCLEOTIDES <I>DE NOVO</I> BIOSYNTHESIS II	18	-1.9327	0.01287554	0.07945564

Appendix 2: Gene Set Enrichment Analysis of Complexes in *E. coli*

Oleate

NAME (Complexes)	*SIZE*	*NES*	*NOM p-val*	*FDR q-val*
NADH:QUINONE OXIDOREDUCTASE I	11	-2.19961	0	0
ATP SYNTHASE F₀ COMPLEX // ATP SYNTHASE F₁ COMPLEX	7	-1.97751	0	6.61E-04
SUCCINATE:QUINONE OXIDOREDUCTASE SUBCOMPLEX	3	-1.67594	0	0.06536648

Acetate

NAME (Complexes)	*SIZE*	*NES*	*NOM p-val*	*FDR q-val*
NADH:QUINONE OXIDOREDUCTASE I	11	-2.31232	0	0
ATP SYNTHASE F₀ COMPLEX // ATP SYNTHASE F₁ COMPLEX	7	-1.95217	0	9.37E-04
NADH:QUINONE OXIDOREDUCTASE I, PERIPHERAL ARM	4	-1.75573	0	0.01386948
ATP SYNTHASE F₁ COMPLEX	4	-1.6581	0.00422833	0.03531452
SUCCINATE:QUINONE OXIDOREDUCTASE SUBCOMPLEX	3	-1.62958	0	0.04581498

Succinate

NAME (Complexes)	*SIZE*	*NES*	*NOM p-val*	*FDR q-val*
ATP SYNTHASE F₀ COMPLEX // ATP SYNTHASE F₁ COMPLEX	7	-2.1168	0	0
NADH:QUINONE OXIDOREDUCTASE I	11	-1.88637	0.004132231	0.00869888
ATP SYNTHASE F₁ COMPLEX	4	-1.77332	0	0.02181596
SUCCINATE:QUINONE OXIDOREDUCTASE SUBCOMPLEX	3	-1.65933	0	0.06052947
THE TOL-PAL CELL ENVELOPE COMPLEX	4	-1.61624	0.016460905	0.08666097

Glycerol

NAME (Complexes)	*SIZE*	*NES*	*NOM p-val*	*FDR q-val*
None				

Glucosamine

NAME (Complexes)	*SIZE*	*NES*	*NOM p-val*	*FDR q-val*
ATP SYNTHASE F₀ COMPLEX // ATP SYNTHASE F₁ COMPLEX	7	-1.84975	0	0.01598191

N-acetylglucosamine

NAME (Complexes)	*SIZE*	*NES*	*NOM p-val*	*FDR q-val*
ATP SYNTHASE F₀ COMPLEX // ATP SYNTHASE F₁ COMPLEX	7	-1.95419	0.002123142	9.76E-04

Maltose

NAME (Complexes)	*SIZE*	*NES*	*NOM p-val*	*FDR q-val*
None				